Estratto dal Volume 136, *Memorie di Scienze Fisiche e Naturali*, «Rendiconti della Accademia Nazionale delle Scienze detta dei XL», serie V, vol. XLII, parte II, tomo II, 2018

ACCADEMIA NAZIONALE DELLE SCIENZE
detta dei XL

The astrochemical observatory: focus on chiral molecules

L'osservatorio astrochimico: obiettivo sulle molecole chirali

Edited by
Andrea Lombardi and Federico Palazzetti

Rome, 22-23 March 2018

ISBN 000-00-00000-00-0

ISSN 0392-4130

ACCADEMIA NAZIONALE DELLE SCIENZE DETTA DEI XL
00161 Roma - Via L. Spallanzani, 7

Rendiconti
Accademia Nazionale delle Scienze detta dei XL
Memorie di Scienze Fisiche e Naturali
136° (2018), Vol. XLII, Parte II, Tomo II, p. 5

EMILIA CHIANCONE*

Welcome address

I would like to welcome you all on behalf of the Academy of the XL and introduce you briefly to our Academy and the origin of its name. Back in 1782, Anton Maria Lorgna, a mathematician and hydraulic engineer from Verona, wanted Italian scientists, who were dispersed in a number of local academies, to have a single voice in Europe. Thus, Lorgna invited the 40 most outstanding scientists from all parts of Italy to join the «Società Italiana» he was founding and to publish their work in the Memorie di Fisica e Matematica, nowadays the Rendiconti. In a few years, the Memorie di Fisica e Matematica became the reference point of Italian scientists in Europe and the «Società Italiana dei XL» established itself as the sole representative of Italian Science. I would like to stress that Lorgna called the Society «Italian» roughly a hundred years before Italy was united; we are very proud of this anticipatory role.

Let me add a few words on the topic of this Symposium and at the same time thank our Academy member Vincenzo Aquilanti and his team for organizing it. Given my background as protein scientist, and my limited knowledge of chirality, let me just refer to Primo Levi and his thoughts on «*Asymmetry and life*» published in the Bollettino dell'Unione Matematica Italiana in 1998. Levi dwells on the fact that all the protagonists of the living world – proteins, nucleic acids, sugars – are asymmetric, that the left-right asymmetry is intrinsic to life and concludes that it coincides with life. It seems to me that this conclusion is relevant to one of the scopes of the Symposium, brought up by the continuously increasing number of chiral molecules discovered in space, namely assessing the role of chirality in the origin and evolution of life.

Let me give the floor to Vincenzo for his opening remarks, while thanking you for your attention.

* President, Accademia Nazionale delle Scienze detta dei XL, Roma (Italy).
E.mail: segreteria@accademiaxl.it emilia.chiancone@uniroma1.it

Rendiconti
Accademia Nazionale delle Scienze detta dei XL
Memorie di Scienze Fisiche e Naturali
136° (2018), Vol. XLII, Parte II, Tomo II, pp. 7-15

VINCENZO AQUILANTI*

The Astrochemical Observatory: Chemistry in the sky

Summary – The sixteen chapters of this book are a collection of short essays and extended abstracts, which originated from presentations at an event that took place in 22 and 23 March 2018 in Villa Torlonia in Rome. The venue was the Library of the Accademia Nazionale delle Scienze detta dei Quaranta (National Academy of Sciences, known as of the Forty). The participants to the conference shared interest for the role of molecules in connection with the modern science of the Universe. The recent designation for this area of research goes under the name of Astrochemistry. A brief history of this discipline is sketched, with particular emphasis on the roots, namely the developments that took place back in time, essentially due to an eminent astronomer, Angelo Secchi: in the Nineteenth century he was known as "the Chemist of the sky": he was curious about the role of chemical elements in the observational data from his telescope, that he had equipped with a spectroscope. The nucleus of the group of scientists carrying out concerted efforts under the denomination "Astrochemical Observatory" operates since a dozen years: it is diffused in various universities and research centers essentially based in central Italy, extended to collaborators in the Nation and abroad. The theme chosen for this year's event that can be considered as one of a series, is molecular chirality, a topic transversal across many disciplines that has relevance also for evolutionary sciences. The conference was dedicated to the memory of Giangualberto Volpi, the founder of a school in chemical kinetics who had died in February 2017: in June 2018, he would have been ninety years old: Volpi's school was based first in Rome on ion-molecule reactions and then in Perugia on neutral reactions. A member of his school, Anna Giardini who later contributed to the topic of chiral recognition, was the special guest of the conference. Anticipations are indicated of future meetings: the one in 2019 will be devoted to chemical kinetics, while other events in preparation will be centered about the figure of Primo Levi, writer, chemist, prominent figure, protagonist of the cultural debate of last century, in occasion of his one hundredth birthday.

* One of the XL – Dipartimento di Chimica, Biologia e Biotecnologie, Università di Perugia, 06123 Perugia, Italy. Consiglio Nazionale delle Ricerche, Istituto di Struttura della Materia, 00016 Roma, Italy. E.mail: vincenzoaquilanti@yahoo.it

Opening the March 2018 event

The call for the present conference had the goal of establishing a starting event for an initiative involving research groups in Italy active in carrying out projects in astrochemistry. The melting pot consisted of a scientific reunion assessing the state of the "Astrochemical Observatory", that had been formalized in 2016 under the auspices of the Italian Accademia Nazionale delle Scienze detta dei XL (National Academy of Sciences, known as of the Forty). The initiative is regarding wide areas covered by the emerging science going under the name of astrochemistry – a new name with an immediate self-explaining connotation. To this theme, several activities had been dedicated already in the recent past, and the particular focus of this gathering has been centered around that of molecular chirality. However, the occasion was taken of extending the presentations to related topics, in order to give an account of the general status of the research in this field from Italian scientists, enlarged to their principal international collaborators. For an account published in 2012 of the preliminary proposals see Figure 1.

Fig. 1. Cover of the Journal where in 2012 an article on the Astrochemical Observatory project was presented, with particular emphasis on the collaborations with Osaka and Taipei laboratories.

Twenty years ago in Rome…

The First European Workshop on an emerging discipline "Exo-Astro-Biology", took place in Frascati, near Rome, in 2001 and included the attendance of many chemists. Proceedings are available (see Figure 2): the concluding sentence of one of the progress reports (Keheyan *et al.* 2001) refers to "astrobiological implications of our laboratory discovery, the detection of aligned benzene in gaseous streams (see the Physical Review Focus, http://focus.aps.org.no.26,29 May 2001, and Chemical,

Fig. 2. The proceedings of the First European Workshop on Exo-/ Astro-biology in 2001.

Engineering News, 11 June 2001, p. 22) and previous evidence on simpler molecules point out that as our future work plan we focus on possible mechanisms for chiral bio-stereochemistry of oriented reactants, for example when flowing in atmospheres of rotating bodies, specifically the planet Earth". A decade later, at the 2010 and 2012 Rome Lincei Conferences on Astrochemistry and Chirality, respectively, the opportunity was provided of presenting an account of the progress regarding that initial proposal.

The search for possible stereodynamical mechanisms of chiral discrimination based upon collisions, involves design of new experiments and the laboratory techniques must be upgraded to distinguish between enantiomers. This objective requires sharpening not only the experimental tools, but also the theoretical ones provided by modern physical chemistry (Aquilanti *et al.* 2008): quantum and semiclassical approaches developed for few-atom reactions need extensions to cases of more complicated many-body systems to explicitly include chirality, starting by defining convenient parametrization of chiral observables for enantiomeric distinguishability. From an experimental viewpoint, progress continues to be required on collisional alignment in gaseous streams and on various aspects of physicochemical sciences, aimed at understanding spatial aspects of molecular structure and dynamics. The main target here is to measure and/or to calculate crucial kinetic parameters (cross sections and rate constants) to be used in models to verify the hypothesis that molecular collision mechanisms can induce chirality discrimination. Experiments involving molecular beams techniques, assisted by model molecular dynamics calculations, are currently being performed and described in some of the papers collected here.

The prequel: Angelo Secchi, the chemist of the sky

The Nineteenth Century Jesuit Angelo Secchi (Reggio Emilia 1818 – Rome 1878) was defined as "the chemist of the sky". He was very well known in his times for many scientific contributions and discoveries: not only he was an astronomer and an astrophysicist, but also established important geophysical benchmarks, such as the definition of the Rome meridian, and laboratory studies of the Earth magnetism and of meteorology. Regarding his contribution to astronomy, during the several years when he acted as the director of the Pontifical Observatory, he had implemented the idea of adding a spectroscope to his telescope and in this way he could follow the "royal road" established by Fraunhofer and others. Importantly, he was the first to focus not only on the spectral lines (which were correctly attributed to atomic spectra) but also to bands, which were subsequently associated to molecular spectra. In this sense he was really doing chemistry. Additionally, one of the main aspects of the great fame of Secchi came when he classified stars according to their chemical compositions: his classification was the first to be proposed and lasted as the standard one for few decades, until the British classification modified his approach by substantial variants.

Angelo Secchi was a member of the Academy of the Forty and was a Jesuit: his laboratory was placed in central Rome at the roof of the S. Ignazio church, which is the headquarter of the Jesuit Order. Unfortunately for him, when in the Seventies of the XIX century, Rome passed from the Pontifical Reign to the newly formed Italian Kingdom, Father Secchi, as functionary of the Papal state, was under scrutiny for removal by the new state and for dismission from his position as Chief Astronomer. The Italian Senate voted by a tiny majority in his favor and for him to continue to be the head of the Observatory, especially thanks to the influence of Quintino Sella – then Minister of Economics of Italy and the president of the newly reorganized Lincei Academy. The Pope established an alternative a new branch of the academy, known as Accademia Pontificia, and Secchi was as appointed the president of it. Exceptionally, he was allowed to continue his activity as Chief Astronomer until his death in 1878. He was a member of the Academy of the Forty, without interruption from 1858 to 1878: to celebrate him, the Academy organizad an important meeting on the occasion of his centennial anniversary: the proceedings of this conference were published in 1979 and a second edition was printed in 1993. In the year 2018 in September, a conference subsequent to the present one, celebrating the bicentennial of his birth, took place: a stamp was issued from the Italian Mail (Figure 3) and proceedings are being prepared from the Academy of the Forty also on this event.

Fig. 3. Celebration of Angelo Secchi (the Chemist of the sky), on the Bicentennial of his birth, by a postcard and a stamp from the Italian Mail in April 2018.

A dedication: Giangualberto Volpi and chemical kinetics

The conference is dedicated to professor Giangualberto Volpi (Figure 4), who died exactly one year before this event in February 2017 and would be ninety-year-old at the time of writing. To his memory, a commemorative article appeared in this Rendiconti, Aquilanti, 2016. He belonged to a team that in the post-war Italy started a pioneering activity on elementary chemical reactions, innovating the instrumentation of chemical physics by introducing the first especially built mass spectrometer in the country, homemade in the laboratory of professor Giorgio Careri in the Physics Institute of the University of Rome. The instrument was essential for a kinetic study of the prototype of all chemical reactions, the isotopic exchange of hydrogen and deuterium, and that work provided the first convincing experimental confirmation of Transition State Theory, which had been formulated about 25 years before by Eyring, Polanyi, Wigner. In successive decades, Volpi established a research activity in the General Chemistry Institute in the University of Rome, devoted to elementary chemical processes, innovating the scope of investigations of the group to the point that it is now recognized as among the first teams to study physics and chemistry involving ions by high pressure mass spectrometry. The group became soon a world leader on ion-molecule reactions, and the results obtained were considered of main interests in radiation chemistry and in the chemistry of plasmas, with applications to the ionosphere research and more recently to astrochemical environments. In fact, well beyond the expectation of scientists of the atmospheres of the planets in the solar system, ion-molecule reactions are being considered as playing an important role even in discussions of the early Universe, regarding the formation of atoms and molecules through reactions of ions. The book reports articles on these and related topics.

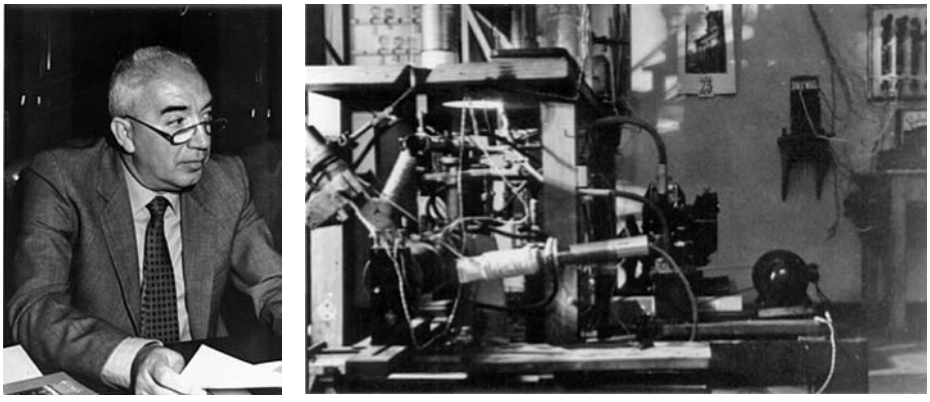

Fig. 4. Gian Gualberto Volpi in his office in Perugia at the beginning of the century. Also shown the mass spectrometer of the Fifties.

Special guest: Anna Giardini and chiral recognition

Anna Giardini's work was recognized worldwide as that of a fine experimentalist with a deep involvement in studying processes of relevance both to theoreticians and to applied scientists. Her enthusiasm and tireless energy were so well known that it is no surprise to us that after retirement from the University she had been still active in the National Research Council Laboratories. As a further impressive demonstration of the ample spectrum of interest that have characterized her scientific career, she more recently focused on the study of ultrafast photophysical and photochemical processes with femtosecond lasers, performing pump-probe spectroscopy experiments of molecules of biological relevance in liquid solutions. Important are her contributions to chirality issues, see Figure 5 and many articles in this book by her former collaborators and students.

Fig. 5. Anna Giardini in her office at La Sapienza of Rome around 2005. Several contributions in this collection come from her main coworkers on chirality issues, such as Professor Maurizio Speranza, and former students Susanna Piccirillo, now at the University of Rome Tor Vergata, Daniele Catone and Mauro Satta, now at CNR, the Italian National Research Council, and others.

The sequel: Primo Levi, chirality and the periodic system

The year 2019 is the centennial of the birth of Primo Levi who was a chemist both as training (doctor in Chemistry in Turin in 1941) and for many years also by profession. Any intent to highlight the significant role in his life and in his work of science (and of chemistry in particular), is often overshadowed by the immense notoriety of his great figure as narrator and witness of his time. The famous book by Levi *Il Sistema Periodico*, "The Periodic System" (1975), see Figure 6, is a paramount

Fig. 6. The first edition of one of Primo Levi's narrative masterpieces, and one where the "fil rouge" is the reference to his chemical background. Note the cover, by a drawing by M. S. C. Escher, showing a three-dimensional paradox inspired by a Möbius band: to the early XIX century mathematician Möbius the geometrical concept now known as chirality is attributed.

example of narrative writing inspired and permeated by scientific philosophy. Additionally, the year 2019 marks the 150th anniversary of the formulation of the periodic system of elements by Medeleev: this milestone was celebrated ten years ago in an interdisciplinary Lincei congress and updates are proposed also in reference to the work of Levi. In Levi, the theme of molecular chirality pervades his writing explicitly or as a metaphor: in future events, presentations of this interdisciplinary theme will also be addressed.

In 2017, the Italian Chemical Society, together with the German counterpart, instituted the two-year Primo Levi Prize and awarded the Nobel Prize laureate Hoffmann with a prestigious ceremony, held in Germany, that has been given a great deal of attention from media. The next award will be organized by the Italian Chemical Society in Rome in December 2019: accompanying events are being planned emphasizing highly interdisciplinary features

As mentioned, Primo Levi was a chemist by profession, his doctoral dissertation concerned Walden's inversion, related to chiral changes: he later published a famous article on molecular chirality and asymmetry of life, whose relevance was underlined by the physicist Tullio Regge, with whom he discussed in more occasions about the possible dialogue between the two cultures. The title of one of his collections is *L'Asimmetria e la Vita* (Asymmetry and Life). The excellence of his

writing pervades his literary works, as a witness to the Holocaust, as a publicist, as a scientific disseminator within narrative contexts, transcending the barriers between the "two cultures".

Concluding the presentation of the book dedicated to the 2018 event, it is an appropriate signal towards the future to indicate that dates and location for the next event, OAK – Observatory for Astrochemical Kinetics, are already settled: again Rome, the Biblioteca dell'Accademia dei XL, 27 and 28 June 2019: old and new participants are cordially invited to joint efforts on the current and future chemical themes inspired by the surprising discovery of myriads of planets outside the Solar System.

BIBLIOGRAPHY

Aquilanti V., Molecular and Nanodynamics: from atoms to biomolecules, 2008. Physica Scripta, 78, 050301.

Aquilanti V., Piccirillo S., Speranza M., Anna Giardini's journey from atoms to biomolecules, 2008. Physica Scripta, 78, 050401.

Aquilanti V., Grossi G., Lombardi A., Maciel G. S., Palazzetti F., 2008. The origin of chiral discrimination: supersonic molecular beam experiments and molecular dynamics simulations of collisional mechanisms. Physica Scripta 78,058119-058125.

Aquilanti V., Grossi G., Lombardi A., Maciel G.S., Palazzetti F., 2011. Aligned molecular collisions and a stereodynamical mechanism for selective chirality. Rend. Fis. Acc. Lincei 22,125-135.

Aquilanti V., 2016. Ricordo di Gian Gualberto Volpi. Rendiconti Accademia Nazionale delle Scienze detta dei XL, Memorie di Scienze Fisiche e Naturali 134° Vol. XL, Parte II, 45-49.

Boato G., Volpi G.G., Experiments on the Dynamics of Molecular Processes: A Chronicle of Fifty Years, 1999. Annual Review of Physical Chemistry, 50, 23-50.

Keheyan Y., Aquilanti V., Brucato J.R., Colangeli L., Cataldo F., Mennella V., 2001. Astrochemical and prebiotical elementary processes. In: European Workshop on Exo-/Astrobiology, Frascati, May 2001, esa SP, August 2001, pp. 357-361.

Palazzetti F., Maciel G.S., Lombardi A., Grossi G., Aquilanti V., 2012. The astrochemical observatory: molecules in the laboratory and in the cosmos. J. Chin. Chem. Soc. 59, 1045-1052.

Secchi A., Sugli spettri prismatici delle stelle fisse, 1867. Rendiconti Accademia Nazionale delle Scienze detta dei XL, 67-152.

Secchi A., Sulla grande nebulosa di Orione, 1868. Rendiconti Accademia Nazionale delle Scienze detta dei XL, 99-134.

Secchi A., Sugli spettri prismatici delle stelle fisse, Memoria Seconda, Pubblicata nel 1869/1876 Rendiconti Accademia Nazionale delle Scienze detta dei XL, 73-133.

Secchi A., Sugli spettri prismatici de' corpi celesti, Memoria Terza, Pubblicata nel 1869-1876. Rendiconti Accademia Nazionale delle Scienze detta dei XL, 191-248.

Rendiconti
Accademia Nazionale delle Scienze detta dei XL
Memorie di Scienze Fisiche e Naturali
136° (2018), Vol. XLII, Parte II, Tomo II, pp. 17-25

ALESSANDRA CIAVARDINI[1] – FLAMINIA RONDINO[2]
ALESSANDRA PALADINI[3] – MAURIZIO SPERANZA[4]
SIMONETTA FORNARINI[4] – MAURO SATTA[5] – SUSANNA PICCIRILLO[6]

The effect of halogen substitution on the aromatic ring in chiral recognition between 1-aryl-1-ethanol and butan-2-ol: Resonant Two Photon Ionization Spectroscopy and Quantum Chemical Calculations

Abstract – Non-covalent intra and intermolecular interactions account for the molecular and chiral recognition properties as well as the functionality of biomolecules.

This minireview presents the results concerning adducts between chiral aromatic alcohols, differently substituted on the aromatic ring, with the two enantiomers of butan-2-ol, which have been investigated by mass-selective resonant two-photon ionization (R2PI) and infrared depleted R2PI (IR-R2PI) techniques. The comparison of the systems allowed us to highlight the significance of specific intermolecular interactions in the chiral discrimination process. The interpretation of the results is based on theoretical predictions at the D-B3LYP/6-31++G** level of theory.

Introduction

The transmission of chiral information, the recognition properties as well as the functionality of biomolecules rely substantially on non-covalent intra and intermol-

[1] Elettra-Sincrotrone Trieste S.c.p.A., in Area di Ricerca, Basovizza (Trieste), Italy.
[2] C.R ENEA Frascati, Via E. Fermi 45 - 00044 Frascati, Roma, Italy.
[3] CNR – ISM, Area della Ricerca di Roma 1, Monterotondo Scalo, Italy.
[4] Dip. di Chimica e Tecnologie del Farmaco, Università di Roma «La Sapienza», Rome, Italy.
[5] CNR-ISMN, Dipartimento di Chimica, University of Rome Sapienza, Rome, Italy.
[6] Dip. di Scienze e Tecnologie Chimiche, Università di Roma «Tor Vergata», via della Ricerca Scientifica - 00133 Rome, Italy. E-mail: piccirillo@fisica.uniroma2.it

ecular interactions and their study is of fundamental interest and has a deep impact on chemistry, biology, pharmacology, materials science and astrophysics. In combination with stronger non-covalent interactions with high directionality, such as conventional hydrogen bonding or metal coordination, other forces such as π···π stacking, lone pair···π or weaker hydrogen bond interactions such as XH···π (X = O, N and C) or CH···X (X = O, N, halogen) interactions often play an essential role in chiral discrimination processes [1]. Indeed, the ability of halogen atoms to work as effective sites for directing molecular recognition processes long remained unexplored, despite in 1970 Hassel *et al.* [2] pointed out the key role of halogen atoms in driving molecular self-assembly processes. Then in the past decade, the effects of halogenation have received a growing interest in many different fields, and the halogen bond has been largely exploited to control the assembly of small molecules in the design of both supramolecular complexes and new materials [3].

A convenient approach to gain detailed information on the nature of the specific intervening forces is to generate tailor-made molecular adducts in the isolated state and to investigate them through high-resolution spectroscopy. Specific interactions, influencing molecular geometries, as well as the dynamics of conceivable reactive processes [4] can be studied without any interference from the environment. The results of gas phase experiments can be used by theoretical chemists as a benchmark for the validation of different approximations for quantum calculations [5].

Here, we highlight and summarize some recent results [6, 7, 8] concerning adducts containing a chiral halogenated molecule, obtained under collision-free conditions in supersonic molecular beams and investigated through resonant two-photon ionization (R2PI) and double-resonance infrared-R2PI (IR-R2PI) spectroscopy coupled with mass spectrometry. In particular, we point out results concerning the effect of the presence of a halogen atom in different positions on the aromatic ring on the structure and the conformational equilibria of the complexes between (*S*)-1-(4-chlorophenyl)ethanol (p-ClE_S), S-1-(4-fluorophenyl)ethanol (p-FE_S), (S)-1-(2-fluorophenyl)ethanol (o-FE_S), R-1-phenyl1-ethanol (E_R) with the two enantiomers of butan-2-ol (B_R and B_S). All figures are adapted from Ref. 6.7,8.

Experimental section

The experimental apparatus for the study of gas phase complexes has been described previously [6, 9] and will be briefly summarized. Neutral clusters are produced in a 10-Hz-pulsed seeded supersonic expansion of vapors of chiral molecules generated in temperature-controlled reservoirs in argon carrier gas. The clusters are ionized via one-color Resonant Two Photon Ionization (1cR2PI) process. The photoions are mass analyzed in a time-of-flight mass spectrometer and detected by a channeltron. One-color R2PI experiments are performed through the ionization of the species of interest by resonant absorption of two photons of the same energy h . The entire TOF mass spectrum is recorded as a function of ν_1. Due to the resonant

step in the two-photon process, the wavelength dependence of a given mass-resolved ion represents the excitation spectrum of the neutral precursor and contains information about its electronic excited state S_1.

The difference in the binding energies of the diastereomeric complexes has been evaluated by the measure of the product/parent dissociation ratio recorded at specific 1c-R2PI transitions.

The vibrational spectra in the OH-stretching region of the neutral precursors are recorded by IR–R2PI double resonance spectroscopy. The IR and UV lasers are counter-propagating and spatially superimposed, the IR laser pump pulse precedes the UV laser by about 100 ns. If a cluster absorbs photons with energies of one or several quanta of a high-frequency vibrational mode, it predissociates very fast by IVR resulting in a depopulation and an R2PI-ion signal depletion. An ion-dip spectrum is recorded by scanning the wavelength of the IR laser with the wavelength of the probe laser being fixed to the specific transition in the R2PI spectrum of a selected cluster. It represents part of the vibrational spectrum of the neutral precursor cluster in the electronic ground state. This methodology also allows the discrimination of different conformers present in the supersonic molecular beam [10]. The IR laser light is generated by a home-made, injection-seeded optical parametric oscillator (OPO), built according to the design developed at the University of Frankfurt [11].

A preliminary analysis of the conformational landscape was carried out by classical molecular dynamics with the MM3 force-field. The optimized structures are classified according to their conformation and energy and the lowest energy structures for each diastereomer (relative energy lower than 2 kcal mol^{-1}) have been re-optimized with the D-DFT approach: we used the B3LYP Hamiltonian with the 6-31++G** basis set. Further details can be found in references 6,7 and 8.

The structure of the bare chromophores

The 1cR2PI excitation spectrum of the halogenated compounds pFE_S, $p\text{-}ClE_S$ and oFE_S are characterized by the presence of low-frequency (40-50 cm-1) band progressions, which are absent in the E_R congener under similar experimental conditions. This behavior is ascribable to the fact that the S1←S0 transition in the halogenated species involves asymmetric structures of the aromatic ring in both the S_0 and S_1 states while the same electronic transition in non-halogenated E_R involves no change of the quasi-C6 symmetry of the ring. According to D-B3LYP/6-31++G** calculations, the band progression observed in the spectra of pFE_S, $p\text{-}ClE_S$ and oFE_S can be related to the $\nu_1(C_1\text{-}C_\alpha)$ torsional mode of the most stable structure of each species, pointing out that only one predominant conformer is identified in the supersonic beam expansion. The presence of one stable conformation is found also in the case of E_R.

The most stable conformational structures of the isolated chromophores which were identified experimentally are remarkably similar. As shown in figure 1 for

p-ClE_S they are characterized by an intramolecular OH···π interaction and a weak attractive C_2H···O interaction. In the case of oFES, there is also a weak $C_\alpha H$···F interaction.

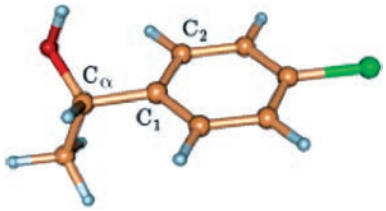

Fig. 1. D-B3LYP/6-31++G** calculated structure for the most stable conformer of isolated p-ClE_S.

Structure and stability of the para halogenated diasteromers

Fig. 2 reports as an example the 1cR2PI excitation spectra of the two complexes of p-FES with R and S-butan-2-ol [6]. Both spectra display a low frequency vibrational progression which can be assitgned to the $\nu_1(C_1\text{-}C_\alpha)$ torsional mode. A spectral chiral discrimination is evident from the spectra: each diastereomer displays distinct features shifted to the red with respect to 0_0^0 electronic transition of the chromophore [12]. The shift is greater for the homochiral complex with respect to the

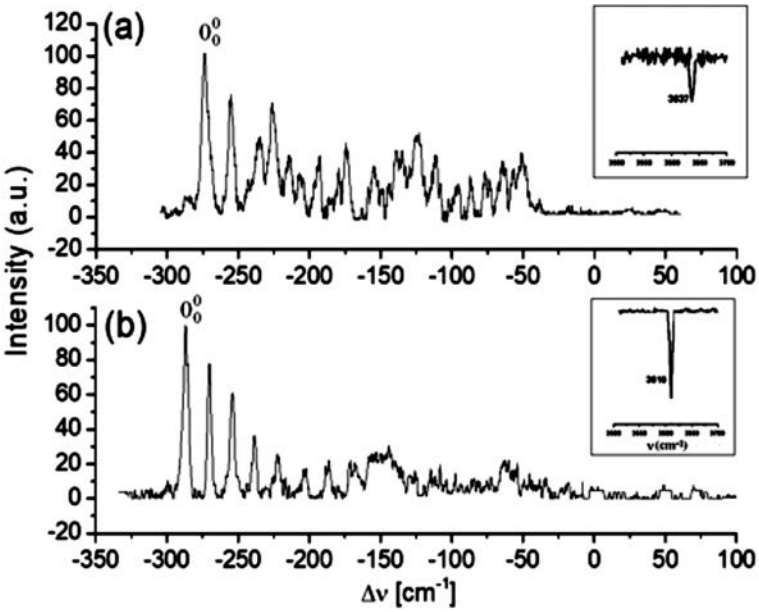

Fig. 2. R2PI excitation spectra and IR-R2PI spectra (inset) of (a) heterochiral [p-FE_S*B_R] and (b) homochiral [p-FE_S*B_S] clusters.

heterochiral complex. Similar results have been found for the non-halogenated adducts and for the para-chloro adducts with butan-2-ol [8]. The measurement of the dissociation ratios in the mass spectra indicates that the homochiral complexes are more stable than the heterochiral complexes for the non halogenated and para fluorinated diasteromers and the relative stability of the specific homo versus hetero complexes is much higher for the para substituted complexes with respect to the non-fluorinated adducts.

The shift in the R2PI spectra is relative to the electronic transition of the isolated FE_S molecule at 37 140 cm^{-1}.

In the inset of figure 2, the IR-R2PI depletion spectra of the complexes is shown, recorded in the 3500-3700 cm^{-1} range with the probe wavelength set on the 0_0^0 origin of the complexes. The bands at 3637 and 3610 cm^{-1} correspond to the OH stretch mode of butanol in the p-$FE_S{\cdot}B_{R/S}$ clusters.

Figure 3 for the non halogenated and figure 4 for the para-halogenated adducts show the D-B3LYP calculated structures which have been assigned on the basis of i) the comparison between calculated and observed vibrational frequencies, ii) the analysis of the specific interactions contributing to the shift of the electronic transition, iii) the relative energy of the complexes. A complete description of all calculated complexes can be found in references 6, 7, 8. These structeres are characterized by an $O^{ch}H{\cdots}O$ hydrogen bond and an $O^{bu}H{\cdots}\pi$ interaction with the aromatic ring (O^{ch} and O^{bu} are the oxygen atoms of chromophore and butan-2-ol). The binding motif is similar, as shown in figure 4: the hydrogen atom attached to the C_2 chiral center of butan-2-ol points towards the aromatic ring, so that $C_2H{\cdots}\pi$ interactions are established. Other $CH{\cdots}\pi$ interactions can be established either by facing the ethyl or the methyl group of butan-2-ol towards the aromatic ring, yet these interactions are stronger if the ethyl points towards the aromatic ring. In the non-halogenated complexes (figure 3) and in the para fluoro or chloro substituted complexes (figure 4) the ethyl group of butan-2-ol is always bent over the aromatic ring. The conformation of butan-2-ol in the clusters is the same in all the adducts and it is

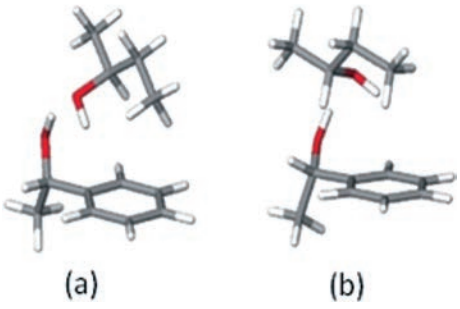

Fig. 3. D-B3LYP/6-31++G** structures of the assigned homochiral and heterochiral conformers of the complexes of of E_R with butan-2-ol. (a) homochiral (b) heterochiral.

one of the two most stable geometries that have been identified by microwave Fourier transform spectroscopy in supersonic beam expansion of isolated butan-2-ol, denoted m-ga [13]. The different chirality of the two stereoisomers of butan-2-ol involves that, in the complex, the hydrogen atom attached to the C_α chiral center of the aromatic molecule and the hydrogen atom attached to the C_2 chiral center of butan-2-ol are facing each other in the hetero complexes, (fig. 4b, as well as 4d, 3b) while they point to opposite directions in the homocomplexes (Fig. 4a as well as 4c, 3a). Consequently $C_\alpha H\cdots HC_2$ repulsive interactions in all the hetero complexes are somewhat more relevant, decreasing the overall CH···π and OH···π interactions with the aromatic ring. This is in agreement with the experimental findings that the homo complexes are more stable than the hetero complexes.

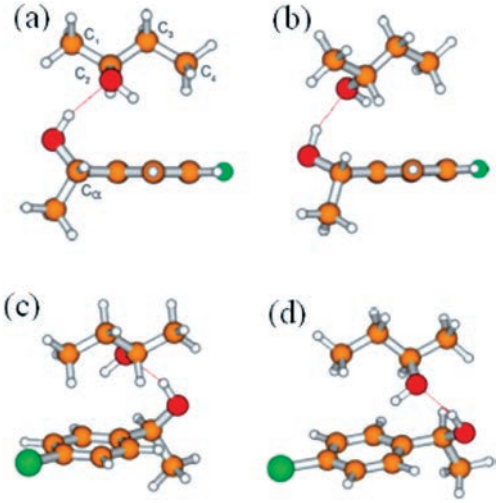

Fig. 4. D-B3LYP/6-31++G** structures of the assigned homochiral and heterochiral conformers of the complexes of p-FES and p-ClES with butan-2-ol. (a) para flluorine substituted complex, homochiral (b) para flluorine substituted complex, heterochiral (c) para chlorine substituted complex, homochiral (d) para chlorine substituted complex, heterochiral.

The comparison between the para halogenated and non-halogenated complexes reveals that the presence of the halogen atom in the para position of the aromatic ring does not affect the overall geometry of the complex, though in the para halogenated homo complexes a contraction of the vdW complex with a shortening of the OH···π distance is found. The strengthening of the attractive interactions in the homo para complexes can be tentatively attributed to the inductive and resonance effects of the halogen atom on the aromatic ring, which modify the distribution of the electron density. This probably leads to an extra stabilization of the homo para substituted complex with respect to the non-substituted homo adduct and could explain the fact that the experimental and theoretical binding energy difference

between the homo and hetero complexes with 2-butanol follows the order E_R*$B_{R/S}$<p-FE_S*$B_{R/S}$ <p-Cl_S*$B_{R/S}$.

Structure and stability of the ortho fluorine substituted complexes

Differently from the non halogenated and para substituted adduct, the R2PI spectrum of the homochiral complex (figure 5a) is blue-shifted with respect to the 0_0^0 transition of the bare chromophore, while in the case of the heterochiral complex (figure 5b) a red shift was measured. Both spectra display a vibrational progression spaced about 20 cm^{-1}. In their respective IR-R2PI spectra, one sharp absorption at 3636 cm^{-1} for the homochiral complex and at 3616 cm^{-1} for the heterochiral complex are measured. The dissociation ratios in the mass spectra are 51% for the homo and 62% for the hetero complex at almost equal values of total ionization energy, hence the hetero/homo ratio in the fragmentation efficiency is lower in the ortho-fluoro substituted complexes with respect to the para-fluoro substituted complexes, in agreement with the calculated binding energy differences.

In the complex formation, the fluorine atom in the ortho position is also available for the formation of an intermolecular C_2H···FC interaction. Considering a structural motif like the one described above for the para and non-fluorinated complexes (fig. 3, 4) the C_2H···FC interaction can be established only in the hetero ortho substituted complex, which indeed adopts a conformation similar to the other discussed hetero structures (figure 5b). In the ortho homo adduct, the establishment of C_2H···FC intermolecular interaction together with an $O^{bu}H$···π interaction is only possible if the conformation of butan-2-ol is different from the m-ga. The best over-

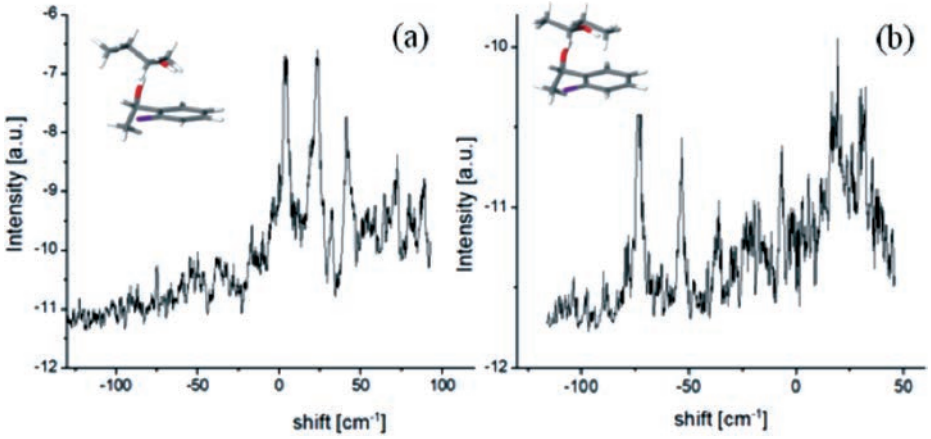

Fig. 5. R2PI excitation spectra and D-B3LYP/6-31++G** structures of (a) homochiral [o-FE_S*B_S] and (b) heterochiral [o-FE_S*B_R] clusters. The shift in the R2PI spectra is relative to the 0_0^0 electronic transition of the isolated o-FE_S molecule at 37587 cm^{-1}.

all agreement with the experimental data is in fact obtained if the spectrum of the homo adduct is assigned to the structure reported in the inset of figure 5a, where the conformation of butan-2-ol is e-ga [13], with the methyl (instead of the ethyl) group interacting with the aromatic ring. The different spectroscopic behavior of this complex acknowledges the role and the importance of CH···F interactions in molecular and chiral recognition processes. While the ortho hetero complex is structurally analogous to the hetero para and non-fluorinated structures, butan-2-ol in the ortho homo adduct adopts a different conformation in order to establish a CH···F intermolecular interaction.

Conclusions

This mini-review resumes the results of a systematic investigation aimed at clarifying, at the molecular level, the potential of the halogen substitution on the aromatic ring to alter the type and magnitude of non-covalent interactions as well as to modify the spectroscopic properties of the adducts. Our results confirm at the molecular level that chiral recognition is a process that involves the conformational adjustments of the partners in order to achieve the best efficacy of non-covalent interactions.

REFERENCES

[1] (a) J. Bella, M. Eaton, B. Brodsky and H.M. Berman, Crystal and molecular structure of a collagen-like peptide at 1.9 A resolution. Science, 1994, 266, 75; (b) H.C. Chang, J.C. Jiang, C.M. Feng, Y.C. Yang, C.C. Su, P.J. Chang and S.H. Lin, Evidence of charge-enhanced C-H-O interactions in aqueous protonated imidazole probed by high pressure infrared spectroscopy. Chem. Phys., 2003, 118, 1802; (c) S. Scheiner, T. Kar and J. Pattanayak, Comparison of Various Types of Hydrogen Bonds Involving Aromatic Amino Acids. J. Am. Chem. Soc., 2002, 124, 13257; (d) P. Milko, J. Roithová and K.A. Schug, Impact of long-range van der Waals forces on chiral recognition in a *Cinchona* alkaloid chiral selector system. Phys. Chem. Chem. Phys., 2013, 15, 6113.

[2] Hassel, O. Structural Aspects of Interatomic Charge-Transfer Bonding. Science 1970, 170, 497-502.

[3] (a) a) Rissanen, K. Halogen Bonded Supramolecular Complexes and Networks. CrystEngComm 2008, 10, 1107-1113. (b) Bouchmella, K.; Boury, B.; Dutremez, S.G.; van der Lee, A. Molecular Assemblies from Imidazolyl-Containing Haloalkenes and Haloalkynes: Competition between Hydrogen and Halogen Bonding. Chem. - Eur. J. 2007, 13, 6130. (c) Metrangolo, P.; Meyer, F.; Pilati, T.; Resnati, G.; Terraneo, G. Halogen Bonding in Supramolecular Chemistry. Angew. Chem., Int. Ed. 2008, 47, 6114-6127 and references therein.

[4] B. Brutschy, Reactions in molecular clusters following photoionization J. Phys. Chem., 1990, 94, 8637-8647.

[5] J.P. Shermann, Spectroscopy and modelling of biomolecular building blocks, Elsevier, Amsterdam, 2007.

[6] Rondino, F.; Paladini, A.; Ciavardini, A.; Casavola, A.; Catone, D.; Satta, M.; Dieter Barth, H.; Giardini, A.; Speranza, M.; Piccirillo, S. Chiral Recognition between 1-(4-Fluorophenyl)

Ethanol and 2-Butanol: Higher Binding Energy of Homochiral Complexes in the Gas Phase. Phys. Chem. Chem. Phys. 2011, 13, 818-824.

[7] Ciavardini, A.; Rondino, F.; Paladini, A.; Speranza, M.; Fornarini, S.; Satta, M.; Piccirillo, S. The Effect of Fluorine Substitution on Chiral Recognition: Interplay of CH-π, OH-π and CH-F Interactions in Gas-Phase Complexes of 1-Aryl-1-Ethanol with Butan-2-ol. Phys. Chem. Chem. Phys. 2013, 15, 19360-19370.

[8] F. Rondino, M. Satta, S. Piccirillo, A. Ciavardini, A. Giardini, M. Speranza, L. Avaldi, A. Paladini Chlorine Para-Substitution of 1 Phenylethanol: Resonant Photoionization Spectroscopy and Quantum Chemical Calculations of Hydrated and Diastereomeric Complexes J. Phys. Chem. A 2016, 120, 5023-5031.

[9] Piccirillo S., Coreno M., Giardini-Guidoni A., Pizzela G., Snels M., Teghil R. (1993). Spectroscopy of 4-fluorostyrene clusters. J Mol Struct 293, 197.

[10] Riehn C., Lahmann C., Wassermann B., Brutschy B. (1992). IR depletion spectroscopy. A method for characterizing a microsolvation environment. Chem Phys Lett 197:443-450.

[11] Reimann B., Buchhold K., Barth H.D., Brutschy B., Tarakeshwar P., Kim K.S., Anisole-(H2O)n(H2O)n (n=1-3)(n=1-3) complexes: An experimental and theoretical investigation of the modulation of optimal structures, binding energies, and vibrational spectra in both the ground and first excited states. J Chem Phys 117, 2002,1.

[12] Speranza, M.; Rondino, F.; Giardini, A.; Paladini, A.; Hortal, A.R.; Piccirillo, S.; Satta, M., Conformational landscape of supersonically expanded 1-(fluorophenyl)ethanols and their monohydrated clusters. ChemPhysChem 2009, 10, 1859-1867.

[13] King, A.K.; Howard, B.J., An investigation into the relaxation of the conformers of butan-2-ol in a supersonic expansion J. Mol. Spectrosc. 2009, 257, 205-212.

Rendiconti
Accademia Nazionale delle Scienze detta dei XL
Memorie di Scienze Fisiche e Naturali
136° (2018), Vol. XLII, Parte II, Tomo II, pp. 27-34

WALTHER CAMINATI* – LUCA EVANGELISTI*
ASSIMO MARIS* – SONIA MELANDRI*,**

Accurate Rotational Spectroscopy for Astrophysical Investigations: the Challenge of Chiral and Flexible Molecules and Molecular Complexes

Summary – In this short review we analyze some results and the challenges related to the analysis of molecular spectra of Complex Organic Molecules (COMs) in the microwave and millimeter frequency range including the detection of their chirality. These analyses are essential for the detection of new molecules of increasing complexity in the huge amount of astronomical data and rich surveys collected by the most recent and advanced radiotelescopes and *in-situ* measurements..

Key words: Molecular Spectroscopy; Rotational Spectroscopy, Complex Organic Molecules; Chirality; Astrochemistry.

The investigation of phenomena related to the chemistry of the Cosmos, in particular regarding the evolution of stars, is strongly based on the identification and quantification of molecules by spectroscopic methods, that is by their emission of light. Spectroscopic lines, in addition to telling us what molecules are present, and their abundance (concentration), are excellent tracers of the physical conditions. For example, temperature (more strictly, rotational temperature) can be measured by comparison of intensities for different rotational lines of the same molecule, gas density can be derived from the collisional excitation of these lines, and radial motion of the cloud; e.g., collapse, can be obtained from the Doppler effect [1]. Already more than 200 molecules have been detected in the gas phase of interstellar clouds

* Dip. di Chimica Giacomo Ciamician, Università di Bologna, Italy.
** E-mail: sonia.melandri@unibo.it

(see for example refs. [1] and [2]) mainly by their rotational spectra and include cations, anions, radicals, small hydrides, oxides, sulfides and halogens but also larger (up to 10 heavy atoms) neutral molecules; the latter, known as Complex Organic Molecules (COMs). Many more complex organic species are expected to be detected thanks to new telescopes: submillimeter observatories such as the Atacama Large Millimeter Array (ALMA), the Stratospheric Observatory for Infrared Astronomy (SOFIA), and the recent Herschel Space Observatory (HSO) which have been and will be providing observational data with unprecedented spectral sensitivity, signal-to-noise ratio and spatial resolution, thus laboratory work is essential to provide the community with the spectral features needed to analyze the cosmological surveys.

The analysis of high resolution spectra of COMs including chiral ones, is sometimes a formidable task because of their high degree of flexibility. The same flexibility belongs to weakly bound molecular complexes (molecules held together by non-covalent interactions) which have been studied in relation to the determination of collision rates which are of vital importance in reactions schemes [3] and are thought to play a role in the chemistry of dense and molecular clouds and in planetary atmospheres [4]. For all of these systems, the presence of several low energy conformations and the presence of large amplitude motions on shallow potential energy surfaces are typical giving rise to complex rotational spectra, which represent a challenge for spectroscopic and computational methods. Therefore a great effort is needed to provide the astronomers with reliable and accurate data for their search of molecules in space.

Usual experimental and theoretical strategies for recording and analyzing the rotational spectra of flexible organic molecules include the use of the cold and isolated conditions of a free jet expansion and heated sources for the non-volatile systems, coupled to absorption or Fourier Transform spectrometers [5, 6] which show an extremely high accuracy, resolution and sensitivity. The introduction of three wave mixing techniques by Patterson *et al.* [7] has expanded applications of microwave spectroscopy into the field of chiral analysis [8-10].

The experimental work is strongly supported and complemented by theoretical modeling and calculations with the aim of assigning the observed spectra and to obtain information on the molecular dynamics which involve, for example, conformational rearrangements [11], tautomeric equilibria [12], large amplitude motions [13], vibro-rotational coupling [14] and the prediction of vibrational spectra [15], see for example the conformational/tautomeric equilibrium of 2-mercaptopyridine [12], represented in figure 1.

Radioastronomical observations encode a huge amount of information. In order to facilitate their decryption, public, on line databases have been built. For instance several different single dish surveys are available through the Spectral Line Search Engine (SLISE at https://www.cv.nrao.edu/~aremijan/PRIMOS/). Atacama Large Millimeter/submillimeter Array data are available at ALMA archive (http://almascience.eso.org/aq/). The analysis of interferometric data is not straightforward, and the reduction of raw data to final spectra requires specific and advanced knowledges.

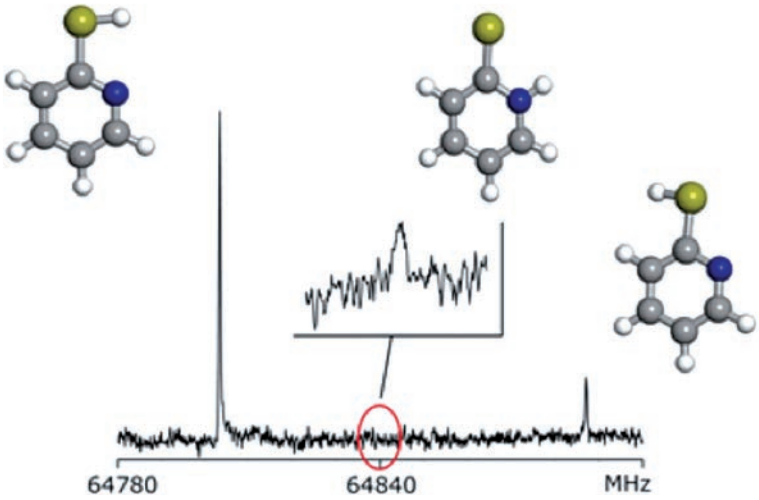

Fig. 1. The precise information on the conformational/tautomeric equilibrium of 2-mercaptopyridine given by millimeter wave free jet absorption spectroscopy.

To overcome this difficulty, a feasibility study to re-image ALMA archival data is currently underway (ALMA Re-I project). ESASky is an open science discovery portal providing full access to the entire sky as observed with Space astronomy missions, as of February 2017 (http://open.esa.int/esasky/), it includes both ESA and international partners data mission.

Once spectral surveys are obtained, the challenge lies in the assignment of the thousands of interstellar molecular lines that are present. This is made easier by the existence of spectral databases for rotational transitions, such as the Splatalogue Database for Astronomical Spectroscopy (http://www.splatalogue.net/), containing the quantal assignments, frequencies, and intensities of both measured and predicted rotational lines for many species.

As an example, we report the analysis of the spectral profile of the Class 0 protostar IRAS 16293-2422 B. The astronomical observations are part of the ALMA project 2012.1.00712.S, aimed to the search of pre-biotic molecules in low-mass protostars. These observations were carried out with 31 antennas of the 12-m main array. They covered four spectral windows: 89.49-89.72, 92.78-93.01, 102.49-102.72 and 103.18-103.41 GHz, each of which with a 0.23 GHz bandwidth and 3840 channels, resulting in a 60 kHz channel spacing corresponding to a velocity resolution of 0.2 km/s. In collaboration with the ALMA Italian Regional Center, we reduced the data according to the standard recipes in the Common Astronomical Software Applications package (v4.2.1) and we extracted the spectrum of the source within one 1”×1” synthesized beam size, centered on the 102.690 GHz peak (RA=16^{h} 32^{m} $22.^{s}612$; Dec=-24°28’32”.588). Then, exploiting the already mentioned Splatalogue data base, we could assign the molecular lines of several species. An excerpt of the

spectra is reported in Figure 2, within the assignment of methylacetylene, ethylene glycol, acetone, glycolaldheyde, ethanol, methylformate. The unassigned lines are indicated with a question mark.

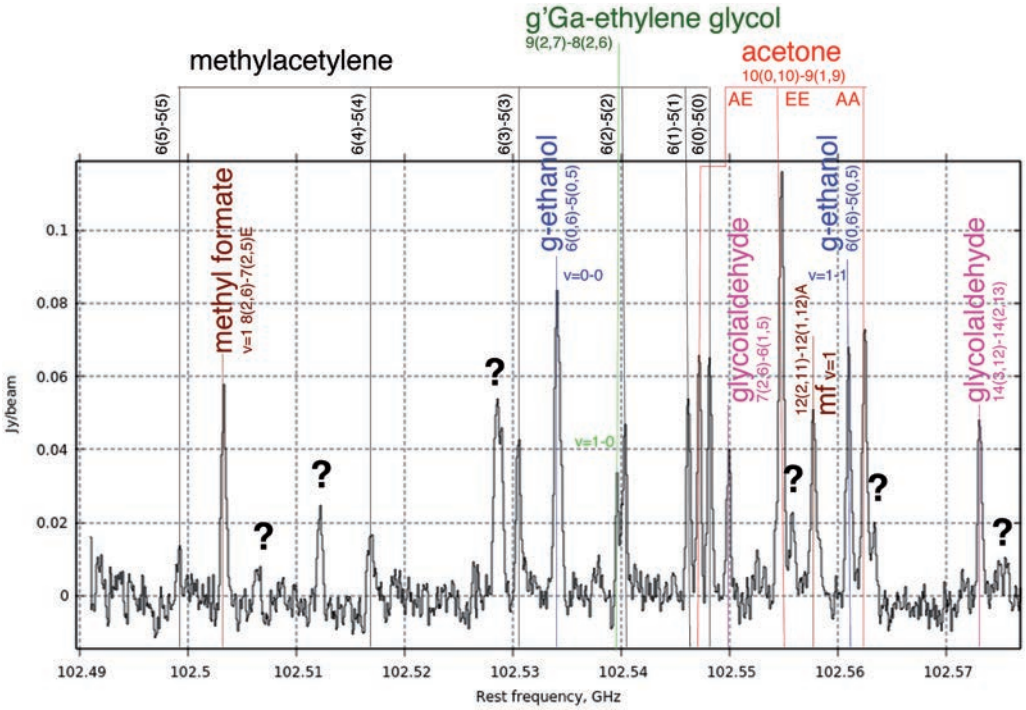

Fig. 2. Line survey and assignment of the protostar IRAS 16293-2422 B (ALMA, band 3).

As regards classical chiral molecules (not taking into account transient chirality, such as in ethyl alcohol or hydrogen peroxide), only propylene oxide has been detected in space [16] but laboratory data exist for many other chiral species such as sugars (see Figure 3) [17, 18] or aminoacids [19].

In 2013, Patterson *et al.* [7] have experimentally demonstrated how to distinguish a pair of enantiomers by microwave spectroscopy using a new three-wave mixing method. The method is based on the fact that for the enantiomers the product of the three electric dipole moments in the principal axis system has opposite sign. Using a special cycle of transitions which needs to have a-, b-, and c-type transitions it is possible to generate a coherent emission signal that is proportional to the product of the three-dipole moment components. The phase of the free induction decay signal is opposite (in the time domain) for different enantiomers. To observe the signal an additional requirement is that the electric fields of the three waves have to be mutually orthogonal. As a result, the signal amplitude is also proportional to the enantiomeric excess.

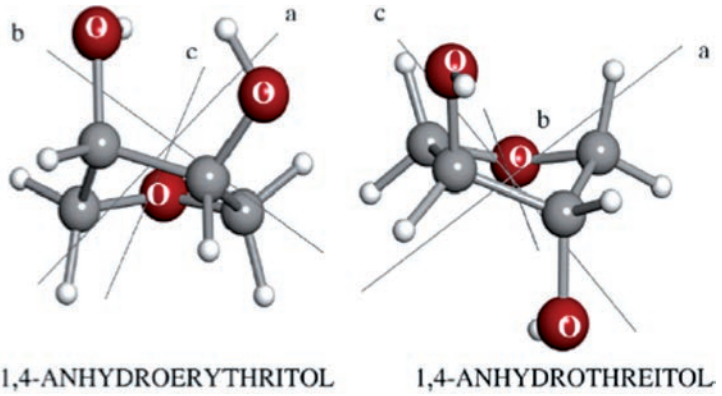

Fig. 3. Sketch of the two most stable conformers of the two isomeric anhydrosugars 1,4-anhydroerythritol and 1,4-anhydrothreitol (AT) and of their principal axes systems (from ref 17b).

Despite several challenges for which the research is still ongoing (such as phase calibration, phase-matching or off-resonant excitation) which has recently been well presented elsewhere [20] and go beyond the aims of this report, it is interesting to highlight a new project for the construction of the first millimeter-wave chirality spectrometer [21, 22]. The success of this project will advance the technologies for the chiral detection and can be applicable to space mission in areas such as Enceladus, Europa, Titan, and Mars. Organic molecules on the planets can be in-situ characterized. This could be the first step for the search of life.

In conclusion, we have discussed how the data obtained from laboratory spectroscopy in the microwave and millimeter wave range are essential for the analysis of the huge amount of data collected and the extremely rich surveys performed by telescopes and especially by the Atacama Large Millimeter Array (ALMA). One of the objectives is the detection of new molecules of increasing complexity and possibly the measurement of their chirality with *in-situ* techniques. All of this represent a challenge from the spectroscopic point of view and for this reason a strong interplay between the laboratory spectroscopists and observational astronomers is required.

Acknowledgements

This paper makes use of the following ALMA data: ADS/JAO.ALMA#2012.1.00712.S. ALMA is a partnership of ESO (representing its member states), NSF (USA) and NINS (Japan), together with NRC (Canada), MOST and ASIAA (Taiwan), and KASI (Republic of Korea), in cooperation with the Republic of Chile. The Joint ALMA Observatory is operated by ESO, AUI/NRAO and NAOJ. We acknowledge the Italian ALMA Regional Center for the availability of high performance computing resources. We wish to thank Camilla Calabrese and Nuria Marcelino for support in the data reduction process.

These investigations have been supported by the Italian MIUR (Finanziamento delle attività base di Ricerca and PRIN 2015 F59J3R 004 PE4) and the University of Bologna (Ricerca Fondamentale Orientata).

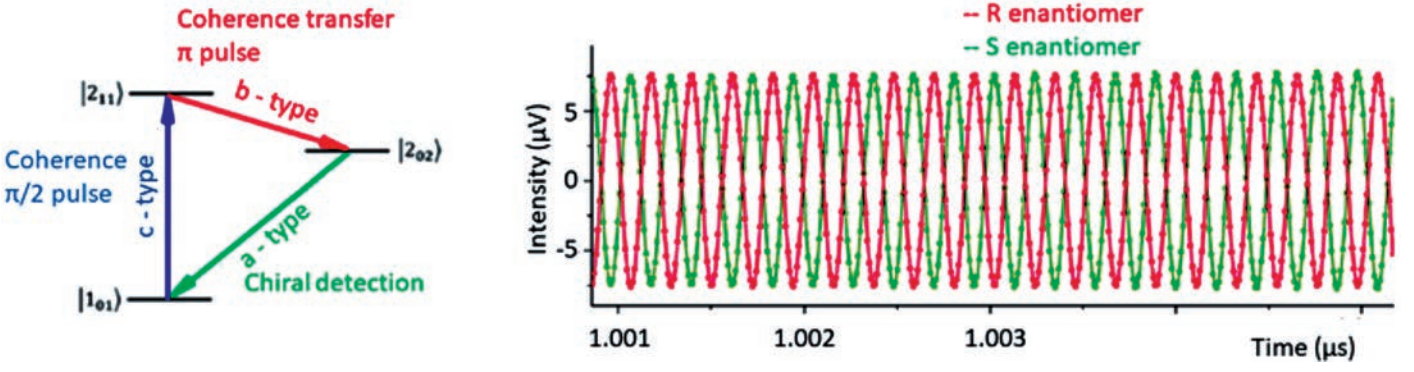

Fig. 4. On the left, the three-wave mixing scheme is shown. The two excitation pulse are applied and the chiral signal (FID) can be measured. On the right it is shown a small interval of the filtered chiral signal obtained using the three-wave mixing experiment. The two enantiomers have opposite phase.

BIBLIOGRAPHIC REFERENCES

[1] E. Herbst, Three milieux for interstellar chemistry: gas, dust, and ice, *Phys. Chem. Chem. Phys.*, **2014**, 16, 3344.
[2] A.G.G. M. Tielens, The molecular universe, Reviews of Modern Physics, **2013**, 85, 1021-1081.
[3] L.A. Surin, I.V. Tarabukin, S. Schlemmer, A.A. Breier, T.F. Giesen, M.C. McCarthy, and A. van der Avoird, Rotational Spectroscopy of the NH_3-H_2 Molecular Complex, *Astrophys. J.* **2017**, 838:27-33.
[4] A. Potepov, Weakly bound molecular complexes in the laboratory and in the interstellar medium: A lost interest?, *Mol. Astrophys.* **2017**, 6, 16-21.
[5] C. Calabrese, A. Maris, L. Evangelisti, L.B. Favero, S. Melandri and W. Caminati, Keto-Enol Tautomerism and Conformational Landscape of 1,3-Cyclohexanedione from Its Free Jet Millimeter-Wave Absorption Spectrum, *J. Phys. Chem.* A **2013**, 117, 13712-13718.
[6] W. Caminati, L. Evangelisti, G. Feng, B.M. Giuliano, Q. Gou, S. Melandri and J.-U. Grabow, On the Cl···C halogen bond: a rotational study of CF3Cl-CO, *Phys. Chem. Chem. Phys.* **2016**,18, 17851-17855.
[7] D. Patterson, M. Schnell, and J.M. Doyle, Enantiomer-specific detection of chiral molecules via microwave spectroscopy. *Nature* **2013**, 497, 475-477.
[8] S. Lobsiger, C. Perez, L. Evangelisti, K.K. Lehmann, and B.H. Pate, Molecular structure and chirality detection by Fourier Transform microwave spectroscopy. *J. Phys. Chem. Lett.* **2015**, 6, 196-200.
[9] D. Patterson and M. Doyle, Sensitive chiral analysis via microwave three-wave mixing. Phys. Rev. Lett. **2013**, 111, 023008.
[10] B.H. Pate, L. Evangelisti, W. Caminati, Y. Xu, J. Thomas, D. Patterson, C. Perez, and M. Schnell, Quantitative Chiral Analysis by Molecular Spectroscopy. In Chiral Analysis - Advances in Spectroscopy, Chromatography and Emerging Methods, 2nd Edition - (P. L. Polavarapu, ed.), Elsevier **2018**, 679-729.
[11] C. Calabrese, A. Maris, L. Evangelisti, A. Piras, V. Parravicini and S. Melandri, Rotational Spectrum and Conformational Analysis of N-Methyl-2-Aminoethanol: Insights into the Shape of Adrenergic Neurotransmitters, Frontiers in Chemistry **2018**, 6, 25.
[12] S. Melandri, L. Evangelisti, A. Maris, W. Caminati, B.M. Giuliano, V. Feyer, K.C. Prince, and M. Coreno, Rotational and Core Level Spectroscopies As Complementary Techniques in Tautomeric/Conformational Studies: The Case of 2-Mercaptopyridine, *J. Am. Chem. Soc.* **2010**, 132, 10269-1027.
[13] a) J.T. Massey, D.R. Bianco, The Microwave Spectrum of Hydrogen Peroxide, *J. Chem. Phys.* **1954**, 22, 442. b) P. Helminger, W.C. Bowman and F. De Lucia, A study of the rotational-torsional spectrum of hydrogen peroxide between 80 and 700 GHz, *J. Mol. Spectr.*, **1981**, 85, 120-130.
[14] M. Tudorie, I. Kleiner, J.T. Hougen, S. Melandri, L.W. Sutikdja, and W. Stahl, A fitting program for molecules with two inequivalent methyl tops and a plane of symmetry at equilibrium: Application to new microwave and millimeter-wave measurements of methyl acetate, *J. Mol. Spectrosc.*, **2011**, 269, 211-225.
[15] A. Maris, C. Calabrese, S. Melandri and S. Blanco, Accurate spectroscopy of polycyclic aromatic compounds: From the rotational spectrum of fluoren-9-one in the millimeter wave region to its infrared spectrum, *J. Chem. Phys.* **2015**, 142, 024317.
[16] B.A. McGuire, P. Brandon Carroll, R.A. Loomis, I.A. Finneran, P.R. Jewell, A.J. Remijan, G.A. Blake, Discovery of the Interstellar Chiral Molecule Propylene Oxide (CH_3CHCH_2O), *Science* **2016**, 352, 1449-1451.

[17] a) B.M. Giuliano, S. Blanco, S. Melandri, and W. Caminati, Laboratory Observation of the Rotational Spectrum of a C4 Sugar, 1,4-Anhydroerythritol, *Astrophysical Journal Suppl. Series* **2008**, 179, 355-359; b) B.M. Giuliano, S. Blanco 1, S. Melandri, W. Caminati, The rotational spectrum of a C4 anhydrosugar, 1,4-anhydrothreitol, *Chem. Phys. Lett.* **2008**, 467.

[18] E.J. Cocinero, A. Lesarri, P. Ècija, F.J. Basterretxea, J.-U. Grabow, J.A. Fernández, and F. Castaño, Ribose Found in the Gas Phase, *Angew. Chem. Int. Ed.* **2012**, 51, 3119-3124.

[19] S. Blanco, M.E. Sanz, J.C. Lopez and J.L. Alonso, Revealing the multiple structures of serine, *PNAS* **2007**, 104, 20183-20188.

[20] M. Holdren, B.H. Pate *et al.*, Enantiomeric Excess measurements using microwave three-wave mixing, 73rd International Symposium on Molecular Spectroscopy **2018** TC06.

[21] S. Yu, T.J. Reck, J. Pearson, M. Malaska, R. Hodyss and B.H. Pate, Millimiter-wave chirality spectrometer (CHIRALSPEC), 73rd International Symposium on Molecular Spectroscopy **2018**, RI03.

[22] https://techport.nasa.gov/view/92667.

Rendiconti
Accademia Nazionale delle Scienze detta dei XL
Memorie di Scienze Fisiche e Naturali
136° (2018), Vol. XLII, Parte II, Tomo II, pp. 35-46

D. CATONE* – N. ZEMA* – T. PROSPERI* – L. AVALDI*
S. TURCHINI*,**

PhotoElectron Circular Dichroism: a versatile probe for chirality

Abstract – The use of circularly polarised light in PhotoElectron Spectroscopy enhances the response to conformational effects in chiral systems. PhotoElectron Circular Dichroism (PECD) provides a rich and detailed dynamics with respect to tiny changes of the electronic and structural properties by means of the dispersion of the intensity of the circular dichroism as a function of photoelectron kinetic energy. This is due to the interference of the outgoing partial waves of the photoelectron in the transition matrix element. Due to this particular interference term in the dipole allowed matrix element, PECD is the chiroptical spectroscopy with the highest asymmetry ratio. State of the art Density Functional Theory (DFT) is an important tool to interpret conformational effects in PECD spectra and to achieve quantitative information.

In this *rendiconto* examples of PECD studies of chiral molecular systems will be presented. They prove that PECD is a versatile tool with high sensitivity to group substitution, isomerism, conformer population, vibrational modes.

Introduction

Chiroptical spectroscopies represent the cornerstone for the stereochemical analysis. Optical Rotatory Dispersion (ORD), Electronic Circular Dichroism (ECD), Vibrational Circular Dichroism (VCD), Raman Optical Activity (ROA) along with Density Functional Theory calculations provide the basis to determine the absolute enantiomer configuration. Chirality affects a wide variety of scientific fields such as

* Istituto Struttura della Materia-CNR (ISM-CNR), Via del Fosso del Cavaliere 100 - 00133 Roma, Italy.
** E-mail: stefano.turchini@ism.cnr.it

enantioselective reactions, chiral recognition in biological processes, homochirality in terrestrial life. The analysis of conformers represents a challenge for spectroscopy; Boltzmann averages over different geometries should be performed in order to reproduce data and the need of a set of independent data is crucial to significantly retrieve the correct weights in the analysis. At variance with, photoabsorption, photoelectron spectroscopy is characterized by two independent quantum labels namely the photon energy and the electron kinetic energy, and provides for each electronic state an electron kinetic energy distribution. The drawback is that the photon energy dependence of the photoelectron cross section of different conformers is faible. In the language of quantum scattering theory this is reflected in a dependence of the photoelectron cross section on the interference of partial waves with the same angular momentum without phase effect. To display the full sensitivity of the electron kinetic distribution to conformer geometry one should select terms with a strong interference. PhotoElectron Circular Dichroism (PECD) presents interference of the l, $l \pm 1$ outgoing partial waves of the photoelectron in the transition matrix element [1] and this is the origin of the extreme sensitivity in electronic and structural properties of chiral molecules [2].

PECD primer

Ritchie [3] pointed out that the PECD appears in the transition matrix element already in the electron dipole term, whereas circular dichroism in absorption is present at the second order perturbation level in the electric dipole/magnetic dipole and electric dipole/electric quadrupole interference terms. Consequently, the detected asymmetries are in the range 10^{-1}-10^{-2} for PECD and 10^{-3}-10^{-4} for CD in absorption. PECD is the chiroptical spectroscopy with the highest asymmetry value. Moreover the variety of spectroscopies and experimental methods based on photoemission can find a specific application to the study of chiral molecules. PECD has found application in valence band [4], core levels [5], resonant photoelectron spectroscopy [6], Auger-photoelectron coincidence spectroscopy [7], multiphoton photoelectron spectroscopy [8], ion-photoelectron coincidence [9], above threshold and tunnel ionization [10], time resolved PES [11].

The photoelectron angular distribution for a circularly polarized radiation and unoriented molecules is written:

$$I_m(\theta) = \frac{\sigma}{4\pi}\left(1 + mDP_1(\cos(\theta)) - 2\beta P_2(\cos(\theta))\right) \quad (1)$$

where P_1, and P_2 are Legendre polynomials, θ is the scattering angle, σ is the total integrated cross section, β is the classical anisotropy parameter and D is the dichroism parameter, which describes the dynamics of the photoionization, $m = \pm 1$ for left and right circularly polarized light. The parameter D is defined for each molecular state and is a function of the electron kinetic energy.

PECD is efficiently modeled by Continuum Multiple Scattering-Xα [12, 13] and B-spline–Linear Combination of Atomic Orbitals (LCAO) – Density Functional Theory (DFT) [14, 15, 16]. PECD has been exploited to study several facets which affect molecular chirality such as isomerism, group substitution, conformer population, clustering, vibrational effects, transient chirality and chiral self-assembled monolayers. Since the early days of the interpretation of PECD conformational geometries were recognized as crucial for the comparison between experiments and theory. A theoretical study on methyl-oxirane derivatives [15] reveals the sensitivity of the D parameter to the changes in the electronic structure due to group substitution also for very localized orbitals. This behavior is associated to the sensitivity of the photoelectron to the whole molecular potential; small variations in the molecular geometry change the molecular potential and could dramatically vary the sine of the phase difference in the D parameter, even for tiny phase differences around zero. Moreover the sine function allows the dichroism to change intensity and sign. At variance the β asymmetry parameter depends on the cosine of the phase difference and is not sensitive to small phase differences. In PECD the final state character plays the most important role; this immediately results from the PECD of the core levels, which are achiral orbitals with localized character. It is worth noticing that also in the case of core levels, despite the local origin of the excitation, PECD displays sensitivity to the absolute enantiomer configuration, as a true chiroptical spectroscopy. Although the first PECD spectra measured with synchrotron radiation were obtained by means of bending magnets, the development of the circular dichroism in photoemission has been associated to the employment of insertion devices fully dedicated to the delivery of photon beams with high flux and large degree of circularly polarization. These insertion devices induce elliptical trajectories of the electron beam in the storage ring, that result in the production of circularly polarized radiation on the central axis of the elliptical path. The two helicity branches are produced by the clockwise/anticlockwise direction of rotation of the elliptical motion. The measurements reported in this *rendiconto* were performed at the Circularly Polarised beamline (CiPo), built and managed by the Istituto di Struttura della Materia – CNR, of the synchrotron radiation facility ELETTRA (Trieste, Italy). The CiPo insertion device is an electromagnetic wiggler that spans the 5-900 eV energy range. PECD measurements are normally taken reversing the photon helicity at 0.05 Hz, recording the two polarity branches of the spectrum. The beamline [17, 18] is equipped with a normal incidence monochromator in the range 5-35 eV (resolving power ~10000 at 16 eV, ~ 6000 at 21 eV) and a grazing incidence spherical grating monochromator in the range 35-900 eV. The polarization ratio is 60% at 15 eV, 90% in the range 40-120 eV in quasi-undulator mode and 80% in the range 120-900 eV in wiggler regime. The electron analyser is a 150 mm electron hemispherical analyser.

Vibrational effects in PECD

The Born-Oppenheimer approximation suggests that the adiabatic coupling between electronic and nuclei allows us to express a molecular state as a product between a vibrational wavefunction depending on the nuclei coordinates and an electronic wavefunction of the electronical coordinates with nuclear coordinates as parameters.

The photoionization matrix element is written as follows:

$$M_{i,f,v,v'} = \left\langle \chi_{f,v'}(\boldsymbol{R}) \middle| \chi_{f,v}(\boldsymbol{R}) \middle\langle \psi_{f,k}^{(-)}(\boldsymbol{r},\boldsymbol{R}) \middle| \mu_{el} \middle| \psi_i(\boldsymbol{r},\boldsymbol{R}) \middle\rangle \right\rangle \tag{2}$$

where $\boldsymbol{r}$ and $\boldsymbol{R}$ are representative of the electronic and the nuclei coordinates, μ_{el} is the electric dipole, $\psi_{f,k}^{(-)}(\boldsymbol{r},\boldsymbol{R})$ and $\psi_i(\boldsymbol{r},\boldsymbol{R})$ are the final and initial electron state, respectively, with the corresponding vibrational function $\chi_{f,v}(\boldsymbol{R})$ and $\chi_{i,v'}(\boldsymbol{R})$. Franck-Condon (FC) approximation considers the electric dipole matrix element independent on the molecular geometry sampled by the vibrations and allows us to factorize the electronic and nuclear contribution.

Violations of the FC approximation are reported due to the influence of shape resonances [19] or of the Cooper minimum [20]. It is worth noting that if the FC approximation holds then PECD should be independent on vibronic effects. D parameter is apt to change as a function of molecular conformation, hence the integral over the electronic coordinates is expected to vary significantly with R, making impossible the separation of the electronic and vibrational contribution. The vibrational intensity of PECD could also display different signs, that is equivalent to a forward-backward asymmetry associated to an opposite sign of the vibronic transitions. Vibrationally resolved K shell circular dichroism in oriented CO [21] is explained in terms of a transition matrix element that employs the integration of the dipole moment over the internuclear distance. A theoretical study on a selected enantiomer of H_2O_2 [22], which is a chiral molecule that interconverts enantiomers and displays lack of optical activity, clearly points out that in the average over the vibrational matrix the vibrational phase effects play a key-role in forward-backward asymmetry; the matrix element is a complex quantity and the difference is dramatically affected by small change of the phase between the different contributions. The PECD of the HOMO of the methyl-oxirane, measured at 21 eV of photon excitation [23], clearly displays a variation of about 40% of the D parameter across the HOMO vibrational envelopes. PECD on the same molecule [24, 25] with photon energy excitation close to the HOMO ionization potential shows a sign inversion in the PECD of different vibrational terms.

It is worth noticing that the tiny changes in the electronic structure due to vibronic effects is highly reflected in the intensity and sign of PECD enlightening the role of the phase difference of the different contributions in the transition matrix element. Figures 1 and 2 report high resolution PECD spectra, together with the PES

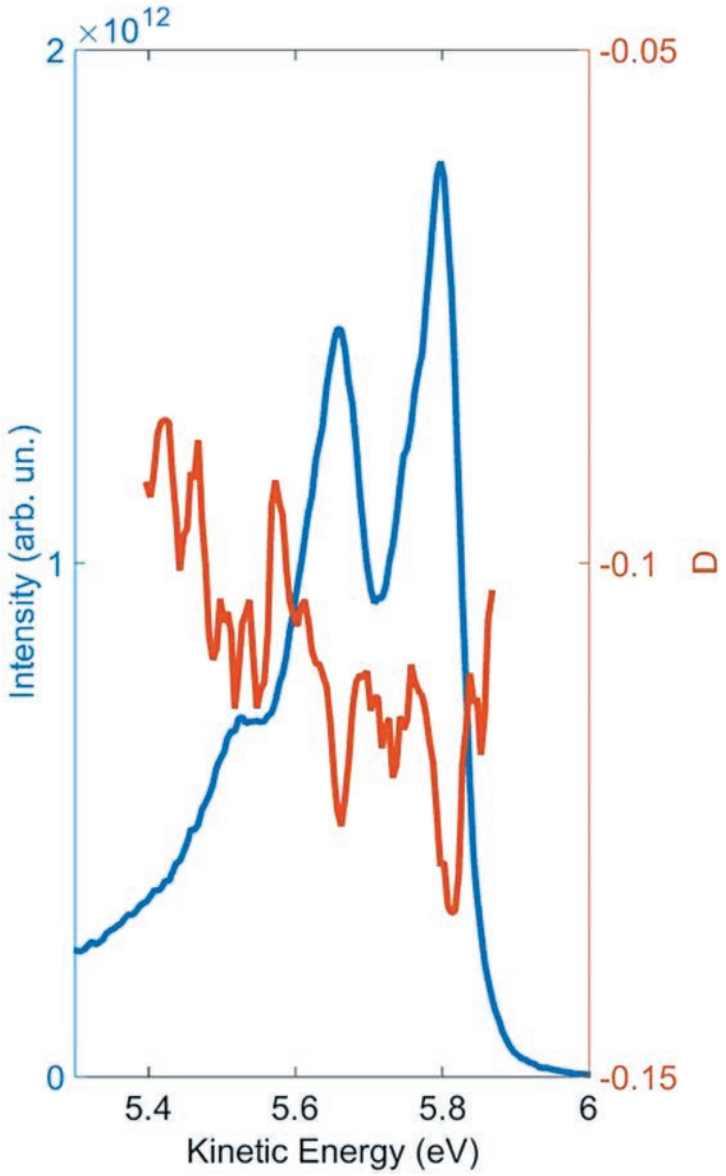

Fig. 1. HOMO PhotoElectron spectrum of S-methyl-oxirane (blue line) measured at 16.6 eV of photon energy together with D parameter (red line).

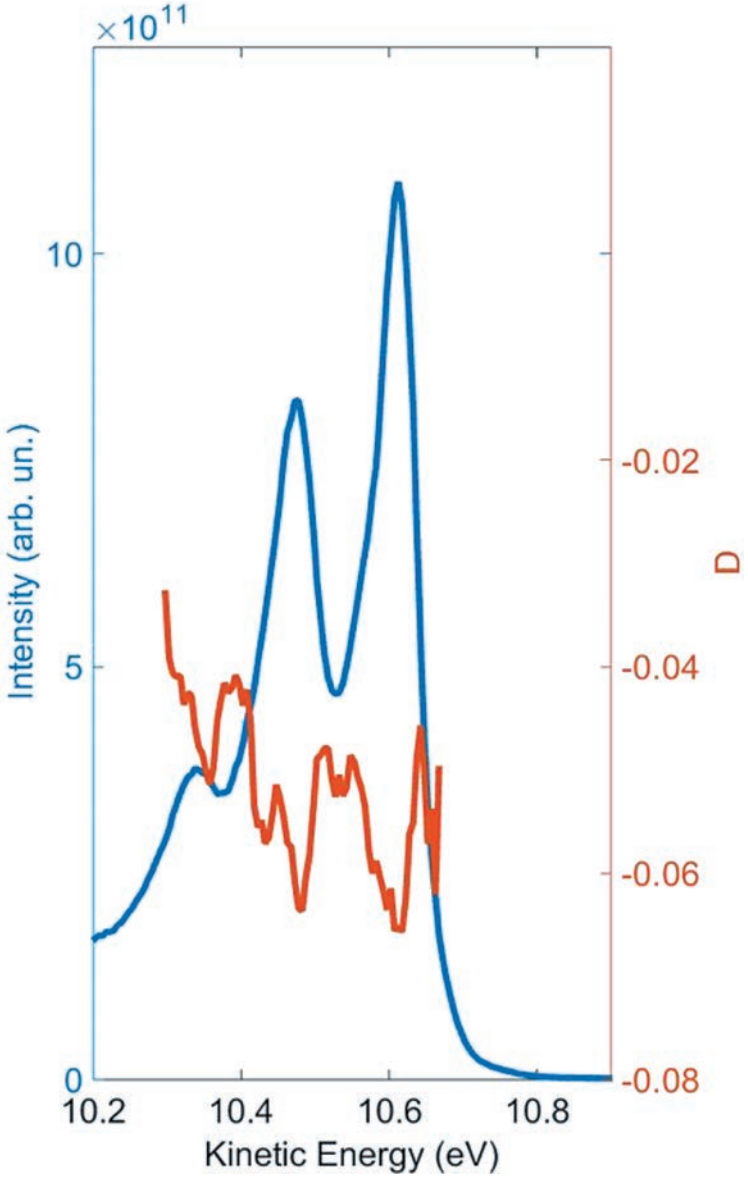

Fig. 2. HOMO PhotoElectron spectrum of S-methyl-oxirane (blue line) measured at 21.4 eV of photon energy together with D parameter (red line).

spectra, of the vibrationally resolved HOMO of methyl-oxirane measured at photon energy 16.6 and 21.4 eV, respectively. Distinct values of D parameter in the vibrational structure are observed as a function of photon energy and vibrational strucure.

Conformer Population studied by PECD

To establish on firm grounds the interpretation of PECD it is desirable to compare the experimental PECD of molecules that are structural isomers and molecules presenting different group substitutions. Alaninol and isopropanolamine are linear saturated bifunctional molecules and are structural isomers with swapped functional groups (-OH,-NH_2). For HOMO and HOMO-1 [26, 27, 28] the DFT theory displays a good agreement in the shape of the dispersion, but it is shifted in kinetic energy toward lower energies for HOMO and toward positive D values in HOMO-1. A better quantitative accord is reported for HOMO-2 and HOMO-3. In the case of the isopropanolamine the comparison with theory improves for HOMO and HOMO-1 with respect to the alaninol case, while it is poor for HOMO-2 and HOMO-3. Theory should give the same level of agreement with respect to the experiments in molecules with the same functional groups and similar skeleton structure. The answer to this issue is clearly important for the interpretation of PECD. From the comparison of the experimental D parameters of the two molecules a similar dichroism dispersion for HOMO and HOMO-1 is found. The difficulty of the theory to represent HOMO and HOMO-1 dichroic dispersion relies in the assignment of the character of the orbitals. For alaninol and isopropanolamine the LB94-DFT method [29] calculates as the main contribution to the HOMO the one of the O 2p and for the HOMO-1 the one of the N 2p, while Hartree-Fock (HF) and OVGF calculations predict a reverse situation. The good agreement of the DFT predicted dichroism with the experiments for isopropanolamine points out that the electronic assignment is O 2p for the HOMO and N 2p for the HOMO-1. On the basis of the topological similarity of the orbitals with respect to the skeleton structure, the good agreement of the experimental dichroism parameter for HOMO and HOMO-1 of the two molecules indicates that the DFT assignment for the HOMO and HOMO-1 of alaninol should be reversed. By means of the PECD dispersion, it is also possible for both molecules to individuate states in the PES spectrum belonging to the minority conformer in the energy range predicted by the OVGF calculations.

Conformational effects in 3-Methylcyclopentanone were observed by PECD varying the conformer population in vapor target at thermal equilibrium [30]. PECD experiment was performed at two different temperature T_1=300 K and T_2=370 K. Assuming a prevailing two conformer population (equatorial and axial conformers) the population at 300 K is P_{eq}=0.9 and P_{ax}=0.1, the population at 370 K is P_{eq}=0.85 and P_{ax}=0.15. Using a Boltzman average for the PECD dispersion at the two temperatures, a 2x2 linear system is formed to retrieve the experimental dichroism parameter of the two conformers. The HOMO experimental dispersions, obtained

solving the linear systems, corresponding to the P_{eq} and P_{ax} show a good agreement with the calculated ones. On the other hand the agreement between the experimental data and the Boltzmann average is good as far as the shape and sign are concerned, but it is only qualitative. These findings directly point out to the contribution of rotations not accounted for in the calculation. PECD is an oscillating signal and sum over conformer contribution in general decreases the intensity. This simple argument explains why the calculated PECD at the equilibrium geometry is usually more intense than the experimental one. However in a great number of experiments calculation at equilibrium geometry reproduces at least qualitatively the experimental data. The above result may suggest that the effect of the average on free rotations results in a superimposed slow varying signal that can shift and distort the shape of the signal of equilibrium geometry. Since PECD strongly depends upon tiny structural variations, the above results pave the road for a quantitative and structural analysis of the conformer population in equilibrium and non-equilibrium states.

Future experimental developments at Elettra

In order to continue the activity described in the previous sections as well as to address other outstanding questions connected with the understanding of the physical mechanism behind the electronic chiral response, the formation of aerosol particles in the atmosphere, the role of spatial and anisotropic properties in biological structure recognition and drug design and the mechanisms of radiation damage and protection in DNA and RNA strands, a project to develop a synchrotron radiation based chemical-physics laboratory at Elettra is under development. The core of the project is a new beamline named MOST (Molecular Science and Technology). The technical specifications of this new beamline are: a wide photon energy range (8 - 1500 eV), full polarization control (horizontal or vertical linear polarization, left or right circular polarization), high flux, (one order of magnitude or more higher than the actual beamline at Elettra), high spectral purity (around a few percents of harmonic content) and superior resolution, taking advantage of the lower emittance of planned Elettra 2.0 source and the lower slope errors of the new optical elements.

The source will consist of two variable polarization undulators, for low and high energy. This configuration has proven to give optimal flux when a wide photon energy range is required, and the most recent soft x-ray beamlines at Elettra are designed like this. The low energy insertion device will be aperiodic to reduce the harmonic content and provide greater spectral purity [31]. The full polarization control will allow an easy determination of asymmetry and dichroic parameters.

The beamline will consist of two branches (figure 3), a low energy branch and a main line where up to three end-stations can be located. The beam emerging from the undulator will be incident on the first optical element, which has the function of absorbing the heat load, deflecting the beam so that gamma rays can be blocked by suitable shielding, and it may also focus the beam. This optical element will deflect

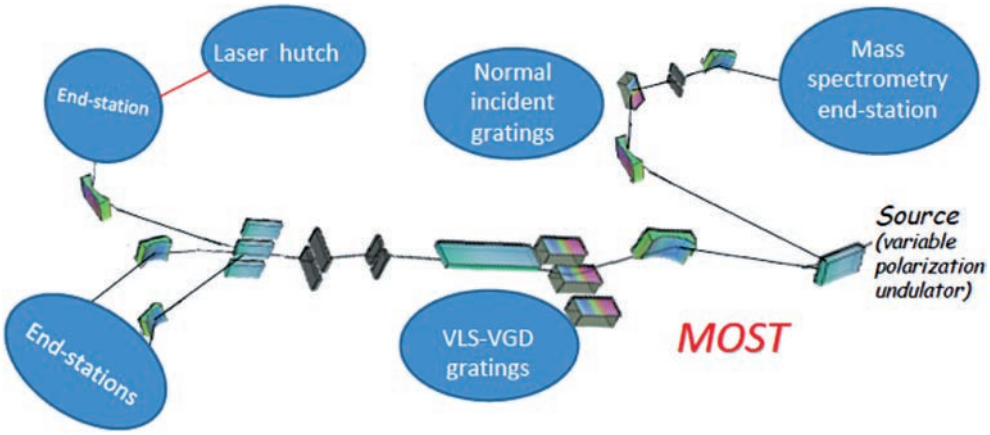

Fig. 3. Schematic layout of the MOST beamline.

the beam either to the main line equipped with a plane grating monochromator or to the low energy branch equipped with a normal incidence monochromator.

As for the main line a design without entrance slits is proposed, an approach widely used for modern beamlines, because since the introduction of top-up operation, Elettra has become a very stable machine, and Elettra 2.0 is expected to be even more stable This shortens the beamline, providing more space after the monochromator for branch lines and experimental stations. Also it may reduce the number of optical elements, increasing flux and reducing cost. The adoption of Variable Line Space (VLS) and Variable Groove Depth (VGD) plane gratings [32] in the monochromators will allow the optimisation of either spectral purity (suppression of higher orders) or flux. The beam will emerge from the exit slit horizontally, and enters a deflection chamber with mirrors to deflect the beam left or right, or allow it to pass straight through. All three branches will have refocusing optics, which provide a small spot in the experimental station. The central branch will provide the full range of energy, and the left and right branches will have lower cut-off energies, depending on the deflection angle chosen for the mirrors. A laser hutch will be constructed, to allow pump-probe experiments with optical laser plus synchrotron light.

The low energy branch line will be equipped with a normal incidence monochromator (refurbishing of the existing one at CIPO beamline which can host two gratings) and cover an energy range 8-35 eV. This branch will serve a permanent end-station devoted to mass spectrometric studies of biomolecules, proteins and ion-molecule reactions. The gratings and focusing optics will be chosen in order to achieve a high flux and optimal suppression of higher orders. The typical resolving power will be at least 10000 over all the energy range.

Conclusions

In the last decade PECD has been established as a promising chiral spectroscopy; it displays the highest chiroptical asymmetry (10^{-1} – 10^{-2}) and benefits from the steep development of circularly polarized VUV sources, such as synchrotron insertion devices and laser high harmonics generation, and from state of the art photoelectron spectroscopy experimental methods. The odd/even interference term of the angular momentum outgoing wavefunction gives rise to the sensitivity to both electronic and structural properties of chiral molecules. DFT-theory is suitable to reproduce experiments and analyzes the experimental signal in terms of conformer population. The future challenge for PECD will be to manage the extreme conformational sensitivity of PECD by means of reliable time consuming calculation approaches.

REFERENCES

[1] Powis I. 2008, Photoelectron circular dichroism in chiral molecules *Adv. Chem. Phys.* **138** 267-329.
[2] Turchini S. 2017, Conformational effects in photoelectron circular dichroism *J. Phys. Condens. Matter* **29** 503001.
[3] Ritchie B. 1976, Theory of the angular distribution of photoelectrons ejected from optically active molecules and molecular negative ions *Phys. Rev. A* **13** 1411-5.
[4] Böwering N., Lischke T., Schmidtke B., Müller N., Khalil T., Heinzmann U. 2001, Asymmetry in Photoelectron Emission from Chiral Molecules Induced by Circularly Polarized Light *Phys. Rev. Lett.* **86** 1187-90.
[5] Hergenhahn U., Rennie E.E., Kugeler O., Marburger S., Lischke T., Powis I., Garcia G. 2004, Photoelectron circular dichroism in core level ionization of randomly oriented pure enantiomers of the chiral molecule camphor *J. Chem. Phys.* **120** 4553-6.
[6] Catone D., Stener M., Decleva P., Contini G., Zema N., Prosperi T., Feyer V., Prince K.C., Turchini S. 2012, Resonant Circular Dichroism of Chiral Metal-Organic Complex *Phys. Rev. Lett.* **108** 83001.
[7] Alberti G., Turchini S., Contini G., Zema N., Prosperi T., Stranges S., Feyer V., Bolognesi P., Avaldi L. 2008, Dichroism in core-excited and core-ionized methyloxirane *Phys. Scr.* **78** 058120.
[8] Lux C., Wollenhaupt M., Bolze T., Liang Q., Köhler J., Sarpe C., Baumert T. 2012, Circular dichroism in the photoelectron angular distributions of camphor and fenchone from multiphoton ionization with femtosecond laser pulses *Angew. Chemie - Int. Ed.* **51** 5001-5.
[9] Fanood M.M.R., Ram N.B., Lehmann C.S., Powis I., Janssen M.H.M. 2015, Enantiomer-specific analysis of multi-component mixtures by correlated electron imaging-ion mass spectrometry *Nat. Commun.* **6** 7511.
[10] Beaulieu S., Ferré A., Géneaux R., Canonge R., Descamps D., Fabre B., Fedorov N., Légaré F., Petit S., Ruchon T., Blanchet V., Mairesse Y., Pons B. 2016, Universality of photoelectron circular dichroism in the photoionization of chiral molecules *New J. Phys.* **18** 102002.
[11] Comby A., Beaulieu S., Boggio-Pasqua M., Descamps D., Légaré F., Nahon L., Petit S., Pons B., Fabre B., Mairesse Y., Blanchet V. 2016, Relaxation Dynamics in Photoexcited Chiral Molecules Studied by Time-Resolved Photoelectron Circular Dichroism: Toward Chiral Femtochemistry *J. Phys. Chem. Lett.* **7** 4514-9.

[12] Powis I. 2000, Photoelectron circular dichroism of the randomly oriented chiral molecules glyceraldehyde and lactic acid *J. Chem. Phys.* **112** 301.
[13] Powis I. 2000, Photoelectron Spectroscopy and Circular Dichroism in Chiral Biomolecules: l-Alanine *J. Phys. Chem. A* **104** 878-82.
[14] Turchini S., Zema N., Contini G., Alberti G., Alagia M., Stranges S., Fronzoni G., Stener M., Decleva P., Prosperi T. 2004, Circular dichroism in photoelectron spectroscopy of free chiral molecules: Experiment and theory on methyl-oxirane *Phys. Rev. A - At. Mol. Opt. Phys.* **70** 014502.
[15] Stener M., Fronzoni G., Di Tommaso D., Decleva P. 2004, Density functional study on the circular dichroism of photoelectron angular distribution from chiral derivatives of oxirane *J. Chem. Phys.* **120** 3284-96.
[16] Giardini A., Catone D., Stranges S., Satta M., Tacconi M., Piccirillo S., Turchini S., Zema N., Contini G., Prosperi T., Decleva P., Di Tommaso D., Fronzoni G., Stener M., Filippi A., Speranza M. 2005, Angle-resolved photoelectron spectroscopy of randomly oriented 3-hydroxytetrahydrofuran enantiomers *ChemPhysChem* **6** 1164-8.
[17] Derossi A., Lama F., Piacentini M., Prosperi T., Zema N. 1995, High flux and high resolution beamline for elliptically polarized radiation in the vacuum ultraviolet and soft x-ray regions *Rev. Sci. Instrum.* **66** 1718-20.
[18] Desiderio D., Difonzo S., Dlviacco B., Jark W., Krempasky J., Krempaska R., Lama F., Luce M., Mertins H.C., Placentini M., Prosperi T., Rinaldi S., Soullie G., Schäfers F., Schmolle F., Stichauer L., Turchini S., Walker R.P., Zema N. 1999, The elettra circular polarization beamline and electromagnetic elliptical wiggler insertion device *Synchrotron Radiat. News* **12** 34-8.
[19] Dittman P.M., Dill D., Dehmer J.L. 1982, Shape-resonance-induced non-Franck-Condon effects in the valence-shell photoionization of O2 *J. Chem. Phys.* **76** 5703.
[20] Rao R.M., Poliakoff E.D., Wang K., McKoy V. 1996, Global Franck-Condon Breakdown Resulting from Cooper Minima *Phys. Rev. Lett.* **76** 2666-9.
[21] Jahnke T., Foucar L., Titze J., Wallauer R., Osipov T., Benis E.P., Alnaser A., Jagutzki O., Arnold W., Semenov S.K., Cherepkov N.A., Schmidt L.P.H., Czasch A., Staudte A., Schöffler M., Cocke C.L., Prior M.H., Schmidt-Böcking H., Dörner R. 2004, Vibrationally Resolved K -shell Photoionization of CO with Circularly Polarized Light *Phys. Rev. Lett.* **93** 083002.
[22] Powis I. 2014, Communication: The influence of vibrational parity in chiral photoionization dynamics *J. Chem. Phys.* **140** 111103.
[23] Contini G., Zema N., Turchini S., Catone D., Prosperi T., Carravetta V., Bolognesi P., Avaldi L., Feyer V. 2007, Vibrational state dependence of B and D asymmetry parameters: The case of the highest occupied molecular orbital photoelectron spectrum of methyl-oxirane *J. Chem. Phys.* **127** 124310.
[24] Garcia G.A., Nahon L., Daly S., Powis I. 2013, Vibrationally induced inversion of photoelectron forward-backward asymmetry in chiral molecule photoionization by circularly polarized light *Nat. Commun.* **4** 3132.
[25] Garcia G.A., Dossmann H., Nahon L., Daly S., Powis I. 2017, Identifying and Understanding Strong Vibronic Interaction Effects Observed in the Asymmetry of Chiral Molecule Photoelectron Angular Distributions *ChemPhysChem* **18** 500-12.
[26] Catone D., Turchini S., Contini G., Zema N., Irrera S., Prosperi T., Stener M., Di Tommaso D., Decleva P. 2007, 2-amino-1-propanol versus 1-amino-2-propanol: Valence band and C 1s core-level photoelectron spectra *J. Chem. Phys.* **127** 144312.
[27] Turchini S., Catone D., Contini G., Zema N., Irrera S., Stener M., Di Tommaso D., Decleva P., Prosperi T. 2009, Conformational effects in photoelectron circular dichroism of alaninol *ChemPhysChem* **10** 1839-46.
[28] Catone D., Turchini S., Contini G., Prosperi T., Stener M., Decleva P., Zema N. 2017, Photoelectron circular dichroism of isopropanolamine *Chem. Phys.* **482** 294-302.

[29] Van Leeuwen R., Baerends E.J. 1994, Exchange-correlation potential with correct asymptotic behavior *Phys. Rev. A* **49** 2421-31.
[30] Turchini S., Catone D., Zema N., Contini G., Prosperi T., Decleva P., Stener M., Rondino F., Piccirillo S., Prince K.C., Speranza M. 2013, Conformational sensitivity in photoelectron circular dichroism of 3-methylcyclopentanone *ChemPhysChem* **14** 1723-32.
[31] Diviacco B., Bracco R., Millo D., Walker R.P., Zalateu M., Zangrando D. 1999, Development of elliptical undulators for ELETTRA *Proceedings of the IEEE Particle Accelerator Conference* vol 4 pp. 2680-2.
[32] Polack F., Lagarde B., Idir M., Cloup A.L., Jourdain E. 2007, Variable Groove Depth Gratings and their Applications in Soft X-ray Monochromators *AIP Conference Proceedings* vol. 879 (AIP) pp 639-42.

Rendiconti
Accademia Nazionale delle Scienze detta dei XL
Memorie di Scienze Fisiche e Naturali
136° (2018), Vol. XLII, Parte II, Tomo II, pp. 47-59

ANTONIO LAGANÀ[1,2] – FERNANDO PIRANI[1] – NOELIA FAGINAS LAGO[1]
GIUSEPPE VITILLARO[2] – ERNESTO GARCIA[3]

Process driven potentials for Open Molecular Science Cloud computational services: the nitrogen case study

Abstract – The paper aims to illustrate the ongoing work to develop Open Molecular Science Cloud services for Astrochemistry enabling distributed computational molecular simulations based on the formulation of the potential energy of their reactive and non reactive state selected elementary components. To this end the paper leverages experimental and theoretical information supporting the building of reliable descriptors of the potential energy, the singling out of the channels driving the dynamical behaviour of the molecular system and the characterizing of the energy dependence of the efficiency of the occurring elementary collisions. In particular, the paper focuses on the advantage of using potential energy surfaces combining longer range (Improved Lennard-Jones) and shorter range (Bond Order) functional forms targeting the full range description of the evolution of the chemical process from asymptotes inward to strong interaction regions and from internal regions backward to the (same or different) asymptote. As a case study we examine here some nitrogen based systems and discuss the connection between the features of the used potential energy surface and some improvements proposed to their currently used formulation.

[1] Dipartimento di Chimica, Biologia e Biotecnologie, Università di Perugia, 06100 Perugia, Italy. E-mail: lagana05@gmail.com
[1] Dipartimento di Chimica, Biologia e Biotecnologie, Università di Perugia, 06100 Perugia, Italy. E-mail: Fernando.Pirani@unipg.it
[1] Dipartimento di Chimica, Biologia e Biotecnologie, Università di Perugia, 06100 Perugia, Italy. E-mail: noelia.faginaslago@unipg.it
[2] CNR ISTM - UOS Perugia, 06100 Perugia, Italy. E-mail: giuseppe@vitillaro.org
[3] Departamento de Quimica Fisica, Universidad del Pais Vasco (UPV/EHU), 01006 Vitoria, Spain. E-mail: e.garcia@ehu.es

1. *Introduction*

The assemblage of appropriate Potential Energy Surfaces (PES)s is of key importance for the accurate evaluation of the dynamics and kinetics properties of molecular systems of interest for astrochemistry [1]. The computational procedure adopted for this purpose is usually articulated into a) the production and/or collection of high resolution experimental and high level ab initio theoretical information on the electronic structure of the involved molecular system, b) the fitting of available data using a suitable formulation of the PES, c) the checking, correcting and coding the PES into a high performing routine, d) the calculation of an extended set of detailed dynamical quantities and their averaging to evaluate the desired observable.

We have already incorporated the steps of the above mentioned procedure into the so called Grid Empowered Molecular Simulator (GEMS) [2-4] implemented as an activity of the Virtual Organization (VO) COMPCHEM [5] first and of the Chemistry Molecular and Materials Science and Technologies (CMMST) Virtual Research Community (VRC) [6] later. According to the dictate of the Open Science consultation document [see ref. 7] we are driving the CMMST VRC Molecular science modelers to adopt an Investigating → Discovering → Analysing → Writing → Publishing → Outreaching → Assessing approach via the development of a dedicated Open Science cloud solution. This is aimed at creating common interfaces and standard maintenance, interoperability and sustainability procedures for data, protocols and methodologies [see http://ec.europa.eu/research/openscience/] for the purpose of offering to everybody the possibility of computing both accurate structural data for chemical compounds and ab initio efficiency parameters for chemical processes.

More specifically, in the recent past, GEMS has been used for the systematic study of the homonuclear chemical processes of Nitrogen. Within this effort, full-dimensional PESs of $N + N_2$ [starting with a LEPS published in ref. 8] were produced. In particular, their Largest-Angle Generalized ROtating Bond Order (LAGROBO) formulation [9] based on Bond Order (BO) coordinates [10] has been used to fit a double barrier Minimum Energy Path (MEP) shown by a set of available high-level ab initio data [11, 12]. Further ab initio calculations were performed later and two new full-dimensional PESs were produced [13, 14] both confirming a double barrier shape of the $N + N_2$ MEP. The investigation was also extended to $N_2 + N_2$ by focusing on the inelastic channel. Accordingly, the PES was formulated as a sum of N_2 intramolecular and intermolecular interactions formulated in terms of distances, spherical harmonics and bond-bond pairwise additive interactions [see for example refs 15-18]. Both the inelastic channel and the LAGROBO approaches were extended also to four nitrogen atom systems. Studies of the interaction components of $N_2 + N_2$ have been reported in [refs. 19-21]. In order to include in the study the switch to atom exchange and fragmentation processes further ab initio

studies were performed for a large set of molecular geometries [22-24] and fitted using also a statistically localized, permutationally invariant, local moving least squares interpolating function [25, 26]. These studies provided also a fitted PES (MN) for the N + N_2 system bearing sufficient flexibility to improve the quality of dynamical studies and to allow a valid description of higher energy processes (including dissociation) [27] even if it cannot be accredited of the necessary accuracy for the calculation of low temperature thermal rate coefficients and low energy detailed state specific collision induced cross sections due to the lack of an attractive long range tail [28]. On the contrary, both the already mentioned Double Many Body Expansion (DMBE) PES [14] and an hybrid LAGROBO and Improved Lennard-Jones [29] (ILJ) PES exhibit an attractive long range tail.

Accordingly, the paper is articulated as follows: in section 2 the evolution towards the provision of cloud services is briefly illustrated, in sections 3 the method adopted for the full range formulation of the potential energy of the two body N-N system is discussed, in section 4 the process-driven method adopted for formulating the full range three body N + N_2 LAG4ILJ PES is discussed, in section 5 the force field approach used for the N_2 dimer is discussed, in section 6 some quantum dynamical effects depending on the inclusion of an accurate long range tail in the N + N_2 potential energy surface are reported, in section 7 some Molecular Dynamics features of the N_2 dimer leveraging the ILJ formulation of the N-N long range interaction and coulombic terms are reported.

2. *The Molecular Science computational platform evolution towards the provision of cloud services*

The work aimed to develop a dedicated Open Science cloud infrastructure for the Molecular Science community started thanks to the COST [www.cost.eu/] Action D23 METACHEM [www.cost.eu/COST_Actions/cmst/D23] launched by the University of Perugia in the year 2000. METACHEM was able to connect the activities of different Molecular Science research laboratories on a shared computing platform made of a geographically distributed cluster of heterogeneous computers connected as a single virtual parallel machine [30]. Grid solutions and paradigms for molecular science research developed by D23 were further enhanced by the next COST Action D37 (Grid Computing in Chemistry: GRIDCHEM) started in the year 2006. GRIDCHEM leveraged the creation and the use of distributed computing infrastructures (the «Grid») to drive collaborative computer modelling and simulation in chemistry towards «new frontiers in complexity and a new regime of time-to-solution» [31].

As a matter of fact, about ten years ago the European projects EGEE [Enabling Grids for E-sciencE, https://cordis.europa.eu/project/rcn/87264_en.html] first and EGI [European Grid Infrastructure, https://en.wikipedia.org/wiki/European-Grid-Infrastructure] later provided European researchers with a world class level platform

for computational collaborations. In particular, during the EGEE-III project, a pilot distributed computational application was assembled to demonstrate the possibility of implementing grid techniques for performing accurate calculations of cross sections and rate coefficients of reactive and non reactive molecular processes for a very large number of molecular geometries [32] and collisional events [33]. This fostered the establishing of the already mentioned COMPCHEM VO[5] and the generalization of the distributed procedures computing the cross sections and the rate coefficients of reactive and non reactive molecular processes into GEMS[2]. This also provided the proper ground for establishing (in the year 2013) a network of (mainly European even if not only) Chemistry Departments sharing their on-line educational services (e-test, learning objects, on-line courses, etc.) leveraging an open collaborative user/producer (Prosumer) [34] model and prompted the assembling at the Dipartimento di Chimica, Biologia e Biotecnologie (DCBB) of the University of Perugia of an embryonic cloud platform of the Beowulf type, named HERLA [https://en.wikipedia.org/wiki/Beowulf_cluster]. The platform consisted in a couple of HPC clusters, (CG/training) and (FE/research), running Scientific Linux 6.x, with two distinct access nodes. The clusters were connected using NIS in a single-image system, and were used the first for students' training (CG) and the second (FE) for scientists' research. Two years later the CMS[2] Consortium of the University of Perugia, of CNR ISTM - UOS Perugia and of the two companies Master-UP srl and Molecular Horizon srl took over the management of HERLA.

More recently cloud images of HERLA (VHERLA) were created and in collaboration with the Department of Physics and Geology (DFG) and INFN Perugia were deployed on a CEPH storage (locate at DCBB) to support the activities of the School Open Science Cloud (SOSC17) held in Perugia on June 2017 and running under the INFN OpenStack platform. The next step of the process consisted in allocating a Virtual Data Center on the GARR Cloud to the end of generating a virtual cluster for Molecular Sciences, with the support of A. Barchiesi (GARR CSD) and G. Attardi (GARR Cloud).

3. *The formulation of the two body N + N potential energy*

A popular formulation of the potential energy of a chemical system for dynamical studies is the one combining locally appropriate (dominant) analytical representations of the interaction by means of appropriate (possibly physically meaningful) switching function (say $g(r)$) turning on and off the various components depending of the value of the internuclear distance r. The obvious starting point of our investigation was the formulation of the potential $V^{(2)}(r)$ of two body (nuclei) systems (here we obviously refer to the Nitrogen-Nitrogen (N-N) one due to the already specified focus of the paper). In the two body problem one can easily compose the $V^{(2)}(r)$ potential (let's call it $V^{(2\text{-}tot)}(r)$ for that purpose) as

$$V^{(2\text{-}tot)}(r) = V^{(2\text{-}spectr)}(r)g(r) + V^{(2\text{-}scatt)}(r)(1 - g(r)). \quad (1)$$

The first term of the sum $V^{(2\text{-}spectr)}(r)$ is usually formulated as a Morse potential

$$V^{(2\text{-}spectr)}(r) = V^{(morse)}(r) = D_e(n^2 - 2n) = D_e(1 - n)^2 - De \quad (2)$$

in which D_e is the dissociation energy of the diatom and $n = \exp(-\gamma\ (r\text{-}r_e))$ is the already mentioned BO variable with γ being a constant proportional to the square root of the force constant of the oscillator. A more flexible formulation of $V^{(2\text{-}spectr)}(r)$ is obtained by the generalization of the Morse functional form to higher powers of n as follows

$$V^{(2\text{-}spectr)}(r) = V^{(BO)}(r) = De \sum_{j=0}^{J} c_j n^j. \quad (3)$$

The value of the c coefficients of eq. 3 are either derived by fitting accurate high level ab initio calculations (see Table 1 for the N-N diatom) or by working out them from spectroscopic force constants [see ref. 35 for the adopted procedure].

Table 1. Coefficients of the N_2 BO potentials formulated using D_e=228.23 kcal/mol and r_e=1.098 Å. The RMSD of BO4 and BO6 from the ab initio data of ref. 36 are 1.035 kcal/mol and 0.650 kcal/mol respectively.

PES	c_1	c_2	c_3	c_4	c_5	c_6
BO_4	2.4200	-1.9573	0.6547	-0.1174		
BO_6	2.9833	-3.7743	2.9145	-1.4858	0.4077	-0.0457

As to the second term of $V^{(2\text{-}tot)}(r)$ (i.e. the $V^{(2\text{-}scatt)}(r)$) it is the already mentioned ILJ potential [29] defined below

$$V^{(2\text{-}scatt)}(r) = V^{(ILJ)}(r) = \varepsilon_o \left[\frac{m}{s(x) - m} \frac{1}{x^{s(x)}} - \frac{s(x)}{s(x) - m} \frac{1}{x^m} \right]. \quad (4)$$

In eq. 4 where $x = r/r_e$, $s(x) = \beta + 4x^2$ (with β ranging from 6 to 10 depending on the hardness of the interacting electronic distributions which is proportional to the cubic root of the polarizability α of the interacting partners). For N-N both ε_o and r_e can also be derived from the polarizability of the interacting partners. The values used for our calculations are: m = 6, ε_o = 6.43 meV, r_e = 3.583 Å and β=6.6055. The BO and the ILJ potentials allow a smooth matching between the atom-atom (scattering) long range and the diatom (spectroscopy) short range components of the formulation of the total two body interaction $V^{(2\text{-}tot)}(r)$ without resorting to a complex formulation of the $g(r)$ switching function. This is useful when dealing with insufficiently dense sets of ab initio electronic structure values.

The formulation of a proper switching function $g(r)$, however, is an important factor for an appropriate connection of the two components of $V^{(2\text{-}tot)}(r)$. The first consideration to make to this end is that $V^{(2\text{-}spectr)}(r)$ and $V^{(2\text{-}scatt)}(r)$ refer, indeed, to different arrangements of the electrons around the nuclei with a strongly bound (the first) and a weakly (or non) bound (the second) nature respectively. Accordingly, n (the BO variable) and x (the reduced ILJ radius) provide clear boundaries ($n = 1$ and $x = 1$) for the interval within which locate the switching function $g(r)$. Within that interval we can either adopt a symmetrically switching function or pilot the switching through the minimum difference between $V^{(2\text{-}spectr)}(r)$ and $V^{(2\text{-}scatt)}(r)$. We are also considering the possibility of adopting a formulation coupling two adiabatic-like components of $V^{(2\text{-}tot)}(r)$ and exploiting high level (experimental and theoretical) information on ionization and polarization energies.

4. *Process Driven Fitting Methods for three body N + N_2 interactions*

The functional representation of the three N atom (N_{L-1}, N_L and N_{L+1}) potential for the $N_{L-1} + N_{L(L+1)} \rightarrow N_{(L-1)L} + N_{(L+1)}$ reactive channel at fixed value of the angle Φ_L (the angle formed by the internuclear distances $r_{L/1,L}$ and $r_{L,L+1}$) can be formulatd in terms of the polar BO coordinates ρ_L and η_L defined (see Fig. 1) as:

$$\rho_L = \left[n^2_{(L-1)L} + n^2_{L(L+1)} \right]^{1/2} \tag{5}$$

and

$$\eta_L = \tan^{-1} \left[\frac{n_{(L-1)L}}{n_{L(L+1)}} \right] \tag{6}$$

using the so called ROtating BO (ROBO) [37] model. In this case one can set the origin of the axes at $n = 0$ (that is at $r = \infty$) for the two involved BO variables without artificial loss of flux. The angle η_L (see Fig. 1) can be taken as a continuity variable in the transformation of the reactant diatom $L(L + 1)$ of channel L into the related product one $(L - 1)L$. At the same time the variable ρ_L (see again Fig. 1) spans the different fixed arrangement angle Φ_L elongations of the system. The corresponding fixed arrangement angle Φ_L ROBO potential channel(s), can be formulated as a polynomial in ρ_L as follows:

$$V_L^{BO}(\Phi_L; \eta_L, \rho_L) = D(\Phi_L; \eta_L) P(\Phi_L; \eta_L; \rho_L) \tag{7}$$

in which $D(\Phi_L; \eta_L)$ represents the fixed collision angle Φ_L depth of the process channel evolving from reactants (at $\eta_L = 0$) to products (at $\eta_L = \pi/2$) while the polynomial $P(\Phi_L, \eta_L; \rho_L)$ represents the shape of the L channel cut while the system elongates (or contracts) out of its (fixed η_L) minimum energy geometry. In the particular case of N + N_2 discussed in ref. 19 the following simple formulation

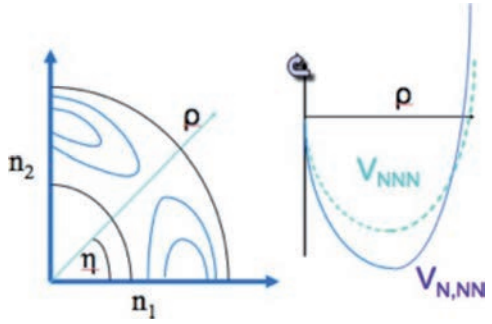

Fig. 1. LHS PLOT: Qualitative isoenergetic contours of the single barrier N+N_2 LAGROBO PES; RHS PLOT: Cuts of the reaction channel at the asymptotes (blue line) and at the saddle (green line) of the N+N_2 LAGROBO PES. For simplicity we drop here the L index for ρ and η and we name n_1 and n_2 the BO variables $n_{L-1,L}$ and $n_{L,L+1}$.

$$D(\Phi_L;\, \eta_L) = -D_e + S_{L1}(\Phi_L)\, \sin(2\eta_L) \tag{8}$$

was adopted to the end of fitting the single barrier of the LEPS thanks both to the collinearity ($\Phi_L^{TS} = 180°$) of the transition state (TS) and to the homonuclear symmetry of the system. In this case, in eq. 8, S_{L1} is equal to the value of the potential energy of the collinear saddle E^{TS}. Corrective S_{Lj} terms depending on the deviation of the actual value of Φ_L from the saddle Φ_L^{TS} one were then added when moving away from the collinear arrangement. In addition, further corrective S_{Lj} terms having the form:

$$S_{Lj} = \sum_{k=1}^{kmax} E^{TS}\, (\Phi_{Lk}^{TS} - \Phi_L)^{2(k\text{-}1)} \tag{9}$$

for the given value of Φ_L were added to the end of changing the topology of the minimum energy path (for example from single to double well). Furthermore, in order to consider all the possible process channels of the system, we combined different fixed Φ_L ROBO formulations into a single LAGROBO (Largest Angle Generalized ROBO) full 3D one and incorporated the long range tail of the potential using an ILJ potential suitably modified to deal with a pseudo-atom diatomic body of the relevant channel. This means that at a value of η_L corresponding to a sufficiently large value of R_{N-N2} (the atom-diatom internuclear distance hereafter called just R) an ILJ potential in R was formulated [29] as:

$$V(R,\, \gamma) = \varepsilon(\gamma) \left\{ \frac{m}{s(R,\, \gamma) - m} \left[\frac{R_m(\gamma)}{R} \right]^{s(R,\gamma)} - \frac{s(R,\, \gamma)}{s(R,\, \gamma) - m} \left[\frac{R_m(\gamma)}{R} \right]^{m} \right\} \tag{10}$$

where $\varepsilon(\gamma)$ and $R_m(\gamma)$ represent, respectively, the depth of the van der Waals potential well and its location in R. In eq 10, the first term describes the R-dependence of

the repulsion, while the second one represents the R-dependence of the long-range attraction with $s(R, \gamma) = \sigma + 4[R/R_m(\gamma)]^2$ and σ being a factor related to the hardness of the two interacting partners. For all values of the orientation angle γ the potential parameters are defined as $R_m(\gamma) = R_{m\perp} \cos^2 \gamma + R_{m\parallel} \sin^2 \gamma$ and $\varepsilon(\gamma) = \varepsilon_\perp \cos^2 \gamma + \varepsilon_\parallel \sin^2 \gamma$, with the $\perp$ and $\parallel$ symbols representing the perpendicular and the collinear arrangements of the system.

By including the ILJ term into the fourth PES of the LAGROBO series the so called LAG4ILJ PES having the advantage of fitting in the most appropriate way both the short and the long-range sets of *ab initio* data was generated. In particular, in the short-range region the calculations were confined, as already mentioned, around the process channel (avoiding so far to compute the (large) fraction of *ab initio* values falling in the forbidden regions) and in the long range region (out of the van der Waals well) concentrate the efforts in best fitting the relevant model parameters.

5. *The Force field of the N_2 dimer*

To realistically describe the total interaction potential energy of the N_2 dimer we had to add the electrostatic (V_{elec}) component to the non-electrostatic (V_{nelec}) one. As discussed earlier the non electrostatic part is properly represented by the already mentioned ILJ potential [29] whereas the electrostatic part is calculated as a simple Coulombic potential

$$V_{tot}(R) = V_{nelec}(R) + V_{elec}(R) = V_{ILJ}(R) + V_{Coul}(R). \quad (11)$$

We can either place the molecular interaction centre on the centre of mass of N_2 to reduce the molecule to a pseudo-atom bearing the total molecular polarizability (CM-CM model) or take into separate account the effects of atomic polarizabilities by means of atom-atom 4 ILJ terms as follows:

$$V_{nelec}(R_{AB}) = \sum_{i,j=1}^{2} V_{ILJ}(R_{ij}) = V_{ILJ}(R_{11}) + V_{ILJ}(R_{21}) + V_{ILJ}(R_{12}) + V_{ILJ}(R_{22}) \quad (12)$$

where i and j indicate the nitrogen atoms of the N_2 molecules A and B within the dimer. This type of potential will be referred to as atom-atom potential.

For the simulation of small gaseous molecules, often partial charges are introduced in the system to calculate the electrostatic interaction. Although such partial charges do not have an actual physical meaning, they are usually chosen so as to best fit a molecular property (often the lowest non-zero multipole is chosen for that purpose). The parameters of the ILJ potential were optimized using different charge schemes. For the N_2 gas, usually either a three site or a four site charge system is adopted [38]. The three-charge system has negative charges on the N atoms and a

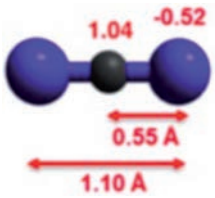

Fig. 2. The charges' scheme adopted to reproduce the electrostatic term of the interaction.

balancing charge on the centre of mass twice the amount needed to get an overall neutral molecule. The negative charges are placed at a distance of 1.10Å from each other, while the positive charge is displaced at a distance of 0.55Å (see Fig. 2). An electrostatic energy contribution is then calculated as the Coulombic sum

$$V_{Coul}(R) = \sum_{i,j} \frac{qiqj}{R_{ij}} \tag{13}$$

where i and j are the relevant point charges located in the N_2 dimer and follow the notation of eq. 12.

6. *The N + N_2 quantum dynamics*

Quantum state to state inelastic probabilities were calculated using the program ABC [39] based on the time-independent hyperspherical coordinate integration of the atom diatom Schrödinger equation for all the reactant states lower than the total energy E_{tot} and a fixed value of the total angular momentum quantum number J. To this end, ABC expands the system wavefunction into a basis set of fixed hyperradius ρ (not to be confused with the above defined BO coordinate ρ) hyperangular functions. The integration is performed by segmenting the ρ interval into several sectors and propagating through them the scattering **S** matrix (from 0 to an asymptotic ρ_{max} value (16 Å)) where the probability **P** matrix is evaluated. Extended convergency checks were performed at total angular momentum $J=0$ for the overall elastic and inelastic collisions. The analysis of the quantum values of the $J=0$ probability associated with inelastic transitions from a given initial rovibrational v, j state to a given final v' vibrational (summed over all rotational) states (v,j|v',all) computed on the DMBE, MN and LAG4ILJ PESs shown in Fig. 3 allows us to accurately quantify the efficiency of the vib-rotational-to-vibrotational energy transfer without resorting to approximations. An important conclusion of such analysis in the energy range of up to 1 eV is the clear predominance of vibrationally elastic events over vibrational excitation and deexcitation. The importance of including the long range tail (as is for the LAG4ILJ PESs) is shown, however, by the enhancement of the efficiency of the vibrational excitation computed on LAG4ILJ of at least one order of magnitude over the DMBE PES and two orders of magnitude over the MN PES and in the corresponding lowering of the energy threshold.

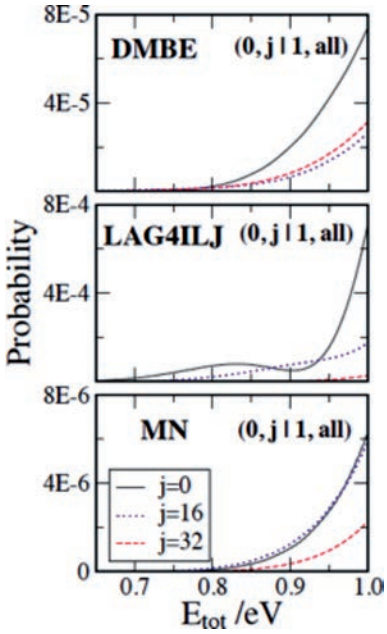

Fig. 3. (v,j|v',all) inelastic transition probabilities computed on the DMBE (upper panel), LAG4ILJ (central panel) and MN (lower panel) PESs plotted as a function of total energy at $J = 0$ and $j = 0, 16, 32$.

A more systematic analysis of the structure of the computed probabilities is given by the comparison of the probability for transitions from a given initial rotational state j to a final

Table 2. Interaction parameters for the N_2 dimer using an atom-atom model.

Charge scheme	ε (kcal/mol)	r_0 (Å	β	q^-(e)
no charges				
no charges	0.074	3.893	8.033 /	
Three Charge model				
This work	0.081	3.770	9.000	-0.52

j´ one (only jumps of two units are allowed by the symmetry of the system) as a function of j. These probabilities clearly indicate that there is a tendency of the system to rotationally excite N_2 and trigger a self-sustained rotational excitation of N_2.

7. *Molecular Dynamics of the N_2 dimer*

Molecular Dynamics (MD) simulations of the N_2 dimer have been performed in the canonical (NVT) ensemble using the DL_POLY program [40]. The size of the simulation box was of 36.11 x 62.52 x 140.00 Å3. A Nose-Hoover thermostat with a relaxation constant of 0.5 ps has been employed to keep the temperature T of the system fixed at 300 K. The cutoff distance for the nonelectrostatic and electrostatic components has been set to 15 Å, and the Ewald method has been applied for the calculation of electrostatic contributions. During the simulations the membrane structure was kept frozen and the gas molecules treated as rigid. Each simulation has been performed for 5 ns after a properly long equilibration period with a fixed time step of 1 fs by collecting data every 2 ps. After each production run, the trajectories were recorded and the results analyzed. The simulation temperatures fluctuated between 20 and 3 percent (relative standard deviations vary from 7% to 1%) in going from lower to higher pressure. We consider here first the case of a single interaction centre located on the centre of mass of the N_2 molecule. The interaction parameters are given in Table 2 with relevant partial charges. It is clear from the Table that an explicit inclusion of the electrostatic term by means of the Coulombic sum only affects the ILJ parameters when large charges are used.

Table 3. Interaction energies (D_e) and equilibrium distance (r_{i0}) of the N_2 dimer calculated by the molecular dynamics simulation compare with the literature.

Charge scheme	D_e(kcal/mol)	r_0 (Å)
no charges		
no charges	0.293	3.78
Three Charge model		
Optimized [43]	0.222	3.94
CCSD T [44]	0.205	3.57
This work	0.2635	3.69

In this case, the introduction of the electrostatic term changes the parameters less than in the CM-CM model. For the three-charge model, ε and r_0 increase slightly with the increase of charges (while β decreases). The optimized charges are again slightly higher than the ones reported in the literature. The computed ε and r_0 values for the ILJ potential are similar to those of the relevant Lennard-Jones one (notice the different symbols). Ravikovich *et al.* have reported values of 0.202 kcal/mol for ε and 4.058Å for r_0 of the LJ CM-CM model with no charges [41]. Those ε and r_0 are higher than ours. The agreement is, though, reasonable when taking into account that they were obtained using a completely different method. We can compare the ε and r_0 parameters of the atom-atom model directly to the TraPPE and MOM LJ

ones for the three-charge model [42]. The ε and r_0 for both the MOM and the TraPPE potential (0.072 kcal/mol and 3.730Å respectively) compare reasonably well with our values. Furthermore, we can compare to ILJ parameters using the three-charge model [see ref. 43]. They obtained optimized values of 0.079 kcal/mol, 3.897Å and 7.720 for ε, r_0 and β respectively when using a charge of -0.5664 on the N atom.

In order to examine the performances of the different approaches, the interaction energies of some highly symmetrical configurations of the N_2-dimer were calculated with the different interaction potentials fitted. The values are presented in Table 3. Three representative configurations (T-shape, parallel and linear) were taken into account and were compared with the interaction energies computed at the CCSD(T)/CBS [44] level, which is a well-recognized standard for evaluating the accuracy of other computational methods. From Table 3 it can be seen that the interaction energies of N_2-dimers calculated with the different fittings are in general in good agreement with the CCSD(T) results for the considered noncovalent interaction.

REFERENCES

[1] Talbi D. (2011). Theoretical approaches for studying Astrochemistry, EPJ Web of Conferences, 18: 02002.
[2] Laganà A., Costantini A., Gervasi O., Faginas Lago N., Manuali C., Rampino S. (2010). J. Grid Comput., 8: 571-586.
[3] Manuali C., Laganà A., Rampino S. (2010). Computer Physics Communications, 181: 1179-1185.
[4] Rampino S., Faginas Lago N., Laganà A., Huarte-Larrañaga F. (2012). Journal of Computational Chemistry 33: 708-714.
[5] Costantini A., Gervasi O., Faginas Lago N., Manuali C., Rampino S. (2010). Journal of Grid Computing, 8(4): 571-586.
[6] Laganà A. (2012). http://www.hpc.unipg.it/ojs/index.php/virtlcomm/article/view/40.
[7] http://ec.europa.eu/research/consultations/science-2.0/science_2_0_final_report.pdf.
[8] A. Laganà A., Garcia E., Ciccarelli L. (1987). J. Phys. Chem., 91: 312–314.
[9] Garcia E., Laganà A. (1995). J. Chem. Phys. 103: 5410-5416.
[10] Johnston H.S., Parr C. (1963). J. Am. Chem. Soc., 85: 2544.
[11] Garcia E., Laganà A. (1997). J. Phys. Chem., 101: 4734-4740.
[12] Garcia E., Saracibar A., Gómez-Carrasco S., Laganà A. (2008). Phys. Chem. Chem. Phys., 10: 2552-2558.
[13] Wang D., Stallcop J.R., Huo W.M., Dateo C.E., Schwenke D.W., Partridge H. (2003). J. Chem. Phys., 118: 2186-2189.
[14] Galvão B.R.L., Varandas A.J.C. (2009). J. Phys. Chem., 113: 14424-14430.
[15] van der Avoird A., Wormer P.E.S., Jansen A.P.J. (1986). J. Chem. Phys. 84: 1629-1635.
[16] Gomez L., Bussery-Honvault B., Cauchy T., Bartolomei M., Cappelletti D., Pirani F. (2007). Chem. Phys. Lett., 445: 99-107.
[17] Hellmann R. (2013). Mol. Phys., 111: 387-401.
[18] Cappelletti D., Pirani F., Bussery-Honvault B., Gomez L., Bartolomei M. (2008). Phys. Chem. Chem. Phys., 10: 4281-4293.

[19] Verdicchio M. (2009). Atmospheric reentry calculations and extension of the formats of quantum chemistry data to quantum dynamics, Master Thesis University of Perugia.
[20] Kurnosov A., Cacciatore M., Laganà A., Pirani F., Bartolomei M., Garcia E. (2014). J. Comput. Chem., 35: 722.
[21] Garcia E., Martínez T., Laganà A. (2015). Chem. Phys. Lett., 620: 103.
[22] Pacifici L., Verdicchio M., Faginas Lago N., Lombardi A., Costantini A. (2013). J. Comput. Chem., 34: 2668-2676.
[23] Paukku Y., Yang K.R., Varga Z., Truhlar D.G. (2013). J. Chem. Phys., 139: 044309.
[24] Paukku Y., Yang K.R., Varga Z., Truhlar D.G. (2014). J. Chem. Phys., 140: 019903.
[25] Bender J.D., Doraiswamy S., Truhlar D.G., Candler G.V. (2014). J. Chem. Phys., 140: 054302.
[26] Bender J.D., Valentini P., Nompelis I., Paukku Y., Varga Z., Truhlar D.G., Schwartzentruber T., Candler G.V. (2015). J. Chem. Phys., 143: 054304.
[27] Esposito F., Garcia E., Laganà A. (2017). Plasma Sources Science and Technology 26(4): 045005.
[28] Garcia E., Aoiz F.J., Rampino S., Laganà A. (2018) Quantum state-to-state inelastic probabilities in N + N2 collisions: the role of the respulsive wall and the long-range interaction, Frontiers in Chemistry, section Physical Chemistry and Chemical Physics (abstract accepted for publication).
[29] Pirani F., Brizi S., Roncaratti L., Casavecchia P., Cappelletti D., Vecchiocattivi F. (2008). Phys. Chem. Chem. Phys., 10: 5489.
[30] Foster I., Kesselman C. Eds., The Grid: Blueprint for a New Computing Infrastructure, Morgan Kaufmann Publ., San Francisco (1999).
[31] https://www.cost.eu/actions/D37/#tabs|Name:overview
[32] Storchi L., Tarantelli F., Laganà A. (2006). Lecture Notes in Computer Science 3980: 675-683.
[33] Gervasi O., Laganà A. (2004). Future Generation Computer Systems, 20(5): 703-716.
[34] Laganà A., Gervasi O., Tasso S., Perri D., Franciosa F. (2018). Lecture Notes in Computer Science 10964: 533-548.
[35] Garcia E., Laganà A. (1985). Mol. Phys. 56: 621-627.
[36] Varandas A.J.C. (1980). J. Chem: Soc. Faraday II, 76: 129.
[37] Laganà A. (1991). J. Chem. Phys. 95: 2216.
[38] Makrodimitris K., Papadopoulos G.K., Schober H., Theodorou D.N. (2001). J. Phys. Chem. B, 105: 777–788.
[39] Skouteris D., Castillo J.F., Manolopulos D.E. (2000). Comp. Phys. Comm. 133: 128-135.
[40] Smith W., Yong C.W., Rodger P.M. (2002). Molecular Simulation, 28(5): 385-471.
[41] Ravikovitch P.I., Vishnyakov A., Neimark A.V. (2001). Phys. Rev. E, 64(1).
[42] Murthy C.S., Singer K., Klein M.L., Mcdonald I. R. (1980). Mol. Phys. 41(6): 1387-1399.
[43] Vekeman J., Faginas-Lago N., Cuesta I.G., Sánchez-Marín J., De Merás A.S. (2018). Lecture Notes in Computer Science, 10964.
[44] Tian L., Feiwu C. (2013). J. Mol. Model. (19)12, 5387-5395.

Rendiconti
Accademia Nazionale delle Scienze detta dei XL
Memorie di Scienze Fisiche e Naturali
136° (2018), Vol. XLII, Parte II, Tomo II, pp. 61-72

STEFANO FALCINELLI*

The double photoionization of propylene oxide

Abstract – A photoelectron-photoion-photoion coincidence technique, using an ion imaging detector and tunable synchrotron radiation in the 18.0 – 37.0 eV photon energy range, inducing the ejection of molecular valence electrons, has been applied to study the double ionization of the propylene oxide, a simple prototype chiral molecule. Energy thresholds for the formation of different ionic products, the related branching ratios, and the kinetic energy distribution of fragment ions are measured at different photon energies. The main recorded two body fragmentation channels yield $C_2H_4^+ + CH_2O^+$, and $C_2H_3^+ + CH_3^+$ product ions (66.70% and 18.70%, respectively). These new experimental data are relevant per se and are mandatory information for further experimental and theoretical investigations of oriented chiral molecules.

Keywords: double photoionization, molecular dications, synchrotron radiation, chiral molecule, propylene oxide, astrochemistry.

1. *Introduction*

The present paper represents an effort to unravel the physical chemistry of the elementary processes induced by the interaction of ionizing vacuum ultraviolet VUV photons with a simple chiral molecules, the propylene oxide, being the first chiral molecule detected by astronomers using highly sensitive radio telescopes in interstellar space [1]. It is well known that the left-right dissymmetry, both at macroscopic and micro-scopic scales, plays a fundamental role in life science. Investigation of molecular enantiomeric nature has therefore a strong impact in chemistry in various subareas such as, heterogeneous enantioselective catalysis, photochemical asymmetric synthe-sis, drug activity, enzymatic catalysis, and chiral surface science involving supramolecular assemblies [2, 3]. The interaction of polarized light with

* Department of Civil and Environmental Engineering, University of Perugia, Via G. Duranti 93 - 06125 Perugia, Italy. E-mail: stefano.falcinelli@unipg.it

chiral systems has been extensively studied since Pasteur's pioneering experiments on optical activity leading to the enantiomer recognition [4]. Although techniques involving optical rotation and circular dichroism in photoabsorption with visible/UV light are routinely used as well established analytical methods, studies of chiral systems using ionizing photons are instead very limited to date (see Ref. [5] and references therein). Progresses in synchrotron radiation techniques allowed intense photon sources with high degree of both linearly and circularly polarized light of both helicities to be used in experiments like that one concerning the present paper. In particular, we intended to study the fragmentation dynamics following the double photoionization of propylene oxide whose importance from an astrochemical point of view has been already mentioned above. In fact, this chiral molecule has been detected in the gas phase in a cold extended molecular shell around the embedded, massive protostellar clusters in the Sagittarius B2 star-forming region, being a material representative of the earliest stage of solar system evolution in which a chiral molecule has been found [1]. To characterize the ionizing VUV interaction with such a molecule, we started by the use of a linearly polarized synchrotron radiation, as that one available at the «Circular Polarization (CiPo)» Beamline at the Elettra Synchrotron Facility of Trieste (Italy), to perform a double photoionization experiment using the same ARPES (Angle Resolved Photo-Emission Spectroscopy) apparatus successfully employed in previous studies, performed by our research team [6-10]. In such an experiment, the double photoionization of propylene oxide molecules in a racemic mixture, has been performed in order to measure: i) the threshold energy for the different ionic products formation; ii) the related branching ratios, and iii) the kinetic energy released (KER) distribution of fragment ions at different photon energies. This preliminary study is important to provide unavailable data on dication energetics and nuclear dissociation dynamics, this being mandatory information for further experimental and theoretical investigations of the interaction between chiral molecules and circularly polarized radiation. For such a reason, we are planning to switch in next future to use the circularly polarized light, as available at «CiPo» Beamline, using the two enantiomers of propylene oxide with the aim to investigate possible differences on the angular and energy distribution of fragment ions and ejected photoelectrons at different photon energies. (Figures 1-5 are adapted from Ref. 11).

2. *Materials and Methods*

The data reported and discussed in this paper were recorded in experiments performed at the ELETTRA Synchrotron Facility of Basovizza, Trieste (Italy). The ARPES end station was employed at the «Circular Polarization (CiPo)» beamline.

For the present experiment we used a 3D-ion-imaging TOF spectrometer that we have successfully applied recently to N_2O [12, 13], CO_2 [14, 15], C_6H_6 [16, 17], and C_2H_2 [18, 19] double photoionization experiments. In particular, this device consists in a time of flight (TOF) spectrometer equipped with an ion position sensitive

detector (stack of three micro-channel-plates with a multi-anode array arranged in 32 rows and 32 columns). It has been especially designed in order to properly measure the spatial momentum components of the dissociation ionic products [20]. The data were accumulated using the same method previously employed, and the analysis has been carried out by using the codes and computational procedure already well tested [12-19]. The energy selected synchrotron light beam operating in the 18-37 eV photon energy range crosses at right angle an effusive molecular beam of the neutral precursor molecule, and the ion products are detected in coinci-dence with photoelectrons coming out from the same double photoionization event under study.

The propylene oxide molecular beams was prepared by effusion from a glass bottle containing a commercial sample (with a 99% nominal purity), and was supplied by a needle effusive beam source taking advantage of its high vapor pressure at a room temperature. A Normal Incidence Monochromator (NIM), equipped with two different holographic gratings, allowing to cover the 18-37 eV energy range by means of a Gold (2400 l/mm) and an Aluminum (1200 l/mm) coated grating has been used. Spurious effects, due to ionization by photons from higher orders of diffraction, are reduced by the use of the NIM geometry.

The resolution in the investigated photon energy range was about 1.5-2.0 meV. More details about the used experimental techniques have been detailed elsewhere [21-27].

3. *Results and Discussion*

In a recent double photoionization experiment of propylene oxide in a photon energy range of 18-37 eV [5] we found the following six two-body fragmentation channels accessible in the Coulomb explosion of the $(C_3H_6O^{2+})^*$ intermediate molecular dication with the measured relative abundances:

$$C_3H_6O + h\nu \rightarrow (C_3H_6O^{2+})^* + 2e^- \rightarrow C_2H_4^+ + CH_2O^+ \quad 66.70\% \quad (1)$$

$$\rightarrow CH_2^+ + C_2H_4O^+ \quad 7.84\% \quad (2)$$

$$\rightarrow CH_3^+ + C_2H_3O^+ \quad 5.00\% \quad (3)$$

$$\rightarrow O^+ + C_3H_6^+ \quad 1.59\% \quad (4)$$

$$\rightarrow C_2H_3^+ + CH_6O^+ \quad 18.70\% \quad (5)$$

$$\rightarrow OH^+ + C_3H_5^+ \quad 0.17\% \quad (6)$$

The measured threshold energy for the double ionization of propylene oxide was 28.3±0.1 eV [6]. In this paper we present the KER distributions of product ions obtained as a function of the investigated photon energy for each reaction (1)-(6) above. Such KER distributions are reported in Figures 1-5. It was not possible to determine KER distributions related to product ions of reaction (6) because the

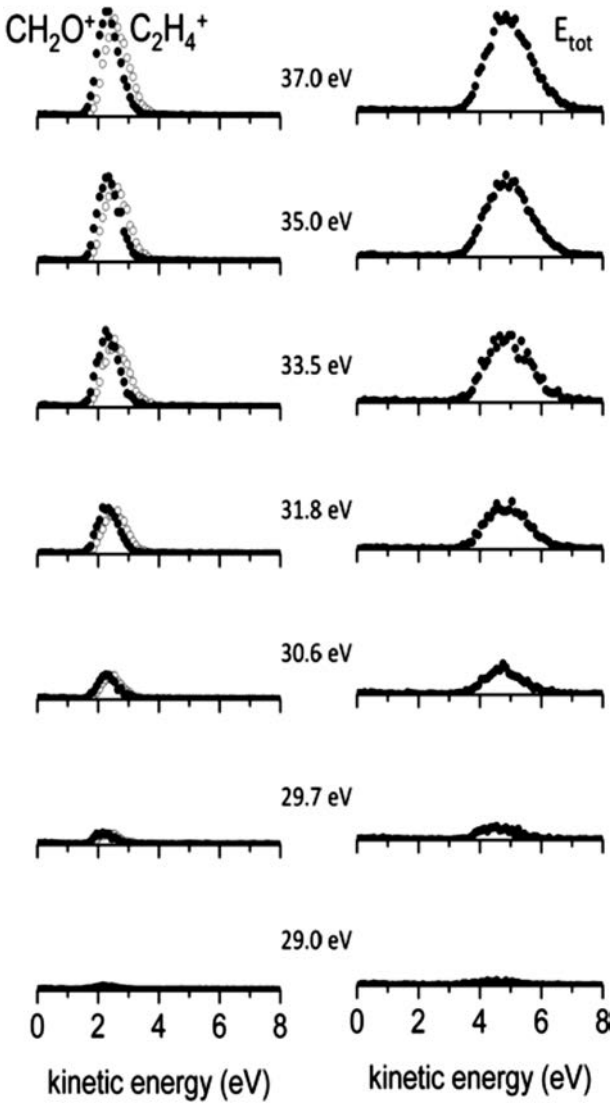

Fig. 1. The kinetic energy released (KER) distribution of the $C_2H_4^+ + CH_2O^+$ products for various investigated photon energies: in the left panel are reported the KER for each fragment ion, whereas in right panel the total KER distributions are shown.

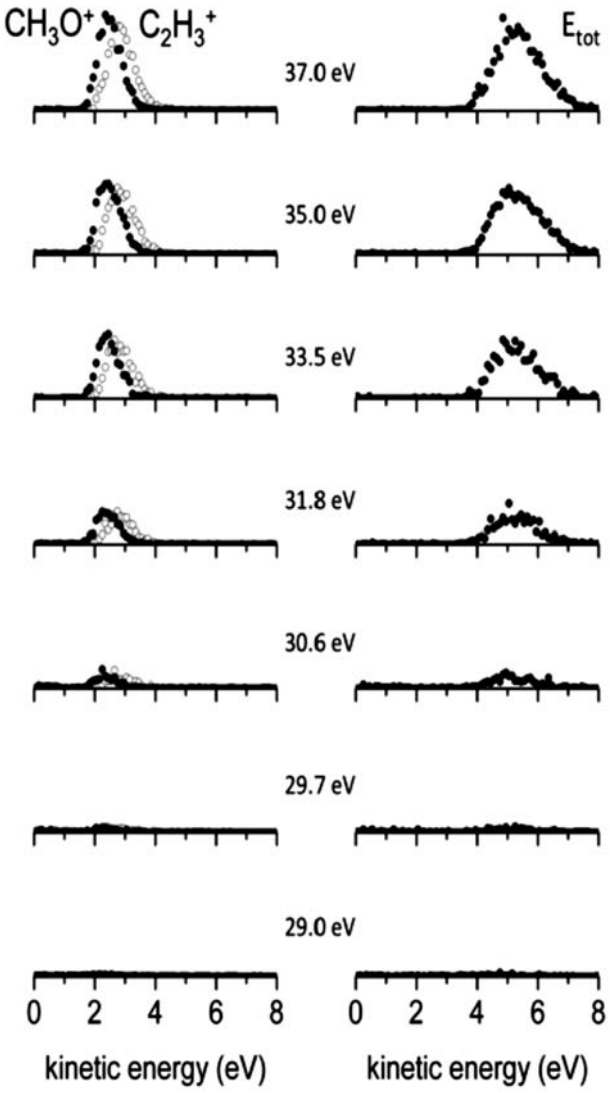

Fig. 2. The kinetic energy released (KER) distribution of the $C_2H_3^+ + CH_3O^+$ products for various investigated photon energies: in the left panel are reported the KER for each fragment ion, whereas in right panel the total KER distributions are shown.

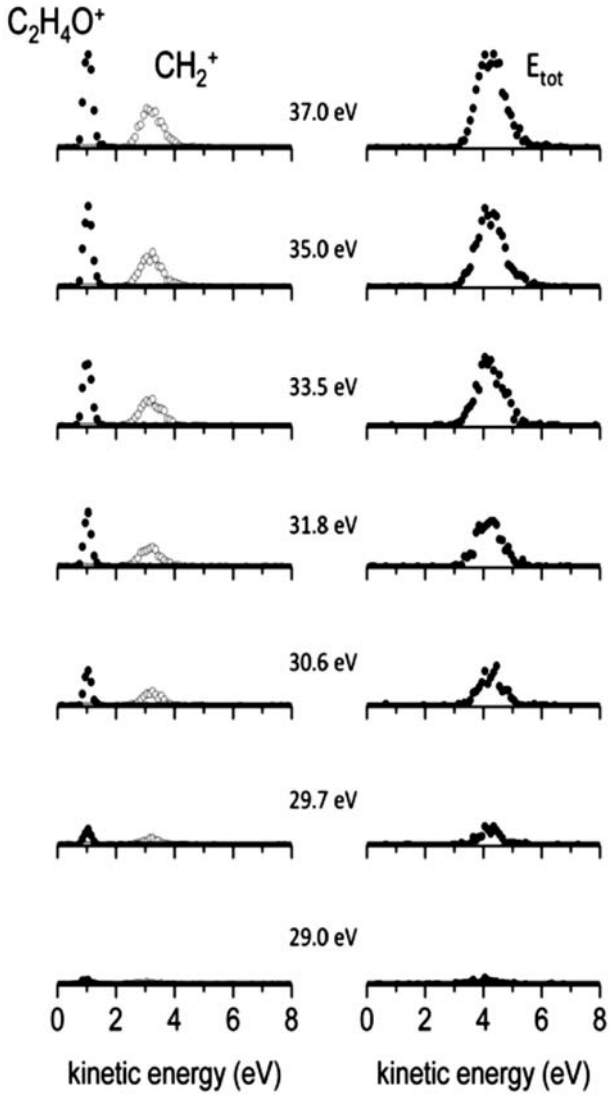

Fig. 3. The kinetic energy released (KER) distribution of the $CH_2^+ + C_2H_4O^+$ products for various investigated photon energies: in the left panel are reported the KER for each fragment ion, whereas in right panel the total KER distributions are shown.

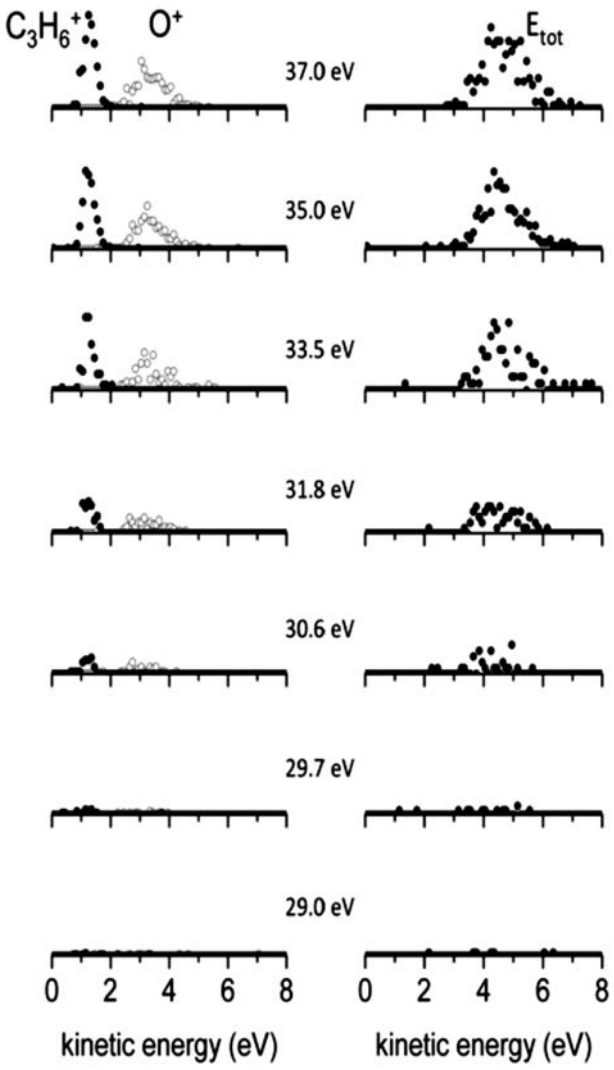

Fig. 4. The kinetic energy released (KER) distribution of the $O^+ + C_3H_6^+$ products for various investigated photon energies: in the left panel are reported the KER for each fragment ion, whereas in right panel the total KER distributions are shown.

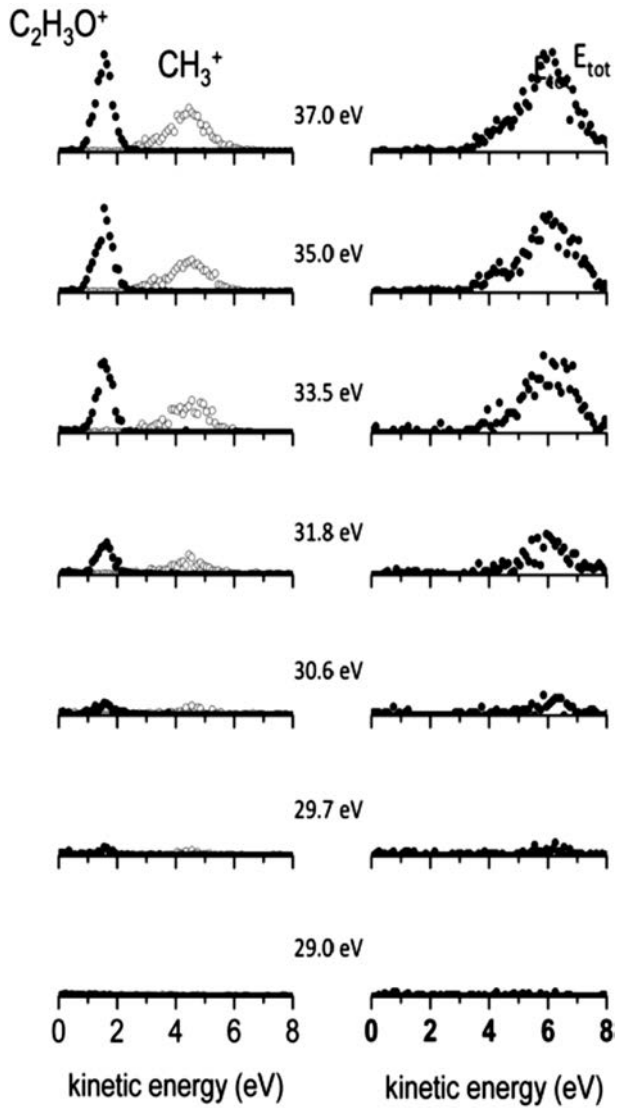

Fig. 5. The kinetic energy released (KER) distribution of the $CH_3^+ + C_2H_3O^+$ products for various investigated photon energies: in the left panel are reported the KER for each fragment ion, whereas in right panel the total KER distributions are shown.

very low intensity of recorded signals for OH^++$C_3H_5^+$ coincidences. All recorded KER distributions of Figures 1-5 do not change appreciably with the photon energy. In particular, they appear rather symmetric and can be easily fitted by a simple Gaussian function. It has to be noted that in such Figures the peaks position and relative shapes, for each analyzed dissociation channel, are practically the same for all investigated photon energies. This could be an indication that each fragmentation channel involves one specific region of the multidimensional potential energy surface, associated to the effective intramolecular interaction within the $(C_3H_6O)^{2+}$ dication frame and responsible of the opening of the various two body fragmentation channels, at all investigated energies. Therefore, for all investigated fragmentation channels the excess of the used photon energy respect to the double ionization threshold energy should be released as electron recoil energy. The only exception is constituted by the recorded total KER distribution for the two CH_3^+ + $C_2H_3O^+$ product ions of reaction (3) shown in the right panel of Fig. 5 as a function of the investigated photon energy. It is evident that such total KER distributions are characterized by a bimodal behavior depending on the two possible microscopic mechanisms for the two body fragmentation of $(C_3H_6O)^{2+}$ dication producing CH_3^+ + $C_2H_3O^+$. In fact, reaction (3) may occurs by two different pathways: in one case (probably the most important one) a direct fragmentation of the $(C_3H_6O)^{2+}$ dication into CH_3^+ + $C_2H_3O^+$ products can occurs, while in a second case the Coulomb explosion of the $(C_3H_6O)^{2+}$ dication takes place by means of a hydrogen migration from the methyl group of propylene oxide molecule to the end carbon atom bound with oxygen. Further experiments performed using isotopically labeled precursor molecules should clarify the relative importance of such different microscopic pathways for reaction (3).

Moreover, future experimental investigations recording the angular distributions of the final ions could be able to investigate in major detail the hypotheses discussed above concerning the microscopic two body dissociation mechanisms following the Coulomb explosion of the $(C_3H_6O)^{2+}$ dication. These experiments are planned in next future at the Elettra Synchrotron Facility to measure the anisotropy parameter [28-30] in the angular distribution of dissociation ion products as a function of the photon energy, and possibly electron kinetic energy spectra as done in previous experiments [31-35].

4. *Conclusions*

In this paper, we presented a study of the double photoionization of a simple chiral molecule of astrochemical interest (the propylene oxide) promoted by direct ejection of two valence electrons. The study has been performed by using linearly polarized synchrotron radiation in order to identify the leading two-body dissociation channels and measure: i) the threshold energy for the different ionic products formation; ii) the related branching ratios, and iii) the KER distribution of fragment ions at different photon energies. This preliminary study is important to provide

unavailable data on $(C_3H_6O)^{2+}$ molecular dications energetics, and nuclear dissociation dynamics, being mandatory information for further experimental and theoretical investigations of the interaction between chiral species and linearly or circularly polarized light. Besides, for all investigated fragmentation channels, the recorded KER distributions indicate that the excess of the used photon energy, respect to the double ionization threshold energy, should be released as electron recoil energy. The CH_3^+ formation by reaction (3) involves two different microscopic mechanisms in the Coulomb explosion fragmentation dynamics of the intermediate $(C_3H_6O)^{2+}$ dication. This is confirmed by the observation of a bimodality in the total KER distribution for the $CH_3^+ + C_2H_3O^+$ product ions of reaction (3), as observed in previous experiments [5,11].

BIBLIOGRAPHIC REFERENCES

[1] McGuire, B.A., Carroll, P.B., Loomis, R.A., *et al.*, (2016). Discovery of the interstellar chiral molecule propylene oxide (CH_3CHCH_2O). *Science* **352**, 1449-1452.

[2] Wan, T.A., Davies, M.E., (1994). Design and synthesis of a heterogeneous asymmetric catalyst. *Nature* **370**, 449-450.

[3] Riviera, J.M., Martin, T., Rebek, J. Jr., (1998). Chiral Spaces: Dissymmetric Capsules Through Self-Assembly. *Science* **279**, 1021-1023.

[4] Pasteur, L., (1848). Recherches sur les relations qui peuvent exister entre la forme crystalline et la composition chimique, et le sens de la polarisation rotatoire. *Ann. Chim. Phys.* **24**, 442.

[5] Falcinelli, S., Vecchiocattivi, F., Alagia, M., Schio, L., Richter, R., P. Stranges, S., *et al.*, (2018). Double photoionization of propylene oxide: A coincidence study of the ejection of a pair of valence-shell electrons. *J. Chem. Phys.* **148**, 114302.

[6] Rosi, M., Falcinelli, S., Balucani, N., Casavecchia, P., Leonori, F., Skouteris, D., (2012). Theoretical Study of Reactions Relevant for Atmospheric Models of Titan: Interaction of Excited Nitrogen Atoms with Small Hydrocarbons. ICCSA 2012, Part I, *Lecture Notes in Computer Science LNCS* **7333**, 331-344.

[7] Falcinelli, S., Pirani, F., Vecchiocattivi, F., (2015). The Possible role of Penning Ionization Processes in Planetary Atmospheres. *Atmosphere* **6(3)**, 299-317.

[8] Alagia, M., Balucani, N., Candori, P., Falcinelli, S., Richter, R., Rosi, M., Pirani, F., Stranges, S., Vecchiocattivi, F., (2013). Production of ions at high energy and its role in extraterrestrial environments. *Rendiconti Lincei Scienze Fisiche e Naturali* **24**, 53-65.

[9] Falcinelli, S., (2017). The Escape of O^+ and CO^+ Ions from Mars and Titan Atmospheres by Coulomb Explosion of CO_2^{+2} Molecular Dications. *Acta Physica Polonica A* **131(1)**, 112-116.

[10] Falcinelli, S., Candori, P., Pirani, F., Vecchiocattivi, F., (2017). The role of the charge transfer in stability and reactivity of chemical systems from experimental findings. *Phys. Chem. Chem. Phys.* **19(10)**, 6933-6944.

[11] Falcinelli, S., Rosi, M., Vecchiocattivi, F., Pirani, F., *et al.*, (2018). Double Photoionization of Simple Molecules of Astrochemical Interest. ICCSA 2018, Part II, *Lecture Notes in Computer Science LNCS* **10961**, 746-762.

[12] Alagia, M., Candori, P., Falcinelli, S., Lavollée, M., Pirani, F., Richter, R., Stranges, S., Vecchiocattivi, F., (2007). Anisotropy of the angular distribution of fragment ions in dissociative double photoionization of N_2O molecules in the 30-50 eV energy range. *J. Chem. Phys.* **126(20)**, 201101.

[13] Alagia, M., Candori, P., Falcinelli, S., Lavollée, M., Pirani, F., Richter, R., Stranges, S., Vecchiocattivi, F., (2006). Double photoionization of N_2O molecules in the 28-40 eV energy range. *Chem. Phys. Lett.* **432**, 398-402.

[14] Alagia, M., Candori, P., Falcinelli, S., Lavollée, M., Pirani, F., Richter, R., Stranges, S., Vecchiocattivi, F., (2009). Double Photoionization of CO_2 molecules in the 34-50 eV Energy range. *J. Phys. Chem. A* **113**, 14755-14759.

[15] Alagia, M., Candori, P., Falcinelli, S., Lavollèe, M., Pirani, F., Richter, R., Stranges, S., Vecchiocattivi, F., (2010). Dissociative double photoionization of CO_2 molecules in the 36-49 eV energy range: angular and energy distribution of ion products. *Phys. Chem. Chem. Phys.* **12**, 5389-5395.

[16] Alagia, M., Candori, P., Falcinelli, S., Pirani, F., Pedrosa Mundim, M.S., Richter, R., Rosi, M., Stranges, S., Vecchiocattivi, F., (2011). Dissociative double photoionization of benzene molecules in the 26–33 eV energy range. *Phys. Chem. Chem. Phys.* **13(18)**, 8245-8250.

[17] Alagia, M., Candori, P., Falcinelli, S., Mundim, M.S.P., Pirani, F., Richter, R., Rosi, M., Stranges, S., Vecchiocattivi, F., (2011). Dissociative double photoionization of singly deuterated benzene molecules in the 26–33 eV energy range. *J. Chem. Phys.* **135(14)**, 144304.

[18] Alagia, M., Callegari, C., Candori, P., Falcinelli, S., Pirani, F., Richter, R., Stranges, S., Vecchiocattivi, F., (2012). Angular and energy distribution of fragment ions in dissociative double photoionization of acetylene molecules at 39 eV. *J. Chem. Phys.* **136**, 204302.

[19] Falcinelli, S., Alagia, M., Farrar, J.M., Kalogerakis, K.S., Pirani, F., Richter, R., *et al.*, (2016). Angular and energy distributions of fragment ions in dissociative double photoionization of acetylene molecules in the 31.9-50.0 eV photon energy range. *J. Chem. Phys.* **145(11)**, 114308.

[20] Lavollée, M., (1990). A new detector for measuring three-dimensional momenta of charged particles in coincidence. *Rev. Sci. Instrum.* **70**, 2968.

[21] Schio, L., Li, C., Monti, S., Salén, P., Yatsyna, V., Feifel, R., Alagia, M., *et al.*, (2015). NEXAFS and XPS studies of nitrosyl chloride. *Phys. Chem. Chem. Phys.* **17(14)**, 9040-9048.

[22] Falcinelli, S., Pirani, F., Alagia, M., Schio, L., Richter, R., Stranges, S., Balucani, N., Vecchiocattivi, F., (2016). Molecular Dications in Planetary Atmospheric Escape. *Atmosphere* **7(9)**, 112.

[23] Falcinelli, S., Rosi, M., Cavalli, S., Pirani, F., Vecchiocattivi, F., (2016). Stereoselectivity in Autoionization Reactions of Hydrogenated Molecules by Metastable Noble Gas Atoms: The Role of Electronic Couplings. *Chemistry Eur. J.* **22(35)**, 12518-12526.

[24] Alagia, M., Bodo, E., Decleva, P., Falcinelli, S., Ponzi, A., Richter, R., Stranges, S., (2013). The soft X-ray absorption spectrum of the allyl free radical. *Phys. Chem. Chem. Phys.* **15(4)**, 1310-1318.

[25] Falcinelli, S., Rosi, M., Candori, P., Farrar, J.M., Vecchiocattivi, F., Pirani, F., Balucani, N., Alagia, M., Richter, R., Stranges, S., (2014). Kinetic energy release in molecular dications fragmentation after VUV and EUV ionization and escape from planetary atmospheres. *Planetary and Space Science* **99**, 149-157.

[26] Pirani, F., Falcinelli, S., Vecchiocattivi, F., Alagia, M., Richter, R., Stranges, S., (2018). Anisotropic forces and molecular dynamics. *Rendiconti Lincei Scienze Fisiche e Naturali* **29(1)**, 179-189.

[27] Alagia, M., Candori, P., Falcinelli, S., Mundim, K.C., Mundim, M.S.P., Pirani, F., *et al.*, (2012). Lifetime and kinetic energy release of metastable dications dissociation. *Chem. Phys.* **398**, 134-141.

[28] Zare, R.N., (1972). Photoejection Dynamics. *Mol. Photochem.* **4**, 1.

[29] Alagia, M., Brunetti, B. G., Candori, P., Falcinelli, S., Teixidor, M. M., Pirani, F., *et al.*, (2004). Threshold-photoelectron-spectroscopy-coincidence study of the double photoionization of HBr. *J. Chem. Phys.* **120(15)**, 6980-6984.

[30] Alagia, M., Brunetti, B.G., Candori, P., Falcinelli, S., Teixidor, M.M., Pirani, F., *et al.*, (2004). Low-lying electronic states of HBr^{2+}. J. Chem. Phys. **120(15)**, 6985-6991.

[31] Alagia, M., Biondini, F., Brunetti, B.G., Candori, P., Falcinelli, S., Teixidor, M.M., Pirani, F., *et al.*, (2004). The double photoionization of HCl: An ion-electron coincidence study. *J. Chem. Phys.* **121(21)**, 10508-10512.

[32] Teixidor, M.M., Pirani, F., Candori, P., Falcinelli, S., Vecchiocattivi, F., (2003). Predicted Structure and Energetics of HCl^{2+}. *Chem. Phys. Lett.* **379**, 139-146.

[33] Alagia, M., Brunetti, B.G., Candori, P., *et al.*, (2006). The double photoionization of hydrogen iodide molecules. *J. Chem. Phys.* **124(20)**, 204318.

[34] Pei, L., Carrascosa, E., Yang, N., Falcinelli, S., Farrar, J.M., (2015). Velocity Map Imaging Study of Charge-Transfer and Proton-Transfer Reactions of CH_3 Radicals with H_3^+. *Journal of Physical Chemistry Letters* **6 (9)**, 1684-1689.

[35] Brunetti, B., Candori, P., Falcinelli, S., Lescop, B., *et al.*, (2006). Energy dependence of the Penning ionization electron spectrum of $Ne^*(^3P_{2,0})$ + Kr. *Eur. Phys. J. D* **38**, 21-27.

Rendiconti
Accademia Nazionale delle Scienze detta dei XL
Memorie di Scienze Fisiche e Naturali
136° (2018), Vol. XLII, Parte II, Tomo II, pp. 73-80

SERGIO ABBATE[1] – GIUSEPPE MAZZEO[1] – GIOVANNA LONGHI[1]

NIR-absorption and NIR-VCD spectroscopy can teach us a lot about OH bonds

Abstract – We briefly review the local mode model and its usefulness to interpret simply and effectively the near infrared absorption and near infrared vibrational circular dichroism spectra (NIR and NIR-VCD respectively). In particular we consider the case of the OH-stretching first overtone region between 6250 and 7700 cm^{-1} (1600 and 1300 nm). With reference and by comparison of newly acquired data for chiral phenylethanol and chiral 2,2,2-trifluorophenylethanol, we show that NIR VCD spectra in that region are quite informative about the OH bond, more than the corresponding fundamental region, between 3000 and 3800 cm^{-1}, which is more accessible to standard instrumentation.

Introduction. The local mode model and NIR spectra

Near-infrared (NIR) vibrational absorption spectroscopy covers the spectroscopic region from straight infrared to the red-visible region (2500-700 nm = 4000-15,000 cm^{-1}): it has been thought generally to be dull and hard to cope with theoretically; for this reason it has been used scarcely in Academia but a lot in industry and for practical reasons, for example in the pharma- industry, agro-food industry, packaging industry and for quality control [1]. The scope of the present chapter is to demonstrate that this spectroscopic region deserves attention also from basic science investigators and can provide useful and fundamental information on molecular structure. This has been recognized for some time, the revived interest dating back to 1980, when considerable progress had been made both experimentally and

[1] DMMT (Dipartimento di Medicina Molecolare e Traslazionale), Università di Brescia, Viale Europa 11 - 25123 Brescia (Italy).
E-mail: sergio.abbate@unibs.it giuseppe.mazzeo@unibs.it giovanna.longhi@unibs.it

theoretically. Indeed, in the eighties, besides the use of long path-length cells employed in order to be able to detect vibrational features with increasingly lower molecular absorption coefficient at decreasing wavelength [2], several methods were proposed and utilized to investigate also gases, like laser intra-cavity photo-acoustic spectroscopy, thermal lensing, etc. [3-7]. Theoretically, the local mode approximation [2, 8-10] accommodated satisfactorily the interpretation of the many spectroscopic data being accumulated; the local mode model stimulated interested, through a renewed attention to the Morse potential and the alike, also from theoretical physicists utilizing methods, as, e.g. Lie-algebraic methods [11]. The local mode model allows one to approximate the NIR spectrum as the succession of overtone spectra at *v*-th order of the uncoupled XH-stretching vibrational modes (X = C, O, N, etc.); the large anharmonicity permitting to overcome inter-mode couplings. Concurrently, in the model no combination or mixed mode involving XH-modes plus bath-modes or bending modes is expected to bear intensity, as generally observed.

Our group contributed to the field by testing whether some NIR chiroptical spectroscopy were possible on chiral compounds, and indeed we found it was [12, 13] in the range from 3000 to 600 nm for molecules not containing electronic chromophores, active in the investigated region. Some fifty compounds were studied in our group, in the group of Nafie and in the group of Stephens even earlier [13-15]: for all of them it was possible to measure vibrational circular dichroism (VCD), which has been measured prevalently in the mid-IR range (3300-1000 $cm^{-1} \approx$ 3000-10000 nm). VCD spectroscopy consists in the difference in absorption of left and right circularly polarized light in the IR and NIR range [16]. Theoretically we also contributed to the further elaboration of the local mode model by introducing the effect of *mechanical anharmonicity* and of *electrical anharmonicity* [16-19] in such a way that the new terms are easily computed from ab-initio/DFT quantum mechanical packages [20-21]. In this way, we provided a protocol for calculating the mechanical anhamonicity parameter χ_n together with the harmonic mechanical frequency ω_n for the *n*-th bond-stretching (or local mode) at ν-th order from the 2nd, 3rd and 4th derivatives K_{nn}, K_{nnn} and K_{nnnn} of the Hessian matrix, to be inserted in the Birge-Sponer or Dunham expansion reported in eq. (1) (all other constants in eq. (1) being easily recognizable fundamental constants):

$$\omega_{nv} = hc\left(\omega_n\left(v+\frac{1}{2}\right) - \chi_n\left(v+\frac{1}{2}\right)^2\right) \qquad \chi_n = \frac{h}{64\pi^2 mc}\left(\frac{5}{3}\frac{K_{nnn}^{\ 2}}{K_{nn}^{\ 2}} - \frac{K_{nnnn}}{K_{nn}}\right) \tag{1}$$

$$\langle \mu_i \rangle_{0v} = \sum_{\alpha=H,X} \Pi^0_{\alpha iz} t_\alpha \langle 0|z|v\rangle + \frac{1}{2}\sum_{\alpha j}\left(\frac{\partial \Pi_{\alpha iz}}{\partial z}\right)_0 t_\alpha \langle 0|z^2|v\rangle + higher-order-terms \tag{2}$$

$$\langle m_i \rangle_{v0} = \sum_{\alpha=H,C} A^0_{\alpha iz}\frac{1}{m_R} t_\alpha \langle v|p|0\rangle + \sum_{\alpha=H,C}\left(\frac{\partial A_{\alpha iz}}{\partial z}\right)_0 \frac{1}{m_R} t_\alpha \langle v|zp|0\rangle + higher-order-terms \tag{3}$$

In eqs. (2) and (3) instead are presented the contributions of electrical anharmonicity to the electric dipole transition moments and magnetic dipole transition moments for the *0* -> *v* transition of the *n*-th local mode; such contributions are the first derivative of the atomic polar tensor Π and atomic axial tensor *A* with respect to the *n*-th XH stretching, involving the α-th atoms (the transition moments just presented enter the dipole strengths and rotational strengths, as for example in refs. [21, 22, and 23]. Explanation of the other constants in eqs. (2) and (3) and generalization to include higher derivatives than the first one may be found in refs. [17, 18 and 19].

Discussion. The first overtone of the OH-stretching region

In this chapter we deal with the first overtone ($\Delta v = 2$) of alcohol molecules. For this and even further overtone regions, since just one OH bond is present, the local mode approximation is well justified. Through the method briefly expounded above, we were able to explain the NIR and NIR-VCD spectra of (*R*)- and (*S*)-borneol between 1600 and 1300 nm. [24] The case of borneol is intriguing, since two features are observed for the OH-stretching in NIR-VCD, instead of just one, as observed in the NIR-absorption spectrum and as expected from the local mode model. The explanation we provided in ref. [24] was that three conformers, corresponding to three different orientations of the OH group, are present in solution and VCD is able to detect them, since the sign of VCD is different for one of them with respect to the other two. Thus VCD adds some information, which absorption is unable to pick, since it has got an implicitly higher resolution, due to sign sensitivity. Not only that, the mechanical anharmonicity parameter and mechanical frequency we were able to calculate in ref. [24] are pretty close in value to the ones for ethylene glycol, that Kjaergaard *et al.* [7] had calculated and measured for the OH bond for overtone up to $v = 5$, as may be appreciated from Table 1.

Cmpd.	Conformer	τ(deg)	%pop	ω(cm^{-1})	χ(cm^{-1})
Borneol	1-f	68	51.5	3807	88.6
(ref. 24)	2-f	174	28.3	3822	86.8
	3-f	300	20.2	3814	90.0
Ethylene	1-b			3806	82.9
glycol	1-f			3856	84.1
(ref. 7)					

Table 1. Comparison of mechanical harmonic frequencies and anharmonicity constant calculated via DFT for the OH bond in borneol [24] and ethylene glycol [7]. One has three conformers for borneol, for which the OH bond is «free» (f) and several conformers for ethylene glycol, for which the OH bond can be either «free» (f) or involved in a donor-type H-bond (b). Results for just one conformer are provided in the latter case.

The new alcohol-cases that we wish to discuss here are (*R*)- and (*S*)-phenyl ethanol (**1**) and (*R*)- and (*S*)-2,2,2-trifluoro-phenyl ethanol (**2**), differing just in the CH_3 group being substituted by a CF_3 group. In Figure 1 we present the superimposed mid-IR and mid-IR-VCD spectra of both enantiomers of **1** and of ***2*** in CS_2 and CCl_4 solution respectively (please notice that the VCD spectra of the two enantiomers of the two compounds are opposite, within experimental error). While the data for ***2*** are from a previous publication of ours [25], the data for **1** are taken from our collection of yet unpublished results.

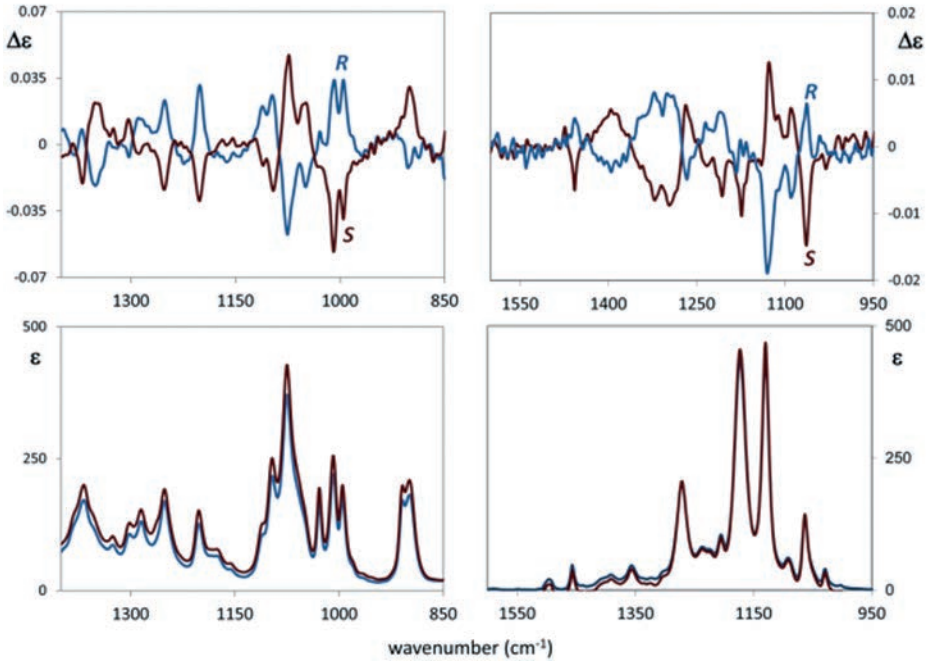

Fig. 1. IR-VCD spectra of phenyl ethanol (**1**) (left) and of 2,2,2-trifluoro-phenyl ethanol (**2**) (right). Spectrum of **1** was recorded in CS_2 solvent at 0.1M concentration in 200 μm cell. Spectrum of 2 was recorded in $CDCl_3$ solvent at ca. 0.1M concentration in 100 μm cell.

We were able to predict [25] the IR and VCD spectra of Figure 1 by DFT calculations carried out by using standard methodology [20, 26]. Computed spectra are not reported here for conciseness. The computed spectra contain fundamental transitions ($\Delta v = 1$) for highly delocalized normal modes resulting from linear combinations of several simple «internal» modes involving CC- and CO- and CF-stretchings and HCC and OH bendings [27]. Besides and more importantly the computed spectra are weighted averages of IR and VCD spectra of different conformers, which are thermally populated through Boltzmann population factors [26]. The conformers

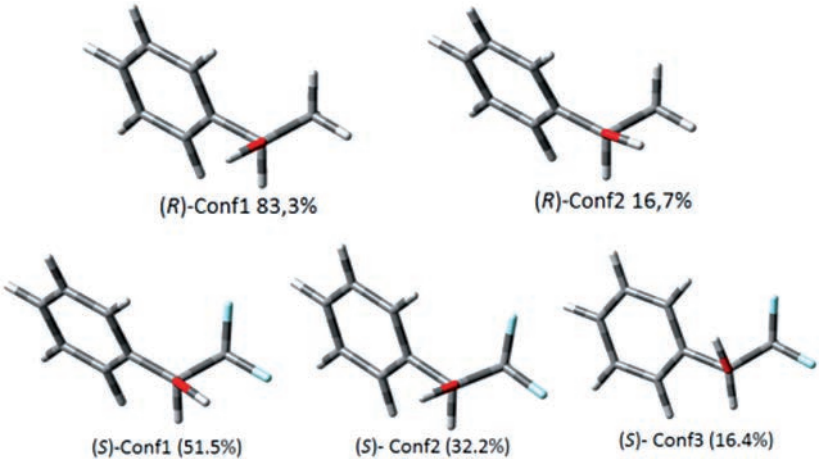

Fig. 2. Calculated conformers of phenyl ethanol (**1**) (first row as *R* configuration) and of 2,2,2-trifluoro-phenyl ethanol (**2**) (second row as *S* configuration). Population factors are reported in brackets.

predicted for these compounds are presented in Figure 2: in the top line one has the conformers for molecule **1** ((*R*)-enantiomer), in the lower line the conformers for molecule ***2*** ((*S*)-enantiomer).

Please notice that the prevalent conformer for **1** (with a population factor larger than 80%) is such that the positive H atom of the OH bond is strongly attracted by the phenyl moiety. Instead in **2** the OH is pointing to the strongly electro-negative CF_3-group (with a population larger than 50%), while the conformer with the OH pointing towards PHE is close to 30% in population. This has consequences on the reproduction of the spectra, especially the VCD ones, of Figure 2; however there is no clear, immediately recognizable signature of each one of the two conformers. Instead, a dramatic difference is observed in NIR-VCD spectra of **1** and **2**, which we recorded on our home-made apparatus in the region of the first OH-stretching overtone ($\Delta v = 2$) (see Figure 3) on the same solution employed for mid-IR VCD measurements.

The NIR absorption spectrum is very simple and almost coincidental in the two cases, namely it is composed by one single band at ca. 1416 nm with a max absorption coefficient $\varepsilon \approx 1.6\ M^{-1}cm^{-1}$, being two order of magnitudes lower than in the mid-IR. The NIR-VCD spectrum (which provides mirror-image spectrum for the two enantiomers, as is in the mid-IR) is composed by a single feature in **1** and by a major feature in **2**, accompanied by a minor one at lower energies (longer wavelengths) and opposite sign. The major feature reaches approximately the value $\Delta\varepsilon \approx \pm 1 \times 10^{-4}$ for **1** and the value $\Delta\varepsilon \approx \pm 1.6 \times 10^{-4}$ for **2**, with two orders of magnitude decrease from the fundamental IR stretching region (*cfr.* Figure 1). The latter fact, namely that absorption and VCD spectra decrease by similar orders of magnitude at each overtone order has been known for some time, even before the advent

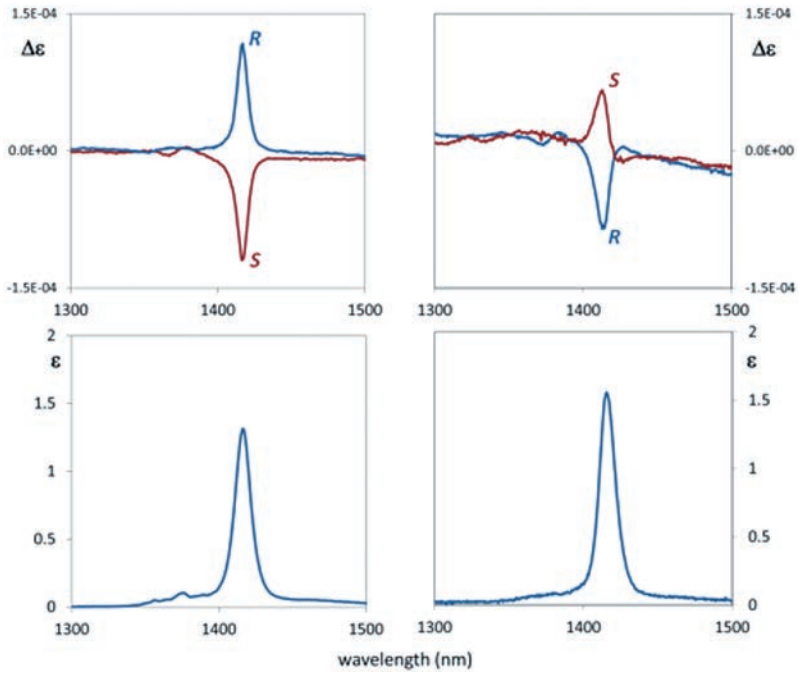

Fig. 3. NIR-VCD spectra of the two enantiomers of phenyl ethanol (**1**) (left) and of 2,2,2-trifluoro-phenyl ethanol (**2**) (right). Spectrum of **1** was recorded in CS_2 solvent at 0.1M concentration in 5 cm quartz cuvette. Spectrum of **2** was recorded in CCl_4 solvent at 0.13 M concentration in 2 cm path-length quartz cuvette.

of DFT calculations [28-30], based on the first extensive application of Van Vleck perturbation theory to the study of VCD anharmonic spectra [31, 32]. However, and most importantly, for the same absolute configuration at the stereogenic carbon, the sign of the major VCD band is reversed. To explain that fact, we first observe that the (C.I.P.) specification of molecular chirality [33] by Cahn, Ingold, and Prelog for **1** is such the groups about the sterogenic carbon C* are in the decreasing order: OH, Phe, CH_3, H, while for **2** the order is: OH, CF_3, Phe, H. Thereby the (*R*) configuration for **1**, as defined by C.I.P. rule, places the chemical groups in the same order as for (*S*)-**2**, once the substitution $CH_3 \Leftrightarrow CF_3$ is made (see Figure 2). Moreover, the different conformational properties pointed out above for **1** and **2** give further meaning to what is observed: as it happens in borneol, different orientations of the OH group, are characterized by different signs in the VCD transition. Indeed, as of Figure 2, the conformer prevailing in **1** is quite different from the conformer prevailing in **2**: in the former case OH tends towards the Phe group (# 2 in C.I.P. rule), while in the latter case the OH tends towards CF_3 (once more # 2 in C.I.P. rule). We think that this fact provides physical grounds to the C.I.P. rule and the

NIR-VCD spectrum is directly related to it. In conclusion, the NIR-VCD spectrum is directly related to the local structure of the vibrational chromophore, not only as regards the geometrical characteristics, but also as regards the different electronic chemical environment, through the electrical anharmonicity parameters. The corresponding IR-VCD spectra, examined extensively by Nafie *et al.* [14] for several compounds, is not as informative as the NIR-VCD ones. We finally wish to report that the importance of the first overtone region for the OH-stretching had been pointed out some time ago by Sandorfy et al. in seminal studies of NIR absorption spectra of simple alcohols [34].

REFERENCES

[1] Jamrógiewigz M., (2012). Application of the near-infrared spectroscopy in the pharmaceutical technology. *J. Pharm. Biomed. Anal.* **66**, 1-10.

[2] Henry B.R., (1977). Use of Local Modes in the Description of Highly Vibrationally Excited Molecules. *Accts. Chem. Res.* **10,** 207-213.

[3] Franko M. & Tran C.D., (2010). *Thermal Lens Spectroscopy*. Encyclopedia Analytical Chemistry, J. Wiley, London.

[4] Swofford R.L., Long M.E., Burberry M.S. & Albrecht A.C., (1977). «Free» O-H overtone absorption of methanols in the visible region by thermal lensing spectroscopy. *J. Chem. Phys.* **66**, 664-668.

[5] Fang H.L., Swofford R.L., (1982). Photoacoustic spectroscopy of vibrational overtones in polyatomic molecules. *Appl. Optics* **21**, 55-60.

[6] Lespade L., Rodin S., Cavagnat D., Martin J.J., Cornut J.C. & Abbate S., (1991) Intracavity dye laser photoacoustic spectroscopy: measurements of the fifth overtone of cyclohexene. *Annales Physique, supplement au n. 2*, **16**, 145-146.

[7] Kjaergaard H.G. & Howard D.L., (2006) Overtone spectroscopy: a sensitive probe of hydrogen bonding. Chemistry in New Zealand, 16-19.

[8] Lawton R.T. & Child M.S., (1981). Local and normal stretching vibrational states of H_2O. *Mol. Phys.* **44**, 709-723.

[9] Lehmann K.K., (1983). On the relation of Child and Lawton's harmonically coupled anharmonic-oscillator model and Darling-Dennison coupling. *J. Chem. Phys.* **79**, 1098.

[10] Mills I.M. & Robiette A.G., (1985). On the relationship of normal modes to local modes in molecular vibrations. *Mol. Phys.* **56**, 743-765.

[11] Iachello F. & Levine R.D., (1995). *Algebraic Theory of Molecules*. Oxford University Press, New York.

[12] Abbate S., Longhi G., Ricard L., Bertucci C., Rosini C., Salvadori P. & Moscowitz A., (1989). Vibrational Circular Dichroism as a Criterion for Local Mode versus Normal Mode Behavior. Near infrared Circular Dichroism Spectra of some Monoterpenes. *J. Am. Chem. Soc.* **111**, 836-840.

[13] Castiglioni E., Lebon F., Longhi G. & Abbate S., (2002). Vibrational Circular Dichroism in the Near Infrared: Instrumental Developments and Applications. *Enantiomer* **7**, 161-173.

[14] Guo C., Shah R.D., Dukor R.K., Freedman T.B., Cao X. & Nafie L.A., (2006). Fourier transform vibrational circular dichroism from 800 to 10,000 cm^{-1}: Near-IR-VCD spectral standards for terpenes and related molecules. *Vibr. Spectrosc.* **42**, 254-272.

[15] Keiderling T.A. & Stephens P.J., (1976). Vibrational circular dichroism of overtone and combination bands. *Chem. Phys. Lett.* **41**, 46-48.
[16] Nafie L.A., (2011). *Vibrational Optical Activity: Principles and Applications*. Wiley, UK.
[17] Abbate S., Longhi G., Castiglioni E. (2012). Near-Infrared Vibrational Circular Dichroism: Nir-Vcd. In Comprehensive Chiroptical Spectroscopy, Volume 1: Instrumentation, Methodologies, and Theoretical Simulations, First Edition. Ed. Berova N., Polavarapu P.L., Nakanishi K. & Woody R.W., **Vol 1**, Ch. 10, 247, John Wiley & Sons, Inc.
[18] Gangemi F., Gangemi R., Longhi G. & Abbate S. (2009). Calculations of overtone NIR and NIR-VCD spectra in the local mode approximation: camphor and camphorquinone. *Vibr. Spectrosc.* **50**, 257-267.
[19] Abbate S., Castiglioni E., Gangemi F., Gangemi R. & Longhi G., (2009). NIR-VCD, vibrational circular dichroism in the near-infrared: Experiments, theory and calculations. *Chirality*, **21**, S242-S252.
[20] Gaussian09. Frisch M.J., *et al*. (2009) Gaussian, Inc., Wallingford, CT.
[21] Stephens P.J., (1985). The theory of vibrational circular dichroism. *J. Phys. Chem.* **89**, 748-752.
[22] Moscowitz A., (1962). Theoretical aspects of optical activity. Part one: small molecules. *Adv. Chem. Phys.* **Vol IV**, 68-112.
[23] Bak K.L., Bludský O. & Jørgensen P., (1995). Ab initio calculations of anharmonic vibrational circular dichroism intensities of trans-2,3-dideuterio-oxirane. *J. Chem. Phys.* **103**:10548-10555.
[24] Gangemi F., Gangemi R., Longhi G. & Abbate S., (2009). Experimental and ab-initio calculated VCD spectra of the first OH-stretching overtone of (1R)-(-) and (1S)-(+)-endo-borneol. *Phys. Chem. Chem. Phys.* **11**, 2683-2689.
[25] Abbate S., Lebon F., Lepri S., Longhi G., Gangemi R., Spizzichino S., Bellachioma G., Ruzziconi R., (2011). Vibrational Circular Dichroism (VCD): a Valuable Tool for Conformational Analysis and Absolute Configuration Assignment of Chiral 1-([2.2.]Paracyclophan-4-yl)-2,2,2-trifluoroethanols. *ChemPhysChem* **12**, 3519-3523.
[26] Stephens P.J., Devlin F.J. & Cheeseman J.R., (2012). *VCD spectroscopy for Organic Chemists*. CRC Press, Boca Raton, FL.
[27] Wilson E.B. Jr., Decius J.C., Cross P.C., (1955). *Molecular Vibrations*. McGraw-Hill, New York, NY.
[28] Abbate S., Longhi G. & Santina C., (2000). Theoretical and experimental studies for the interpretation of vibrational circular dichroism spectra in the CH-stretching overtone region. *Chirality* **12**, 180-190.
[29] Polavarapu P.L., (1996). Vibrational optical activity of anharmonic oscillator. *Mol. Phys.* **89**, 1503-1510.
[30] Abbate S., Gangemi R., Longhi G., (2002). Dipole and rotational strengths for overtone transitions of a C2-symmetry HCCH molecular fragment using Van Vleck perturbation theory. *J. Chem. Phys.* **117**, 7575-7586.
[31] Faulkner T.R., Marcott C., Moscowitz A., Overend J., (1977). Anharmonic effects in vibrational circular dichroism. *J. Am. Chem. Soc.* **99**, 8160-8168.
[32] Faulkner T.R., Marcott C., Moscowitz A., Overend J., (1977). Vibrational circular dichroism in bromochlorofluoromethane and bromochlorofluoromethane-d. Calculation of the rotational strengths associated with the fundamentals and the binary overtones and combinations. *J. Am. Chem. Soc.* **99**, 8169-8175.
[33] Cahn, R.S., Ingold, C., Prelog, V., (1966). Specification of molecular chirality. *Angew. Chem. Intl. Ed.* **5**, 385-415.
[34] Péron, J.-J., Sandorfy, C., (1976). The anharmonicity of the OH stretching vibration of hydrogen bonded methanol in binary systems. *J. Chem. Phys.* **65**, 3153-3157.

Rendiconti
Accademia Nazionale delle Scienze detta dei XL
Memorie di Scienze Fisiche e Naturali
136° (2018), Vol. XLII, Parte II, Tomo II, pp. 81-89

FERNANDO PIRANI[1] – DANIELA ASCENZI[2]

Stereodynamical effects by anisotropic intermolecular forces

Abstract – Alignment and/or orientation of molecules (i.e. non-statistical spatial distributions of their rotational angular momenta, their molecular axes and/or their molecular planes) can be naturally induced during two body collisions in gas phase. The nature and strength of the intermolecular forces involved, and their anisotropies govern the collision dynamics and a deep understanding of the physical mechanisms underlying collisional alignment/orientation is crucial to control the stereodynamics of elementary chemical-physical processes. By using different experimental techniques and theoretical methodologies the effect of polarization on elementary processes involving neutral and ionic species are presented and discussed for both weakly and strongly interacting systems.

1. *Introduction*

Electric and magnetic field gradients, arising from anisotropic intermolecular forces, can induce molecular polarization, *i.e.* alignment and/or orientation of a molecule as a consequence of collisions with other atoms or molecules. A deep knowledge of these phenomena, today still not fully understood, is of general relevance to control the stereodynamics of elementary chemical-physical processes, occurring both in gaseous and condensed phases and involving neutral and ionic species (Vattuone *et al.* 2010). The possibility of aligning/orienting molecules in gaseous streams by virtue of collisions may have some implications in understanding the origin of

[1] Dipartimento di Chimica, Biologia e Biotecnologie Università di Perugia, Via Elce di Sotto 8, Perugia, Italy. E-mail: fernando.pirani@unipg.it
[2] Dipartimento di Fisica, Università di Trento, Via Sommarive 14 - 38123 Trento, Italy. E-mail: daniela.ascenzi@unitn.it

chiral discrimination and chiral selectivity emerging in vortices formed both in the liquid and in the gas phase (Lombardi *et al.* 2018 and references therein; Su *et al.* 2013). It is intriguing to think that polarization phenomena involving chiral molecules might have implications for the emergence of homochirality in the Universe and connections might be proposed with vortex generation in the atmospheres of rotating planets and satellites or in the protoplanetary disk phase of stellar formation.

This short review paper reports on results obtained, by exploiting an integrated experimental-theoretical approach, within a long-standing collaboration between the research groups in Perugia and Trento. By combining information obtained with different techniques and experimental set-ups, it will be highlighted how molecular polarization, induced in a *natural way* by anisotropic forces, plays a role on the stereodynamics of reactive and non-reactive collisions.

2. *Molecular alignment by weak anisotropic forces*

Several experimental findings suggest that, when only weak van der Waals forces are operative among the colliding partners, molecular alignment is the result of a combined effect of several elastic/inelastic collisions occurring along preferential directions in environments where anisotropic velocity distributions are operative. It is the case of supersonic expansions leading to the formation of *seeded molecular beams*, where hundreds of collisions among seeded molecules and lighter carrier atoms occur preferentially in the forward direction of the expansion. Two limiting collision regimes can be identified in the expansion zone, with increasing distance from the nozzle, where different relative collision velocities (defined as *velocity slip*) and gas densities are present (see top part of Figure 1). Molecules emerging from the nozzle suffer hundreds of collisions (both elastic and inelastic and at different impact parameters) and are accelerated, focused in the forward direction and aligned, as pictorially shown in the central and bottom part of Figure 1.

Two different experimental ways to probe the alignment degree far from the beam source have been used in the Perugia laboratory: the first one exploits the measure of the beam transmittance across a Stern-Gerlach magnetic selector and it is applicable only to paramagnetic molecules such as O_2 (Aquilanti *et al.* 1994, 1995a, b, 1998). The second one, of more general applicability, involves measurements of beam intensity attenuation in scattering experiments with a spherical target (Aquilanti *et al.* 1997).

The magnetic analysis performed on O_2 seeded beams has shown that molecules achieve a high and anomalous paramagnetism, related to a non-statistical distribution of their magnetic sublevels. The paramagnetic degree is found to increase with the final speed achieved by the molecules within the same velocity distribution, and with the pressure employed in the source (Aquilanti *et al.* 1994, 1995a). In other words, molecules flying in the head of the molecular beam, with intermediate and high supersonic character, exhibit the highest polarization degree. In addition, it was sug-

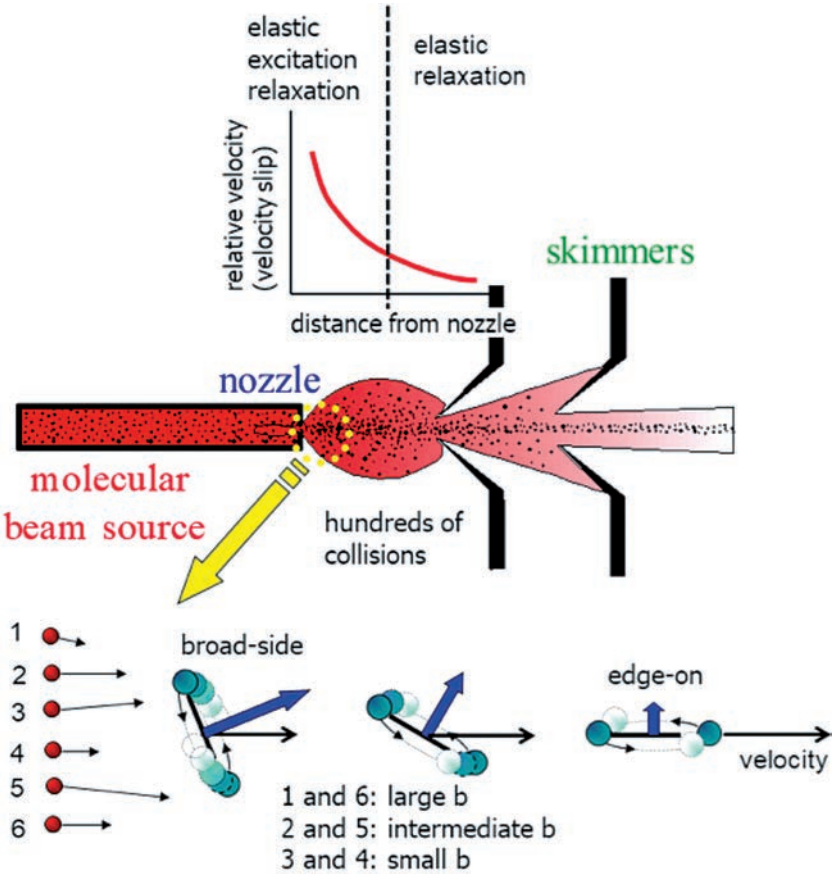

Fig. 1. *Center*: a pictorial view of the formation of a skimmed molecular beam by expansion of a gas mixture through a nozzle. *Top*: dependence of the *velocity slip* with the nozzle distance. The vertical dashed line defines the two different limiting regions: at short distance from the nozzles many body elastic and inelastic collisions lead to molecular rotational excitation and relaxation. At larger distances only elastic and inelastic processes at low energy (rotational relaxation) can occur, producing the sequence of events illustrated in the bottom part. *Bottom*: effect of collisions at different impact parameters *b*. Collisions at large impact parameters (1 and 6) are mostly elastic and lead to focusing in the forward direction; collisions at intermediate *b* (2 and 5) lead bending of the rotational plane (promoting alignment in the «edge-on» configuration); collisions at small *b* (3 and 4) lead to acceleration and relaxation.

gested that a high simultaneous/combined polarization of **K** (the rotational angular momentum) and **S** (the electronic spin angular momentum) is achieved by faster molecules (Aquilanti *et al.* 1999). A key for understanding the origin of such effect is to consider that during the collision, the intermolecular electric field strength is sufficient to decouple **K** from **S** (which are coupled to give the spin-rotational angular momentum **J** in the isolated O_2 molecule)**,** and its anisotropy (or gradient) tends to form states with *zero helicity*, that is exhibiting *zero projection* of **K** along the flying direction. Under such conditions, the unique quantization axis for **S** is the direction of the orbital angular momentum of the collision complex. After the collision **K** couples again with **S** and a polarization transfer between **K** and **S** can occur.

The extent of molecular alignment has been found to depend on the geometric features of the nozzle, on the gas density and on the resolution conditions adopted in the detection of aligned molecules (Aquilanti *et al.* 1994, 1995a, b, 1997, 1998, 1999), but it turned out to be nearly independent on the type of lighter carrier species. The latter finding led to the introduction of the *reduced speed* (i.e. the ratio between the selected molecular velocity v and the peak velocity of the molecular beam v_p) as a proper scaling factor for the alignment degree. Hence, exploiting the velocity selection technique, it has been possible to sample in a controlled way molecules flying at the same speed but having a different alignment degree, as detailed in panel *a)* of Figure 2 (Aquilanti *et al.* 1994, 1995a). By combining velocity selection with scattering experiments it was possible to measure not only velocity dependences of the cross section for projectile molecules flying with the same *reduced speed*, but also of the cross section anisotropy due to the change of the speed ratio. Results for the O_2-Kr system are shown in panel *b)* of Figure 2 (Aquilanti et al,1998). Scattering experiments were particularly useful in the case of diamagnetic N_2 projectiles (Aquilanti *et al.* 1997).

An integrated investigation exploiting scattering and spectroscopic probes has been performed on some seeded beams of hydrocarbon molecules (Pirani *et al.* 2001, 2003), while other cases of molecular polarization have been investigated with different techniques, as discussed in (Aquilanti *et al.* 2005).

3. *Molecular orientation by intermediate strength forces*

Molecular orientation controlled by anisotropic intermolecular forces of intermediate strength manifests even in single collision events if the molecules involved are in low lying rotational states. Orientation can be achieved in the presence of a permanent dipole moment for the molecular target, and the water molecule, having a large dipole moment but an electronic polarizability very close to that of O_2 and Ar, is the ideal candidate to investigate the role of different contributions to anisotropic intermolecular interactions, with special reference to intermolecular hydrogen bonds, and their effects on collision dynamics properties (Cappelletti *et al.* 2012). Even working with rotationally hot and randomly oriented projectile-target

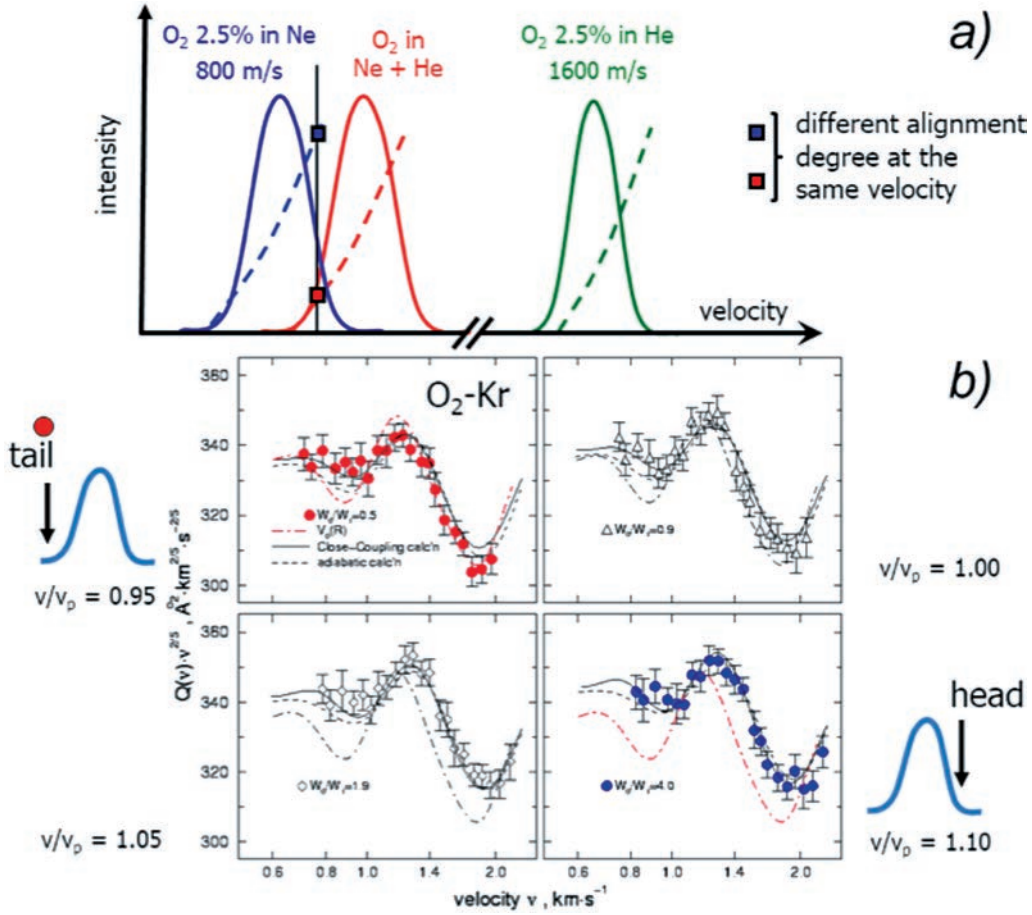

Fig. 2. *a)*: velocity distributions (solid lines) of O_2 supersonic beams seeded in increasingly lighter mixtures of atomic carriers: Ne (blue), He (green) and a Ne+He mixture (red). The dashed lines represent the speed dependence of the alignment for molecules flying within the same velocity distribution. By probing the tail of the Ne+He seeded beam (red square) or the head of the Ne seeded beam (blue square) O_2 molecules having the same speed but different alignment degree can be selected. *b)*: integral cross sections for scattering of O_2 molecules having different *reduced speed* (hence different alignment degrees) and using Kr as the spherical target.

molecule pairs, there is clear evidence that an electrostatic interaction contribution is operative, arising from the partial polarization achieved by water molecules during the collisions (Roncaratti *et al*. 2014 a, b). The anisotropic intermolecular potential between two water molecules is sufficiently strong to couple their permanent dipole moments within the field gradient, thus transforming *free rotations* into *pendular states,* a particular case of bending motion. H_2O molecules with very similar rotational periods and in low lying rotational states are more efficiently coupled, in what has been pictorially described as a *synchronized dance of water molecules* (Roncaratti *et al*. 2014 a, b).

4. *Molecular orientation by strong intermolecular forces*

Molecular orientation effects become dominant in each collision events when the anisotropic intermolecular forces have high intensities. Such a situation can occur under an ample variety of conditions, but here we will focus on collisions involving charged species. Physical and chemical processes involving ions occur in many gaseous and plasma environments (e.g. ionospheres of planets and satellites, interstellar medium, laboratory plasmas for technological applications), where ion–molecule reactions participate in the balance and redistribution of charges in the above-mentioned systems, as well as to the synthesis/destruction of chemical species. In the case of ion–molecule reactions, alignment/orientation is a general phenomenon due the large electric fields generated by the charged particle. Polarization might lead to stereodynamic effects that can either enhance or suppress reactivity. The former effect is achieved when alignment/orientation drives the collision complex into the most appropriate configurations for reaction (see the enhanced reactivity at low collision energies in the $H_2^+ + H_2 \rightarrow H_3^+ + H$ reaction, Allmendinger *et al*. 2016). The latter occurs when long-range interaction potentials reorient the reacting couple either in a non-reactive or in a configuration unfavorable for reaction, as in the case of the H-atom transfer reaction between H_2 and H_2O^+, where reorientation of H_2O^+, facilitated by rotational excitation, is necessary to promote reactivity (Li *et al*. 2014). Another example is represented by the positive temperature dependence shown in the rate constants of the barrierless and exothermic charge exchange reactions between Ar^+ and N_2^+ ions and diatomic interhalogen molecules ICl and ClF (Shuman et al. 2017). The extent of long-range ion-molecule interaction potentials are also at the basis of the effects observed on bimolecular reactivity by different rotational isomers (conformers) of a polyatomic molecule in the gas phase (Chang *et al*. 2013; Rösch *et al*. 2014).

Collisions with He^+ are an important pathway for the decomposition of «complex organic molecules» (COMs, i.e. molecules containing at least six atoms) in the interstellar medium. Within this framework, we recently investigated charge transfer reactions of He^+ with dimethyl ether CH_3OCH_3 (DME) and methylformate $HCOOCH_3$ (MF), two amongst the most abundant COMs with a prebiotic rele-

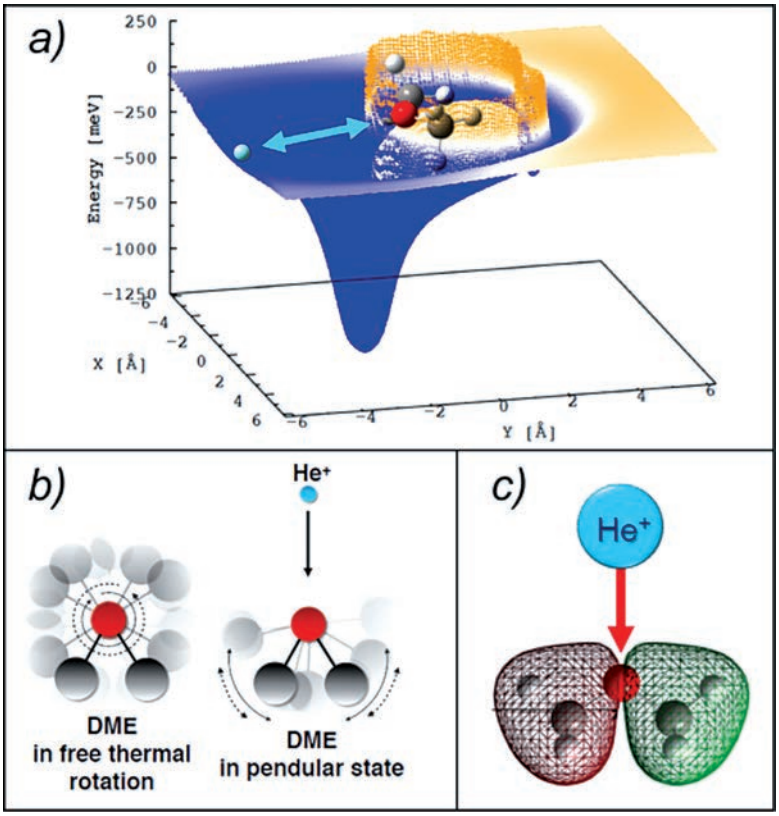

Fig. 3. *a)*: Cut of the potential energy hypersurface (with the He^+ ion confined in the plane defined by the C-O-C atoms) for the entrance channel of the He^+-DME system. *b)* Pictorial representation of the formation of a *pendular state* during collisions between He^+ and DME: at large ion-neutral distances the molecule is rotating freely (left), while at shorter distances (right) the PES anisotropy is so prominent that free rotations are hampered and DME librates around the direction of preferential orientation; *c)* electron density distribution for one of the inner valence molecular orbitals of DME involved in the electron transfer process with He^+.

vance for their capability of acting as building blocks for sugars and biopolymers (Balucani *et al.* 2015). Using the Guided Ion Beam Mass Spectrometer in Trento reactive cross sections and branching ratios (BRs) as a function of the collision energy have been measured (Cernuto *et al.* 2017, 2018). Due to the large dipole moments exhibited by the neutral collision partners the studied systems present large interaction anisotropies that can induce strong steroedynamic effects and influence the outcome of reactive collisions. The experimental evidence is that electron exchange processes are completely dissociative, leading to extensive fragmentation of the neutral partner, and cross section trends with collision energies are at odds

with those expected from simple *capture models*. By investigating the nature of the non-adiabatic transitions between the reactant and product potential energy surfaces using an improved Landau-Zener model, we were able to identify three critical elements at the basis of such discrepancy: the strong anisotropy of the potential energy hypersurface (PES) in the entrance channel, the crossings among entrance and exit PESs and the symmetry of the electron density distributions of the molecular orbitals involved in the electron transfer to He^+ (Cernuto *et al.* 2017, 2018). The presence of deep potential wells for selected configurations of the reacting couple induces pronounced orientations of the polar neutrals in the electric field generated by the cation (*i.e.* formation of *pendular states* in which the molecule librates around a preferential direction), thus channelling most of the molecules in narrow angular cones confined around the most attractive configurations of the interacting systems. A cut of the PES for the He^+-DME system is reported in panel *a)* of Figure 3, while a pictorial view of the formation of *pendular states* is shown in panel *b)* of the same Figure. The crossing positions among entrance and exit PESs force He^+ to capture an electron from an inner valence molecular orbital of the organic molecules, thus producing quickly dissociating molecular cations in highly excited states. The symmetry of the electron density distribution of the molecular orbitals from which the electron is removed affects the probability of electron transfer to He^+. For both DME and MF the overlap integral between the orbitals involved in the electron exchange is unfavourable (see panel *c)* of Figure 3 for the He^+-DME case), thus originating the paradox that the most attractive geometry is the least efficient for charge transfer.

As general conclusion, it is proper to stress that molecular polarization effects, induced in all investigated cases by anisotropic intermolecular forces of different strength, tend to become more prominent under sub-thermal conditions. Hence they should be properly taken into account when modelling non-reactive as well as reactive systems in low temperature environments such as the interstellar medium and planetary atmospheres.

REFERENCES

Allmendinger P., Deiglmayr J., Hçveler K., Schullian O., Merkt F. (2016). Observation of enhanced rate coefficients in the $H_2^+ + H_2 \rightarrow H_3^+ + H$ reaction at low collision energies. J. Chem. Phys., 145, 244-316.

Aquilanti V., Ascenzi D., Cappelletti D., Pirani F. (1994). Velocity dependence of the collisional alignment of oxygen molecules in gaseous expansions. Nature 371:399-402.

Aquilanti V., Ascenzi D., Cappelletti D., Pirani F. (1995a). Rotational alignment in supersonic seeded beams of molecular oxygen. J. Phys. Chem. 99: 13620-13626.

Aquilanti V., Ascenzi D., Cappelletti D., Franceschini S., Pirani F. (1995b). Scattering of rotationally aligned oxygen molecules and the measurement of anisotropies of van der Waals forces. Phys. Rev. Lett. 74:2929-2932.

Aquilanti V., Ascenzi D., Cappelletti D., Fedeli R., Pirani F. (1997). Molecular beam scattering of nitrogen molecules in Supersonic seeded beams: A probe of the Rotational alignment. J. Phys. Chem. A 101:7648-7656.

Aquilanti V., Ascenzi D., Cappelletti D., de Castro Vitores M., Pirani F. (1998). Scattering of aligned molecules. The potential energy surfaces for the Kr-$O_2$and Xe-O_2 Systems. J. Chem. Phys. 109: 3898-3910.

Aquilanti V., Ascenzi D., de Castro Vitores M., Pirani F., Cappelletti D. (1999). A quantum mechanical view of molecular alignment and cooling in seeded supersonic expansion. J. Chem. Phys. 111: 2620-2632.

Aquilanti V., Bartolomei M., Pirani F., Cappelletti, Vecchiocattivi F., Shimizu Y., Kasai T. (2005). Orienting and Aligning molecole for stereochemistry and photodynamics. Phys. Chem. Chem. Phys. 7:291-300.

Balucani N., Ceccarelli C., Taquet V. (2015). Formation of complex organic molecules in cold objects: the role of gas-phase reactions. Monthly Notice Royal Astronomical Society 449, L16

Cappelletti D., Ronca E., Belpassi L., Tarantelli F., Pirani F. (2012). Revealing charge-transfer effects in gas-phase water chemistry. Acc. Chem. Res. 45:1571-1580.

Cernuto A., Tosi P., Martini L.M., Pirani F., Ascenzi D. (2017). Experimental investigation of the reaction of helium ions with dimethyl ether: stereodynamics of the dissociative charge exchange process. Phys. Chem. Chem. Phys. 19:19554-19565.

Cernuto A., Pirani F., Martini L.M., Tosi P., Ascenzi D. (2018). The selective role of long range forces in the stereodynamics of ion molecule reactions: The He^+ + methyl formate case from guided ion-beam experiments. ChemPhysChem 19:51-59.

Chang Y.-Pin., Długołęcki K., Küpper J., Rösch D., Wild D., Willitsch S. (2013). Specific Chemical Reactivities of Spatially Separated 3-Aminophenol Conformers with Cold Ca^+ Ions. Science 342, 98-101

Li A., Li Y., Guo H., Lau K.C., Xu Y., Xiong B., Chang Y.C., Ng Y.C. (2014). Communication: The origin of rotational enhancement effect for the reaction of H_2O^+ +H_2 (D_2). J. Chem. Phys. 140, 011102-011111.

Lombardi A., Palazzetti F. (2018). Chirality in molecular collision dynamics. J. Phys. Condensed Matter 30, 063003.

Pirani F., Cappelletti D., Bartolomei M., Aquilanti V., Scotoni M., Vescovi M., Ascenzi D., Bassi D. (2001). Orientation of benzene in supersonic expansions, probed by IR-laser absorption and by molecular beam scattering. Phys. Rev. Lett. 86, 5053-5038.

Pirani F., Bartolomei M., Aquilanti V., Scotoni M., Vescovi M., Ascenzi D., Bassi D., Cappelletti D. (2003). Collisional orientation of the benzene molecular plane in supersonic seeded expansions, probed by infrared polarized laser absorption spectroscopy and by molecular beam scattering. J. Chem. Phys. 119265, 276.

Roncaratti L.F., Cappelletti D., Pirani F. (2014). The spontaneous synchronized dance of pair of water molecules. J. Chem. Phys. 140124318.

Roncaratti L.F., Cappelletti D., Candori P., Pirani F. (2014). Polar molecules engaged in pendular states captured by molecular-beam scattering experiments. Phys. Rev. A 90:012705.

Rösch D., Willitsch S., Chang Y.-Pin, Küpper J. (2014). Chemical reactions of conformationally selected 3-aminophenol molecules in a beam with Coulomb-crystallized Ca^+ ions. J. Chem. Phys. 140,124202.

Shuman N., Martinez O., Ard S., Wiens J., Keyes N., Guo H., Viggiano A. (2017). Surprising behaviors in the temperature dependent kinetics of diatomic interhalogens with anions and cations. J. Chem. Phys. 146, 214307.

Su, T.-M., Palazzetti F., Lombardi A., Grossi G., Aquilanti V. (2013). Molecular alignment and chirality in gaseous streams and vortices. Rendiconti Lincei-Scienze Fis. & Nat. 24, 291-297.

Vattuone L., Savio L., Pirani F., Cappelletti D., Okada M., Rocca M. (2010). Interaction of rotationally aligned and of oriented molecules in gas phase and at surfaces. Prog. Surf. Sci. 85, 92-160.

Rendiconti
Accademia Nazionale delle Scienze detta dei XL
Memorie di Scienze Fisiche e Naturali
136° (2018), Vol. XLII, Parte II, Tomo II, pp. 91-98

PIERGIORGIO CASAVECCHIA[1] – ADRIANA CARACCIOLO[1]
GIANMARCO VANUZZO[1] – NADIA BALUCANI[1]

Crossed molecular beam experiments on bimolecular reactions of relevance in astrochemistry: the case of atomic oxygen reactions with small unsaturated hydrocarbons

Abstract – The presence of atomic oxygen in the interstellar medium is one of the factors that limit the growth of the carbon skeleton of organic molecules, as it easily degrades organic molecules into CO or one of its precursors (e.g. HCO). Yet, its reactions can actually lead to the formation of O-rich organic molecules like esters or carboxylic acids. In this contribution, we summarize recent experimental work on the reactions between atomic oxygen and small unsaturated hydrocarbons performed in our laboratory by means of the crossed molecular beam techniques with mass spectrometric detection. Our results show that, even if C-C bond fission dominates the reaction mechanism in most cases, interesting O-bearing radicals are formed that can further foster the chemical complexity of interstellar organic molecules.

1. *Introduction*

Oxygen is an important player in the chemistry of the Universe, being the third most abundant element. Even though its mole fraction is only 477 ppm, it is more abundant than carbon (326 ppm) and nitrogen (102 ppm) and exhibits a rich chemistry, contrarily to the two most abundant elements, hydrogen and helium, characterized by mole fractions of 90.9964% and 8.8714%, respectively. Among the various extraterrestrial environments, interstellar clouds (that is, the regions of the

[1] Dipartimento di Chimica, Biologia e Biotecnologie, Università degli Studi di Perugia, Via Elce di Sotto, 8 – 06123 Perugia, Italy.
E-mail: piergiorgio.casavecchia@unipg.it; nadia.balucani@unipg.it

interstellar medium where most of matter outside solar systems gathers, with number densities as low as 10^4 molecules/cm^3 and temperatures ranging from 10 to 100 K) are the subject of great interest, because these are the regions of galaxies where new stars, and their solar systems, are formed (Caselli and Ceccarelli, 2012). Since we cannot directly reconstruct the evolution of our own star and solar system, neither can we observe the birth of a new star in real time because the timescale is outside the human range, the best approach to understand how Sun and its Solar System were formed is to analyze different interstellar objects in different evolutionary stages and try to recreate the sequence of steps that leads from a diffuse cloud to a Sun-like star and its planets (Caselli and Ceccarelli, 2012). The observation of relatively complex organic molecules (McGuire, 2018) in all the stages that are believed to lead to star formation seems to suggest that interstellar clouds can be the chemical factories where massive synthesis of organic molecules occurs, thus providing the newly formed solar systems with the inventory of the simple organic molecules necessary to trigger (if the planet conditions are favorable) the emergence of life (Caselli and Ceccarelli, 2012; Balucani, 2009). This vision gains support from the observation of plenty of complex chemicals (including aminoacids and other prebiotic molecules) in the small bodies of our solar systems (asteroids, meteorites, comets and even interplanetary dust particles) that are supposed to be the carriers that bring interstellar molecules (and the products of their chemical evolution) to the newly formed planets (Ehrenfreund *et al*., 2002).

Given the predominance of hydrogen, oxygen is mainly sequestered as water. In cold objects, it is assumed to be strongly depleted from the gas-phase being the main constituent of the water-ice mantles that cover interstellar dust particles (Occhiogrosso *et al*., 2013). Also, a significant fraction is segregated into CO, a very abundant interstellar molecule. Yet, the presence of residual oxygen in atomic form can have a strong influence in the formation and destruction of interstellar complex organic molecules (Occhiogrosso *et al*., 2013). In particular, because of its capability of reacting with organic molecules in a destructive way, the presence of atomic oxygen can severely reduce the chemical complexity of the available organic species.

In this contribution, we will show several cases in which atomic oxygen degrades organic molecules. In particular, we will analyze several examples of reactions with unsaturated hydrocarbons. As we are going to see, oxygen atoms are even more effective than we thought in inducing the break-up of C-C bonds and in degrading them directly towards CO or CO precursors. However, at the same time the reactions of atomic oxygen with organic molecules allow for the formation of other complex molecular species (Balucani *et al.* 2015, Skouteris *et al*. 2018) that can, instead, foster the chemical growth of prebiotic molecules. Quite interestingly, indeed, among the so-called interstellar complex organic molecules (iCOMs), those which are by far the most abundant do contain oxygen, namely formaldehyde, methanol, dimethyl ether, methyl formate etc. (Ceccarelli *et al*., 2017, McGuire, 2018). In this contribution, we will briefly summarize the main results obtained in

our laboratory by means of the crossed molecular beam technique with mass spectrometric detection on the reactions of atomic oxygen with unsaturated hydrocarbons (Casavecchia *et al.*, 2015). Among the results we have obtained, the focus will be on the product branching ratios. We will also analyze the effect of those revised branching ratios in the chemistry of interstellar clouds and the role of atomic oxygen in the organic chemistry of interstellar objects (Occhiogrosso *et al.*, 2013).

2. *Experimental method*

In our laboratory, we use the crossed molecular beam technique coupled to mass spectrometric detection. The basic scheme of our apparatus follows the classical design by Lee and coworkers (for a scheme of our apparatus in its recent version see Casavecchia *et al.* 2015, 2009; for the original work by Lee and coworkers, see Lee *et al.* 1969). Our machine features an efficient radio frequency discharge beam source for the production of intense supersonic beams of atomic or diatomic radicals (see Alagia *et al.* 1996 and Leonori *et al.* 2010). When applied to the production of beams of atomic oxygen, we obtain a very high degree of dissociation starting from a dilute mixture of molecular oxygen in helium or neon. Atomic oxygen is produced mainly in its ground ^{3}P state, with a small percentage (around 5%, see Alagia *et al.* 1996) in the first electronically excited state ^{1}D.

The observables of this experimental technique are the product angular and time-of-flight distributions (Balucani *et al.*, 2006). From these quantities, we can gain insights into the reaction mechanism and product branching ratios. In particular, the product branching ratios are of interest in the context of applied chemistry, because the products of one elementary reaction are the reactants of subsequent ones in the intricate networks of elementary chemical reactions that account for the global transformation. Since most of the kinetics experimental techniques are designed to record the disappearance rate of one reactant, rather than determining the appearance rate of products, our experimental results nicely complement the results of kinetics experiments.

3. *The reaction of atomic oxygen with hydrocarbon containing a triple bond*

In our laboratory, we have investigated the reaction of atomic oxygen in its ground state with ethyne and propyne (Leonori *et al.*, 2014; Vanuzzo *et al.* 2016). No experimental evidence of the reactions involving O(^{1}D) was obtained at the mass-to-charge ratios investigated. In both cases, we have verified that the initiation of the reaction occurs with the addition of the electrophilic atomic oxygen to the π system of the alkyne. In the case of ethyne, because of its symmetric structure, only two sets of products have been observed, that is HCCO + H (O/H exchange channel) and CO + CH_2 (C-C bond breaking channel). The O/H exchange channel is dominant (accounting for *ca.* 80%) under all the experimental conditions investi-

gated. There is no experimental evidence of the occurring of intersystem crossing (ISC) to the underlying singlet potential energy surface. Several theoretical studies (Gimondi *et al*., 2016; Rajak and Maiti, 2014; Nguyen *et al*., 2006) confirm our data in this respect. In the case of the reaction with propyne, given that also in this case the initial attack is towards the π system of the molecule, the asymmetry of the molecule makes more channels possible. In addition, the occurrence of ISC is very important in this case. In Table 1 are reported the product branching ratios (B. R.) under the conditions of our experiments.

Table 1. Experimental branching ratios of the two simplest O + alkyne reactions at E_c~10 kcal/mol.

Reaction channel	O + HCCH	B. R.	O + CH_3CCH	B. R.
H	H + HCCO	**0.79**	H + CH_3CCO	**0.04**
CH_3	-		CH_3 + HCCO	**0.10**
CO	CH_2 + CO	**0.21**	C_2H_4/$CHCH_3$+CO	**0.74**
HCO	-		HCO + C_2H_3	**0.11**
H_2	-		CHCCO + H_2	**0.01**

4. *The reaction of atomic oxygen with hydrocarbons containing one double bond*

In our laboratory, we have investigated the reaction of atomic oxygen in its ground state with ethene, propene and 1-butene (Fu *et al*., 2012; Balucani *et al.* 2015b; Leonori *et al*., 2015; Caracciolo *et al*., 2017). In all cases, we have verified that the initiation of the reaction occurs with the addition of the electrophilic atomic oxygen to the π system of alkenes. The main result of our investigation is that there is a facile pathway leading directly to the formation of formaldehyde, accounting for 20%, 44% and 15% of the reaction involving ethene, propene and 1-butene, respectively (see Table 2 and Caracciolo *et al*., 2017). This was unexpected for the reactions with propene and 1-butene. ISC is also important for these reactive systems, but its extent varies from system to system, as a result of the detailed characteristics of the associated triplet and singlet potential energy surfaces and their coupling terms. In the case of the reaction $O(^3P)+C_2H_4$, we have compared our detailed observables with the predictions of quasiclassical trajectories calculations on an accurate potential energy surface where the occurrence of ISC was explicitly considered. This comparison fully corroborates our experimental findings (Fu *et al*. 2012; Balucani *et al*. 2015b).

Table 2. Experimental branching ratios of the two simplest O + alkene reactions at E_c ~ 9 kcal/mol.

Reaction channel	$O + CH_2=CH_2$	B. R.	$O + CH_3\text{-}CH=CH_2$	B. R.
H	$H + CH_2CHO$	**0.30**	$H + CH_3CHCHO$	**0.07**
H	$H + CH_3CO$	**0.03**	$H + CH_3COCH_2$	**0.05**
CH_3	$CH_3 + HCO$	**0.34**	CH_3+CH_2CHO/CH_3CO	**0.32**
H_2CO	$CH_2 + H_2CO$	**0.20**	$CHCH_3/C_2H_4 + H_2CO$	**0.44**
H_2	$H_2 + CH_2CO$	**0.13**	$CH_3CHCO + H_2$	**0.03**
C_2H_5	-		$C_2H_5 + HCO$	**0.09**

5. *Astrophysical implications*

The new branching ratios derived in our laboratory for the reactions $O+C_2H_2$, CH_3CCH, C_2H_4 and CH_2CCH_2 have been tested in astrochemical models of interstellar clouds (Occhiogrosso *et al.* 2013) for four different scenarios corresponding to the conditions of *i*) diffuse clouds, *ii*) translucent clouds, *iii*) dark cores and *iv*) hot cores. Important differences were noted with respect to the previous models referring to the data set of UMIST 2006 (one of the most used databases for astrochemistry, now evolved in the more recent UMIST 2012, see Woodall *et al.* 2007 and McElroy *et al.*, 2013). The new branching ratios affect the abundances of several observed species in the case of hot cores. The main differences have been highlighted in Figure 2 and Table 6 of the paper by Occhiogrosso *et al.* 2013. Apart from some interesting effects on the species which are already considered in the models (such as CH_2, CH_3, CH_2CO or C_2H_2 and C_2H_4 themselves), the inclusion of new species can have a profound influence in the outcome of astrochemical models. For instance, in Figure 2 the abundances of the newly inserted species CH_2CHO/CH_3CO and CH_3CCO reach very high, unrealistic values because no destruction pathways were included. This is a way to estimate the maximum impact of these species in different evolutionary stages of hot cores. In real cases, when chemical destruction routes will be included, their reactions with other constituents of hot cores (ion species, for instance, or other abundant reactive radicals) could lead to more complex molecules bearing an oxygen atom. We remind that several of the hot cores considered in Occhiogrosso *et al.* (2013) are the objects where a large number of molecular species, complex to some extent and rich in oxygen (*e.g.* methyl acetate, ethyl formate, methoxymethanol), have been detected (McGuire, 2018). In other words, even if the presence of atomic oxygen impedes the growing up of the skeleton of C-atoms, it might lead to the formation of O-rich organic molecules.

This suggestion is actually supported by two modelling studies, in which the reactions of atomic oxygen with organic radicals already bearing an oxygen atom were invoked to lead to the formation of methyl formate, glycolaldehyde and acetic acid. Methyl formate, indeed, results from the sequence of reactions (S1) (see Balucani *et al.*, 2015a), while glycolaldehyde and acetic acid result from the sequence of reactions (S2a,b) (see Skouteris *et al.*, 2018) in the gas phase, starting from saturated molecules which can well be formed by surface-induced hydrogenation on interstellar dust particles:

$$CH_3OCH_3 \xrightarrow{OH,Cl} CH_3O\dot{C}H_2 \xrightarrow{O} CH_3OCHO \quad (S1)$$

$$CH_3CH_2OH \xrightarrow{OH,Cl} CH_3\dot{C}HOH \xrightarrow{O} CH_3COOH \quad (S2a)$$

$$CH_3CH_2OH \xrightarrow{OH,Cl} \dot{C}H_2CH_2OH \xrightarrow{O} HCOCH_2OH \quad (S2b)$$

In this sense, the role of atomic oxygen is strategical in converting the saturated species possibly produced by heterogeneous processes on the dust surface into much more complex and variegated species.

In conclusion, as expected, the reactions of atomic oxygen with organic molecules have the capability of degrading them by inducing the fission of C-C bonds. At the same time, however, new radicals containing an O-atom are formed and they can, in turn, lead to the formation of O-rich organic molecules. Some of these species (glycolaldehyde, acetic acid) are widely detected in space and are considered to be prebiotic species, being potential precursors of sugars and aminoacids.

A more general conclusion is that only the detailed knowledge of the reactions leading to the formation of the most important prebiotic molecules will help us to understand if the chemistry that precedes life emergence is common in the Universe and, in turn, if life is possible outside our Solar System.

Acknowledgments. Financial support by «Fondazione Cassa Risparmio Perugia» (Project 2015.0331.021 Scientific&Technological Research) and MIUR (PRIN 2015, STARS in the CAOS, 2015F59J3R) is gratefully acknowledged.

REFERENCES

Alagia M., Aquilanti V., Ascenzi D., Balucani N., Cappelletti D., Cartechini L., Casavecchia P., Pirani F., Sanchini G., Volpi G. G. (1997). Magnetic analysis of supersonic beams of atomic oxygen, nitrogen and chlorine generated from a radio-frequency discharge. Israel Journal of Chem. 37, 329.

Balucani N. (2009). Elementary reactions and their role in gas-phase prebiotic chemistry. International Journal of Molecular Sciences 10, 2304.

Balucani N., Capozza G., Leonori F., Segoloni E., Casavecchia P. (2006). Crossed molecular beam reactive scattering: from simple triatomic to multichannel polyatomic reactions. International Reviews in Physical Chemistry 25, 1952.

Balucani N., Ceccarelli C., Taquet V. (2015a). Formation of complex organic molecules in cold objects: the role of gas-phase reactions. Monthly Notices of the Royal Astronomical Society 449, L16.

Balucani N., Leonori F., Casavecchia P., Fu B., Bowman J. M. (2015b) Crossed molecular beams and quasiclassical trajectory surface hopping studies of the multichannel nonadiabatic $O(^3P)$+ethylene reaction at high collision energy. The Journal of Physical Chemistry A 119, 12498.

Caracciolo A., Vanuzzo G., Balucani N., Stranges D., Cavallotti C., Casavecchia P. (2017). Observation of H-displacement and H_2 elimination channels in the reaction of $O(^3P)$ with 1-butene from crossed beams and theoretical studies. Chemical Physics Letters 683, 105; and to be published.

Casavecchia P., Leonori F., Balucani N., Petrucci R., Capozza G., Segoloni E. (2009). Probing the dynamics of polyatomic multichannel elementary reactions by crossed molecular beam experiments with soft electron-ionization mass spectrometric detection. Physical Chemistry Chemical Physics 11, 46.

Casavecchia p., Leonori F., Balucani N. (2015). Reaction dynamics of oxygen atoms with unsaturated hydrocarbons from crossed molecular beam studies: primary products, branching ratios and role of intersystem crossing. International Reviews in Physical Chemistry 34, 161.

Ceccarelli C., Caselli P., Fontani F., Neri R., López-Sepulcre A., Codella C., Feng S., Jiménez-Serra I., Lefloch B., Pineda J. E., Vastel C., Alves F., Bachiller R., Balucani N., Bianchi E., Bizzocchi L., Bottinelli S., Caux E., Chacón-Tanarro A., Choudhury R., Coutens A., Dulieu F., Favre C., Hily-Blant P., Holdship J., Kahane C., Jaber Al-Edhari A., Laas J., Ospina J., Oya Y., Podio L., Pon A., Punanova A., Quenard D., Rimola A., Sakai N., Sims I. R., Spezzano S., Taquet V., Testi L., Theulé P., Ugliengo P., Vasyunin A. I., Viti S., Wiesenfeld L., Yamamoto S. (2017). Seeds Of Life In Space (SOLIS): The organic composition diversity at 300–1000 au scale in solar-type star-forming regions. The Astrophysical Journal 850, 176.

Ehrenfreund P., Irvine W., Becker L., Blank J., Brucato J. R., Colangeli L., Derenne S., Despois D., Dutrey A., Fraaije H., Lazcano A., Owen T., Robert F. (2002). Astrophysical and astrochemical insights into the origin of life. Reports on Progress in Physics 65, 1427.

Fu B., Han Y.-C., Bowman J. M., Angelucci L., Balucani N., Leonori F., Casavecchia, P. (2012) Intersystem crossing and dynamics in $O(^3P) + C_2H_4$ multichannel reaction: experiment validates theory. Proceedings of the National Academy of Sciences of the United States of America 109, 9733.

Ilaria Gimondi, Carlo Cavallotti, Gianmarco Vanuzzo, Nadia Balucani, Piergiorgio Casavecchia (2016). Reaction dynamics of $O(^3P)$ + propyne: II. Primary products, branching ratios, and role of intersystem crossing from ab initio coupled triplet/singlet potential energy surfaces and statistical calculations. The Journal of Physical Chemistry A 120, 4619.

Lee Y. T., McDonald J., LeBreton P., Herschbach D. (1969). Molecular beam reactive scattering apparatus with electron bombardment detector. Review of Scientific Instruments 40, 1402.

Leonori F., Hickson K. H., Le Picard S., Wang X., Petrucci R., Foggi P., Balucani N., Casavecchia P. (2010). Crossed-beam universal-detection reactive scattering of radical beams characterized by laser-induced-fluorescence: the case of C_2 and CN. Molecular Physics 108, 1097.

Leonori F., Balucani N., Capozza G., Segoloni E., Volpi G. G., Casavecchia P. (2014). Dynamics of the $O(^3P) + C_2H_2$ reaction from crossed molecular beam experiments with soft electron ionization detection. Physical Chemistry Chemical Physics 16, 10008.

Leonori F., Balucani N., Nevrly V., Bergeat A., Falcinelli S., Vanuzzo G., Casavecchia P., Cavallotti C. (2015). Experimental and theoretical studies on the dynamics of the $O(^3P)$ + propene reaction: primary products, branching ratios, and role of intersystem crossing. The Journal of Physical Chemistry C 119, 14632

McGuire B. A. (2018). 2018 Census of interstellar, circumstellar, extragalactic, protoplanetary disk, and exoplanetary molecules. The Astrophysical Journal Supplement Series 239, 17.

McElroy D., Walsh C., Markwick A.J., Cordiner M.A., Smith K., Millar T.J. (2013). The UMIST database for astrochemistry 2012. Astronomy and Astrophysics 550, A36.

Nguyen T. L., Peeters J., Vereecken L. (2006). Quantum chemical and theoretical study of the $O(^3P) + C_2H_2$ reaction: a multistate process. The Journal of Physical Chemistry 110, 6696.

Occhiogrosso A., Viti S., Balucani N. (2013). An improved chemical scheme for the reactions of atomic oxygen and simple unsaturated hydrocarbons - implications for star-forming regions. Monthly Notices of the Royal Astronomical Society 432, 3423.

Rajak, K., Maiti, B. (2010). Trajectory surface hopping study of the $O(^3P) + C_2H_2$ reaction dynamics: effect of collision energy on the extent of intersystem crossing. The Journal of Chemical Physics 140, 044314.

Skouteris D., Balucani N., Ceccarelli C., Vazart F., Puzzarini C., Barone V., Codella C., Lefloch B. (2018). The genealogical tree of ethanol: gas-phase formation of glycolaldehyde, acetic acid and formic acid. The Astrophysical Journal 854, 135.

Vanuzzo G., Balucani N., Leonori F., Stranges D., Nevrly V., Falcinelli S., Bergeat A., Casavecchia P., Cavallotti, C. (2016). Reaction dynamics of $O(^3P)$ + propyne: I. primary products, branching ratios, and role of intersystem crossing from crossed molecular beam experiments. The Journal of Physical Chemistry A 120, 4603.

Woodall J., Agúndez M., Markwick-Kemper A. J. , Millar T. J. (2007). The UMIST database for astrochemistry 2006. Astronomy and Astrophysics 466, 1197.

Rendiconti
Accademia Nazionale delle Scienze detta dei XL
Memorie di Scienze Fisiche e Naturali
136° (2018), Vol. XLII, Parte II, Tomo II, pp. 99-105

M. SATTA[1] – M.H.D. VAN DER WIEL[2] – D.A. NAYLOR[3]
G. MAKIWA[3] – A. ABERGEL[4]

HF molecule as a tracer of column density in interstellar diffuse gas: the adsorption on dust grain surfaces

Abstract – The HF molecule has been proposed as a sensitive tracer of diffuse interstellar gas, but at higher densities its abundance could be influenced heavily by freeze-out onto dust grains, and hence it can lead to a distortion as a mass tracer if these freeze-out effects are not properly taken into account. At this regard it is important to refer to the study of the spatial distribution of a collection of absorbing gas clouds, some associated with the dense, massive star-forming core NGC6334 I, and others with diffuse foreground clouds elsewhere along the line of sight. A far-infrared spectral imaging has been used from the Herschel SPIRE iFTS to construct a map of HF absorption at 243 mm in a region surrounding NGC6334 I and I(N). These data also imply a lack of gas-phase HF in the envelope of core I(N). Using a simple description of adsorption onto and desorption from dust grain surfaces, it can be shown that the overall lower temperature of the envelope of source I(N) is consistent with freeze-out of HF, while it remains in the gas phase in source I. The HF molecule can be used as a tracer of column density in diffuse gas ($n_H \approx 10^2$–10^3 cm^{-3}), and it may uniquely traces a relatively low-density portion of the gas reservoir available for star formation that otherwise escapes detection. At higher densities prevailing in protostellar envelopes ($\geq 10^4$ cm^{-3}), there are evidences of HF depletion from the gas phase under sufficiently cold conditions.

[1] CNR-ISMN, Department of Chemistry, University of Rome «Sapienza», Italy.
[2] Centre for Star and Planet Formation, Niels Bohr Institute & Natural History Museum of Denmark, University of Copenhagen, Denmark.
[3] Institute for Space Imaging Science, Department of Physics & Astronomy, University of Lethbridge, Canada.
[4] Institut d'Astrophysique Spatiale, CNRS, Univ. Paris-Sud, Université Paris-Saclay, France.

Introduction

Atomic fluoride is the only element in the interstellar chemistry which is mainly neutral, because of its ionization potential >13.6 eV, reacts exothermically with H_2 to form neutral HF, and lacks an efficient chemical pathway to produce its hydride cation HF^+ due to the strongly endothermic nature of the reaction with H_3^+. For these reasons chemical models predict that essentially all interstellar F is locked in HF molecules [1, 2], which has been confirmed by observations across a wide range of atomic and molecular ISM conditions [3]. Galactic [4] and extragalactic [5] interferometric observations show that CF^+, the next most abundant F bearing species after HF, has an abundance roughly two orders of magnitude lower than HF. As for destruction of HF, the most efficient processes are UV photodissociation and reactions with C^+, but both of these are unable to drive the majority of fluoride out of HF [2]. Because of the constant HF/H_2 abundance ratio and the high probability that HF molecules are in the rotational ground state, measurements of HF J=0→1 absorption provide a straightforward proxy of H_2 column density. This has led to the suggestion that, at least in diffuse gas, HF absorption is a more reliable tracer of total gas column density than the widely used carbon monoxide (CO) rotational emission lines, and is more sensitive than CH or H_2O absorption [6].

Based on the above arguments, HF absorption measurements are a good tracer of overall gas column density. However, HF itself may suffer from freeze-out effects [7, 8] and the density and temperature conditions needed for HF adsorption onto dust grains have been studied in astrophysical contexts [9]. (Figure 1 is adapted from Ref. 9).

Discussion

Any freeze-out of interstellar HF will obfuscate the direct connection between HF absorption depth and H_2 column density described above. A proper analysis [9] of these freeze-out effects has been carried out by studying the filamentary, star-forming cloud NGC 6334, at a distance of 1.35 kpc, which harbors a string of dense cores: specifically the region of ~ 2.4 × 1.6 pc surrounding the embedded cores NGC 6334 I and NGC 6334 I(N) (See Fig. 1). The mass of source I(N) exceeds that of sister source I by a factor of ~ 2-5, but the ratio of their bolometric luminosities is 30-140 in favour of source I because of the markedly lower temperature for source I(N). Core I is in a more evolved stage of star formation than core I(N).

Envelope of core I(N) is more massive than that of core I, but has a similar size, hence its total gas column density toward core I(N) should be higher. On the contrary the map of equivalent width of the HF 1 ← 0 absorption neglects this assumption. This can be explained if the the lack of HF absorption associated with the I(N) core is not due to the difference in total (H_2) column, but to the fact that HF is primarily frozen out onto dust grains in core I(N), while HF is in the gas phase in core I.

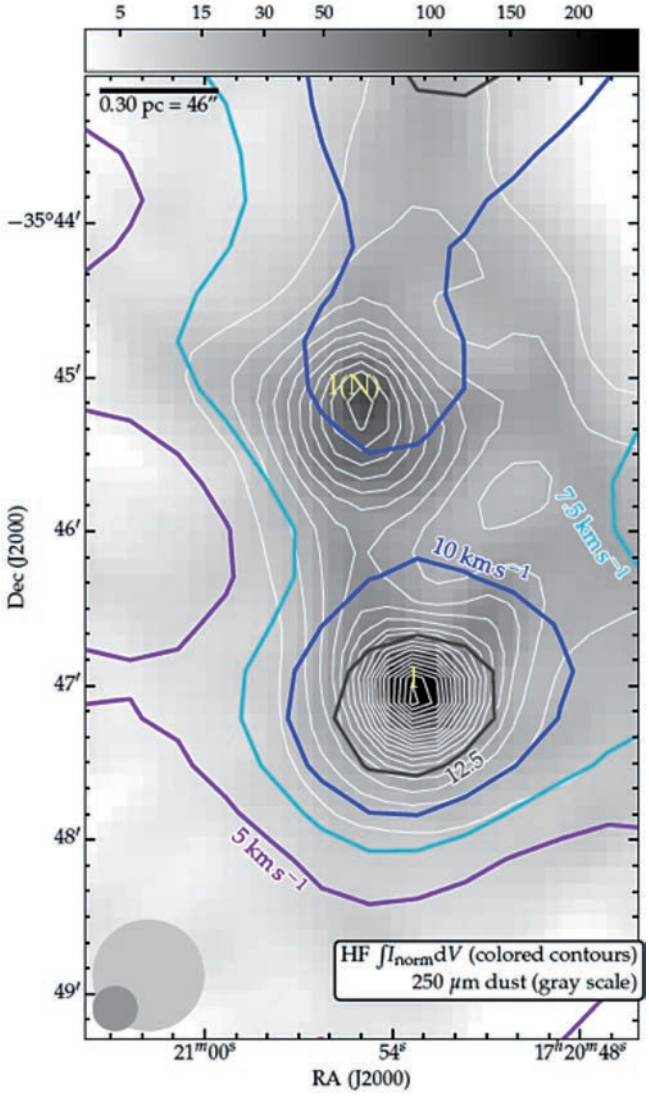

Fig. 1. Map of equivalent width of the HF 1←0 absorption signature measured with Herschel SPIRE iFTS (see ref. 9).

To support the hypothesis of HF being depleted from the gas phase in core I(N), a rudimentary model has been adopted (see ref 9 and references therein). We assume that thermal desorption is the dominant mechanism that drives molecules from the grain surface back into the gas phase, where λ, and ξ, are respectively the adsorption and the desorption rate:

$$\lambda\left(n_{\mathrm{H}},\, T_{gas}\right) = 4.55\times10^{-18}\left(\frac{T_{gas}}{m_{HF}}\right)^{0.5} n_H \quad [s^{-1}] \tag{1}$$

$$\xi\left(T_{dust}\right) = \nu_{vib} exp\left(\frac{-E_{b,HF}}{kT_{dust}}\right) \qquad [s^{-1}] \tag{2}$$

Here, T_{gas} and T_{dust} are the temperatures of gas and dust, m_{HF} is the molecular weight of HF, n_H is the density of hydrogen nuclei, ν_{vib} is the vibrational frequency of the HF molecule in its binding site, for which we adopt 10^{13} s^{-1}, k is the Boltzmann constant, and $E_{b,HF}$ is the binding energy of HF to the dust grain surface. Typical interstellar dust grains, especially those embedded in cold, star-forming regions, are covered in one or multiple layers of ice consisting of various molecules, mainly H_2O, CO, and CO_2 [10]. We collect binding energy values for several types of grain surfaces in Table 1. For CO and CO_2 ice covered grains we adopt calculated binding energies from the literature [11, 12], while for hydrogenated bare silicate grains and H_2O ice covered grains, these values result from ab initio chemical calculations 9.

To calculate the HF binding energies we carry out quantum calculations within the Kohn-Sham implementation of Density Functional Theory using the Quantum Espresso Simulation Package [13]. Perdew-Burke-Ernzerhof exchange-correlation functional ultrasoft pseudopotentials are used. KS valence states are expanded in a plane-wave basis set with a cutoff at 340 eV for the kinetic energy. The selfconsis-

Surface topology	E_b,HF (Kcal/mol)
SiH_2···FH	2.23
SiH(OH)···FH	15.69
$Si(OH)_2$···FH···$(OH)_2$Si	17.01
$Si(OH)_2$·H_2O·HF	25.42
$(CO)_{ICE}$···FH	2.13
$(CO_2)_{ICE}$···FH	2.22
$(H_2O)_{ICE}$···FH	12.68

Table 1. Binding energies for HF onto various surfaces.

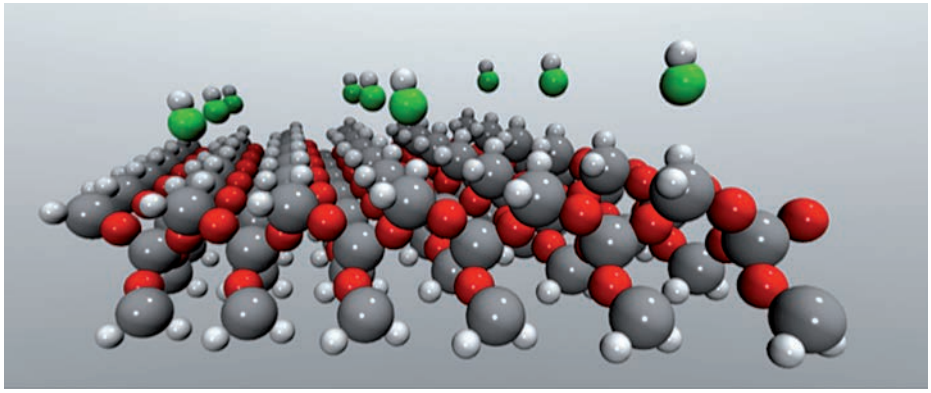

Fig. 2. Schematic view of the SiH_2···FH topology.

tency of the electron density is obtained with the energy threshold set to 10^{-5} eV. Calculations are performed using the primitive unit cell containing a total number of 46 atoms for bare hydrogenated silica, and 54 atoms for hydrogenated silica covered with one layer of H_2O ice. The geometry optimization is used within the conjugate gradients scheme, with a threshold of 0.01 eV $Å^{-1}$ on the Hellmann-Feynman forces on all atoms; the Si atoms of the bottom layers are fixed at their bulk values.

In amorphous silica, exposed to terrestrial atmosphere, the most stable surface [α-Quartz(001)] is characterized by five types of terminal chemical groups: $=SiH_2$, ≡SiH, =Si-O-Si= (siloxane bridges), ≡SiOH (single silanol), $=Si(OH)_2$ (geminal silanol). $=SiH_2$ and ≡SiH groups are less probable because siloxane and silanol groups have lower energy content with respect to them. At T > 500 K silanol groups are converted in siloxane bridges, with H_2O production (dehydroxilation). The binding energy of HF with the SiH terminus of hydrogenated crystalline silica is based on calculations for the hydroxylated alpha-quartz (001) surface. The binding energy

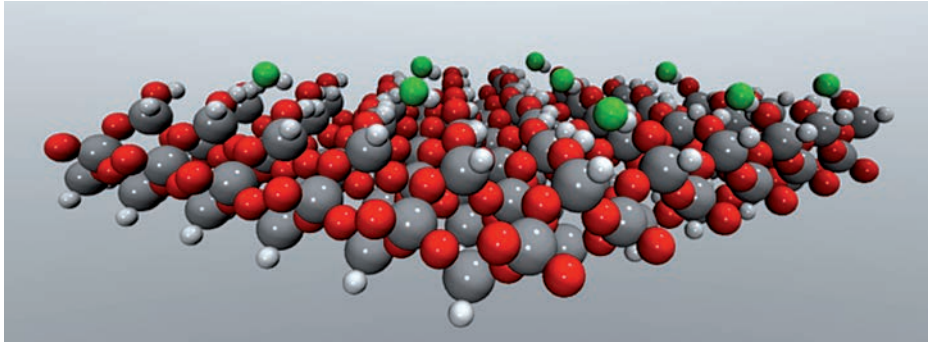

Fig. 3. Schematic view of the SiH(OH)···FH topology.

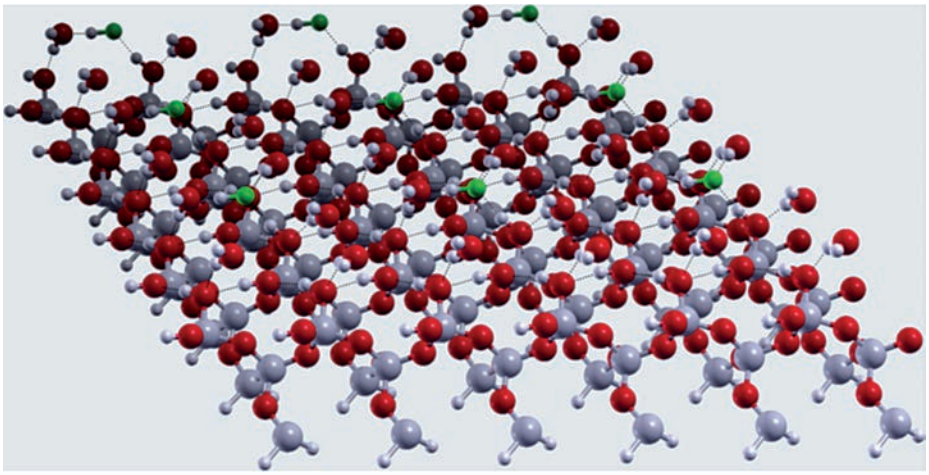

Fig. 4. Schematic view of the $Si(OH)_2 \cdot H_2O \cdot HF \cdots$topology.

of HF with one layer of H_2O ice on amorphous hydrogenated silicate is estimated by assuming that the the most common structure in this case is the HF molecule interacting with a H_2O molecule bonded to silanol (SiOH), which is the most abundant surface group in amorphous silica [14].

The binding energies of HF with CO and CO_2 ice (Table 1) are taken from calculations for molecules in the gas phase. We consider the gas phase binding energies of HF with CO and CO_2 to be similar to those of HF with CO and CO_2 ices adsorbed on an inert surface such as that of hydroxylated amorphous silica. This approximation is based on the weak interactions of these ices with hydroxylated silica and within the CO and CO_2 molecular solids, so that the electronic density of CO and CO_2 in solid form is not significantly altered with respect to their state in the gas phase. Hence, the binding energy of the HF molecule with CO or CO_2 as calculated in the gas phase is applicable for the condensed phase. The situation is notably different for interactions with H_2O in the gas or adsorbed form, because of its stronger interaction with silica and HF. For HF interacting with H_2O ice, we use binding energies from calculations 9.

The binding energy of HF with the SiH and SiOH terminus of hydrogenated crystalline silica are shown in fig. 2 and 3. The binding energy of HF with one layer of H_2O ice on amorphous hydrogenated silicate (See fig. 4) is estimated by assuming that the the most common structure in this case is the HF molecule interacting with a H_2O molecule bonded to silanol (SiOH), which is the most abundant surface group in amorphous silica.

The analysis of the radial dependence of adsorption and desorption timescales (see eq. 1 and 2) of HF from various types of grain surfaces indicates that the grains are mainly supposed to be made of: $(CO)_{ICE}$, $(CO_2)_{ICE}$, SiH_2 $(H_2O)_{ICE}$, whereas H_2O

and OH groups seems to not play any role in the grain adsorption of HF in these ISM molecular clouds.

Summarizing, this work uses HF as a sensitive tracer for (molecular) gas at relatively low densities that may be contributing mass to star forming cores. The HF signature reveals a gas reservoir that is inconspicuous in traditional dense gas tracers such as CO. In addition, we show that gas phase HF in higher density environments ($>10^5$ cm^{-3}) is extremely sensitive to interactions with dust grains and will be depleted significantly at low dust temperatures 9.

REFERENCES

[1] *Chemistry of Hydrogen Fluoride in the Interstellar Medium*, Zhu, C., Krems, R., Dalgarno, A., & Balakrishnan, N. 2002, ApJ, 577, 795.

[2] *The Chemistry of Fluorine-bearing Molecules in Diffuse and Dense Interstellar Gas Clouds*, Neufeld, D.A., Wolfire, M.G., & Schilke, P. 2005, ApJ, 628, 260.

[3] *Detection of hydrogen fluoride absorption in diffuse molecular clouds with Herschel/HIFI: an ubiquitous tracer of molecular gas*, Sonnentrucker, P., Neufeld, D.A., Phillips, T.G., *et al.* 2010, A&A, 521, L12.

[4] *Widespread galactic CF+ absorption: detection toward W49 with the Plateau de Bure Interferometer*, Liszt, H.S., Guzmán, V.V., Pety, J., *et al.* 2015, A&A, 579, A12.

[5] *Detection of extragalactic CF + toward PKS 1830-211 Chemical differentiation in the absorbing gas*, Muller, S., Kawaguchi, K., Black, J.H., & Amano, T. 2016, A&A, 589, L5.

[6] *The CO-to-H-2 Conversion Factor*, Bolatto, A.D., Wolfire, M., & Leroy, A.K. 2013, ARA&A, 51, 207.

[7] *Herschel observations of EXtra-Ordinary Sources (HEXOS): Detection of hydrogen fluoride in absorption towards Orion KL*, Phillips, T.G., Bergin, E.A., Lis, D.C., *et al.* 2010, A&A, 518, L109.

[8] *Hydrogen fluoride in high-mass star-forming regions*, Emprechtinger, M., Monje, R.R., Van der Tak, F.F.S., *et al.* 2012, ApJ, 756, 136.

[9] *Three-dimensional distribution of hydrogen fluoride gas toward NGC 6334 I and I(N)*, Van Der Wiel, M.H.D., Naylor, D.A., Makiwa, G., Satta, M., Abergel, A., A&A 2016, 593, Article number A37.

[10] *Observations of the Icy Universe*, Boogert, A.C.A., Gerakines, P.A., & Whittet, D.C.B. 2015, ARA&A, 53, 541.

[11] *Theoretical influence of third molecule on reaction channels of weakly bound complex CO_2… HF systems*, Chen, S.-J., Chen, C., & Hong, Y.-S. 2006, International Journal of Quantum Chemistry, 106, 1640.

[12] *Predicted properties of the CO-HF isomer using a six-dimensional morphed potential*, Rivera-Rivera, L.A., McElmurry, B.A., Lucchese, R.R., & Bevan, J.W. 2012, Journal of Molecular Structure, 1023, 43.

[13] *QUANTUM ESPRESSO: a modular and open-source software project for quantum simulations of materials*, Giannozzi, P., Baroni, S., Bonini, N., *et al.* 2009, Journal of Physics Condensed Matter, 21, 395502.

[14] *Accurate amorphous silica surface models from first-principles thermodynamics of surface dehydroxylation*, Ewing, C.S., Bhavsar, S., Götz, V., McCarthy, J.J., & Johnson, K.J. 2014, Langmuir, 30, 5133.

Rendiconti
Accademia Nazionale delle Scienze detta dei XL
Memorie di Scienze Fisiche e Naturali
136° (2018), Vol. XLII, Parte II, Tomo II, pp. 107-113

ANDREA LOMBARDI[1] – FEDERICO PALAZZETTI[1]
VINCENZO AQUILANTI[1] – KING-CHUEN LIN[2] – DOCK-CHIL CHE[3]
MASAAKI NAKAMURA[3] – TOSHIO KASAI[2]

Excited CO Formation in Interstellar Molecular Clouds: Methyl Formate Photodissociation by Ultraviolet Radiation

Summary – Progress in astrochemistry is driven by observations. Typically, the molecules in the Interstellar Medium dark and dense clouds are studied by the infrared and millimeter spectroscopy by radiotelescopes. A careful analysis of their signatures in the spectra helps to characterize these regions where new stars and planets are born. The rotational transition lines of carbon monoxide, CO, are the most important tracer of molecular gas within molecular clouds. However, the accuracy of the interpretation of the detected signals depends on the quality of the kinetic models, used to simulate molecular environments, that in order to be reliable require accurate knowledge of the dynamics and reactive kinetics properties of the individual molecules. A certain lack of knowledge in current models surely affects reactive and dissociation processes involving complex organic molecules. For example, these can be exposed to far Ultra-Violet (FUV) radiation in photodissociation regions and also in the inner regions of molecular clouds (collision of cosmic rays with gas phase particles can results in UV emissions) and generate vibro-rotationally excited molecular fragments upon photodissociation, such as rotationally hot CO molecules. In this work we establish a possibly fruitful dialogue between the chemistry and astrophysics communities considering a molecular beam experiment of UV photodissociation of methyl formate, abundant and ubiquitous in space, as a source of accurate information about the generation of vibrationally and rotationally excited CO dissociation fragments in molecular clouds. The scheme can be extended to many complex organic molecules, for which experimental and theoretical photodissociation studies are feasible.

[1] Dipartimento di Chimica, Biologia e Biotecnologie, Università di Perugia.
[2] National Taiwan University, Taiwan.
[3] Osaka University, Osaka, Japan.

Introduction

The advent of a new interdisciplinary field of scientific research, astrochemistry [1], as the investigation of the chemical nature of the Universe, originates from astronomical and radioastronomical observations and space mission data collections. The interpretation of the resulting ample phenomenology needs to be assisted by laboratory experiments and theoretical and computational modeling. This search has already led to the identification of a constantly increasing number of molecules, even complex organic molecules, but progress in space exploration and direct sampling promise further insight into the evolution of the universe, from a chemical point of view, since its formation up to the the generation of protobiological molecules.

In this respect, the discovery of amino-acids in meteorites, and possibly in other spatial environments, has contributed to the debate on the origin of the building blocks of life in space. The recent discovery of propylene oxide (PO) in the Interstellar Medium (ISM) [3] has induced large interest in spite that it is just a further addition to a now long list of molecules, being this molecule an ideal candidate as a prototype for studies aiming at elucidating the insurgence and establishment of homochirality since the origin and early evolution of life, an issue still lacking convincing explanations.

The trend in the discovery of Complex Organic Molecules (COMs) [4] confirm a diffuse presence in the Interstellar Medium (ISM), since besides protostellar hot cores and corinos, COMs are found at all stages of star formation, in cold cores, protoplanetary disks, shocks, jets and outflows [5].

Their widespread presence in the ISM suggests that in building kinetic models of spatial environments one should assess the role of COM breakings upon photodissociation, since such processes involve the production of the simple basic diatomic molecules such as, for example, carbon monoxide CO and the hydroxyl radical OH, generated in excited rotational and vibrational states.

The observation of molecules, in any astrophysical environment, relies upon experiments based on measurements of radiative spectra, but sufficiently high spectral resolution and sensitivity allow in principle to measure also absorption spectra from different rotational levels, including the ground state, permitting to probe the column density of the detected molecule, temperature and molecule abundances.

Carbon monoxide, a basic reactant for the formation of small organic molecules and aminoacids and, at the same time, the detectable product of their decomposition by photodissociation, is one of the most abundant molecules in space, with a specific relationship to hydrogen and a main tracer of molecular clouds, due to the ease of detection of its Ultraviolet (UV) and millimeter (mm) photon emission.

Privileged environments for CO generated by photodissociation are arguably regions of the ISM, so called “neutral”, in which the gas heating and chemical processes are mostly regulated by far UV. These are termed Photo-Dissociation Regions (PDRs) and are the source of most of the non-stellar infrared (IR) and the millimeter and submillimeter CO emission from galaxies [6].

The importance of PDRs has become increasingly apparent with advances in Infra-Red (IR) and submillimeter astronomy. The IR emission from PDRs corresponds to rovibrational lines of H_2, rotational lines of CO, broad mid-IR features of polycyclic aromatic hydrocarbons (PAH) and a luminous underlying IR continuum from interstellar dust. The transition of H to H_2 and C to CO actually occurs within PDRs. Comparison of observations with theoretical models of PDRs enables one to determine the density and temperature structure, the elemental abundances, the level of ionization, and the radiation field. Complex Organic Molecules (COMs) are abundant especially in the deep part of clouds, where actually the far UV radiation is more attenuated. In these regions, however, the effect of cosmic rays is the leading one, which causes the presence of secondary UV radiation, due to collisions with molecules (mainly H_2).

If the temperature is sufficiently high, molecules, also the more complex ones, can be desorbed from grain surface.

Generation of excited CO molecules, could affect the emission spectra, which follow a proper excitation of the molecular emitting levels. The emitted radiation is directly linked to the population of the upper level (it may also depend on the population of the lower level) and to the physical and chemical properties of the environments located between the source and the observer. The presence of dust particles is an example of effect inducing additional absorption and scattering which may considerably alter the observed emitted spectrum.

In this work, we accont for molecular beam experiment of UV photodissociation of methyl formate, abundant and ubiquitous in space, as a source of accurate information about the generation of vibrationally and rotationally excited CO dissociation fragments in molecular clouds.

Population of levels by collisional processes

The collisions between molecules are the basic processes leading to energy transfer and internal excitation and population of higher states. Their efficiency relies on the nature of the colliding partners, the chemical composition and the density of the medium and the local temperature, which influences statistically the average degree of excitation and, consequently, determines the intensities of the radiation emission. Other important mechanism can be effective, such as radiative and chemical level pumping. When relatively complex organic molecules are available, and photons with frequencies close to far-UV radiation are present, photodissociation might occur generating excited fragments, such as CO, OH or HCO. This scheme, is a mechanism that indirectly pumps radiation energy into the rotational and vibrational manifold of diatomic molecules, such as the tracer CO.

The level population in the conditions typical of the interstellar medium is generally not in line with a thermal distribution. For a given molecule, the assignment of a set of transitions allows to draw a so-called Boltzmann plot, reporting the log-

arithm of the column density, denoted as $N(j)$ and corresponding to the j-level relative population divided by its statistical weight g_j, versus the related energies (often expressed in Kelvin). The corresponding points are aligned when thermodynamic equilibrium or local thermodynamic equilibrium (LTE) is fulfilled and the temperature is simply obtained from the slope of the curve.

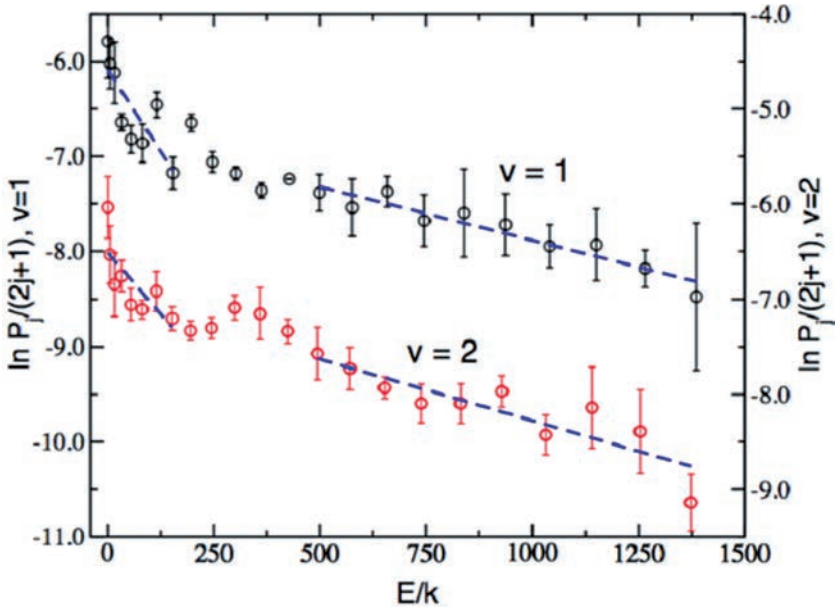

Fig. 1 Boltzmann plots of data of rotational populations of vibrationally excited CO molecules (v = 1 and v = 2), from laser photodissociation of a molecular beam of methyl formate. Thermal bimodality is exhibited by changes in slopes (dashed lines are a guide for readers' eyes adapted from Ref. 7).

$$P(j) = g_j \frac{P(\mathrm{O})}{g_0} e^{-(E_j - E_0)/kT}$$

Fig. 1 shows an example of Boltzmann plot measured downstream of a molecular beam experiment involving photodissociation of methyl formate [7].

The drawback of such an idealized picture come from the low-density conditions typical of the interstellar medium, meaning low collision frequencies, which prevent molecular encounters to be the leading process in establishing thermal equilibrium, even locally, for the level population.

In other words, LTE is rarely fulfilled. Then, knowledge of the collisional rate coefficients involving the most abundant species, i.e. H, H_2, He, electrons and Carbon and Oxygen carrier molecules, such as the molecular tracer CO, is required to solve the coupled differential equations describing the evolution of the different excited states of each molecule. Under similar conditions, the interpretation of the

emission spectra to infer the physical and chemical properties of the molecular clouds also requires the simultaneous solution of the radiative transfer part, which contributes to de-excitation in competition with collisions.

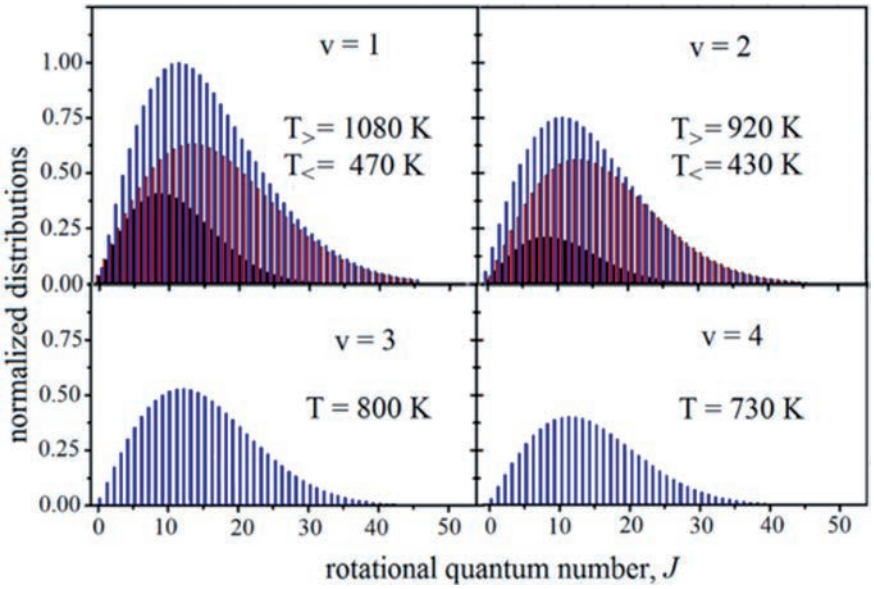

Fig. 2 Reconstructed rotational quantum number distributions from the estimated rotational temperature values from Boltzmann deconvolutions. Two components, designated by $T_<$ and $T_>$, are disentangled and attributed as arising from events emerging directly from pathways into the channel CH_3OH + CO or from alternative paths along the radical channel adapted from Ref. 7.

To better understand the observational data, it is necessary to enhance the models including physical chemical networks containing gas-phase and grain-surface reactions. The determination of collisional rates for all the relevant interstellar molecules is therefore a major challenge in the interpretation of astrochemical observations. In the specific case outlined above, when photodissociation occurs, the network should include such processes and the correct share of single excited states in which the fragments are produced.

This situation is not limited to astrochemical models. In general, whatever the conditions, the modeling of gas phase systems requires an accurate description of the molecular energy transfer and photodissociation and reactive processes, which have to be carefully represented within the kinetic models. So many other research areas fields are included, such as combustion chemistry, chemistry of plasmas, gases under flow conditions (e.g. in aircraft and spacecraft design [8]). The additional obstacle here, is the lack of general and local equilibrium for any of the degrees of freedom, which prevents to assume statistical population averaging, and forces to

resort to a state-to-state level of details for the rate coefficients and to detailed dynamics simulations to obtain reactive mechanisms, branching ratios and dissociation pathways. Important attempts are currently being carried out in the gas dynamics community to develop kinetic models at a state-specific level [9-12].

The excitation and de-excitation of molecules, occurring upon collision, as well their decomposition patterns are strongly dependent on the features of the intermolecular potentials [10] and part of the efforts to improve the accuracy of models must be spent to obtain a realistic description of the intermolecular interactions. A further key point is that energy transfer is state-specific in its nature, since it depends on the initial quantum states of the colliding molecules, and this dependency is more pronounced when excited states are involved, as for hypersonic flows and high temperature plasmas, an aspect typical of planetary atmosphere chemistry [8].

Photossociation as a vibrational and rotational pumping mechanism

Besides collisional excitation, photodissociation processes of small and medium size molecules abundantly present in molecular clouds, can convert the UV radiation into significant amounts of vibrational and rotational energy of the preferred dissociation fragments, such as CO.

As an example, the methyl formate molecule ($HCOOCH_3$) is one of the most abundant species in hot molecular cores [14]. Together with acetic acid and the sugar glycolaldehyde, these $C_2H_4O_2$ molecules are the first triad of isomers detected in interstellar clouds. The abundance of methyl formate is an average of 100 times the amount of acetic acid, the second most abundant isomer and this must depend upon formation pathways and quantum yields of photodissociation. In the last ten years some significant experimental and theoretical studies of the photodissociation of methyl formate around the lower energy limit of the far-UV radiation, have been carried out (see e.g. Ref. [7,15]), showing that the main dissociation pathways involve CO fragment formation with a significant vibrational and rotational excitation. This suggests a possible role of such processes in determining the CO level population. Fig. 2 shows the rotational distribution of CO fragments from methyl formate photodissociated at 248 nm [7].

Concluding remarks

Small organic molecules, e.g. methyl formate, are sources of excited molecular fragments, such as the tracer CO. Performing properly designed molecular beam experiments, assisted by theoretical and computational modeling, provide accurate rate coefficients of collisional energy transfer processes in the range of conditions typical of the interstellar medium. In particularly, experiments of photodissociation allow to reconstruct the energy disposal and the molecular vibro-rotational state distributions, enriching current astrochemical data base by updated kinetics and population data.

BIBLIOGRAPHIC REFERENCES

[1] Palazzetti, F., Maciel, G.S., Lombardi, A., Grossi, G., Aquilanti, V.: The astrochemical observatory: molecules in the laboratory and in the cosmos. J. Chin. Chem. Soc. 59, 1045-1052 (2012).
[2] Pizzarello, S., Groy, T.L.: Molecular asymmetry in extraterrestrial organic chemistry: an analytical perspective. Geochim. Cosmochim. Acta 75, 645-656 (2011).
[3] McGuire, B., Carroll, P.B., Loomis, R.A., Finneran, I.A., Jewell, P.A., Remijan, A.J., Blake, G.A.: Discovery of the interstellar chiral molecule propylene oxide (CH_3CHCH_2O). Science 352, 1449–1452 (2016).
[4] Ceccarelli, C., Cernicharo J.: Organic Molecules in the Interstellar Medium, in Origins and Evolution of Life: An Astrobiological Perspective, p. 85, Cambridge University Press, 2011, Cambridge, UK.
[5] van Dishoeck, Ewine F.: Astrochemistry: overview and chellenges, in Astrochemistry VII - Through the Cosmos from Galaxies to Planets, Proceedings IAU Symposium No. 332 (2017).
[6] Hollenbach, D.J., Tielens, A.G.G.M.: Photodissociation Regions in the Interstellar Medium of Galaxies, Rev. Mod. Physics, 71, 173 (1999).
[7] Lombardi, A., Palazzetti, F., Aquilanti, V., Li, H.-K., Tsai, P.-T., Kasai, T., Lin, K.-C., Aquilanti, V. Rovibrationally Excited Molecules on the Verge of a Triple Breakdown: Molecular and Roaming Mechanisms in the Photodecomposition of Methyl Formate, J. Phys. Chem. A 120, 5155-5162 (2016).
[8] Capitelli, M., Bruno, D., Colonna, G., D'Ammando, G., Esposito, F., Laricchiuta, A., Pietanza, L.D. Molecular Physics and Kinetics of High Temperature Planetary Atmospheres, Rendiconti Lincei 22, 201-210 (2011).
[9] Panesi, M., Jaffe, R.L., Schwenke, D.W., Magin, T.E.: J. Chem. Phys. 138, 044312 (2013).
[10] Laganà, A., Lombardi, A., Pirani, F., Belmonte, P.G., Ortega, R.S., Armenise, I., Cacciatore, M., Esposito, F., Rutigliano, M.: Open Plasma Phys. J. 7, 48-59 (2014).
[11] Celiberto, R., et al. Atomic and molecular data for spacecraft re-entry plasmas, Plasma Sources Sci. Tech. 25, 033004 (2016).
[12] Armenise, I., Kustova, E. State-to-state models for CO_2 molecules: From the theory to an application to hypersonic boundary layers, Chemical Phys. 415, 269-281 (2013).
[13] F. Fantuzzi, S. Pilling, A. C. F. Santos, L. Baptista, A. B. Rocha, H. M. Boechat-Roberty, Photodissociation of methyl formate in circumstellar environment: stability under soft X-rays, Monthly Notices of the Royal Astronomical Society (2011), 417, 2631-2641.
[14] Lee, S.H., Photodissociation dynamics of methyl formate at 193.3 nm: Branching ratios, kinetic-energy distributions, and angular anisotropies of products, J. Chem. Phys. (2008), 129, 194304.

Rendiconti
Accademia Nazionale delle Scienze detta dei XL
Memorie di Scienze Fisiche e Naturali
136° (2018), Vol. XLII, Parte II, Tomo II, pp. 115-129

NAYARA D. COUTINHO[1] – YAGO S. SILVA[2] – DARIO DE FAZIO[1]
SIMONETTA CAVALLI[1] – VALTER H. CARVALHO-SILVA[2]
VINCENZO AQUILANTI[1,3]

Chemical Kinetics under Extreme Conditions: Exact, Phenomenological and First-Principles Computational Approaches

Abstract – Modern experimental and theoretical advances in chemical kinetics are documenting an ample spectrum of phenomena on reactions occurring under conditions relevant for astrochemistry, from those of interest for formation of molecules in the early universe to those encountered in interstellar medium. Here, we present a set of exact, phenomenological and first-principles tools to describe temperature dependence of rate constants under extreme conditions, showing non-Arrhenius behavior, especially at low temperatures. We are mainly concerned with illustrating case studies on (i) *super*-Arrhenius kinetics, including treatment of diffusion and viscosity in supercooling and glass material; (ii) *sub*-Arrhenius kinetics, regarding quantum mechanics proton or atomic hydrogen transfer in chemical reactions of interest in astrochemistry, astrobiology, and also in atmospheric and industrial applications; and (iii) *anti*-Arrhenius kinetics, where processes with no energetic obstacles are rate-limited by molecular reorientation requirements, such as documented for OH + HX (X = Br and I) elementary chemical reaction.

1. Introduction

The understanding of the history, role and fate of molecules in the universe requires information of the kinetics of the involved elementary processes, particularly

[1] Dipartimento di Chimica, Biologia e Biotecnologie, Università di Perugia, Via Elce di Sotto 8, 06123, Perugia, Italy.
[2] Grupo de Química Teórica e Estrutural de Anápolis, Ciências Exatas e Tecnológicas. Universidade Estadual de Goiás, CP 459, 75001-970 Anápolis, GO Brazil.
[3] Istituto di Struttura della Materia, Consiglio Nazionale delle Ricerche, 06100, Rome, Italy.

on their rates, and often in a wide range of conditions and specifically as a function of temperature. The temperature dependence of the rate constant of the primordial chemical reaction process is therefore crucial in order to establish the molecular abundances and the early universe evolution. The rate constants for most rate processes depend on absolute temperature according to the Arrhenius law: however, modern experimental progress in the age of nanotechnologies and computational progress, that are manifesting in a variety of approaches, has shown that when extended to low temperatures, deviations are observed even with no apparent changes in the chemical mechanism or in the physical nature of the moieties. Indeed, these advances have assisted to control the physical chemistry of materials in a large variety of environments and in the progress of new sciences, such as astrochemistry and astrobiology.

The deviations from linearity in Arrhenius plot leads to distinct regimes, denoted *sub*-Arrhenius, *super*-Arrhenius and *anti*-Arrhenius: the first two case correspond, respectively, to higher or lower reactivity as temperature decreases, and therefore to a decrease or increase of the apparent activation energy; the last and extreme case arises when the activation energy has negative value. To describe these behavior, recent systematic investigations lead to a simple formulation in terms of a single deformation parameter, denominated as *deformed*-Arrhenius (*d*-Arrhenius). which is inspired by Tsallis non-extensive statistical mechanics and exploits Euler's expression of the exponential function as the limit of a succession.

Special attention requires the chemistry of the early Universe, which plays an important role in our understanding of the formation of the first cosmological objects. Molecular formation began in the recombination era, when the temperature was low enough for the newly formed atoms to survive and participate in further evolution. At the end of the era, atomic density was still too low for three body reactions to play any significant role: however, it was then that the first molecular species were postulated to be formed through radiative association. The formation of molecular species in the primordial Universe is extremely important, because roto-vibrational quantum states became available to participate in the cooling process, permitting the dissipation of the radiative energy and balancing the increase of the gravitational energy during the collapse of the first cosmological objects. Gas phase chemistry of formation and destruction of these molecules is therefore very important to get a good understanding of how galaxies and clusters came to be.

Accordingly, this paper aims to illustrate the recent advances in the understanding of chemical kinetics in extreme temperature conditions, mainly in astrophysical environment. In the Section 2 we show the new paradigms and the current state of kinetic theory for *super*-Arrhenius, *sub*-Arrhenius and *anti*-Arrhenius behavior. In sections 3 and 4 we present an exact quantum dynamics study of the F + HD and H + HeH^+ reactions for ultra-cold collision energies with an emphasis on the application of the *d*-Arrhenius formula and of the relevance of these results in the early universe scenario. Concluding remarks follow in Section 4.

2. Low temperature: *Sub*, *super* and *anti*-Arrhenius Behavior

The rate constant k for the most rate processes depend on absolute temperature according to the well-known Arrhenius law [1]:

$$k(\beta) = Ae^{-Ea\beta} \tag{1}$$

where A is the pre-exponential factor, Ea the apparent activation energy and $\beta = \frac{1}{k_B T}$, where k_B is the Boltzmann constant. However, modern experimental techniques and theoretical approaches are providing an ample phenomenology of deviations from Arrhenius behavior, especially at low temperatures. In order to provide a description of *non*-Arrhenius behavior, recent systematic investigations led to a simple formalism in terms of a single parameter, d. The use of the *deformed* Arrhenius law [2, 3]:

$$k(\beta) = A(1 - d\varepsilon\beta)^{\frac{1}{d}}, \tag{2}$$

known as the Aquilanti-Mundim formula, permitting one to evaluate prototypical systems where the temperature dependence of the rate constant according to this equation is described by $\varepsilon > 0$ and $d > 0$ or $d < 0$, corresponding to convex (*super*-Arrhenius), concave (*sub*-Arrhenius) in the semi-log plots against reciprocal temperature (see figure 1). In the limit $d \longrightarrow 0$, the term $(1 - d\varepsilon\beta)^{\frac{1}{d}}$ can be identified with the Arrhenius exponential law (Eq. (1)). Other case for $\varepsilon < 0$ will also be documented and indicated as *anti*-Arrhenius.

In the next section the recent paradigm and the current state are illustrated for: (i) *super*-Arrhenius kinetics, for example cases where transport mechanisms accelerate processes when increasing temperature; (ii) *sub*-Arrhenius kinetics, where quan-

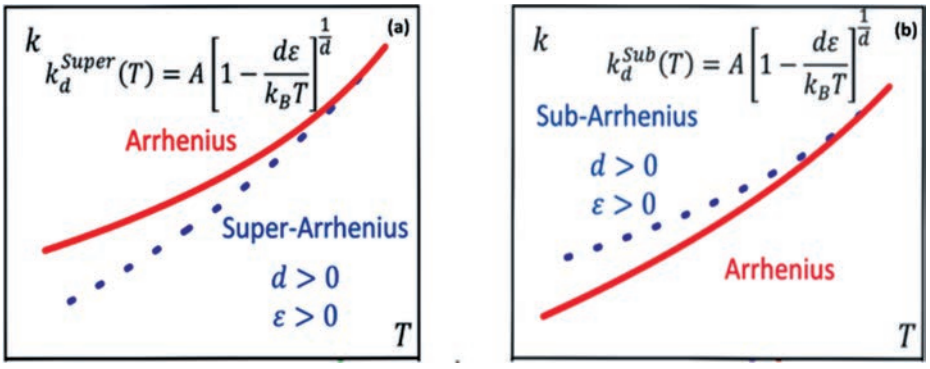

Fig. 1. Experimental, theoretical and simulation data are universally analyzed by an Arrhenius plot, where k is reported against T. Deviations from linearity at low temperatures can be observed in the plot as showing either a «concave» behavior (*sub*-Arrhenius), i.e., higher than expected rates as temperature decreases, or a «convex» curve (*super*-Arrhenius), i.e., lower than expected rates as temperature decreases.

tum mechanical tunneling favors low temperature reactivity; (iii) *anti*-Arrhenius kinetics, where processes with no energetic obstacles are limited by molecular reorientation requirements.

2.1. *The* super-*Arrhenius case*

Super-Arrhenius behavior is one that deserves particular attention, and its occurrence is varied and demanding. It often manifests because of collective phenomena, such as those amenable of treatment by the non-extensive thermodynamics of Tsallis, and covers on ample set of phenomena: rates of enzymatic catalysis promoted processes [4–6], food preservation processes [7, 8], basic features of the dynamics of complex or glass-forming liquids and solids [9-14] and geochemistry [15]. A significant number of studies in the temperature-dependence of rates of enzymatic catalysis reactions has inspired several formulations for the description of the mechanism involved in these processes [16-19]. Results in the kinetics of catalytic reactions of the dehydrogenase and oxidase enzymes has shown an unequivocal *super*-Arrhenius behaviour [4, 5, 20, 21].

A similar behavior is found in the temperature dependence of food processes. We propose in Ref. [7] the use of Equation 1 to describe the non-Arrhenius behavior in these processes, showing that the *d*-Arrhenius formula is suitable for describing the effect of temperature on non-enzymatic browning of onion and on the rate of growth of several species of bacteria. The *d*-Arrhenius rate law provides a means to account for convex curvature. Such factors include particle diffusion and constraints on proposed microscopic model, in particular requiring that any successful approach to *super*-Arrhenius processes should be consistent with the microcanonical rate constant [7, 21].

A most fundamental case of *super*-Arrhenius temperature-dependence occurs for the diffusion in supercooled systems near the glass transition temperature, T_g. An interesting example is the diffusion of krypton in methanol and ethanol mixtures at low temperature near their glass transition temperatures [22-24]. Furthermore, in the vicinity of the glass transition temperature the viscosity and diffusion coefficients of polymers and other glass forming liquids are strong functions of temperature, and it is a frequently occurring observation that materials exhibit deviation from Arrhenius behavior. Non-Arrhenius relaxation rates in glassy materials can be associated with thermally activated rearrangements of increasing numbers of molecules as temperature decreases.

To account for the *super*-Arrhenius behavior in classical collective phenomena, it is shown that is inversely proportional to the barrier height, ε, and directly proportional to a limit critical temperature, $T^{\dagger}$, which can be related to freezing in the degree of freedom of the system:

$$d = \frac{k_B T^{\dagger}}{\varepsilon} \tag{3}$$

2.2. *The* sub-*Arrhenius cases*

There are uncountable cases of concave deviation on the temperature rate constants for the elementary chemical reactions that can be classified as exhibiting a *sub*-Arrhenius behavior. In systems with no apparent changes in the chemical mechanism, this behavior can be attributed in most cases to quantum mechanical tunneling [2, 25]. Several investigations have provided examples of chemical reactions within this regime. A series of experimental kinetic data and of benchmark theoretical calculations [26-33] has established that, for example, the prototypical quantum mechanically investigated reaction of a fluorine atom with molecular hydrogen represents (See Section 3) an archetypical case of *sub*-Arrhenius behavior [34, 35], as has been experimentally confirmed [36].

To account for the *sub*-Arrhenius behavior in elementary chemical reactions, it has been shown that can be considered as inversely proportional to the square of the barrier height (ε) and directly proportional to the square of the frequency for crossing the barrier ($v^{\neq}$) at a maximum in the potential energy surface:

$$d = -\frac{1}{3}\left(\frac{hv^{\neq}}{2\varepsilon}\right)^2, \tag{4}$$

agreeing with Wigner's tunnel formula.

This definition can be incorporated in transition-state theory to cover cases where reaction rates as a function of temperature deviate from Arrhenius law. When deviation can be ascribed to quantum mechanical tunneling, an explicit derivation is given and inserted in a proposed variant of transition-state-theory – *deformed* transition-state-theory (*d*-TST) – which permits comparison with experiments and tests against alternative formulations. The application of *d*-TST to several hydrogen transfer reactions has been showing promising results. Temperature ranges for the validity of the approach are assessed with respect to features of the potential energy barrier to reaction [37]. Elementary reactions, widely investigated both experimentally and theoretically, which have been described successfully, are F + H_2 [2, 35], CH_4 + OH [38], CH_3Cl + OH [38], H_2 + CN [38], OH + HCl [39], abstraction and dissociation in the nitrogen trifluoride channels [40], and proton rearrangement in curcumin [41] and methylhydroxycarbene [42] and recently *d*-TST is shown to be suitable for describing the overall rate constant for the CH_3OH + H reaction [43].

As discussed in Refs. [44, 45], the degree of concavity in the Arrhenius plot can characterize the degree of tunneling in chemical reactions. The crossover temperature, $T_c = \hbar v^{\neq}/k_B$, is the parameter that delimits the degree of tunnelling regimes. The ranges of tunnelling regimes are important to quantify how the tunnelling affects the rate constant in particular cases. From a mathematical viewpoint, the *d*-TST formulation has clear limitations in the description of the deep tunnelling

regime (Wigner limit) [46, 47], since the Euler limit deformation of the exponential function fails to quantify the distributions of reactive particles with energy less than the height of the barrier. However, the flexibility of the distribution formula permits to cover the *sub*-Arrhenius behaviour, specifically typical of quantum tunnelling, smoothly extending into the Boltzmann distribution [48] of the classical regime.

Formula (2) is found adequate for moderate tunneling, $T > T_c$. Rarer cases of deep tunneling can be dealt by introducing a modified form [49]:

$$k_d^{ASCC}(T) = A\left(1 - \frac{d\varepsilon}{k_B T + h\nu^{\neq}}\right)^{\frac{1}{d}}. \tag{5}$$

Its derivation and performances will be further discussed elsewhere.

2.3. Anti-*Arrhenius cases*

The rates of some processes increase as temperature decreases accordingly to an apparently negative activation energy. These processes can be classified as *anti*-Arrhenius. In gas-phase reaction the *anti*-Arrhenius behavior is frequently found in molecule-radical reactions [50-55]. Using a first-principles Born-Oppenheimer molecular dynamics approach, we were able to provide an interpretation of the negative dependence of the rate constant on temperature for the OH + HBr and OH + HI reactions [56-59], confirming the suggestion obtained experimentally that this phenomenon has stereodynamical origin, which until now has been neglected by theoretical studies. The analysis of simulations showed that for low temperature, the reactants reorient to find the propitious alignment leading to reaction; however, this adjustment is progressively less effective for higher temperatures, where the wandering paths evidence the «roaming» effect. Additionally, the smaller number of reactive trajectories and the time required for the mutual reactant orientations for the hydrogen exchange for the OH + HI suggest a greater role of stereodynamics here, which may be related to the higher observed rate constant for the same temperature compared to the OH + HBr reaction.

Currently, there is ample activity investigating whether advances in molecular dynamics simulations can provide quantitatively rate constants [60-62]. However, the methods have difficulty in estimating the rate constants, generally leading to overestimates and the discrepancy with experimental data is larger for high temperatures. With our methodology, we also find overestimating rate constant for OH + HBr and HI reactions [56, 57]. These uncertainties are often associated to inherent difficulties of possible direct evaluations from molecular dynamics simulation, and are ascribed to the statistical validity of samplings of the system phase space and the accurate characterization of transition state features [63-65]. These crucial issues in the applications of TST-type approaches to calculations of rates constitute hard problems in the extraction of rate constants from first-principles molecular dynamics

experiments, preventing them to represent an at least semiquantitative alternative to direct exact or approximate quantum mechanical methods, often prohibitive to be implemented.

As a final example on how the study of the *anti*-Arrhenius behavior offers opportunities for fundamental research and can guide scientific progress in different areas, we note a recent paper where the stereodirectionality effect contributed to understand the negative activation energy in addition reactions of arylchlorocarbenes to alkenes [66].

3. An exact triatomic treatment: the $F + H_2 \longrightarrow HF + H$ reaction and its isotopic variants

The rate constants for the $F + H_2$ reaction and its isotopic variants arouses great attention from experimental and theoretical chemical kinetics studies [67-69]. This reaction is a prototypical exothermic elementary reaction driven by the tunneling effect. Furthermore, because of the population inversion of the vibrational levels in the HF product, this reaction was studied in much detail for leading to vibrational population inversion of interest of chemical lasers [70].

For this reaction, the results of rigorous quantum scattering calculations, see ref. [71] for details, show a linear behavior of the rate constant at high temperature, when the thermal contributions are more pronounced; however, a strong curvature was observed at low temperature. We compare the abilities that two different approaches, namely the Bell's 1935 [72] and *d*-Arrhenius [2, 48, 73] formulas, have to account for the deviation of the rate constant from the Arrhenius law in a temperature interval at the borderline between moderate and deep tunneling regimes, see Figure 2.

The rate constant obtained from close coupling calculations employing FXZ PES [74] has been fitted to the Bell's 1935 formula:

$$k(T) = A \left[\frac{RT \exp\left(-\varepsilon/RT\right) - \hbar\nu^{\neq} \exp\left(-\varepsilon/\hbar\nu^{\neq}\right)}{RT - \hbar\nu^{\neq}} \right] \tag{6}$$

as presented in Ref. [71]. Here, the *d*-Arrhenius [2, 48, 73] formula in Eq. (2) and Eq. (5) has been used to described the rate constants.

From Figure 2 one can note that the two formulas fit satisfactory well the close coupling data in the range of temperatures studied with a mean percent error within or close to the numerical accuracy of the data. Nevertheless, it had been shown in ref. [71] that Bell's formulas reproduce much better the data (a factor near to five) with respect to *d*-Arrhenius. As introduced in the section 2.2, *d*-Arrhenius formula has clear limitations in the description the rate constant below of the crossover temperature, $T_c = \hbar\nu^{\neq}/\boldsymbol{k}$, which for the F + HD reaction is equal to 178 K. In general, Bell's venerable approach turns out as very useful for extending the study of reactivity at very low temperatures, describing a dependence of rate constants in agree-

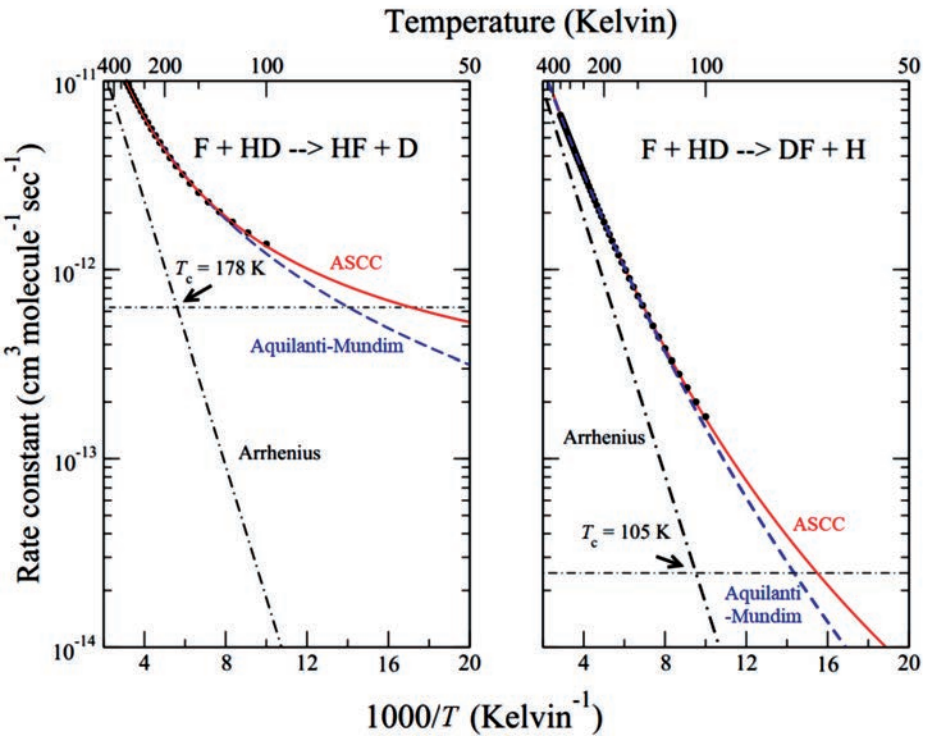

Fig. 2. Arrhenius plot for F + HD ⟶ FH + D reaction (reproduced and updated from ref. [71]). Filled circles indicate the results obtained from close coupling quantum scattering calculations employing FXZ PES, whereas lines are obtained by: red solid lines for the ASCC formula, Eq. (5), and dashed blue lines for the Aquilanti-Mundim formula, Eq.(2). The dot-dashed black lines are the classical Arrhenius results. The crossover temperature T_c is indicated by arrow.

ment with Wigner threshold law. However, the ASCC formula shown here is definitively better and recommended.

The current challenge is to describe the temperature dependence on the rate constants for temperatures below 1K, where an *anti*-Arrhenius behavior, due to the presence of a resonance state near to reaction threshold, has been predicted by recent results not published yet.

4. An exact treatment of the ion-molecular reaction $H + HeH^+ \longrightarrow H_2 + He^+$: role in the primordial universe

Because H and He are the dominant species in the early Universe scenario and can be ionized to H^+ and He^+ by cosmic rays, the first collisions of the He chemistry are $He + H_2^+$ and $He^+ + H_2$. The former collision is an adiabatic process on the HeH_2^+ ground electronic surface and was extensively investigated in the past [75].

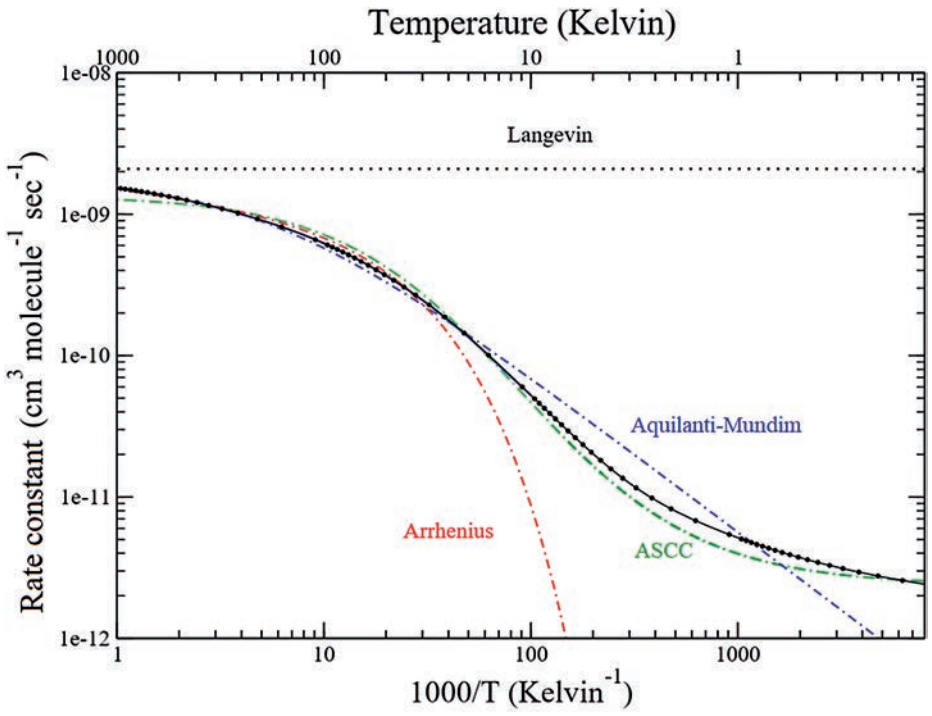

Fig. 3. Rate constants for the H + HeH^+ reaction as a function of temperature. A log-log plot is here used to emphasize the cold regime. The figure is adapted from [75], to be consulted for further details. The dashed black line, labeled Langevin, is the capture model value obtained by using for the dipole polarizability of the incoming hydrogen atom the exact analytical value of 4.5 a.u. The dashed blue and red lines are the results of the fits to the solid black line using Aquilanti-Mundim and ASCC formula (with A = cm^3.molecule^-1.sec^-1, ε = 0.2644 kJ.mol^{-1} and $\nu^{\neq}$ = 3.49 cm^{-1}).

The chemical reaction H + HeH^+ reaction plays an important role in astrophysics, because it is the key step in one of the main mechanisms of hydrogen molecule formation in the primordial plasma, strongly affecting the hydrogen abundance in the red shift range 150-300 nm. The temperature dependence of the rate of this simple exothermic process is therefore crucial in order to establish the molecular abundances and the early universe evolution. Also, the existence of HeH^+ in many different astrophysical environments (planetary nebulae, dense molecular clouds, white dwarfs) has been discussed in several papers [76, 77]. Because of the many astrochemical applications, accurate reaction data are required in the full collision energy range, from the ultra-cold regime to the three-body breakup and beyond.

The dynamics of the H + HeH^+ reaction has been studied from 0.001 K to 2000 K by close coupling quantum reactive scattering calculations, exact when the potential energy surface is given [78]. The main tools that allow the covering of so large a range of temperature, varying by six orders of magnitude, have been the

implementation of the Enhanced Renormalized Numerov method [79] to improve the convergence in the ultra-cold regime and a massive parallelization of the code [74] to treat the large number of partial waves required for this ionic system.

The large difference at higher temperatures (see Fig. 3), where the rates are about double in the new time independent calculations, may have important consequences in the early universe scenario. In fact, a higher reactivity of the HeH^+ cation makes the title reaction more competitive with radiative dissociation favoring the formation of the H_2 (at higher red shifts, where the HeH^+ mechanism is the main channel of formation of the hydrogen molecule. It is highly relevant to date the formation of the first stars and galaxies because the H_2 molecule is, in the present state of the astrophysical knowledge [80], the most important coolant species in the early universe scenario.

5. Conclusion

In summary, in our journey to the understanding of the microscopic ingredients which are the driving-force in physical and chemical processes under extreme conditions, and specially at low temperatures, we can highlight some interesting new entries: (i) the introduction of a deviation parameter *d* covering uniformly a variety of rate processes, from quantum mechanical tunneling and stereodynamical effects to Pareto-Tsallis distributions process culminating in deformed version of the Arrhenius law, the Aquilanti-Mundim *d*-Arrhenius; (ii) a relationship among the deformation parameter *d* with structural properties of the physical and chemical processes evaluated; (iii) explanation of the role of stereodynamical and roaming effects for elementary chemical reactions under *anti*-Arrhenius behavior; and (iv) presentation of exact rate constant at extreme low temperature for three-body reactions which emphasize the limitations of the phenomenological formulas available and the need of advance in formulations which describe processes in this regime.

BIBLIOGRAPHIC REFERENCES

[1] S. Arrhenius, On the reaction rate of the inversion of non-refined sugar upon souring, Z. Phys. Chem. 4 (1889) 226-248.

[2] V. Aquilanti, K.C. Mundim, M. Elango, S. Kleijn, T. Kasai, Temperature dependence of chemical and biophysical rate processes: Phenomenological approach to deviations from Arrhenius law, Chem. Phys. Lett. 498 (2010) 209-213.

[3] V. Aquilanti, N.D. Coutinho, V.H. Carvalho-Silva, Kinetics of Low-Temperature Transitions and Reaction Rate Theory from Non-Equilibrium Distributions, Philos. Trans. R. Soc. London A. 375 (2017) 20160204.

[4] A. Kohen, R. Cannio, S. Bartolucci, J.P. Klinman, Enzyme dynamics and hydrogen tunnelling in a thermophilic alcohol dehydrogenase, Nature. 399 (1999) 496-499. http://dx.doi.org/10.1038/20981.

[5] Z.D. Nagel, M. Dong, B.J. Bahnson, J.P. Klinman, Impaired protein conformational landscapes as revealed in anomalous Arrhenius prefactors, Proc. Natl. Acad. Sci. 108 (2011) 10520-10525.
[6] M.P. Meyer, D.R. Tomchick, J.P. Klinman, Enzyme structure and dynamics affect hydrogen tunneling: The impact of a remote side chain (I553) in soybean lipoxygenase-1, Proc. Natl. Acad. Sci. 105 (2008) 1146-1151.
[7] N.D. Coutinho, V.H.C. Silva, K.C. Mundim, H.C.B. de Oliveira, Description of the effect of temperature on food systems using the deformed Arrhenius rate law: deviations from linearity in logarithmic plots vs. inverse temperature, Rend. Lincei. 26 (2015) 141-149.
[8] M.. Peleg, M.D. Normand, M.G. Corradini, The Arrhenius Equation Revisited, Crit. Rev. Food Sci. Nutr. 52 (2012) 830-851.
[9] P.G. Debenedetti, F.H. Stillinger, Supercooled liquids and the glass transition, Nature. 410 (2001) 259-267.
[10] R.S. Smith, B.D. Kay, Breaking Through the Glass Ceiling: Recent Experimental Approaches to Probe the Properties of Supercooled Liquids near the Glass Transition, J. Phys. Chem. Lett. 3 (2012) 725-730.
[11] N.J. Luiggi Agreda, Aquilanti-Mundim deformed Arrhenius model in solid-state reactions, J. Therm. Anal. Calorim. (2016) 1175-1184.
[12] T. Hecksher, A.I. Nielsen, N.B. Olsen, J.C. Dyre, Little evidence for dynamic divergences in ultraviscous molecular liquids, Nat. Phys. 4 (2008) 737-741.
[13] S. Vyazovkin, S. Vyazovkin, S. Vyazovkin, J.R. Hulett, I.W.M. Smith, G. Tan, Q. Wang, H. Zheng, W. Zhao, S. Zhang, Z. Liu, A. Khawam, D.R. Flanagan, A.K. Galwey, P. Simon, H.L. Friedman, S. Vyazovkin, N. Sbirrazzuoli, M.C. Smith, C.-H. Chang, W. Chao, L.-C. Lin, K. Takahashi, K.A. Boering, J.J.-M. Lin, J.M. Valverde, D.S. Achilias, G.Z. Papageorgiou, G.P. Karayannidis, J.W. Huang, N. Bosq, N. Guigo, J. Persello, N. Sbirrazzuoli, J.-W. Huang, Y.-L. Wen, C.-C. Kang, M.-Y. Yeh, S.-B. Wen, S. Biswas, B. Dutta, S. Bhattacharya, S. Vyazovkin, I. Dranca, A. Codou, N. Guigo, J. van Berkel, E. de Jong, N. Sbirrazzuoli, G. Stoclet, G.G. du Sart, B. Yeniad, S. de Vos, J.M. Lefebvre, N. Bosq, N. Guigo, E. Zhuravlev, N. Sbirrazzuoli, M. Martinez-Palau, L. Franco, J. Puiggali, D. Turnbull, J.C. Fisher, K. Chen, A.N. Baker, S. Vyazovkin, N. Guigo, N. Sbirrazzuoli, S. Vyazovkin, R. Farasat, B. Yancey, S. Vyazovkin, M. Tansho, Y. Furukawa, D. Nakamura, R. Ikeda, A. Toda, M. Hikosaka, K. Yamada, S. Vyazovkin, B. Yancey, K. Walker, H.E. Kissinger, T. Sasaki, R. Farasat, S. Vyazovkin, R. Farasat, S. Vyazovkin, S. Vyazovkin, N. Sbirrazzuoli, I. Dranca, K. Miura, M.L. Williams, R.F. Landel, J.D. Ferry, P. Badrinarayanan, W. Zheng, S.L. Simon, G.Z. Papageorgiou, D.S. Achilias, G.P. Karayannidis, C.A. Angell, M.R. Kamal, E. Rabinowitch, S. Vyazovkin, N. Sbirrazzuoli, A. Omrani, A.A. Rostami, F. Ravari, A. Mashak, O. Zabihi, A. Hooshafza, F. Moztarzadeh, H. Payravand, A. Afshar, R. Alizadeh, A.M. Stolin, A.G. Merzhanov, A.Y. Malkin, C. Alzina, N. Sbirrazzuoli, A. Mija, M. Vafayan, M.H. Beheshty, M.H.R. Ghoreishy, H. Abedini, M. Khoshkish, M. Vafayan, H. Bouhendi, S. Vyazovkin, J.A. Huidobro, I. Iglesias, B.F. Alfonso, A. Espina, C. Trobajo, J.R. Garcia, M.J. Starink, S. Vyazovkin, P. Simon, P.S. Thomas, J. Okuliar, A.S. Ray, W. Tang, D. Chen, J. Cai, S. Chen, P. Budrugeac, P. Budrugeac, Y. Han, H. Chen, N. Li, T. Dubaj, Z. Cibulková, P. Šimon, A. Ortega, C. Popescu, A time to search: finding the meaning of variable activation energy, Phys. Chem. Chem. Phys. 18 (2016) 18643–18656.
[14] V.K. de Souza, D.J. Wales, Energy landscapes for diffusion: Analysis of cage-breaking processes, J. Chem. Phys. 129 (2008) 164507.
[15] G. Schubert, Treatise on Geophysics, 2007.
[16] A. Warshel, R.P. Bora, Perspective: Defining and quantifying the role of dynamics in enzyme catalysis, J. Chem. Phys. 144 (2016) 180901.
[17] D.G. Truhlar, Transition state theory for enzyme kinetics, Arch. Biochem. Biophys. 582 (2015) 10-17.

[18] P. Singh, Z. Islam, A. Kohen, Examinations of the Chemical Step in Enzyme Catalysis, in: Methods Enzymol., 2016.
[19] J.P. Klinman, A. Kohen, Evolutionary Aspects of Enzyme Dynamics, J. Biol. Chem. 289 (2014) 30205-30212.
[20] J.P. Klinman, A. Kohen, Hydrogen Tunneling Links Protein Dynamics to Enzyme Catalysis, Annu. Rev. Biochem. 82 (2013) 471-496.
[21] D.G. Truhlar, A. Kohen, Convex Arrhenius plots and their interpretation, Proc. Natl. Acad. Sci. 98 (2001) 848-851.
[22] J. Matthiesen, R.S. Smith, B.D. Kay, Mixing It Up: Measuring Diffusion in Supercooled Liquid Solutions of Methanol and Ethanol at Temperatures near the Glass Transition, J. Phys. Chem. Lett. 2 (2011) 557-561.
[23] J. Matthiesen, R.S. Smith, B.D. Kay, Using Rare Gas Permeation to Probe Methanol Diffusion near the Glass Transition Temperature, Phys. Rev. Lett. 245902 (2009) 1-4.
[24] A.C.P. Rosa, P. Vaveliuk, K.C. Mundim, M.A. Moret, A model for diffusive systems: Beyond the Arrhenius mechanism, Phys. A Stat. Mech. Its Appl. 450 (2016) 317-322.
[25] D. De Fazio, V. Aquilanti, S. Cavalli, A. Aguilar, J.M. Lucas, Exact quantum calculations of the kinetic isotope effect: Cross sections and rate constants for the F + HD reaction and role of tunneling, J. Chem. Phys. 125 (2006) 133109.
[26] J.-C. Rayez, L. Bonnet, P. Larrégaray, A. Perrier, Transition State Theory: A Reaction Dynamics Tool Applied to Gas-Surface Reactions, Mol. Sci. 3 (2009) A0029.
[27] L. Bonnet, J.-C. Rayez, Dynamical derivation of Eyring equation and the second-order kinetic law, Int. J. Quantum Chem. 110 (2010) 2355-2359.
[28] L. Bonnet, On the dynamical foundations of transition state theory: a semiclassical analysis, Ann. Phys. (N. Y). 314 (2004) 99-118.
[29] S.J. Klippenstein, V.S. Pande, D.G. Truhlar, Chemical kinetics and mechanisms of complex systems: a perspective on recent theoretical advances., J. Am. Chem. Soc. 136 (2014) 528-46.
[30] J.L. Bao, P. Sripa, D.G. Truhlar, Path-dependent variational effects and multidimensional tunneling in multi-path variational transition state theory: rate constants calculated for the reactions of HO^2 with tert-butanol by including all 46 paths for abstraction at C and all six paths for , Phys. Chem. Chem. Phys. 18 (2015) 1032-41.
[31] S. Chapman, B.C. Garrett, W.H. Miller, Semiclassical transition state theory for nonseparable systems: Application to the collinear $H+H_2$ reaction, J. Chem. Phys. 63 (1975) 2710-2716.
[32] P. Hänggi, M. Borkovec, Reaction-rate theory: fifty years after Kramers, Rev. Mod. Phys. 62 (1990) 251-341.
[33] Y. V. Suleimanov, F.J. Aoiz, H. Guo, Chemical Reaction Rate Coefficients from Ring Polymer Molecular Dynamics: Theory and Practical Applications, J. Phys. Chem. A. 120 (2016) 8488-8502.
[34] V. Aquilanti, S. Cavalli, D. De Fazio, A. Volpi, A. Aguilar, J.M. Lucas, Benchmark rate constants by the hyperquantization algorithm. The F + H^2 reaction for various potential energy surfaces: features of the entrance channel and of the transition state, and low temperatur e reactivity, Chem. Phys. 308 (2005) 237-253.
[35] V. Aquilanti, K.C. Mundim, S. Cavalli, D. De Fazio, A. Aguilar, J.M. Lucas, Exact activation energies and phenomenological description of quantum tunneling for model potential energy surfaces. The F+H^2 reaction at low temperature, Chem. Phys. 398 (2012) 186-191.
[36] M. Tizniti, S.D. Le Picard, F. Lique, C. Berteloite, A. Canosa, M.H. Alexander, I.R. Sims, The rate of the F + H^2 reaction at very low temperatures., Nat. Chem. 6 (2014) 141-5.
[37] V.H. Carvalho, V. Aquilanti, H.C.B. de Oliveira, K.C. Mundim, Deformed Transition State Theory: Inclusion of the Tunneling Effect by Euler Exponential, Limit of Validity and Description of Bimolecular Reactions, Rev. Process. Químicos. 9 (2015) 226-228.

[38] V.H. Carvalho-Silva, V. Aquilanti, H.C.B. de Oliveira, K.C. Mundim, Deformed transition-state theory: Deviation from Arrhenius behavior and application to bimolecular hydrogen transfer reaction rates in the tunneling regime, J. Comput. Chem. 38 (2017) 178-188.
[39] N.D. Coutinho, F. Sanches-Neto, V. Silva, H.C.B. de Oliveira, L. Ribeiro, V. Aquilanti, Kinetics of the OH + HCl H_2O+Cl reaction: rate determining roles of stereodynamics and roaming, and of quantum tunnelling, Chem. J. J. Comput. (2018).
[40] D. Claudino, R. Gargano, V.H. Carvalho-Silva, G.M. e Silva, W.F. da Cunha, Investigation of the Abstraction and Dissociation Mechanism in the Nitrogen Trifluoride Channels: Combined Post-Hartree–Fock and Transition State Theory Approaches, J. Phys. Chem. A. 120 (2016) 5464-5473.
[41] L.G. Santin, E.M. Toledo, V.H. Carvalho-Silva, A.J. Camargo, R. Gargano, S.S. Oliveira, Methanol solvation effect on the proton rearrangement of curcumin's enol forms: an ab initio molecular dynamics and electronic structure viewpoint, J. Phys. Chem. C. 120 (2016) 19923-19931.
[42] S.F. de A. Morais, K.C. Mundim, D.A.C. Ferreira, An alternative interpretation of the ultracold methylhydroxycarbene rearrangement mechanism: cooperative effects., Phys. Chem. Chem. Phys. 17 (2015) 7443-8.
[43] F.O. Sanches-Neto, N.D. Coutinho, V.H. Carvalho-Silva, A novel assessment of the role of the methyl radical and water formation channel in the CH_3OH + H reaction, Phys. Chem.Chem. Phys. 19 (2017) 24467-24477.
[44] S.G. Christov, The Characteristic (Crossover) Temperature in the Theory of Thermally Activated Tunneling Processes, Mol. Eng. 7 (1997) 109-147.
[45] R.P. Bell, The Tunnel Effect in Chemistry, Champman and Hall, London, 1980.
[46] E.P. Wigner, On the Behavior of Cross Sections Near Thresholds, Phys. Rev. 73 (1948) 1002-1009.
[47] T. Takayanagi, N. Masaki, K. Nakamura, M. Okamoto, S. Sato, G.C. Schatz, The rate constants for the H+H_2 reaction and its isotopic analogs at low temperatures: Wigner threshold law behavior, J. Chem. Phys. 86 (1987) 6133.
[48] V.H.C. Silva, V. Aquilanti, H.C.B. De Oliveira, K.C. Mundim, Uniform description of non-Arrhenius temperature dependence of reaction rates, and a heuristic criterion for quantum tunneling vs classical non-extensive distribution, Chem. Phys. Lett. 590 (2013) 201-207.
[49] V. Aquilanti, F. Sanches-Neto, N.D. Coutinho, V.H. Carvalho-silva, to be published.
[50] R.S. Timonen, J.A. Seetula, D. Gutman, Kinetics of the Reactions of Alkyl Radicals (CH_3, C_2H_5,i-C_3H_7,and t-C_4H_9)with Molecular Bromine, J. Chem. Inf. Model. 94 (1990) 3005-3008.
[51] J.A. Seetula, Kinetics and thermochemistry of the R+HBr reversible arrow RH+Br (R = C_2H_5 or beta-C_2H_4Cl) equilibrium - An ab initio study of the bond energies in partly chlorinated ethanes and propanes, J. Chem. Soc. Trans. 94 (1998) 891-898.
[52] V.I. Jaramillo, S. Gougeon, S.D. Le Picard, A. Canosa, M.A. Smith, B.R. Rowe, A consensus view of the temperature dependence of the gas phase reaction: OH + HBr → H^2O + Br, Int. J. Chem. Kinet. 34 (2002) 339-344.
[53] D. Stone, D.M. Rowley, Kinetics of the gas phase HO_2 self-reaction: effects of temperature, pressure, water and methanol vapours., Phys. Chem. Chem. Phys. 7 (2005) 2156-2163.
[54] R. Atkinson, R. Perry, J.P. Jr, Rate constants for the reactions of the OH radical with (CH) NH,(CH) N, and CHNH over the temperature range 298-426° K, J. Chem. Phys. 68 (1978) 1850-1853.
[55] P. Campuzano-Jost, J.N. Crowley, Kinetics of the Reaction of OH with HI between 246 and 353 K, J. Phys. Chem. A. 103 (1999) 2712-2719.
[56] N.D. Coutinho, V.H.C. Silva, H.C.B. de Oliveira, A.J. Camargo, K.C. Mundim, V. Aquilanti, Stereodynamical Origin of Anti-Arrhenius Kinetics: Negative Activation Energy and Roaming for a Four-Atom Reaction, J. Phys. Chem. Lett. 6 (2015) 1553-1558.

[57] N.D. Coutinho, V. Aquilanti, V.H.C. Silva, A.J. Camargo, K.C. Mundim, H.C.B. De Oliveira, Stereodirectional Origin of anti-Arrhenius Kinetics for a Tetraatomic Hydrogen Exchange Reaction: Born-Oppenheimer Molecular Dynamics for OH + HBr, J. Phys. Chem. A. 120 (2016) 5408-5417.

[58] N.D. Coutinho, V.H. Carvalho-Silva, H.C.B. de Oliveira, V. Aquilanti, The HI + OH → H_2O + I reaction by first-principles molecular dynamics: Stereodirectional and anti-Arrhenius kinetics, 2017.

[59] N.D. Coutinho, V. Aquilanti, F.O. Sanches-Neto, V.H. Carvalho-Silva, First-principles molecular dynamics and computed rate constants for the series of OH-HX reactions (X= H or the halogens): non-Arrhenius kinetics, stereodynamics and quantum tunnel, Press. (2018).

[60] M. Döntgen, M.-D. Przybylski-Freund, L.C. Kröger, W.A. Kopp, A.E. Ismail, K. Leonhard, Automated discovery of reaction pathways, rate constants, and transition states using reactive molecular dynamics simulations., J. Chem. Theory Comput. 11 (2015) 2517-24.

[61] K.L. Fleming, P. Tiwary, J. Pfaendtner, New Approach for Investigating Reaction Dynamics and Rates with Ab Initio Calculations., J. Phys. Chem. A. 120 (2016) 299-305.

[62] V. Imandi, A. Chatterjee, Estimating Arrhenius parameters using temperature programmed molecular dynamics, J. Chem. Phys. 145 (2016) 034104.

[63] J. Xie, W.L. Hase, Rethinking the SN2 reaction, Science. 352 (2016) 32-33.

[64] P. Manikandan, J. Zhang, W.L. Hase, Chemical Dynamics Simulations of X– + CH_3Y → XCH3 + Y– Gas-Phase SN2 Nucleophilic Substitution Reactions. Nonstatistical Dynamics and Nontraditional Reaction Mechanisms, J. Phys. Chem. A. 116 (2012) 3061-3080.

[65] M.A.F. de Souza, T.C. Correra, J.M. Riveros, R.L. Longo, Selectivity and mechanisms driven by reaction dynamics: the case of the gas-phase $OH(^{\cdot})$ + CH_3ONO_2 reaction., J. Am. Chem. Soc. 134 (2012) 19004-10.

[66] L. Wang, K. Krogh-Jespersen, R.A. Moss, Activation Parameters for Additions to Alkenes of Arylchlorocarbenes with Enhanced Electrophilicity, J. Org. Chem. 80 (2015) 7590–7593.

[67] K. Liu, Crossed-Beam Studies of Neutral Reactions: State-Specific Differential Cross Sections, Annu. Rev. Phys. Chem. 52 (2001) 139-164.

[68] X. Yang, State-to-State Dynamics of Elementary Bimolecular Reactions, Annu. Rev. Phys. Chem. 58 (2007) 433-459.

[69] X. Li, Z. Sun, Dynamical resonances in F+ H_2/HD reaction scattering, Theor. Chem. Acc. 137 (2018) 19.

[70] N. Bloembergen, C.K.N. Patel, P. Avizonis, R.G. Clem, A. Hertzberg, T.H. Johnson, T. Marshall, R.B. Miller, W.E. Morrow, E.E. Salpeter, A.M. Sessler, J.D. Sullivan, J.C. Wyant, A. Yariv, R.N. Zare, A.J. Glass, L.C. Hebel, G.E. Pake, M.M. May, W.K. Panofsky, A.L. Schawlow, C.H. Townes, H. York, Report to the American Physical Society of the study group on science and technology of directed energy weapons, Rev. Mod. Phys. 59 (1987) S1.

[71] S. Cavalli, V. Aquilanti, K.C. Mundim, D. De Fazio, Theoretical reaction kinetics astride the transition between moderate and deep tunneling regimes: The F + HD case, J. Phys. Chem. A. 118 (2014) 6632-6641.

[72] R.P. Bell, Quantum Mechanical Effects in Reactions Involving Hydrogen, Proc. R. Soc. London. Ser. A, Math. Phys. 148 (1935) 241-250.

[73] V. Aquilanti, E.P. Borges, N.D. Coutinho, K.C. Mundim, V.H. Carvalho-Silva, From statistical thermodynamics to molecular kinetics: the change, the chance and the choice, Rend. Lincei. Sci. Fis. e Nat. 29 (2018) 787-802.

[74] D. De Fazio, J.M. Lucas, V. Aquilanti, S. Cavalli, Exploring the accuracy level of new potential energy surfaces for the F + HD reactions: from exact quantum rate constants to the state-to-state reaction dynamics, Phys. Chem. Chem. Phys. 13 (2011) 8571-8582.

[75] D. De Fazio, The H + HeH^+ → He + H^{2+}reaction from the ultra-cold regime to the three-body breakup: Exact quantum mechanical integral cross sections and rate constants, Phys. Chem. Chem. Phys. 16 (2014) 11662-11672.

[76] G.J. Harris, A.E. Lynas-Gray, S. Miller, J. Tennyson, The role of HeH^+ in cool helium rich white dwarfs, 617 (2004)L143-L146.
[77] W. Roberge, A. Dalgarno, The Formation and Destruction of HeH^+ in Astrophysical Plasmas, 255 (1982) 489-496.
[78] D. Skouteris, J.F. Castillo, D.E. Manolopoulos, ABC: a quantum reactive scattering program, 133 (2000) 128-135.
[79] F.D. Colavecchia, F. Mrugała, G.A. Parker, R. T Pack, Accurate quantum calculations on three-body collisions in recombination and collision-induced dissociation. II. The smooth variable discretization enhanced renormalized Numerov propagator, J. Chem. Phys. 118 (2003) 10387-10398. doi:10.1063/1.1573186.
[80] D. Galli, F. Palla, The Dawn of Chemistry, Annu. Rev. Astron. Astrophys. 51 (2013) 163-206.

Rendiconti
Accademia Nazionale delle Scienze detta dei XL
Memorie di Scienze Fisiche e Naturali
136° (2018), Vol. XLII, Parte II, Tomo II, pp. 131-140

CESARE CECCHI-PESTELLINI*

Chiral Selection in Space: Role of Cosmic Dust

Abstract – It is well known that the amino acids occurring in proteins (natural amino acids) are exclusively of L-configuration. Among the many scenarios put forward to explain the origin of this chiral homogeneity, one involves the asymmetric photolysis of amino acids present in space, triggered by circularly polarized ultraviolet radiation. Here, I propose that amino acids formed in the cavities of dust aggregates in protoplanetary discs are exposed to asymmetric photolysis induced by an effective ultraviolet circularly polarization generated in situ.

1. *Introduction*

The origin of homochirality of amino acids and sugars is so far an unfilled gap for the theories of the chemical origin of life. Why amino acids occurring in proteins are, almost exclusively, of L-conformation and only D-conformation sugars enter the RNA and DNA molecules is, in fact, the most crucial question to be answered before indulging in any chemical, biological or philosophical discussion on the origin of life.

Quantitative analyses of cosmic debris show some amino acids presenting an excess of the L-conformation enantiomer (e.g., Engel & Nagy 1982), while both rare and common sugar monoacids (aldonic acids) may contain significant excesses of the D-enantiomer (Cooper & Rios 2016) in straightforward similarity with terrestrial biomolecular homochirality. This coincidence is too striking to be fortuitous; it points out that products of routine cosmic chemistry contributed to the early Earth organic pool and facilitated prebiotic molecular evolution.

Several controversial theories have been developed to explain an abiogenic origin of the chiral homogeneity in terms of the physico-chemical processes involved.

* INAF – Osservatorio Astronomico di Palermo, Piazza del Parlamento 1 - 90134 Palermo (PA), Italy.

For evident reasons, the highest astrophysical relevance has been awarded to processes involving radiation and magnetic fields. Among photochemical effects, only Circularly Polarized Light (CPL) and a static magnetic field collinear with a light beam are truly chiral systems and thus can potentially produce an enantiomeric enhancement within initially racemic mixtures.

The interaction of CPL with an isotropic medium containing chiral molecules in the presence of a constant external magnetic field may be described by several phenomenological constants, relating to optical activity and dichroism, summarized by slightly different dielectric constants associated with right- and left-handed CPL (e.g., Jorissen & Cerf 2002).

In this work I propose a new scenario in which amino acids formed in the cavities of dust grain aggregates (Duley, 2000, Williams & Cecchi-Pestellini 2016) in protoplanetary discs, are exposed to asymmetric photolysis induced by an effective ultraviolet CPL generated *in situ*. The enantiomeric excess of chiral biomolecules produced and protected in the cavities of grain aggregates may have contributed to the early Earth organic pool and facilitated prebiotic molecular evolution.

2. *The possible role of cosmic dust in the emergence of life on Earth*

Only a very small fraction of the organic compounds in nature are found in planets or comets and other condensed objects. By far the larger quantity – more than 99.9% by mass – reside in the enormous molecular clouds in interstellar space of the Milky Way and other spiral galaxies. Abiotic organic chemistry, as observed in molecular clouds, offers a glimpse of the chemical evolution preceding the onset of life on our own planet, and allows us to evaluate the possibility that, during the evolution from a molecular cloud to a planetary system, complex organic molecules are formed, transformed and preserved until they are incorporated into comets and meteorites.

Do complex organic molecules survive the processes of star and planet formation? The formation of a planetary system is a violent event, so the intricate chemical history of the gas from which the planet forms may be obliterated, requiring chemical evolution to be continuously restarted. On the other hand, the chemical mechanisms that generate biomolecules in space could be transferred to newly formed planets during a bombardment phase by the dust grains aggregates, comets, asteroids, and meteorites, so there is a potential connection between prebiotic organic chemistry and the chemistry of the interstellar medium. These exogenous products could, of course, have been complemented by substances arising on Earth.

Cosmic dust may have contributed to the emergence of life on Earth many times during the long evolutionary pathway that eventually gave rise to our planetary system, in the following ways: (1) contributing precursors for prebiotic chemistry in larger bodies, (2) serving as building blocks from which future comets, asteroids, and other celestial bodies may originate, (3) inducing the formation of the Earth

itself and – more generally – planets, (4) delivering complex organic molecules to the early Earth and Mars during the late heavy bombardment 4.5 billion years ago, (5) providing a stable and reducing environment for the ingredients needed to start life early and quickly, and (6) contributing to chiral selection in space. While there is considerable agreement regarding the points from (1) to (4), the last two issues are rather speculative and no general, or even partial consensus on the production and selection of chiral organic molecules in protoplanetary discs has been reached. The present proposal is based on these last two hypotheses.

3. *The potential of ice cavity gas-phase chemistry for chemical complexity*

All the early speculations about the origins of life on Earth were based on Solar System processes. Of these speculations, the more influential were the suggestions of possible Miller–Urey type syntheses in a reducing planet atmosphere, following production and recombination of radicals, and of catalytic, Fisher–Tropsch type processes in the early stages of the solar nebula. In 1957 Miller showed that formaldehyde and hydrogen cyanide were key intermediates in the synthesis of glycine. This led Orò. and his co-workers (1961) to study the products of a solution of ammonium cyanide (NH_4CN) in water, discovering that NH_4CN was converted in adenine, one of the four bases of DNA. Such, and other similar, discoveries determined the direction of research on prebiotic chemistry for many years. However, our understanding of the atmosphere on early Earth has changed since then, and it is now believed that the atmosphere consisted mostly of carbon dioxide, nitrogen, and water. Under such conditions, prebiotic molecules are produced only in trace amounts.

However, in the complex process leading to the formation of circumstellar discs around young stars from prestellar dense molecular clouds, physical conditions similar to those envisaged in the early prebiotic experiments may arise. In the high densities of the discs, these ice-coated dust grains collisionally agglomerate, assembling in loosely packed structures with much of their internal volume being vacuum and trapped ices. Sputtering of silicate, carbon solids, and PAHs by cosmic-rays will inject heavier atoms, ions and molecules into these ices.

The timescale for the accretion of volatiles on grains is much faster than that of grain aggregation, implying that the latter process occurs when dust grains have already accreted ice mantles. Interstitial voids must occur even in highly organized, densely packed structures. For example, dense packing of like spheres in a face-centered cubic lattice leaves 26% of space unoccupied. In surface chemistry the time delay between the adsorption and reaction steps may be substantial if the reaction products are non-volatile, but they can be short for prompt reactions. The products of surface reactions are either retained on dust or desorbed to the ambient gas. Duley (2000) noted that the interior of dust aggregates offers a different intermediate possibility: the re-accretion of reaction products by other components of the aggregate. This re-deposition may occur on the surface of other dust particles or on com-

ponents of an ice mantle. As desorbed products can be in an energetic state, these secondary reactions might be expected to mimic some aspects of high-temperature chemistry. Aggregate grains bring together all components of the interstellar gas and dust, a unique situation, outside planetary systems. As reaction products can remain trapped within aggregates and are shielded from radiation, conditions exist for the formation of larger molecules. The feedstock for this chemistry would be the ices accumulated during aggregation, together with light atoms and radicals from the ambient gas that diffuse into the interior of the aggregate.

Dust aggregates can be impulsively heated by collisions with other aggregates or grains and by cosmic-ray impacts. The heat released during a collision may lead to the vaporization of the ice content filling the cavities, in which radicals and molecules from the ice enter a transient, warm, high pressure gas phase, giving rise to: (1) a solid-state chemistry involving elements such as Si, Mg and Fe sputtered from silicate particles; (2) facilitated secondary reactions and rapid quenching of the reaction products; (3) a hydrogen rich atmosphere inside the cavities. The resulting mixture is a reasonable analogue of the conditions that Stanley Miller supposed as plausible for the primitive Earth atmosphere. Therefore, grain aggregates may represent in the interstellar medium the equivalent of terrestrial micro-laboratories containing raw materials of reducing chemical composition suitable for conversion into complex organic molecules. The final products are likely to be very similar to those obtained from laboratory chemistry under terrestrial conditions. Because of the reducing atmosphere in the cavities large organic molecules are allowed to form. Recent numerical experiments (Saitta & Saija 2014) based on ab-initio molecular dynamics simulations of aqueous systems subject to electric fields (e.g. describing lightning) and on metadynamics analysis of chemical reactions showed that glycine spontaneously forms from mixtures of simple molecules. Formic acid and formamide are key intermediate products of the early steps of the Miller reactions. Formamide represents the simplest molecule containing the peptide bond. It is therefore of great interest as an important precursor in the abiotic synthesis of amino acids, and of further prebiotic chemistry. Remarkably, when nitrogen compounds are present in the initial mixture, the processing of interstellar ice analogues produces formamide (e.g., Jones *et al*. 2011), and under suitable conditions aminoacids (e.g., Muñoz-Caro *et al*. 2002), and sugars (de Marcellus *et al.* 2015).

4. *Chiral selection in protoplanetary discs*

The formation yield of complex molecules depends critically on the dose of ultraviolet radiation impinging on the molecular material. Cecchi-Pestellini *et al*. 2005 showed that the interiors of grain aggregates are, in fact illuminated by a substantial fraction of the incident radiation. In addition to implications for the photochemistry of icy mixtures trapped in aggregate cavities, such residual radiation acquires polarization properties, that are directly related to asymmetric photo-reactions of chiral molecules.

The most general state of polarization of an electromagnetic field is elliptic and the direction of propagation is given by the Poynting vector $\boldsymbol{S}$. The latter has a fixed direction for a plane homogeneous wave and/or for a scattered field in the far zone. In both these cases the plane of polarization ellipse is orthogonal to the Poynting vector, so that the state of polarization is conveniently described by the Stokes parameters constructed with the components of the field orthogonal to the direction of propagation. In the interstitial material and in the cavities of the aggregate the direction of propagation of the field changes from point to point. The plane of polarization ellipse is in general not orthogonal to the vector $\boldsymbol{S}$. Consequently, the state of polarization of the field cannot be described by the usual Stokes parameters but it needs a more general description (Carozzi *et al*. 2000), e.g., through the definition of the real vector $\boldsymbol{V} = i\,(\boldsymbol{E} \times \boldsymbol{E}^*)$, where $\boldsymbol{E}$ is the electric field and $\boldsymbol{E}^*$ is its complex conjugate. The magnitude of $\boldsymbol{V}$ is $2/\pi$ times the area of the polarization ellipse. When $\boldsymbol{V} = 0$ the field is linearly polarized, otherwise the electric field rotates, as a function of time, in a counterclockwise sense with respect to $\boldsymbol{V}$. As a consequence, the sign of $V_S = \boldsymbol{V}\,\boldsymbol{S}/|\boldsymbol{S}|$ gives the sense of field rotation with respect to the direction of propagation of the electromagnetic energy. The components of the vector $\boldsymbol{V}$ are found expanding the spectral density tensor (the representation of the coherency dyad $\rho = \boldsymbol{E} \otimes \boldsymbol{E}^*$ in rectangular coordinates) in terms of the unit matrix $\mathbf{1}_3$ and of the eight Gell-Mann matrices that are the generators of the group SU(3). Details on the generalized description of the polarization of electromagnetic waves can be found in Borghese *et al*. 2005.

This has interesting consequences, e.g., when a linearly polarized wave impacts on the aggregate, the net result is the creation of additional components of the fields that thus lose their original state of being linearly polarized, acquiring a degree of circularity. In other words, the field depolarizes (becomes elliptically polarized) in the inner cavities of the aggregate giving rise to CPL, and thus providing a photoselective mechanism.

4.1 *A proof of concept*

I approximate the aggregate with a simple model consisting of a homogeneous sphere with radius ρ_0 embedding a spherical cavity with radius ρ_c. The incident field is assumed to propagate along the z axis and the reference plane is chosen to be the x-y plane (Fig. 1a). The location of the embedded cavity is determined by the couple of polar angles θ_c and φ_c, and by the distance from the center of the host sphere. I consider host spheres with radii around the value $\rho_0 = 100$ nm, taken as a reference. Dust particles of these sizes are efficient in causing interstellar extinction at visual wavelength. I choose four candidates for the interstitial material, namely silicates, amorphous carbon, water ice, and a Bruggeman mixture (Bohren & Huffman 1983) of 30% silicates, 30% amorphous carbon and 40% water ice. The Bruggeman mixing rule is applied only to the interstitial material, whereas the cavity is treated as a separate entity.

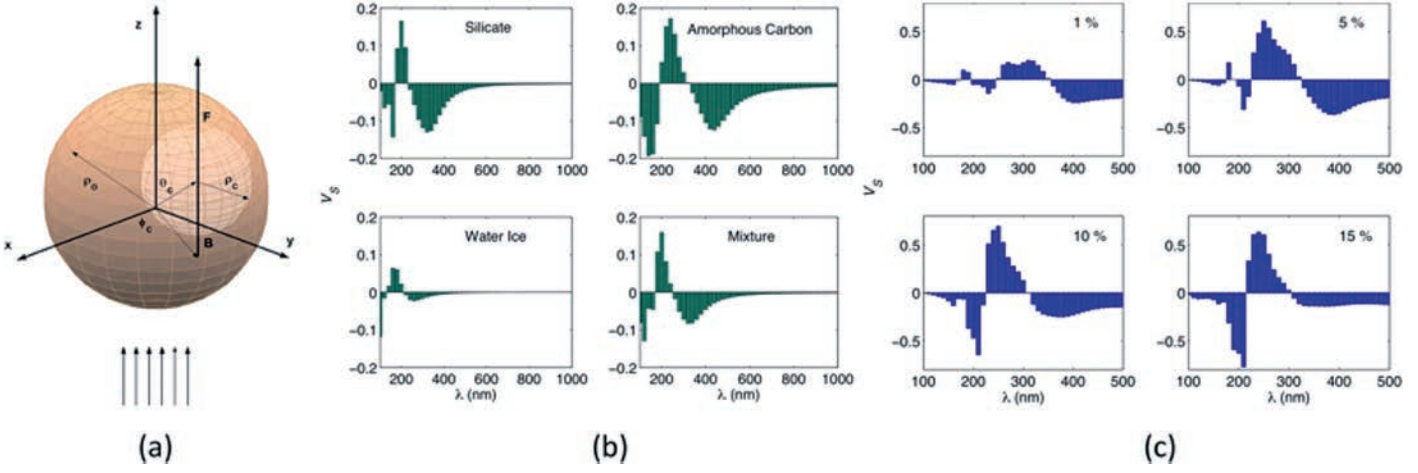

Fig. 1. (a) geometry of the interaction between the impinging wave and the «aggregate»; (b) V_S computed at the point B as a function of the wavelength for a aggregate and cavity radii of 100 and 74 nm (40% in volume), respectively, using different dust materials; (c) same as in (b) but with the variable cavity size; the dust material is the Bruggeman mixture.

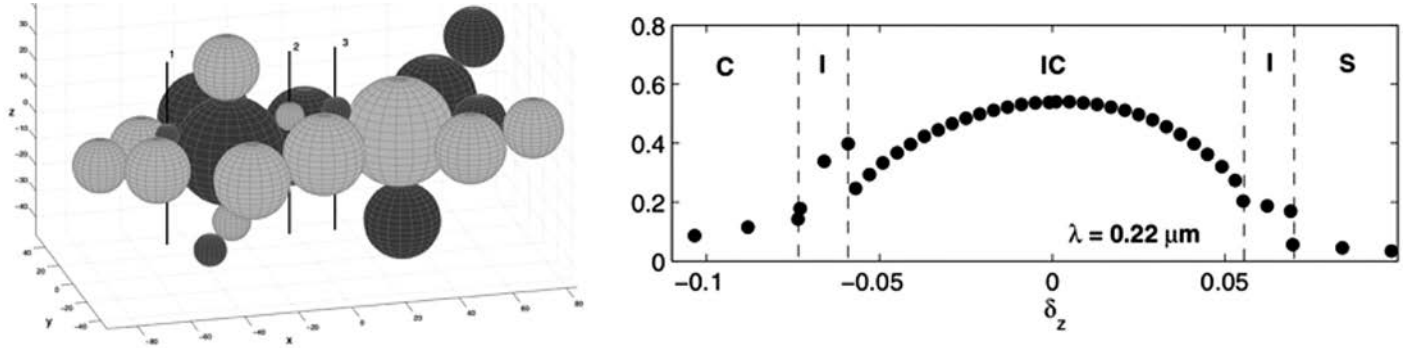

Fig. 2. Left panel – Geometry of the aggregate of spheres of different radii. The darker spheres have a core of carbon, whereas the lighter ones have a core of silicates. All the spheres are covered by a mantle of water ice whose thickness is 25% of the corresponding radius. Vertical lines indicate the position of resulting interstitial cavities; Right panel – V_S within cavity 2 as a function of the penetration of the radiation into the aggregate, for incidence along the z axis and polarization along the x axis. δ_z is the z coordinate scaled by the size of the aggregate. S: silicate sphere; I: ice layer; IC: interstitial cavity; C: carbon sphere.

V_S is computed at B and F (see Fig. 1a), i.e. the points at which the parallel to the z axis through the center of the cavity crosses its surface. Calculations show that: the largest depolarization effects occur for cavities tangent to the surface of the host sphere; rotating the position of the cavity with respect to both the x and y axes the sign of V_S is unchanged; the depolarization appears to be almost independent of the refractive index, the maximum value of V_S occurring in the range 100 – 500 nm for any choice of the material, while no depolarization occurs above 1 μm; depolarization effects are only slightly dependent on the volume of the embedded cavity (Fig. 1c); for evident symmetry reasons the field does not depolarize at points B and F when the cavity is centered on the z axis; the sign of field rotation alternates with wavelength (Fig. 1b).

This last property is particularly intriguing. In fact, every proposed mechanism for asymmetric photolysis induced by an external source of ultraviolet CPL has to meet with the Kuhn-Condon rule (e.g., Mason 2000). The most effective proposed external ultraviolet CPL sources operate only at a single photochemically active circular dichroic band, which is not shared by all biogenic amino acids. (Cerf & Jorissen 2000). In the present model the CPL, that spans a wide wavelength region from 100 nm to 1 μm, for volumes of the embedded cavity larger than the 5% of the volume of the host sphere, changes twice the sense of field rotation at approximately 200 and 300~nm. The inversion at 200 nm which fits exactly the circular dichroic spectra of Tryptophan and Proline occurs, for instance in an aggregate with radius $\rho_0 = 150$ nm, embedding a cavity with a volume about 40% of the volume of the host sphere.

4.2 *A more realistic case*

As a natural extension of the synthetic aggregate presented in the previous paragraph, dust grains are modelled here as a fluffily substructured collection of 25 stratified spheres, composed by a solid refractory core (silicates or amorphous carbon) covered by an icy water mantle (Fig. 2, left panel). The radii of the subunits are randomly chosen. Such a model includes the presence of interstitial voids generated by coagulation of particles.

A more realistic aggregate allows the possibility to assess the presence of trends and regularities in the wave depolarization pattern. V_S is computed at several points within the cavities for incidence along all coordinate axes (which is equivalent to a rotation of the target grain), in the wavelength range from 0.1 to 0.3 μm. The results indicate that a much lower depolarization occurs for incidence along the x axis, as well as along the y axis. Generally, the sign of V_S changes for rotations of the aggregate with respect to a fixed direction of incidence and of polarization.

Major results of the study are as follows: (1) in all examined cases a net depolarization is present; (2) depolarization in a given cavity depends exclusively on the environment, i.e., morphology and chemical composition of the aggregate close to

the cavity; (3) any time there is significant depolarization in an interstitial cavity, a significant amount occurs in its icy boundaries (see Fig. 2, right panel), the most interesting region for photochemistry; (4) in all examined cases, the depolarization depends on the wavelength, with V_S varying both in sign and/or in value, in going from $\lambda = 0.1$ to 0.2 μm; (5) significant depolarization occurs when the projected section of the target aggregate on a plane perpendicular to the direction of incidence of the wave bears enough asymmetry; (6) the sign of V_S changes erratically from cavity to cavity; there is however a tendency of CPL sign to be the different in the inner and outer parts of the aggregate; (7) rotations can affect the sign of Vs, but, on average, a net depolarization of a given sign is always present, i.e., the integral of V_S over the rotation angle is never zero; (8) the depolarization appears to be essentially determined by the geometry of the nearest environment.

Since the sign of V_S is not the same in different cavities of the same aggregate, it is not clear whether or not the depolarization, i.e., the presence of an effective CPL within the ice layers, might be relevant to the selection of chiral molecules.

5. *Discussion and conclusions*

In this work, I address the problem of field depolarization within interstellar dust aggregates, in which coagulation generates interstitial cavities partly filled with icy condensed gas. The present calculations show that a net depolarization effect is always present in all cavities, although the signs of generated CPL depend on the location within the aggregate in an unclear way. This prevents the establishment of a net enantiomeric excess of a given symmetry.

Since the effect is purely geometric, it is not chiral since it does not provide a symmetry breaking. In fact, the sign of the induced circular polarization changes with rotation of the cavities with respect to axes parallel to the propagation of the wave. The breaking of spatial symmetry may be provided by dust grain alignment with respect to the stellar incident field. When embedded in a protoplanetary disc, real aggregates can be efficiently aligned by interacting with the gaseous flow both in subsonic and supersonic regimes. The alignment arises from grains having irregularities that scatter atoms with different efficiency in the right and left directions. Although, the tendency for grains is to align with long axes perpendicular to the magnetic field, paramagnetic dissipation is not involved (Lazarian & Hoang 2007), and the specific chemical composition of a dust aggregate is irrelevant. In conclusion, if the aggregates in the protoplanetary disc are aligned, they must share the same geometrical asymmetry: the denser part leading and the more porous one following. Because the more porous part has more cavities a net enantiomeric excess of chiral biomolecules is to be expected in the aggregates.

The ubiquitous mutual presence of ultraviolet linearly polarized radiation and dust aggregation in star forming regions may provide the conditions for a widespread universal replication of the chiral selection.

REFERENCES

[1] Borghese, F., Denti, P., Saija, R. & Cecchi-Pestellini, C. 2005, *On The Polarization And Depolarization Of The Electromagnetic Waves*, Journal of Physics: Conference Series, 6, 59.
[2] Bohren, C.F. & Huffman, D.R. 1983, *Absorption And Scattering Of Light By Small Particle*, J. Wiley & Sons.
[3] Carozzi, T., Karlsson, R. & Bergman, J. 2000, *Parameters Characterizing Electromagnetic Wave Polarization*, Physical Review E, 61, 2024.
[4] Cecchi-Pestellini, C. *et al.* 2005, *Ultraviolet Radiation Inside Interstellar Grain Aggregates. I. The Density Of Radiation*, Astrophysical Journal, 624, 223.
[5] Cerf, C. & Jorissen, A. 2000, *Is Amino-Acid Homochirality Due To Asymmetric Photolysis In Space?*, Space Science Review, 92, 603.
[6] Cooper, G. & Rios, A.C. 2016, *Enantiomer Excesses Of Rare And Common Sugar Derivatives In Carbonaceous Meteorites*, Proceedings of the National Academy of Sciences of the U.S.A., 113, 10.1073.
[7] de Marcellus, P. *et al.* 2015, *Aldehydes And Sugars From Evolved Precometary Ice Analogs: Importance Of Ices In Astrochemical And Prebiotic Evolution*, Proceedings of the National Academy of Sciences of the U.S.A., 112, 965.
[8] Duley, W.W. 2000, *Chemistry In Grain Aggregates: A Source Of Complex Molecules?*, Monthly Notices of the Royal Astronomical Society, 319, 791.
[9] Engel, M.H. & Nagy, B. 1982, *Distribution And Enantiomeric Composition Of Amino Acids In The Murchison Meteorite*, Nature, 296, 837.
[10] Jones, B.M., Bennett, C.J. & and Kaiser, R.I. 2011, *Mechanistical Studies on the Production of Formamide (H_2NCHO) Within Interstellar Ice Analogs*, Astrophysical Journal, 734, 78.
[11] Jorissen, A & Cerf, C. 2002, *Asymmetric Photoreactions As The Origin Of Biomolecular Homochirality: A Critical Review*, Origins Of Life And Evolution of the Biosphere, 31, 167.
[12] Lazarian, A. & Hoang, T. 2007, *Grain Alignment Induced By Radiative Torques: Effects Of Internal Relaxation Of Energy And Complex Radiation Field*, Astrophysical Journal, 669, 77.
[13] Mason, S.F. 2000, *Extraterrestrial Handedness Revisited*, Origins of Life and Evolution of Biosphere, 30, 435.
[14] Miller, S.L. 1957, *The Mechanism Of Synthesis Of Amino Acids By Electric Discharges*, Biochimica et Biophysica Acta, 23, 480.
[15] Muñoz-Caro, G.M. *et al.* 2002, *Amino acids from ultraviolet irradiation of interstellar ice analogues*, Nature, 416, 403.
[16] Orò, J. & Kinball, A. 1961, *Synthesis of purines under possible primitive earth conditions. I. Adenine from hydrogen cyanide*, Archives of Biochemistry and Biophysics, 94, 217.
[17] Saitta, A.M. & Saija, F. 2014, *Miller experiments in atomistic computer simulations*, Proceedings of the National Academy of Sciences of the U.S.A., 111, 13768.
[18] Williams, D.A. & Cecchi-Pestellini, C. 2016, *The Chemistry of Cosmic Dust*, Royal Society of Chemistry Publishing.

Rendiconti
Accademia Nazionale delle Scienze detta dei XL
Memorie di Scienze Fisiche e Naturali
136° (2018), Vol. XLII, Parte II, Tomo II, pp. 141-149

SAVINO LONGO*

The State-to-state kinetics: from a Sumerian prototype to astrobiology

Abstract – The state-to-state (STS) kinetics, in which molecules in different internal states are considered as different species in the description of chemical reactions, is one of the most productive concepts in theoretical chemistry with an endless record of successful applications. An example is the formulation of scenarios for the production of oxygen on Mars. In the STS formulation of a chemical problem, distribution functions appear, which describe the population of molecules in these different states. The problem of composition change with time can be solved only when these distributions, and their changes too, are included in the calculations. Remarkably, the basic ideas of this approach are already found, in the author's opinion, in a 40-centuries old Sumerian tablet which reports a fully theoretical cattle breeding account. This document also anticipates some basic ideas of computer science, like the execution of a program and the management of a structure of data. 40 centuries later, ideas from this prototype may help to explain the predominance of a single chiral version in biological molecules and organisms.

Introduction: the state-to-state kinetics and its importance

One of the most productive concepts of modern theoretical chemistry is the *state-to-state kinetics* (STS in the following) [1-3]. It is based on the known fact that in some chemical reactions networks, the internal state of molecules has such a strong effect on reactivity, that the molecular species must be conceived as mixtures of several components, each component of the mixture being the ensemble of molecules in a given state. According to this view the species is therefore represented as a probability distribution, the state- or energy- distribution. This concept has found

* Chemistry Department of the University of Bari and CNR, Via Orabona 4 - 70126 Bari, Italy. E-mail: savino.longo@uniba.it

wide application to the determination of chemical reaction rates in fields as different as atmospheric science, astrophysics, catalysis, energy production and many others.

A large number of very important examples can be used to illustrate the importance of the STS concept [3]. One which is gaining recently much visibility for its relevance to space technology and Mars colonization scenarios is the following: CO_2, the most important component of Mars atmosphere, may be converted to CO and atomic oxygen by a reaction where electrons in a gas are used to pump up energy into the vibrational degrees of freedom of the CO_2 molecule [4-5]. Since the most effective dissociation path is through the asymmetric stretching mode, it is necessary to distinguish the 22 vibrational levels of this mode. Electron impact processes, the so-called eV, however, can only pump energy into the lowest vibrational levels, say the first 4 or 5. Subsequently, CO_2 molecules reach the dissociation limit with the help of a different process, named VV_1, where a low excited CO_2 molecule interacts with a more excited one pushing this last to higher excitation

$$CO_2(1)+CO_2(v)\rightarrow CO_2(0)+CO_2(v+1)$$

This mechanism, which was extensively studied by Russian scientists in the 70's-80's [6], works like a «conveyor belt» where molecules are moved up the ladder until they reach dissociation, i.e.

$$CO_2(1)+CO_2(21)\rightarrow CO_2(0)+CO+O$$

Note that no dissociation occurs until the top of the internal energy ladder is reached.

A remarkable aspect of the STS reaction schemes is that the knowledge of the concentration of a given species is no more sufficient to specify its state. Knowledge of a «hidden distribution» becomes necessary, the distribution of individual molecules in individual conditions (internal state, speed, age, depending on the problem). This distribution must be computed, stored and updated in order to determine the reaction rate. The equation, or scheme, normally used to update this internal distribution is called «Master Equation». This is a classical probability expression, not to be confused with the Pauli Master Equation in spin relaxation problems. The state of the system is specified only if the distribution of molecules into this collection of states is provided.

A very early example of the role of distributions in a growth problem

Surprisingly, early studies of this idea are very old. It is claimed in the present work that they are as old as 40 centuries, and possibly more. The oldest «paper» is not even paper but a clay table: a Sumerian tablet kept in the Louvre museum (the AO5499 table). This table was found in the Puzriš-Dagan excavation, the modern

Drehem. It dates back to king Shulgi period of neo-Sumerian culture in Ur, giving to the tablet an estimated date of 2000-2100 BC. The tablet is fully written in Sumerian, on both sides. The text of AO5499 describes what is presented as a cattle breeding account, and names it the «problem of the scribe Idua». It looks at a first view as an accurate account of cows (ab_2) and bulls (gu_4) during several years (figure 1), but, as it was recognized long ago [6], the «problem of Idua» is actually the first known model of a growth process formulated on pure theoretical basis [7-8]. It introduces a distribution of cattle ages. Only adult cows ($ab_2.mah_2$) reproduce. On AO5499 the problem is solved reporting the numbers of individuals as a function of age and time (Figure 1). While a description of AO5499 and its recognition as a theoretical problem is found for example in [7], here we will adopt the modern terminology while connecting this problem to the STS kinetics.

The process involved is actually very clear and self-explanatory even after four millennia. The state of the cattle is defined by a vector N of dimension 5. This vector contains the number of cows with ages from 0 to the mature state named mah_2. In this specific example mah_2=4 which means that N is a vector of mah_2+1=5 elements, marked in the tablet as follows: calf ($ab_2.amar.ga$), 1 year old ($mu\ 1$), 2 years old, 3 years old, adult ($ab_2.mah_2$), see again figure 1.

The number of individuals of age x becomes equal to the number of individuals of age x+1 at the next «step», in this way:

$$N(0) \rightarrow N(1) \rightarrow N(2) \text{ and so on}$$

But adult cows only increase in number, with no mortality, betraying the theoretical nature of the problem

$$N(mah_2) \leftarrow N(mah_2)+N(mah_2\text{-}1)$$

The number of newborns, N(0), is calculated by a simple model: the number of newborns is equal to the number of mature cows N(mah_2), but they are distributed between males and females in alternation. This regular alternation is another, even stronger, clue of the theoretical nature of the account.

The Idua problem, from a modern perspective, anticipates many important concepts:

(1) A growth process is influenced by the distribution of different states of individuals (the STS concept);

(2) the distribution can be represented by a collection of individuals in different states (similar to a modern event-driven simulation);

(3) the evolution is essentially obtained by shifting the recorded data in a sequence (the modern «stack» concept in computer Science).

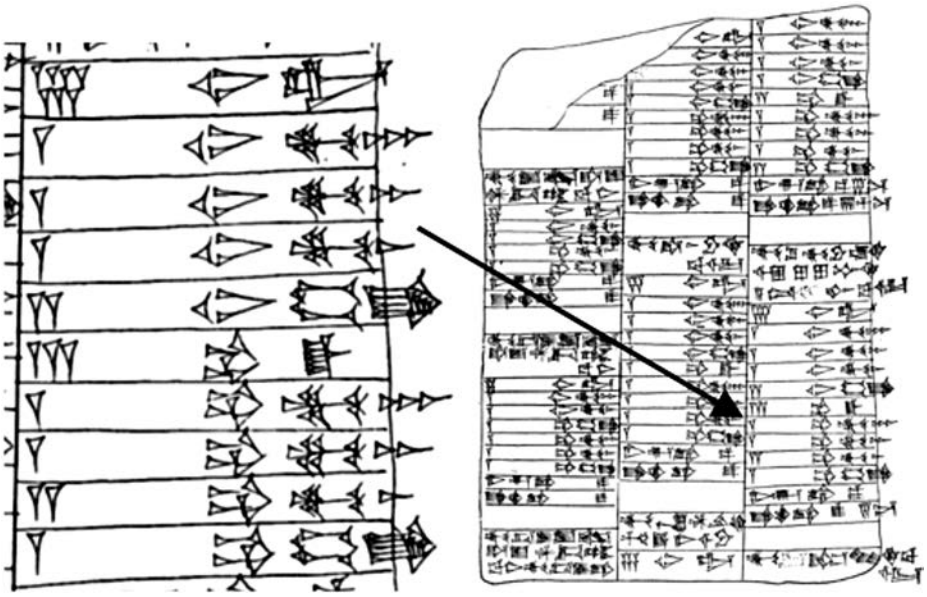

Fig. 1. The AO5499 tablet. Left: the calculated age distribution after 7 yrs. including (from above) 7 adult cows, one 3 years old, one 2 years old, one 1 year old, 2 heifer calves; 3 adult bulls, one 3 years old, one 2 years old, two 1 year old, 1 bull calf. Right: full obverse of the tablet (the simulation continues on the other side). The attribution of the problem to Idua is on the left bottom corner. Adapted from the Cuneiform Digital Library Initiative archive [7].

Idua sequences: new applications for a 40 centuries old idea

In a modern revisit of the problem of Idua, simple computer programs can be used to produce a variety of «Idua sequences», using parameter values no more limited by the original application. An example, in figure 2, extends considerably the number of states (using mah_2=20 instead of 4). The evolution of this more extended simulation displays better the structure of the sequence. The employ of these or similar deterministic sequences in chemical kinetics is suggestive, since they express in a very simple form the effect of internal distribution evolution in a multiplication process. The example in figure 2 already presents a nontrivial kinetics, due to the delays introduced by the necessity for new individuals to reach the uppermost level and contribute to the production rate. Even leaving, as here, the production rule strictly equal to those reported in the original Idua problem, the growth can be strongly influenced by different choices for the initial distribution of ages.

The study of the mathematical and numerical properties of «Idua sequences» by modern standards can be an interesting topic for new researches in theoretical chemistry and numerical analysis.

Fig. 2. Author's computer-generated «Idua sequence» with $mah_2 = 20$ and an arbitrary initial population (upper row) with only two individuals with initial state 6 and 11: time flows from top to bottom. New individuals in the 0 state appear only after 10 time-units and the internal population is continuously evolving.

It is not difficult to imagine chemical systems for which an Idua sequence could provide an insightful model: a possibility is a population of molecules which receive free energy from a substrate in successive steps and, when the stored energy is high enough to compensate for a thermodynamic or kinetic threshold, undergo *self-replication*, i.e. a reaction of the form

$$A(i) + S^* \rightarrow A(i+1) + S$$
$$A(n) + S^* \rightarrow 2A(0) + S$$

where S and S* are the energy-poor and energy-reach version of an environmental species. The self-replication step is the last one. Note the difference between self-replication and the CO_2 dissociation reaction in the previous section.

Chiral selection and prebiotic evolution

Computational models including the STS concept and self-replication, like those described by Idua sequences and in the previous section, may look artificial, but they have been actually much studied in the past and applied to some of the most fundamental problems in chemistry and biology. An example from the study on the origin of life and astrobiology is the attempt to explain the predominance of biological molecules, as well as whole organisms, which have a well-defined chirality

(L *levo* or D *destro*). This last is the geometrical property which distinguishes a left hand from a right one (thereby its name, from *χειρ*, hand). The two chiral variants, called *enantiomers*, have the same thermodynamic stability and should be present in biological systems with the same occurrence, all the opposite of what is actually found. Explanations of this predominance of a single chirality in biomolecules included many possible external causes which may have favored the formation of one species, by a process of chirality induction, or inheritance, from the environment in which the formation occurs. Among the causes considered there were the chirality of crystal surfaces on which biomolecules where first produced, polarized light, electroweak interactions, the effect of fluid vortexes [9-12].

A new concept was tested by a series of computer simulations in the group of the author a few years ago [13]. The concept is based on the breakup of the celebrated law of large numbers in statistics in a system of self-replicating individuals. The actual model proposed was very complex, involving an internal «genetic code» for any individual, but here it will be described in a simpler way to catch its essential features. The model is based on a simulation of an ensemble of individuals of two different chiral states L and D which can self-reproduce, move by drift and diffusion, and compete for «chemical energy» resources, these last are in the form of «activated cells» which appear randomly in the simulation domain.

An element of strong similarity of this computer experiment with the Idua problem is that the individuals, or «agents» in the simulation have an internal state and that this state is updated at any computational step based on the events occurring in the simulations. Only individuals reaching the uppermost level in the internal scale can reproduce themselves, with the same chirality e.g. a L individual produces another L individual and a D individual produces another D.

An essential breakthrough of this scenario is that, in the random process of replication of the two species competing for the same resources (energy, space, etc.), anomalous fluctuations, similar to critical fluctuations in thermodynamics, arise, which may push one of the alternative species to full extinction even when this last is an extremely unlike outcome according to the law of large numbers (see figure 3).

In this way a mechanism of selection between two isomers L and D initially in a racemic mixture is demonstrated. A very interesting feature of this mechanism is that it is not based on external chiral influences. The selection of a single chiral variant is, of course, random, but the selection process is immensely more effective than in a typical random process. Details of this mechanism have been discussed on ref. [13] where a quantitative explanation of the outcome is also provided based on the numerical solution of the corresponding Master Equation. It was also shown that the chiral symmetry breaking mechanism is critically dependent on the order of the destruction process, which must be pseudo-first order and not higher, e.g. second order. As an alternative to using a Master equation, accurately devised deterministic sequences could be used in the future to mimic the essential features of these prebiotic models and gain further insight into the process.

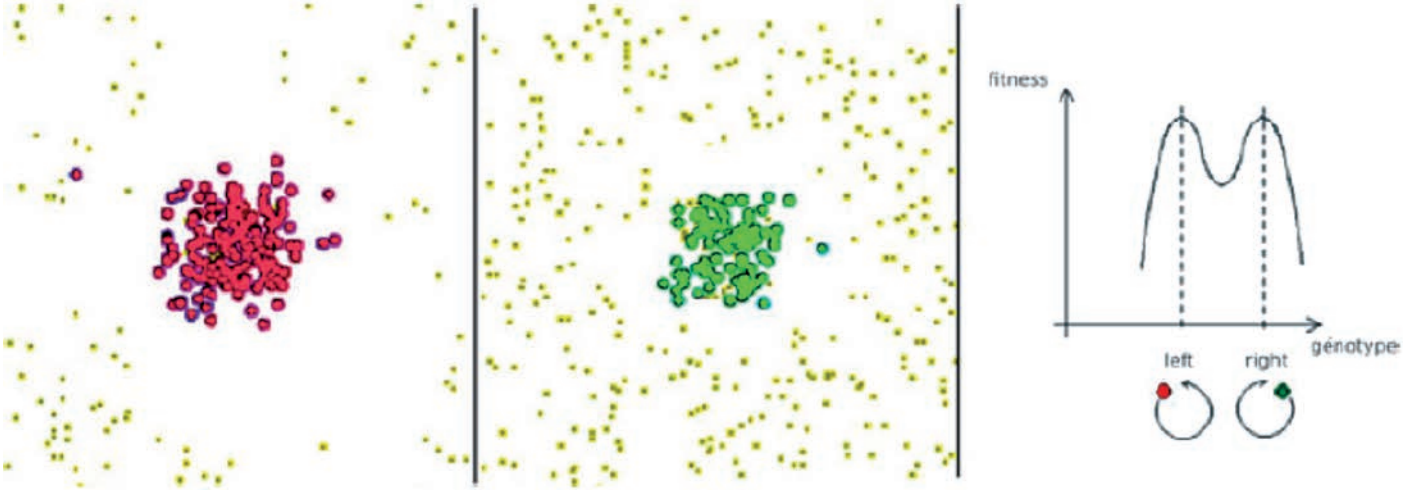

Fig. 3. In this figure, chiral species colonize a 2D space in a demonstration based on the model developed in [8]. The yellow dots are the energy reservoirs S* that bring the chiral species to a higher energy state. The chiral species are represented by circles with different colors, purple-red (L) vs. green-yellow (D). All simulations start from situations where no chirality is predominant. Left panel: simulation in which only the former chiral version remains; central panel: same situation, but opposite dominant chiral version. In the right panel, the chiral symmetry breaking exemplified by this simulation is shown. Adapted from [12].

Conclusions

The STS approach may allow us to formulate appropriate models for countless problems involving molecules which are reacting while performing transitions between their internal states. An example is the production of oxygen out of carbon dioxide on Mars. All these models assume that molecules or species climb a ladder of internal states whose uppermost step is the condition where a reaction is possible. Although this approach, so formulated, looks intrinsically tied to molecules, the inspiration behind it is much more general: an evolving distribution of individual conditions influences the global changes of the population. This idea, quite remarkably, was reported in written form, and concretely demonstrated by a test case, about four millennia ago on a clay tablet. On this tablet the formulation and solution of a problem of growth driven by a distribution of age is presented in the form of cattle accounting during several years. 40 centuries later a variant of this approach shows how a single chiral variety emerges in the course of prebiotic evolution as well as in developed organisms. This is possible since, in its very essence, the STS approach is a special case of an ancient idea of enormous versatility: is it is possible to produce a theoretical model of the changes in a system by defining a rule to calculate the next step in time and iterating the calculation process. Even more important, it is possible to get insight from the observation of the evolution of this virtual world as it evolves on the screen of the computer today, or on the tablet of the scribe in the past.

REFERENCES

[1] Levine, Raphael D. *Molecular reaction dynamics*. Cambridge University Press, 2009.
[2] Capitelli, M., Celiberto, R., Colonna, G., Esposito, F., Gorse, C., Hassouni, K., … & Longo, S. (2015). *Fundamental aspects of plasma chemical physics: Kinetics* (Vol. 85). Springer Science & Business Media.
[3] Steinfeld, J.I., Francisco, J.S., & Hase, W.L. (1989). *Chemical kinetics and dynamics* (Vol. 3). Englewood Cliffs (New Jersey): Prentice Hall. Chapter 9.
[4] Guerra, V., Silva, T., Ogloblina, P., Grofulovi, M., Terraz, L., da Silva, M.L., … & Guaitella, O. (2017). The case for in situ resource utilisation for oxygen production on Mars by non-equilibrium plasmas. *Plasma Sources Science and Technology*, *26*(11), 11LT01.
[5] Diomede, P., van de Sanden, M.C., & Longo, S. (2017). Insight into CO_2 dissociation in plasma from numerical solution of a vibrational diffusion equation. *The Journal of Physical Chemistry C*, *121*(36), 19568-19576.
[6] Rusanov, V.D.; Fridman, A.A.; Sholin, G.V. The Physics of a Chemically Active Plasma with Nonequilibrium Vibrational Excitation of Molecules. *Sov. Phys. Usp.* **1981**, *24*, 447-474.
[7] Nissen, Damerow & Englund, Archaic Bookkeeping (1993) 97-102.
[8] Cuneiform Digital Library Initiative, https://cdli.ucla.edu: result for AO5499.
[9] Viedma, C. (2001). Enantiomeric crystallization from DL-aspartic and DL-glutamic acids: implications for biomolecular chirality in the origin of life. *Origins of Life and Evolution of the Biosphere*, *31*(6), 501-509.

[10] Avetisov, V.A., Kuz'min, V.V., & Anikin, S.A. (1987). Sensitivity of chemical chiral systems to weak asymmetric factors. *Chemical physics*, *112*(2), 179-187.
[11] Aquilanti, V., and G. S. Maciel. «Observed molecular alignment in gaseous streams and possible chiral effects in vortices and in surface scattering». *Origins of Life and Evolution of Biospheres* 36.5-6 (2006): 435-441.
[12] Cecchi-Pestellini C. Chiral Selection in Space, *Rendiconti Accademia dei XL*, XLII, II, 1.
[13] Longo, S., & Coppola, C.M. (2013). Stochastic models of chiral symmetry breaking in autocatalytic networks with anomalous fluctuations. *Rendiconti Lincei*, *24*(3), 277-281.

Rendiconti
Accademia Nazionale delle Scienze detta dei XL
Memorie di Scienze Fisiche e Naturali
136° (2018), Vol. XLII, Parte II, Tomo II, pp. 151-162

ALESSANDRA F. ALBERNAZ[1] – VINCENZO AQUILANTI[2,3]
PATRICIA R. P. BARRETO[4] – ANA CARLA P. BITENCOURT[5]
CONCETTA CAGLIOTI[2,*] – ROBENILSON F. DOS SANTOS[6,7]
ANDREA LOMBARDI[2] – GLAUCIETE S. MACIEL[8]
FEDERICO PALAZZETTI[2] – MIRCO RAGNI[5]

Mapping the configurations of four-bar mechanisms as chirality change processes: a clue in evolutionary science

Abstract – The mechanism of four bars is a prototypical tool of kinematics that has found numerous applications in a variety of areas, since the Industrial Revolution until the Robotics, is here mapped on a screen, developed for representing the configurations of quadrilaterals as functions of their diagonals. The method permits to successfully compact and classify the large amount of structural data obtained during the years on a representative class of peroxides and persulfides. It is based on the two-dimensional representation of the distances sensitive to the variation of the dihedral angle around the O - O and S - S bonds of peroxides and persulfides, with a consequent change in chirality. The screen representation was inspired by the geometrical interpretation of the 6*j* symbols formulated in the asymptotic limit through the Ponzano - Regge theory, thus applying the properties of the tetrahedra and

[1] Instituto de Física, Universidade de Brasília, CEP 70919-970, Brasília, DF, Brazil.
[2] Dipartimento di Chimica, Biologia e Biotecnologie, Università di Perugia, via Elce di Sotto 8, 06123 Perugia, Italy.
[3] Istituto di Struttura della Materia - Consiglio Nazionale delle Ricerche, 00016 Rome, Italy.
[4] Instituto Nacional de Pesquisas Espaciais (INPE)/MCT, Laboratorio Associado de Plasma (LAP), CP515, Sao Jose dos Campos, Sao Paulo CEP 12247-970, Brazil.
[5] Departamento de Física, Universidade Estadual de Feira de Santana, Avenida Transnordestina s/n, 44036-900 Feira de Santana, BA, Brazil.
[6] Instituto de Fisica, Universidade Federal da Bahia, Campus Universitario de Ondina, CEP 40210-340 Salvador, BA, Brazil.
[7] Instituto Federal de Alagoas - Campus Piranhas, CEP 57460-000 Piranhas, AL, Brazil.
[8] Secretaria de Estado da Educação do Distrito Federal, 70040-020, Brasilia, DF Brazil.
* Corresponding author: concettacaglioti@hotmail.com

quadrangles, together with the symmetry properties of the 6*j* symbols. A first information obtainable from these diagrams is the systematic screening of available data: those used here are homogeneous and their accuracy can be improved so that the screen can provide information on the features regulating specific properties. A presentation is also given on a scrutiny of various systems encountered in nature, such as macromolecules, bacteria, vertebrates and invertebrates, demonstrating the ubiquity of the four-bar linkage: for these systems the screen provides a representation to be applied in order to analyze the functional configurations.

1. Introduction

Interest in peroxides and persulfides, the arguably simplest cases of chiral molecules (the two mirror forms being interconverted through torsional motions [1, 2]), greatly increased in the scientific community when hydrogen peroxide was discovered in the interstellar medium [3]. Necessity of compacting and classifying the great variety of data accumulated on these molecules by our group, lead us to develop a method that allows one to visualize their structural, thermodynamic and kinetic data [4-7]. We present a method alternative to the Ramachandran diagram familiar in biochemistry that consists of a plot as a function of distances only, while the Ramachandran diagram is instead a plot as a function of two dihedral angles that visualizes various properties such as the allowed geometries for the various aminoacids that form the peptides. In molecular sciences, angles are much harder to be experimentally accessible, and *e. g.* for peroxides and persulfides, a diagram as a function of the distances is one of choice. Therefore, the proposal is here made that the method be extended also to wide classes of molecules.

The recently established connections between classical and quantum mechanical tools of angular momentum in quantum mechanics [8], on which the idea of a screen is originated, is connected to the four-bar mechanism [9] that is at the basis of the operation of a great variety of several machines moderately extended to robotics. Interestingly it is also observed in both the simplest and the most complex living beings. The screen could be employed to interpret and analyze their motions and the functionally relevant configurations.

The paper is structured as follows: in Section 2, the example of peroxides and persulfides serves to introduce a description of the application of the screen to this ample class of molecules; in Section 3, we report various cases encountered considering living beings that operate through the four-bar mechanism; in Section 4, we give concluding remarks. (Figures 1 and 2 are adapted from Ref. 15).

2. The *screen* applied to peroxides and persulfides

Geometrical features of peroxides and persulfides can be characterized according to their dihedral angle [10-12]. The nomenclature defines *cis* geometries with reference to molecules having dihedral angle of 0°, *trans* geometries with those

having dihedral angles of 180°; for the equilibrium geometries, especially interesting from the view point of chirality since correspond to the pair of enantiomers, the dihedral angle is typical of each molecule. In this section, we will illustrate the method of the screen applied to peroxides and persulfides, defining the quadrilaterals, quadrangles and tetrahedra associated to these class of molecules and showing comparisons between the interatomic distances here introduced and the nomenclature adopted for the 6*j* symbols which occur in the quantum theory of angular momentum.

2.1. *Quadrilaterals, quadrangles and tetrahedra associated to peroxides and persulfides*

In planar Euclidean geometry a quadrilateral is defined as a geometrical object with four sides and four vertices, where the two diagonals join its opposite vertices. The sum of the four inner angles is 360°. In projective and affine geometries, a complete quadrilateral is formed by four points and six lines, where diagonals are considered as further sides. A complete quadrangle includes four incident lines in six points. In projective geometry, quadrangles and quadrilaterals are treated on the same footing. Such objects can be seen in tridimensional geometry as tetrahedral for which the volume is zero.

From a molecular view point, let us consider for definiteness a generic peroxide (Fig. 1), $R_1O_1O_2R_2$, and define a quadrilateral using the four centers in the following way: O_1R_1-O_2R_1-O_1R_2-O_2R_2, these distances define the sides of a quadrilateral, where O_1O_2 and R_1R_2 are the diagonals, to be eventually taken as our variables.

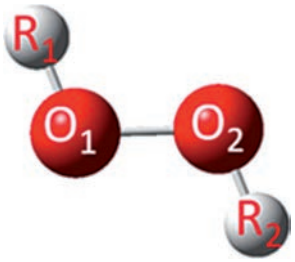

Fig. 1. A generic peroxide, the substituents are indicated with R_1 and R_2, while the oxygen atoms with O_1 and O_2 (for persulfides, O_1 and O_2 are replaced by S_1 and S_2 indicating sulfur atoms). Adapted from ref. [17].

The sides of the quadrilateral are conveniently classified as follows: *a* is the shortest side, *c* is opposite to *a*, *d* is longer than b. The quadrilaterals are identified as biconcave, concave and convex, depending on the number of diagonals located in and out the quadrilateral: the biconcave quadrilateral has two external diagonals, the concave an internal and an external diagonal, and the convex two internal diagonals. Thus, a quadrilateral can be representative of the geometries, as shown in Fig. 2.

Biconcave Concave Convex

Fig. 2. Classification of quadrilaterals based on the number of internal and external diagonals. The parameters R_1O_1, O_1R_2, R_2O_2 and O_2R_1 are indicated by solid lines, while the diagonals O_1O_2 and R_1R_2, x and y, respectively, are indicated by dotted lines. Adapted from ref. [17].

2.2. *6-distance and 6j symbols*

This 6-distance system presents interesting analogies with the *6j* symbol, which represents the matrix element in the passage between two different coupling schemes of quantum mechanical angular momenta. The notation consists of six elements, the angular momenta, distributed in two rows and three columns:

$$\begin{Bmatrix} j_2 & j_1 & j_{12} \\ j & j_3 & j_{23} \end{Bmatrix}. \tag{1}$$

The Ponzano-Regge paper [13] gives a geometrical interpretation of the *6j* symbol in the form of a tetrahedron whose edges are identified with angular momenta of lengths corresponding to their values.

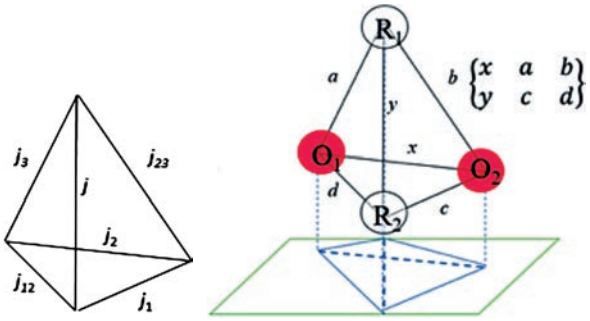

Fig. 3. In the right, the tetrahedron representation of the six entries of a *6j* symbol in in the geometrical interpretation of Ponzano-Regge. In the left, a tetrahedron built on the six distances that characterize a peroxide: its projection on the plane gives a quadrilateral of four sides (continuous line) and two diagonals (dashed lines).

The *6j* notation can be applied to the 6-distance system that we introduced as follows:

$$\begin{Bmatrix} O_1O_2 & O_2R_2 & O_1R_2 \\ R_1R_2 & O_1R_1 & O_2R_1 \end{Bmatrix} \tag{2}$$

in the first column, we report the diagonals (the distance O_1O_2 and R_1R_2), while in the remaining columns the sides O_2R_2, O_1R_1, O_1R_2, O_2R_1 are given. In the case of peroxides and persulfides, the variation of the distance R_1R_2 is the most suitable for monitoring transitions with chirality changing [17, 18]. Different choices of the diagonals are possible, based on the symmetry properties of *6j* symbols:

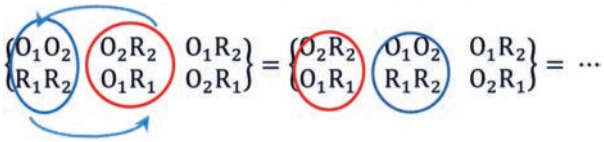

(3)

The quantum mechanical *6j* symbol is invariant under exchange of two columns and this allows us to make alternative choices for the diagonals. They are also invariant under the exchange of rows of two columns and this allows us to generalize the concept of tetrahedron

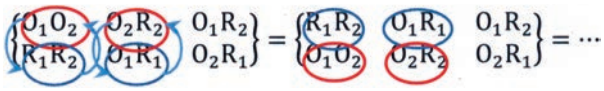

(4)

A further symmetry property of the *6j* symbols is the Regge symmetry, which consists in subtracting the length of the sides from the semi perimeter of the quadrilateral, obtaining the Regge conjugate:

$$\begin{Bmatrix} x & a & b \\ y & c & d \end{Bmatrix} = \begin{Bmatrix} x & s-a & s-b \\ y & s-c & s-d \end{Bmatrix} \tag{5}$$

We will not exploit this property, although surprisingly connected with the Grashof classification of four bar mechanism, as shown in [17].

2.3. *The screen*

The *screen* was initially applied to the *6j* symbol of quantum mechanical angular momentum theory in order to represent the allowed range of a tetrahedral through the plot of two discrete variables [8]. In a similar way, it has been recently applied to represent the field of existence of the tetrahedron associated to molecular structures, as exemplified for peroxides and persulfides [17, 18]. The screen is a plot of the two diagonals of a quadrilateral, x and y, that span the range given by the triangular inequalities $b - a \leq x \leq b + a$ and $d - a \leq y \leq d + a$. The curve inside the screen, the *caustic* curve, reports the values of x and y associate to the planar projection of the tetrahedron, being the quadrilateral a tetrahedron of zero-volume. The caustic curve touches the axes in four points, called *gates*, that are named with the four cardinal points: north N, south S, east E, and west W. There are two further

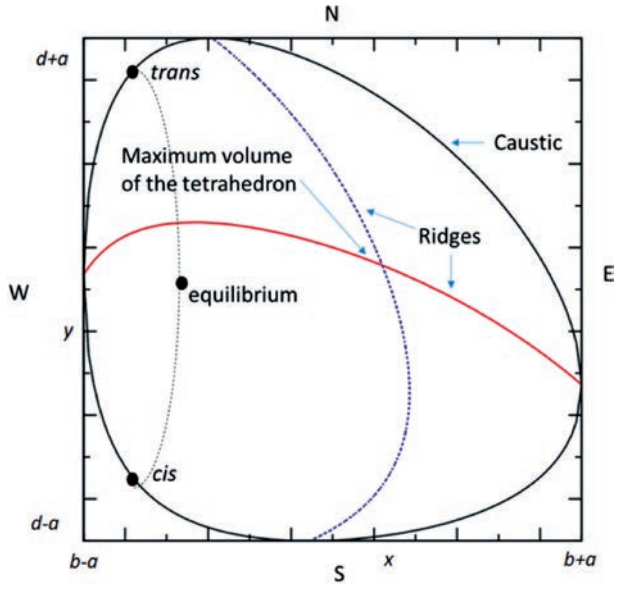

Fig. 4. Screen of a generic tetratomic molecule, the x and y diagonals vary between $b - a$ and $b + a$, and $d - a$ and $d + a$, respectively. The gates N, S, E and W are indicated. The *trans* and *cis* geometries are defined along the caustic curve, while the equilibrium geometry occurs inside the caustic. There the related tetrahedron has volume non-zero. The crossing point of the ridge corresponds to the maximum volume of the tetrahedron for cuts along x and y.

curves defined in the screen, the *ridges*, that mark configurations of the associated tetrahedron when two specific pairs of triangular faces are orthogonal. The crossing point of the ridges corresponds to the maximum value of the volume of the tetrahedron for cuts along x or y. Regarding peroxides and persulfides, *cis* and *trans* geometries are located along the caustic, corresponding to the configuration of a tetrahedron of zero-volume. The equilibrium geometry, corresponding to one of the two enantiomers, is placed within the caustic, where a tetrahedron of non-zero volume is defined. The figure shows only one of the enantiomers, while the other one is located at the same values of x and y on the opposite side of the tetrahedron.

3. The four-bar linkage

The 6-distance system we have just described is reminiscent of a famous mechanism of kinematics known as the four-bar linkage. It consists of four movable bars, or links; their paths is determined by their reciprocal ratio that also permits to classify the performances of the linkage. One of the four links is usually fixed, the *ground link*, and is directly connected to the adjacent links, called *input* and *output link*. The remaining link, opposite to the ground link, is called *floating link*. Assu-

ming the ground link horizontal, the input and output links can make four kinds of rotations: a 360 degrees motion called, the *crank*; a rotation within a limited range that does not include 0 and 180°, the *rocker*; a rotation that excludes 0°, the 0-rocker; a rotation that excludes 180°, the π-*rocker*, again similar to the rocker and the previous case, but excludes 180°. Quadrilateral linkages are also classified according to the lengths of the bars. As well known*, if the sum of the longest and the shortest bars is less than or equal to the sum of the remaining two, they are said to accomplish the condition of Grashof and the shortest link can rotate fully with respect to the neighboring links.*

3.1. *Four-bar mechanism in biological systems*

The considerations made so far can be obvious when extended to more complex systems. The four-bar mechanism is well suited to the study of biological systems because it considers changes in the structural elements that may have occurred, for example during the evolutionary process. Biomechanical systems are defined by morphology and functional properties and the relationship between form and function can have a deep impact on the way in which selection becomes morphological evolution. The biological evolution (the endless change that living beings encounter), as described by Darwin, can be seen as involving an optimization procedure and one can try to understand the intrinsic mechanism occurring in nature and making evolution proceed. The analysis of the four-bar system often provides a rigorous method to simplify the study of much more complex biological mechanisms (see for example [19]).

Macromolecules: DNA and proteins. We start this account with the application of four-bar linkage to macromolecules. DNA turned out to be not simply a genetic material in cells, but also a powerful building material in the nanometer world. The DNA origami is a technique that consists in folding DNA in two- and three- dimensional arrangements (see for example [20]). It is employed in nanotechnology to connect or functionalize different nanostructures, such as gold nanoparticles, quantum dots and single-walled carbon nanotubes, or even to construct nanostructures composed exclusively of DNA. The ability to use DNA origami to design and fabricate a series of classical kinematics joints on a nanometric scale, such as a revolved articulation, prismatic and universal joints, as well as kinematic mechanisms, has been demonstrated including a four-bar spatial link, called the Bennett mechanism [21]. A general algorithm for kinematic projection analysis was developed for mechanisms such as four-bar and five-bar links. The origami DNA kinematics leads to the study of robotics mechanisms and the application of well-developed kinematics theories and the use of computational tools for the design of nanorobots and nanomachines. This technique permits to design custom structures with high addressability that helps in nanoscience research. It is a promising material to be used for diag-

nostics and human health care therapies. DNA nanostructures such as tetrahedra are able to get across the cell membrane and are easily modified to carry RNA, antibodies or small molecules of drugs. The most surprising property of origami DNA-based therapy is the possibility to decide the ability to release drugs. Similarly to DNA, proteins are to be seen as highly refined natural molecular machines, which owe their properties to the complex tertiary structures through a precise spatial positioning of different functional groups. The idea of designing new molecular machines beyond the limits of natural proteins makes the design of new protein structures a challenging perspective, analogously to the approach of DNA nanotechnology, where complex tertiary structures are designed by complementary nucleotide segments. The technology of origami proteins permits to construct different molecular machines [22]. Polypeptides and polynucleotides can be self-assembled in complex tertiary structures in the form of a tetrahedron, four-sided pyramid or triangular prism. The tetrahedral structure has demonstrated biocompatibility since the protein is bent correctly and does not trigger a stress response, and the structures are produced efficiently and compatible with cell physiology.

Bacteria. Bacteria have the ability to move in the medium in which they are located. This is a very important property, because it allows them to escape unfavorable situations or to approach a source of nourishment. This mechanism is called chemotaxis (phenomenon of removal or approach towards a particular substance). Most of bacteria follow spatial gradients of chemical and physical stimuli, a better characterized chemotaxis is found in aminoacid gradients or sugars, but other physiological stimuli like pH, osmolarity, redox potentials and temperature are also known. These multiple environmental stimuli are integrated and elaborated to generate a coordinated behavior of chemotaxis, which has a high sensitivity. Chemotaxis over the years has become a very detailed topic with experimental observations and mathematical models of the dynamics of bacterial populations. The importance of orientation and active movement for survival has led to the emergence and evolution of a variety of motility mechanisms. Bacteria respond to a wide range of stimuli such as concentration of chemicals (chemotaxis), light (phototaxis), electric fields (galvanotaxis), magnetic fields (magnetotaxis), pH (pH-taxis), and temperature (thermotaxis) (see for example [23]. Bacterial chemotaxis is described by a four-bar mechanism and its dynamics can be optimized by an algorithm that also considers the management of the constraints established by the kinematic analysis of the problem. Various algorithms have been proposed for the optimization of the movement that leads to the improvement of bacterial nutrition, based on the design of a four-bar mechanism that follows a linear vertical path (for details see [24]).

Invertebrates. There are examples of four-bar mechanism among invertebrates (animals without vertebral column). Such mechanism can be observed for example in the movement of the wings of insects [25] and jump of locusts [26]. Mantis shrimp (Stomatopoda) generates extremely rapid and powerful predator shots

through a series of structural modifications of the raptorial appendages (the second pair of thoracic limbs is modified in raptor appendices), whose mechanism is also an application of the four-bar linkage [27]. The mechanism adopted by jumping spiders of the family of the Salticidae [28] found applications in robotics.

Fish. In many biological systems, the elements that constitute the skeleton cannot be moved directly by the muscles. This is the case of the movement of the head of fishes during the feeding, because of the absence of lateral muscles strong enough to move the suspensors (cheeks) and opercles [29] (gill cover) in lateral direction (abduction). These elements can be moved through a linkage between bones and ligaments. A certain number of teleosts (fish with a bone skeleton) feed on snail, by crushing the shells, and evolved by developing a four-bar mechanism that involves the cranial elevation and the jaw protrusion mechanism to generate a powerful bite [30]. The lower jaw of a fish is an example of a simple system of biological levers: an input lever, where force is applied, and an output lever, which transmits force; the kinematic transmission is a simple function of the ratio of these lengths. Syngnathidae fishes (seahorses, needlefish and sea dragons) have a highly modified skull characterized by a long tubular snout with small jaws at the end. Previous studies have shown that these species feed by an extremely fast aspiration with a movement characterized by a rapid elevation of the head accompanied by rotation of the hyoid and a four-bar planar model is proposed to explain the coupled movement of the neurocranium and hyoid. The four-bar model indicates a clear coupling between the rotation of the hyoid and the elevation of the neurocranium [31].

Mammals. Relevant examples among mammals are given by kangaroos and elephants. Kangaroo is an animal that jumps with two paws in the synchronous phase. In this case the movement of the jump can be obtained with a four-bar mechanism: a rocker mechanism is adopted to generate repeated movements of contraction and lengthening of the legs to generate the jump [32]. The articulation of the knee of elephant [33] that shows unique morphological characteristics is mainly linked to the support of the enormous body weight of the animal.

4. Concluding remarks

The screen representation of a four-bar mechanism was initially inspired by the *6j* symbols of quantum mechanical angular momentum theory, to represent the allowed range of the tetrahedron associate to the coupling scheme of angular momenta, through plot of two of the discrete variables. It has been recently applied to the mapping of structural properties of peroxide and persulfides, in order to monitor chirality changing transitions [17]. Its applications can be extended to other kind of information, such as thermodynamic and kinetic properties. It can be also extended to other types of chiral stereogenic units, such as those defined by asymmetric carbon connected to four different ligands or to describe the peptide bond, through a reference system of distances only.

The screen is closely related to the four-bar mechanism, the simplest movable closed chain linkage, that is present in systems of growing dimensions, from macromolecules to bacteria, invertebrates and vertebrates. For these systems, the screen represents a promising method for the analysis of the involved kinematics. Interesting perspectives concern its application to extremophiles, organisms that thrive in physically and chemically extreme conditions, nowadays investigated in astrochemistry and astrobiology [34].

Acknowledgments. The authors gratefully acknowledge the Italian Ministry for Education, University and Research (MIUR) for financial support through SIR 2014 (Scientific Independence of Young Researchers), award number: RBSI14U3VF. Robenilson Ferreira is grateful to Brazilian CAPES for a sandwich doctoral (PDSE88881.134388/2016-01) fellowship to the Perugia University.

BIBLIOGRAPHY

[1] Barreto P.R.P., Vilela A.F.A., Lombardi A., Maciel G.S., Palazzetti F., Aquilanti V. 2007. The Hydrogen Peroxide–Rare Gas Systems: Quantum Chemical Calculations and Hyperspherical Harmonic Representation of the Potential Energy Surface for Atom–Floppy Molecule Interactions *J. Phys. Chem. A*, 111, 12754-12762.

[2] Maciel G.S., Barreto P.R.P., Palazzetti F., Lombardi A., Aquilanti V., 2008. A quantum chemical study of H2S2: Intramolecular torsional mode and intermolecular interactions with rare gases *J. Chem. Phys.* 129, 164302.

[3] Bergman P., Parise B., Liseau R., Larsson B., Olofsson H., Menten K.M., Guesten R. Detection of Interstellar Hydrogen Peroxide 2011 *Astron. Astrophys.* 531, Art. No. L8.

[4] Maciel G.S., Bitencourt A.C.P., Ragni M., Aquilanti V. 2007. Quantum study of peroxidic bonds and torsional levels for ROOR' molecules (R, R' = H, F, Cl, NO, CN) *J. Phys. Chem. A* 111, 12604-12610.

[5] Maciel G.S., Bitencourt A.C.P., Ragni M., Aquilanti V. 2007. Alkyl peroxides effect of substituent groups on the torsional mode around the O – O bond. *Int. J. Quant. Chem.* 107, 2697-2707.

[6] Aquilanti V., Ragni M., Bitencourt A.C.P., Maciel G.S., Prudente F.V. 2009. Intramolecular Dynamics of RS–SR′ Systems (R, R′ = H, F, Cl, CH_3, C_2H_5): Torsional Potentials, Energy Levels, Partition Functions *J. Phys. Chem. A*, 113 (16), pp 3804-3813.

[7] Barreto, P.R.P., Palazzetti, F., Grossi, G., Lombardi, A., Maciel, G.S., Vilela, A.F.A. 2010. Range and strength of intermolecular forces for van der Waals complexes of the type H2Xn Rg, with X = O, S and n = 1, 2 *Int. J. Quant. Chem.* 110, 777-786.

[8] Ragni M., Littlejohn R.G., Bitencourt A.C.P., Aquilanti V., Anderson R.W. 2013. The screen representation of spin networks: images of 6j symbols and semiclassical features (2013) LNCS 7972, 60-72. Springer, Heidelberg.

[9] Toussaint G., (2003). Simple Proofs of a Geometric Property of Four-Bar Linkages. The American Mathematical Monthly, Vol. 110, No. 6 (Jun.-Jul., 2003), pp. 482-494.

[10] Barreto P.R.P., Albernaz A.F., Palazzetti F., Lombardi A., Grossi G., Aquilanti V. 2011. Hyperspherical representation of potential energy surfaces: intermolecular interactions in tetra-atomic and penta-atomic systems *Physica Scripta* 84, 028111.

[11] Barreto P.R.P., Albernaz A.F., Palazzetti F., 2012. Potential energy surfaces for van der Waals complexes of rare gases with H_2S and H_2S_2: Extension to xenon interactions and hyperspherical harmonics representation *Int. J. Quant. Chem.*, 112, 834-847.
[12] Palazzetti F., Munusamy E., Lombardi A., Grossi G., Aquilanti V. 2011. Spherical and hyperspherical representation of potential energy surfaces for intermolecular interactions *Int. J. Quant. Chem.* 111 (2), 318-332.
[13] Ponzano G., Regge T. 1968. Semiclassical Limit of Racah Coe cients in Spectroscopic and Group Theoretical Methods in Physics, ed F. Bloch et al. (Amsterdam: North-Holland) pp. 1-58.
[14] Aquilanti V., Grossi G., Lombardi A., Maciel G.S., Palazzetti F. 2008. The origin of chiral discrimination: supersonic molecular beam experiments and molecular dynamics simulations of collisional mechanisms *Physica Scripta* 78, 058119.
[15] Lombardi A., Palazzetti F., Maciel G.S., Aquilanti V., Sevryuk M.B. 2011. Simulation of oriented collision dynamics of simple chiral molecules, *Int. J. Quant. Chem*. 111, 1651-1658.
[16] Aquilanti, V., Bitencourt A.C.P., Caglioti C., dos Santos R.F., Lombardi A., Palazzetti F., Ragni M. (submitted).
[17] Aquilanti V., Caglioti C., Lombardi A., Maciel G.S., Palazzetti F. 2017. Screens for displaying chirality changing mechanisms of a series of peroxides and persulfides from conformational structures computed by quantum chemistry *LNCS*, 354-368.
[18] Aquilanti V., Caglioti C., Casavecchia P., Grossi G., Lombardi A., Palazzetti F., Pirani F. 2017. The astrochemical observatory: Computational and theoretical focus on molecular chirality changing torsions around O – O and S – S bonds. AIP Conference Proceedings 1906, 030010.
[19] Alfaro M.E., Bolnick D.I., Wainwright P.C. 2004. Evolutionary Dynamics of Complex Biomechanical Systems: An Example Using The Four-Bar Mechanism *Evolution*, 58(3) pp. 495-503.
[20] Endo M., Sugiyama H., DNA Origami Nanomachines. 2018 *Molecules* 23, 1766.
[21] D. Lei, A. E. Marras, J. Liu, C-M. Huang, L. Zhou, C. E. Castro, H.-J. Su, G. 2018. Ren Three-dimensional structural dynamics of DNA origami Bennett linkages using individual-particle electron tomography *Nature Comm.* 9, 592.
[22] Ljubetic A. Lapenta F., Gradišar H., Drobnak I., Aupic J., Strmšek Ž., Lainšcek D., Hafner-Bratkovic I., Majerle A., Krivec N., Bencinal M., Pisanski T., Velicković T.C., Round A., Carazo J.M., Melero R., Jerala R. 2017. Design of coiled-coil protein-origami cages that self-assemble in vitro and in vivo *Nature Biotechnology* 35, 1094-1101.
[23] Paulick A., Sourjik V. 2018. FRET Analysis of the Chemotaxis Pathway Response *Methods Mol. Biol.* 1729, 107-126.
[24] Hernández-Ocaña B., Pozos-Parra M.D.P., Mezura-Montes E., Portilla-Flores E.A., Vega-Alvarado E., Calva-Yáñez M.B., 2016. Two-Swim Operators in the Modified Bacterial Foraging Algorithm for the Optimal Synthesis of Four-Bar Mechanisms *Comput. Intell. Neurosci.* Article Number: 4525294 (18 pages).
[25] Zbikowski R., Galinski C., Pedersen C.B. 2005. Four-Bar Linkage Mechanism for Insect like Flapping Wings in Hover: Concept and an Outline of Its Realization *J. Mech. Des.* 127, 817-824.
[26] Patek S.N., Nowroozi B.N., Baio J.E., Caldwell R.L., Summers A.P. 2007. Linkage mechanics and power amplification of the mantis shrimp's strike *Journal Exp. Biol.* 210, 3677-3688.
[27] Mo X., Ge W., Wang S., Zhao D. 2016. Mechanical Design and Dynamics Simulation of Locust-Inspired Straight Line Four-Bar Jumping Mechanism *LNEE* 408, 429-442.
[28] Afolayan M.O., Oyegbade B.I. 2015. Development of a Robot Imitating Nomadic Spiders *Br. J. Appl. Sci. Technol.* 11, 1-12.
[29] Olsen A.M., Camp A.L., Brainerd E.L. 2017. The opercular mouth-opening mechanism of largemouth bass functions as a 3D four-bar linkage with three degrees of freedom *J. Exp. Biol.* 220, 4612-4623.

[30] Baliga V.B., Mehta R.S. 2015, Linking Cranial Morphology to Prey Capture Kinematics in Three Cleaner Wrasses: Labroides dimidiatus, Larabicus quadrilineatus, and Thalassoma lutescens *J. Morph.* 276, 1377-1391.
[31] Roos G., Leysen H., Wassenbergh S.V., Herrel A., Jacobs P., Dierick M., Aerts P., Adriaens D. 2009. Linking Morphology and Motion: A Test of a Four-Bar Mechanism in Seahorses *Physiol. Biochem. Zool.* 82, 7-19.
[32] Jun B.R., Kim Y.J., Jung S. 2016. Design and Control of Jumping Mechanism for a Kangaroo-inspired Robot 6th IEEE RAS/EMBS International Conference on Biomedical Robotics and Biomechatronics (BioRob) June 26-29, UTown, Singapore.
[33] Weissengruber G.E., Fuss F.K., Egger G., Stanek G., Hittmair K.M., Forstenpointner G. 2006. The elephant knee joint: morphological and biomechanical considerations *J. Anat.* 208 pp. 59-72.
[34] Seckbach J., Oren A. 2001. From Extremophiles to Astrobiology. In: Chela-Flores J., Owen T., Raulin F. (eds) First Steps in the Origin of Life in the Universe. Springer, Dordrecht.

Rendiconti
Accademia Nazionale delle Scienze detta dei XL
Memorie di Scienze Fisiche e Naturali
136° (2018), Vol. XLII, Parte II, Tomo II, pp. 163-173

VINCENZO AQUILANTI[1,2] – PIERGIORGIO CASAVECCHIA[1]
DOCK-CHIL CHE[3] – STEFANO FALCINELLI[4] – KING-CHUEN LIN[5]
ANDREA LOMBARDI[1] – TOSHIO KASAI[5] – MASAAKI NAKAMURA[5]
FEDERICO PALAZZETTI[1,*] – FERNANDO PIRANI[1] – PO-YU TSAI[6]

The ORCHID project: a search for the Origin of Chiral Discrimination**

Abstract – Control of translational, internal and orientational molecular degrees of freedom in elementary chemical processes constitutes a challenge for the modeling and applications of physical chemistry. In this paper, we focus on the peculiar part arguably played by orientational control for unveiling the stereodynamical nature of processes involving molecular chirality – one of the most fascinating issues of molecular science, crucial in view of the intriguing ubiquitous role of selective left-right asymmetry in the bio-world. Typically, investigations of processes involving explicitly molecular chirality exploit circular polarization, *e.g.* from laser and/or synchrotron radiation sources. We take an alternative stereodynamical view that relies on advances in molecular-beams orientation techniques: (i) through gas flowing in supersonic regimes, designated as «natural», not requiring external fields and (ii) using elec-

[1] Dipartimento di Chimica, Biologia e Biotecnologie, Università di Perugia, via Elce di Sotto 8, 06123 Perugia, Italy.
[2] Istituto di Struttura della Materia - Consiglio Nazionale delle Ricerche, 00016 Rome, Italy.
[3] Graduate School of Science, Department of Chemistry, Osaka University, Toyonaka, 560-0043 Osaka, Japan.
[4] Dipartimento di Ingegneria Civile ed Ambientale, Università di Perugia, Via G. Duranti 93, 06125 Perugia, Italy.
[5] Department of Chemistry, National Taiwan University, Taipei 106, Taiwan.
[6] Department of Chemistry, National Chung Hsing University, Taichung 402, Taiwan
* Corresponding author: federico.palazzetti@unipg.it
** The research project ORCHID is an integrated search of stereodynamical mechanisms for the ORigin of CHIral Discrimination by oriented molecular beams, synchrotron radiation, molecular dynamics and computational modeling. It received financial support in 2015, by the «Ministero per l'Istruzione, l'Università e la Ricerca» through the program SIR (Scientific Independence for Young Researchers) and is nowadays part of the Astrochemical Observatory.

trostatic techniques. These perspective corroborates the following objectives: (a) extension and probing of the natural orientation technique to chiral molecules by elastic and/or inelastic collisions, that permits to design crossed molecular beam experiments to be implemented for the first-time demonstration of left-right spatial asymmetry in molecular encounters; ii) the novel experimental proposals exploiting hexapolar orientation are applied to experiments on the orientation control of molecular collisions in dynamics and photochemistry.

1. *Introduction*

The experimental techniques and the interpretative tools of modern physical chemistry are applied in this work to specific issues regarding the broad theme of the origin and manifestation of molecular chirality [1, 2]. This theme has exceeded the scope of chemical research and is central also to the physical and biological sciences [3, 4]. The origin of chiral specificity as a signature of life on our planet, and the high enantiomeric selectivity of processes involved in the most important biological molecules, rank among the most intriguing natural phenomena that is of great interest, not only for basic research but also for technology (chiral recognition and asymmetric synthesis in organic, industrial and pharmaceutical chemistry). The recent discovery of propylene oxide, one of the simplest organic chiral molecules, in the interstellar medium [5] (and previously the discovery of hydrogen peroxide, arguably the simplest chiral molecule [6]), has provided additional interest on the occurrence of this phenomenon also in astrochemical environments.

Several hypotheses have been formulated on the natural origins of chiral discrimination in the bio-world. Some of them are controversial and none was convincing enough to receive global consensus. A scenario attributes chiral bias just to chance and statistical fluctuations, followed by some amplification mechanisms: crystalline solids of chiral compounds formed from a melt normally solidify as a racemic conglomerate, and yield an enantiomeric excess if crystallization occurs under constant stirring. A hypothesis considers that asymmetric distributions of enantiomers originated from parity violation, due to weak nuclear forces, leads to an energy difference between enantiomers of chiral molecules, but the energy difference is extremely small and the transmission of this asymmetry to the molecular scale has eluded theoretical modeling and experimental verification (see [7] and references therein).

On the other hand, polarized fields can certainly act as a chiral environment and there is plenty of experimental evidence concerning the role of electric and magnetic fields [8]. Enantioselective photochemistry with circularly polarized light is well established and experimental observations of dichroic effects in photoionization can be obtained by very intense synchrotron radiation sources [9, 10]. The magnetochiral dichroism induced by magnetic fields and unpolarized light may be enantioselective in photochemical reactions, and recently has been observed in organic molecules [11].

A key experiment has recently demonstrated preferential population of the rotamers in haloalkanes induced by whirling flows [12]. Such rotational-translational motions (vortices) are chiral force fields and are present in a large variety of contexts, from planetary atmospheres to the interstellar space. Also, liquid vortices have been shown to induce chiral discrimination in mesophase achiral aggregates [13]. It was theoretically proved that in collisions between unpolarized projectiles and chiral molecules, the differential cross sections for enantiomers differ if these are oriented: if a chiral framework is provided, the enantiomers will scatter the projectiles in different directions [14]. The key role of orientation has been further confirmed by experiments of scattering of polarized electrons by thin films of oriented chiral molecules impinging on surfaces [15], and by the demonstration of stereodynamic effects in scattering from surfaces of molecules oriented according to the techniques mentioned above [16]. Ionization cross sections of chiral molecules by electron impact have also been theoretically investigated, demonstrating the dependence of these observables on the polarization of the incident electron beam [17]. No experimental evidence has been provided on the left-right asymmetry of outcomes of molecular encounters, for which crucial is the unique availability of molecular orientation techniques (see [18] and references therein).

The control of translational and internal molecular states is a main challenge in the realization of stereodynamics experiments. Additionally, control of the molecular orientation is a fundamental prerequisite in order that the phenomenon of chiral selectivity can be demonstrated even without circularly polarized light: this is the strongest point towards the goal of establishing a phenomenology for the origin of chirality as a steric property in the area of chemical kinetics. To this aim, orientational techniques exploit innovative approaches based on (a) properties of expansions of gas mixtures in supersonic flow regimes and hexapolar electrostatic fields. Control through gas flows, referred to as the «natural» alignment technique, has been revealed and characterized in the Perugia laboratory, but knowledge of possible chirality effects in streams is in its infancy and has to be further investigated as a basic scientific issue, a bonus being to prove or disprove any role in prebiotic issues [19-26]. All this is motivating this project (see the logo in Fig. 1) involving the study of left and right asymmetries in elastic and inelastic angular distributions in the collisions of oriented chiral molecules, verifying the anticipation of molecular dynamics simulations, to be performed to design, assist and interpret the demanding experiments and their results. Control through hexapolar electric fields had been widely used for linear and symmetric-top molecules and is being adapted for the first time to the orientation of chiral molecules [27-30]. This requires dealing with molecules of an unprecedented complexity and an elaborate theoretical approach for data analysis. Crossed molecular beam experiments are being performed for the first-time demonstration of left-right spatial asymmetry in molecular encounters: these experiments allow us to obtain information on reaction mechanisms, on the partitioning of product energy and on features of the potential energy surfaces.

Fig. 1. The Orchid in the logo of the project not only stands for the acronym of ORigin of CHIral Discrimination, but is also appropriate being the great varieties of this flower often scrutinized for their chiral properties. One of them is the spiral arrangement of the five petals.

The paper is structured as follows: in Section 2, the theoretical models and computational simulations of chiral selective processes are reported; in Section 3, we describe the on-going molecular beam scattering experiments; in Section 4, we report the state-of-the-art of enantioselective photodissociation experiments; finally, in Section 5 we give concluding remarks.

2. *Theoretical models and computational simulations*

A preliminary assessment of enantioselective collisional mechanisms requires a detailed characterization of the potential energy surface that can describe accurately the intermolecular interactions. An efficient and accurate approach is based on semiempirical methods, which are tested and improved by comparison with results of electronic structure calculations and leads to suitable analytical expressions for the interactions, also by explicitly exploiting the strength and range parameters obtained from collision observables. This approach permits an internally consistent reproduction of the interactions of the most significant configurations of the systems, allowing us to perform extensive molecular dynamics simulations of collisions involving chiral molecules. Extensive investigations have been carried out on hydrogen peroxide and persulfide, which are arguably the simplest cases of chiral molecules

[31-33]. Molecular dynamics simulations of elastic collisions between oriented chiral molecules and rare gas atoms have shown that the latter are deflected with a specific angular distribution discriminating the two enantiomers [34]. For studies concerning unimolecular processes involving propylene oxide and its interactions with rare gas atoms see [35-37].

3. *Chirality discrimination in molecular collisions*

In this section, we describe two unique molecular-beams experiments of remarkable complexity, built and operating in the Perugia laboratory: chiral selection originates in molecular collisions and is determined by the different interaction between a couple of identical (RR) or different enantiomers (RS). Orientational control through the natural alignment technique would permit to highlight such a difference [37-39]. In Fig. 2, we report the configuration of an experimental apparatus

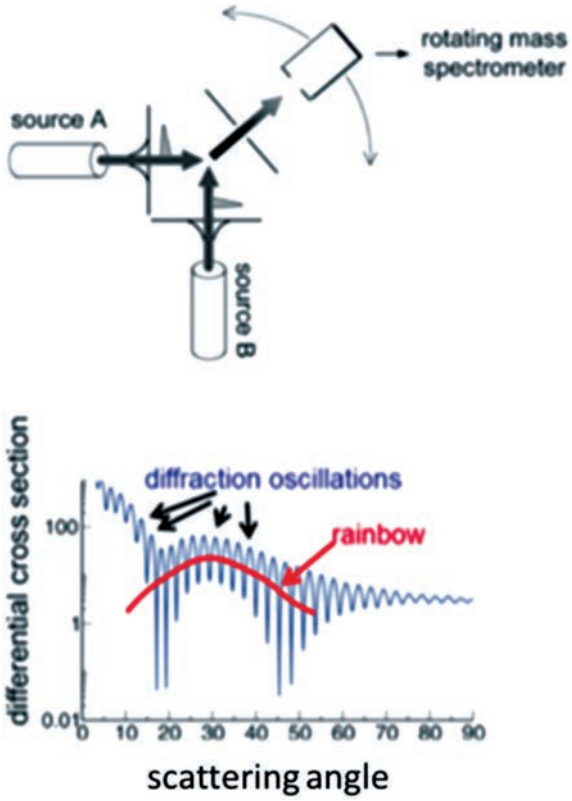

Fig. 2. The apparatus for the realization of differential scattering experiments. The velocity plot shows the quantum interference pattern that can be observed in this kind of experiments due to diffraction oscillations and to the rainbow effect (Adapted from Ref. 38).

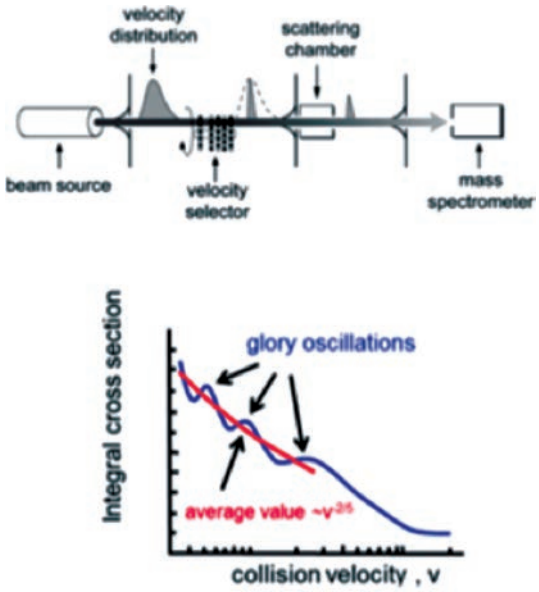

Fig. 3. A typical experimental setup for measuring integral cross sections by the attenuation of a molecular beam at selected velocities by a target gas in the scattering chamber. The plot shows glory oscillations superimposed to an average velocity dependence $v^{-2/5}$ due to the R^{-6} dependence of long-range interactions (Adapted from Ref. 38).

consisting of two crossed molecular beams and a rotating detector, for differential cross section measurements. Under high angular and energy resolution conditions, it permits the manifestation of rainbow and diffraction quantum interference effects, in the angular dependence of the differential cross sections.

In Fig. 3, we show an apparatus for the measurement of the integral cross sections as a function of the collision velocity, consisting of a molecular beam, velocity selected by a mechanical device consisting of a series of rotating slotted disks, of a scattering chamber and of a quadrupole mass spectrometer as a detector. This type of measurements exhibit, under favorable conditions, quantum interference phenomena that are given the names of analogous optical phenomena. In particular, diffraction and rainbow patterns are a manifestation of the rise of repulsive walls and of the strength of the attraction in the neighborhood of the potential wells; the glory quantum interference is instead a probe of the position and depth of the potential well. A chiral discrimination phenomenon is expected to be observed in the angular distribution of the fragments produced by collision of two identical enantiomers, RR, or opposite enantiomers, RS. Measurements of differential cross section, performed by the apparatus in Fig. 2, are suitable for this kind of enantiomeric selection.

The apparatus in Fig. 3, suitable for measurements of integral cross section, permits to probe the different energy interaction between couple of enantiomers RR

and RS. On this regard, we have estimated the interaction averaged over all the relative orientations of a couple of propylene oxide molecules RR and RS. Propylene oxide has been amply characterized by our group both from a theoretical and an experimental point of view. The average binding energy is estimated as about 3-4 kJ/mol at an equilibrium distance of 4-4.5 Å. Considering the information provided by spectroscopic measurements, we have estimated a difference in energy between RR ad RS couples of *ca.* 0.2 kJ/mol, that is about 5% of the total interaction energy. Ongoing experiments have been carried out involving propylene oxide. Additionally, for this molecule double ionization (valence shell) thresholds have been recently measured by synchrotron radiation [40].

4. *Chirality discrimination in photodissociation*

Enantioselective photodissociation experiments are performed on molecules oriented by an electrostatic hexapole, combined with the ion photofragment imaging detection technique. The photodissociation is induced by a linearly polarized laser, which is a non chiral source, but the aim is to point out the role of the orientation in originating chiral discrimination. The interpretation of the chiral effect involved is visualized by a semiclassical vector scheme in the electric dipole approximation in the molecular (body fixed) reference frame *xyz* (Figure 4, upper panel). The vectors to be considered are the velocity of the photofragments **v**, that identifies with the *z*-axis, the transition dipole moment **μ** and the permanent electric dipole moment **d**. The angle θ between **v** and **d** has range $0 \leq \theta \leq \pi$ and the angle Θ between vectors **v** and **μ** has also range $0 \leq \Theta \leq \pi$, while the angle ψ, given by the intersection of the *x*-axis with the projection of **μ** onto the *xy*-plane, has range $0 \leq \psi < 2\pi$. Achiral molecules do not distinguish the sign of ψ, while for chiral molecules, a symmetry breaking occurs and the sign of ψ is characteristic of a specific enantiomer. It is important to note that the sign of ψ can be determined from the photofragment angular distribution of oriented (chiral) molecules via linearly polarized photolysis light. Prerequisite is that the three vectors must have a three-dimensional arrangement. It can be shown that, under sliced imaging conditions, θ and ψ can be determined from specific light polarization and orienting field arrangement.

In Figure 4 (lower panel), we report the simulation of the photofragment angular distribution obtained by ion imaging for a prototypical chiral molecule. A racemic mixture, as well as an achiral molecule, gives a symmetric distribution of the photofragments [41]. On the contrary, the separate enantiomers give an asymmetric distribution, characteristic of the corresponding mirror form. Recent experiments of enantioselective photodissociation involved the hexapole oriented 2-bromobutane [42-44].

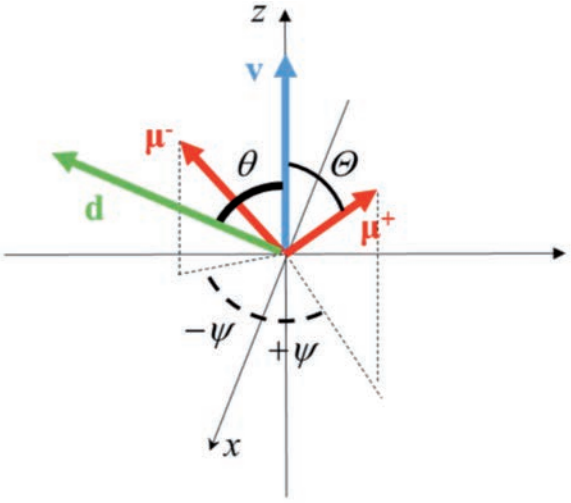

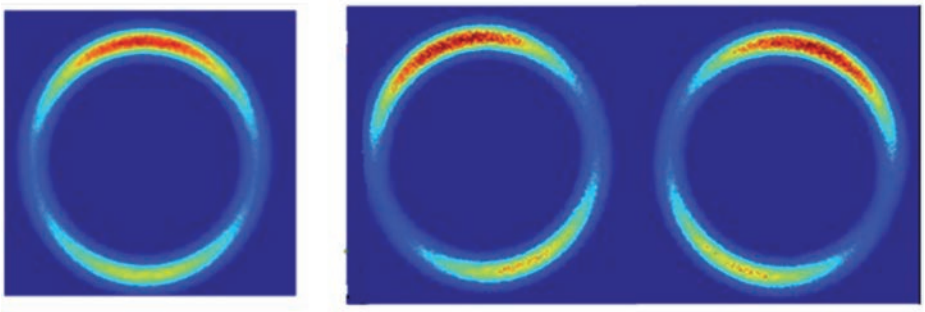

Achiral molecule or racemic mixture

Separate enantiomers

Fig. 4. The upper panel reports the vectors and the angular coordinates that describe the angular distribution of the photofragment in the *xyz* Cartesian coordinate reference frame. The origin of the axes is the center-of-mass of the fragment, the *z*-axis is parallel to the direction of the velocity recoil vector **v** and the permanent dipole moment vector **d** is coplanar to the *xz*-plane. The angle between **v** and **d** is denoted by θ ($0 \le \theta \le \pi$), while the angle between **v** and $\boldsymbol{\mu}$ is indicated by Θ ($0 \le \Theta \le \pi$). The $\boldsymbol{\mu}$ vectors are indicated by the superscripts + and – that correspond to the enantiomers. The directions of $\boldsymbol{\mu}^+$ and $\boldsymbol{\mu}^-$, as well as the sign of ψ, the angle between the *x*-axis and the projection of $\boldsymbol{\mu}$ on the *xy*-plane ψ ($0 \le \psi < 2\pi$), are specific for each enantiomer. (Lower panel) In the left, we report the photofragment angular distribution of an achiral molecule, or similarly of a racemic mixture. In the right, the photofragment angular distributions given by separate enantiomers (Adapted from Ref. 41).

5. *Concluding remarks*

We have provided an account of molecular chirality manifestations in molecular beam experiments and the corresponding theoretical modeling. Chiral effects are expected to show up in the intermolecular interactions involving homo- and heterochiral molecular pairs and in the collision observables, where molecular alignment can arguably highlight such role of the stereodynamics. In dissociation experiments photoinitiated by linearly polarized laser, being a non-chiral source, molecular orientation is a fundamental prerequisite for the observation of chiral effects.

Acknowledgments. The authors gratefully acknowledge the Italian Ministry for Education, University and Research (MIUR) for financial support through SIR 2014 (Scientific Independence of Young Researchers), award number: RBSI14U3VF.

REFERENCES

[1] Aquilanti, V., Maciel, G.S. 2006. Observed molecular alignment in gaseous streams and possible chiral effects in vortices and surface scattering. Orig. Life Evol. Biosph. 36, 435-441.
[2] Palazzetti, F., Maciel, G.S., Lombardi, A., Grossi, G., Aquilanti, V. 2012. The astrochemical observatory: molecules in the laboratory and in the cosmos. J. Chin. Chem. Soc. 59(9), 1045-1052.
[3] Lombardi, A., Palazzetti, F., Aquilanti, V., Pirani, F., Casavecchia, P. 2017. The astrochemical observatory: experimental and computational focus on the chiral molecule propylene oxide as a case study 2017 Lecture Notes in Computer Science 10408, 267-280.
[4] Aquilanti, V., Caglioti, C., Casavecchia, P., Grossi, G., Lombardi, A., Palazzetti, F., Pirani, F. 2017. The astrochemical observatory: computational and theoretical focus on molecular chirality changing torsions around O - O and S - S bonds. In: 1906 AIP Conference Proceedings Article no. 030010.
[5] McGuire, B.A., Carroll, P.B., Loomis, R.A., Finneran, I.A., Jewell, P.R., Remijan, A.J., Blake, G.A. 2017. Discovery of the interstellar chiral molecule propylene oxide (CH_3CHCH_2O) Science 2(5), 99-110.
[6] Bergman, P., Parise, B., Liseau, R., Larsson, B., Olofsson, H., Menten, K.M., Gusten, R., 2011. Detection of interstellar hydrogen peroxide. A&A 531, L8.
[7] Aquilanti, V., Grossi, G., Lombardi, A., Maciel, G.S., Palazzetti, F. 2008. The origin of chiral discrimination: supersonic molecular beam experiments and molecular dynamics simulations of collisional mechanisms. Phys. Scr. 78(5), 7 p. Article no. 058119.
[8] Su, T.-M., Palazzetti, F., Lombardi, A., Grossi, G., Aquilanti, V. 2013. Molecular alignment and chirality in gaseous streams and vortices. Rendiconti Lincei 24(3), 291-297.
[9] Stranges, S., Turchini, S., Alagia, M., Alberti, G., Contini, G., Decleva, P., Fronzoni, G., Stener, M. 2005. Valence photoionization dynamics in circular dichroism of chiral free molecules: the methyl-oxirane. J. Chem. Phys. 122, 244303.
[10] Turchini, S., Zena, N., Contini, G., Alberti, G., Alagia, M., Stranges, S., Fronzono, G., Stener, M., Decleva, P., Prosperi, T. 2004. Circular dichroism in photoelectron spectroscopy of free chiral molecules: experiment and theory on methyl-oxirane. Phys. Rev. A 70, 014502.

[11] Rikken, G.L.J.A., Raupach, E. 2000. Enantioselective magnetochiral photochemistry. Nature 405, 932-935.
[12] Lee, H.-N., Chang, L. -C., Su, T.-M. 2011. Optical rotamers of substituted simple alkanes induced by macroscopic translation-rotational motions. Chem. Phys. Lett. 507, 63-68.
[13] Ribò, J.M., Crusats, J., Sagués, F., Claret, J., Rubires, R. 2001. Chiral sign induction by vortices during the formation of mesophases in stirred solutions. Science 292, 2063-2066.
[14] Lombardi, A., Palazzetti, F., Maciel, G.S., Aquilanti, V., Sevryuk, M.B. 2011. Simulation of oriented collision dynamics of simple chiral molecules. Int. J. Quan. Chem. 111(7-8), 1651-1658.
[15] Ray, K., Ananthavel, S.P., Waldeck, D.H., Naaman, R. 1999. Asymmetric scattering of polarized electrons by organized organic films of chiral molecules. Science 283, 814-816.
[16] Gerbi, A., Vattuone, L., Rocca, M., Valbusa, U., Pirani, F., Cappelletti, D., Vecchiocattivi, F. 2005. Stereodynamic effects int the adsorption of propylene molecules on Ag(001). J. Phys. Chem. B 109, 22884-22889.
[17] Thompson, D.G. 2004. Chiral effects in the ionization of chiral molecules by electron impact. J. Phys. B At. Mol. Opt. Phys. 37, 1013-1024.
[18] Aquilanti, V., Grossi, G., Lombardi, A., Maciel, G.S., Palazzetti, F. 2011. Aligned molecular collisions and a stereodynamical mechanism for selective chirality. Rendiconti Lincei 22(2), 125-135.
[19] Aquilanti, V., Ascenzi, D., Cappelletti, D., Pirani, F. 1994. Velocity dependence of collisional alignment of oxygen molecules in gaseous expansions. Nature 371, 399-402.
[20] Aquilanti, V., Ascenzi, D., de Castro Vitores, M., Pirani, F., Cappelletti, D. 1999. A quantum mechanical view of molecular alignment and cooling in seeded supersonic expansion. J. Chem. Phys. 111, 2620-2632.
[21] Pirani, F., Cappelletti, D., Bartolomei, M., Aquilanti, V., Scotoni, M., Vescovi, M., Ascenzi, D., Bassi, D. 2001. Orientation of benzene in supersonic expansions, probed by IR-laser absorption and by molecular beam scattering. Phys. Rev. Lett. 86, 5038-5053.
[22] Pirani, F., Bartolomei, M., Aquilanti, V., Scotoni, M., Vescovi, M., Ascenzi, D., Bassi, D., Cappelletti, D. 2003. Collisional orientation of the benzene molecular plane in supersonic seeded expansions, probed by infrared polarized laser absorption spectroscopy and by molecular beam scattering. J. Chem. Phys. 119, 265-276.
[23] Pirani, F., Maciel, G.S., Cappelletti, D., Aquilanti, V. 2006. Experimental benchmarks and phenomenology of interatomic forces: open shell and electronic anisotropy effect. Int. Rev. Phys. Chem. 25, 165-199.
[24] Pirani, F., Cappelletti, D., Bartolomei, M., Aquilanti, V., Demarchi, G., Tosi, P., Scotoni, M. 2007. The collisional alignment of acetylene molecules in supersonic seeded expansions probed by infrared absorption and molecular beam scattering. Chem. Phys. Lett. 437, 176-182.
[25] Aquilanti, V., Bartolomei, M., Pirani, F., Cappelletti, D., Vecchiocattivi, F., Shimizu, Y., Kasai, T. 2005. Orienting and aligning molecules for stereochemistry and photodynamics. Phys. Chem. Chem. Phys. 5, 291-300.
[26] Lombardi, A., Maciel, G.S., Palazzetti, F., Grossi, G., Aquilanti, V. 2010. Alignment and chirality in gaseous flows. J. Vac. Soc. Jpn. 53(11), 645-653.
[27] Che, D.-C., Palazzetti, F., Okuno, Y., Aquilanti, V., Kasai, T. 2010. Electrostatic hexapole state selection of the asymmetric-top molecule propylene oxide. J. Phys. Chem. A 114(9), 3280-3286.
[28] Che, D.-C., Kanda, K., Palazzetti, F., Aquilanti, V., Kasai, T. 2012. Electrostatic hexapole state-selection of the asymmetric-top molecule propylene oxide: rotational and orientational distributions. Chem. Phys. 399, 180-192.
[29] Palazzetti, F., Maciel, G.S., Kanda, K., Nakamura, M., Che, D.-C., Kasai, T., Aquilanti, V. 2014. Control of conformers combining cooling by supersonic expansion of seeded molecular

beams with hexapole selection and alignment: experiment and theory on 2-butanol. Phys. Chem. Chem. Phys. 16(21), 9866-9875.

[30] Kasai, T., Che, D.-C., Okada, M., Tsai, P.-Y., Lin, K.-C., Palazzetti, F., Aquilanti, V. 2014. Directions of chemical change: experimental characterization of the stereodynamics of photodissociation and reactive processes. Phys. Chem. Chem. Phys. 16(21), 9776-9790.

[31] Barreto, P.R.P., Vilela, A.F.A., Lombardi, A., Maciel, G.S., Palazzetti, F., Aquilanti, V. 2007. The hydrogen peroxide-rare gas systems: quantum chemical calculations and hyperspherical harmonic representation of the potential energy surface for atom-floppy molecule interactions. J. Phys. Chem. A 111(49), 12754-12762.

[32] Maciel, G.S., Barreto, P.R.P., Palazzetti, F., Lombardi, A., Aquilanti, V. 2008. A quantum chemical study of H_2S_2: intramolecular torsional mode and intermolecular interactions with rare gases. J. Chem. Phys. 129(16), 10 p. Article no. 164302.

[33] Barreto, P.R.P., Palazzetti, F., Grossi, G., Lombardi, A., Maciel, G.S., Vilela, A.F.A. 2010. Range and strength of intermolecular forces for van der waals complexes of the type H2Xn-Rg, with X = O, S and n = 1, 2. Int. J. Quan. Chem. 110(3), 777-786.

[34] Aquilanti, V., Caglioti, C., Lombardi, A., Maciel, G.S., Palazzetti, F. 2017. Screens for displaying chirality changing mechanisms of a series of peroxides and persulfides from conformational structures computed by quantum chemistry 2017 Lecture Notes in Computer Science 10408, 354-368.

[35] Elango, M., Maciel, G.S., Palazzetti, F., Lombardi, A., Aquilanti, V. 2010. Quantum chemistry of C_3H_6O molecules: structure and stability, isomerization pathways, and chirality changing mechanisms. J. Phys. Chem. A 114(36), 9864-9874.

[36] Elango, M., Maciel, G.S., Lombardi, A., Cavalli, S., Aquilanti, V. 2011. Quantum chemical and dynamical approaches to intra and intermolecular kinetics: the $C_nH_{2n}O$ (n = 1, 2, 3) molecules. Int. J. Quantum Chem. 111, 1784-1791.

[37] Barreto, P.R.P., Albernaz, A.F., Aquilanti, V., Faginas-Lago, N., Grossi, G., Lombardi, A., Palazzetti, F., Pirani, F. ????. Potential Energy Surface for the Interaction of Helium with the Chiral Molecule Propylene Oxide Lecture Notes in Computer Science 10964, 593-604.

[38] Lombardi, A., Palazzetti, F., Aquilanti, V., Grossi, G. 2017. Chirality in molecular collisions. In: 1906 AIP Conference Proceedings Article no. 030012.

[39] Lombardi, A., Palazzetti, F. 2018. Chirality in molecular collision dynamics J. Phys. Cond. Mat. 30(6), 19 p. Article no. 063003.

[40] Falcinelli, S., Vecchiocattivi, F., Alagia, M., Schio, L., Richter, R., Stranges, S., Catone, D., Arruda, M.S., Mendes, L.A.V., Palazzetti, F., Aquilanti, V., Pirani, F. 2018. Double photoionization of propylene oxide: a coincidence study of the ejection of a pair of valence shell electrons. J. Chem. Phys. 148, 114302.

[41] Palazzetti, F., Tsai, P.-Y., Lombardi, A., Nakamura, M., Che, D.-C., Kasai, T., Lin, K.-C., Aquilanti, V. 2013. Aligned molecules: chirality discrimination in photodissociation and in molecular dynamics. Rendiconti Lincei 24(3), 299-308.

[42] Nakamura, M., Yang, S.-J., Tsai, P.-Y., Kasai, T., Lin, K.-C., Che, D.-C., Lombardi, A., Palazzetti, F., Aquilanti, V. 2016. Hexapole-oriented asymmetric-top molecules and their stereodirectional photodissociation dynamics. J. Phys. Chem. A 120(27), 5389-5398.

[43] Nakamura, M., Yang Jr., S.-J., Lin, K.-C., Kasai, T., Che, D.-C., Lombardi, A., Palazzetti, F., Aquilanti, V. 2017. Stereodirectional images of molecules oriented by a variable-voltage hexapolar field: fragmentation channels of 2-bromobutane electronically excited at two photolysis wavelengths. J. Chem. Phys. 147(1), 7 p. Article no. 013917.

[44] Nakamura, M., Palazzetti, F., Tsai, P.-Y., Yang, S.-Jr., Lin, K.-C., Kasai, T., Che, D.-C., Lombardi, A., Aquilanti, V. Vectorial imaging of the photodissociation of 2-bromobutane oriented *via* hexapolar state selection. Phys. Chem. Chem. Phys. DOI:10.1039/c8cp04270e (in press).

Symposium

The astrochemical observatory: focus on chiral molecules

L'osservatorio astrochimico: obiettivo sulle molecole chirali

Rome, March 22-23, 2018

Biblioteca dell'Accademia Nazionale delle Scienze detta dei XL
Scuderie Vecchie di Villa Torlonia - Via L. Spallanzani, 1/A

PROGRAM

THURSDAY, MARCH 22

- E. CHIANCONE: *Welcome address*
- V. AQUILANTI: *Opening remarks*
- P. LAZZARETTI: *Anapolar interaction of aminoacids and sugar in nonuniform magnetic fields: could energetic stabilization of a preferred enantiomer take place in interstellar space?*
- S. PICCIRILLO: *Chiral recognition in gas-phase molecular aggregates: the effect of halogen substitution*
- L. EVANGELISTI: *Microwave spectroscopy for chiral molecules: challenges for astrochemical observations*
- S. TURCHINI: *PhotoElectron Circular Dichroism: a versatile probe for chirality*
- S. STRANGES: *Low symmetry effect on the photoelectron dynamics of chiral molecules*
- S. FALCINELLI: *The double photoionization of propylene oxide*
- S. MELANDRI: *Accurate rotational spectroscopy for astrophysical investigations: the challenge of complex organic molecules and molecular complexes*

FRIDAY, MARCH 23

- W. CAMINATI: *Rotational spectroscopy and astrochemical observation: Some historical notes, recent advancements, and some contributions towards the observation of chiral and atropisomeric species*
- S. ABBATE, G. LONGHI: *Study of Near IR vibrational absorption and vibrational circular dichroism and of the role of mechanical and electrical anharmonicities*

– A. MARIS: *Spectroscopic signatures of bifunctional alkanes for search in the interstellar medium*
– F. PIRANI: *Stereodynamical effects by anisotropic intermolecular forces*
– P. CASAVECCHIA: *Astrochemical kinetics by crossed molecular beams*
– A. FILIPPI, M. SPERANZA: *Spectroscopic Discrimination Complexes Involving an Axially Chiral Receptor*
– M. SATTA: *HF molecule as a tracer of column density in interstellar diffuse gas: the adsorption on dust grain surfaces*
– D. ASCENZI: *Role of ions in astronomical environments*
– C. CECCHI PESTELLINI: *Chiral selection in space: the role of cosmic dust*
– S. LONGO: *Modeling of organic matter delivery from Space by sub-mm grains*
– P. DE BERNARDIS, G. SETTI, M. TAVANI: *News from the Universe (to be confirmed)*
– A. LOMBARDI, F. PALAZZETTI: *The project orXid, ORigin of CHiral Discrimination: A physico-chemical view*
– L. AVALDI: *Molecular Science and Technology @ Elettra: proposal of a new beamline*

Additional communications and conclusions

***Scientific and organizing committee*:**

Vincenzo Aquilanti (University of Perugia, Uno dei XL, Linceo)
Andrea Lombardi (University of Perugia)
Federico Palazzetti (University of Perugia)

INDICE

INDICE DEGLI AUTORI

Direttore responsabile: Prof. A. Vigna Taglianti
Autorizzazione del Tribunale di Roma n. 7269 del 28-12-1959
Finito di stampare nel febbraio 2019
S.T.I. (Stampa Tipolitografica Italiana) - Via Sesto Celere, 3 - 00152 Roma